

3
2002

This is to certify that the
thesis entitled

DESIGN OF A CENTRIFUGAL PUMP FOR
LIQUID FUEL PUMPING APPLICATION

presented by

David Thiepxuan Cao

has been accepted towards fulfillment
of the requirements for

M.S. degree in Mechanical Engineering


Major professor

Date 05-01-02



PLACE IN RETURN BOX to remove this checkout from your record.
TO AVOID FINES return on or before date due.
MAY BE RECALLED with earlier due date if requested.

DATE DUE	DATE DUE	DATE DUE

**DESIGN OF A CENTRIFUGAL PUMP FOR LIQUID FUEL
PUMPING APPLICATION**

By

David Thiepxuan Cao

A THESIS

Submitted to

Michigan State University

in partial fulfillment of requirements

for the degree of

MASTER OF SCIENCE

Department of Mechanical Engineering

2002

ABSTRACT

DESIGN OF A CENTRIFUGAL PUMP FOR LIQUID FUEL PUMPING

APPLICATION

By

David Thiepxuan Cao

This thesis studied the conventional and un-conventional design method of centrifugal pump of a liquid fuel to raise a low-pressure fuel supply to the pressure required for the combustion system. In addition, the operating processes of the current automotive fuel pump systems were analyzed. From this study, the feasibility in the replacement of automotive fuel pumps by the centrifugal pump was clarified.

The fuel property requirements are: Density ($\rho = 770 \text{ kg/m}^3$), Viscosity ($\mu = 0.001 \text{ N-sec/m}^2$). The duty points are: Head ($H = 50.36\text{m}$), Low flow rate ($Q = 3.9 \cdot 10^{-5} \text{ m}^3/\text{s}$), High rotational speed ($N = 9000\text{rpm}$). The “conventional pump design method” resulted in a centrifugal pump with a very poor theoretical efficiency, $\eta = 7 \%$. Because of the poor performance, an “unconventional pump design method” has been carried out and the theoretical efficiency have been significantly improved, $\eta = 54.15 \%$.

Modifications of pump geometry in un-conventional design method were manipulated to optimize the pump performance. In the first case, the theoretical optimal pump efficiency is highest, $\eta = 65.5942 \%$, when the number of blades is four and the exit blade angle is $\beta_2 = 90^\circ$. In the second case, the theoretical optimal pump efficiency is $\eta = 65.0498 \%$, when the number of blades is four and the exit blade angle is $\beta_2 = 70^\circ$.

In memory of my parents' invaluable sacrifices and tireless support throughout my life

ad.

Sta

dis

wo

"D

the

at

sp.

Er.

cor

Use

wo

fr.

Un

To

Un

Ye

d.

ACKNOWLEDGEMENTS

The author would like to express his deep gratitude and great appreciation to his advisor, Professor Abraham Engeda at Mechanical Engineering Department of Michigan State University. All the valuable advice, the considerate guidance, the constructive discussion, the willing attitude from his advisor throughout the course of the research work encouraged and supported him to accomplish the final goal in this Thesis. The “Design of A Centrifugal Pump for Liquid Fuel Pumping Application” was achieved with the best results and the expected success.

Special thanks are given to Professor S. Paul Hess of Mathematical Department at Grand Rapids Community College for his helpful discussions. The author greatly appreciates Professor Craig W. Somerton, and Professor Norbert Müller at Mechanical Engineering Department of Michigan State University for being members in examining committee for Thesis defense.

Mr. Craig Gunn at Michigan State University is gratefully acknowledged for his useful help in preparing this thesis and the materials in publication of technical writing works. Moreover, the author also appreciates the assistance, the criticism and great friendships from all other students at the Turbomachinery Lab of Michigan State University: Yinghui Dai, Faisal Omar Mahroogi, Jae Wook Song, Mukarrum Raheel, Toshiyuki Sato, Zeyad Alsuhaibani, Donghui Zhang, and Guy Phuong

The last thing but not the least important thing, the author would like to thank all the members in his family: his Dad, Man Xuan Cao, his Mother, Nguyet Xuan Tran, his younger brother, Hongan Xuan Cao. They continuously gave the author with great love during the time of the research work at Michigan State University.

LIST

LIST

NOV

CHA

1.1

1.2

1.3

1.4

1.5

1.6

1.7

1.8

1.9

1.10

Fig.

CH.

2.1

2.2

TABLE OF CONTENTS

LIST OF TABLES.....	x
LIST OF FIGURES.....	xi
NOMENCLATURE.....	xvi
CHAPTER 1: INTRODUCTION TO CENTRIFUGAL PUMP.....	1
1.1 Introduction.....	1
1.2 Basics components of a centrifugal pump.....	2
1.3 Inlet and flow mechanism in the inlet	2
1.4 Inducer.....	3
1.5 Impeller.....	5
1.5.1 Types of impeller.....	5
1.5.2 Flow mechanism in the impeller.....	7
1.5.3 Governing equations.....	11
1.5.4 Velocity triangles.....	13
1.5.5 Slip factor and various slip factor equations.....	14
1.5.6 Relative velocity in the impeller and rothalpy.....	18
1.6 Diffuser.....	19
1.6.1 Flow mechanism in vaneless and vaned diffusers.....	19
1.6.2 Governing equations.....	20
1.7 Volute.....	20
1.7.1 Flow mechanism in volutes.....	20
1.7.2 Governing Equations.....	21
1.8 Design considerations and sixteen principal design variables.....	21
1.9 Pump performance parameters and dimensionless design coefficients.....	23
1.9.1 Overall performance parameters.....	23
1.9.2 Dimensionless design coefficients.....	26
1.10 Some loss factors influencing the pump performance.....	27
1.10.1 Disk friction losses on the impeller–External losses.....	27
1.10.2 Leakage losses –External losses.....	28
1.10.3 Incidence Losses–Internal losses.....	29
1.10.4 Friction losses –Internal losses.....	31
1.10.5 Viscosity.....	31
1.10.6 Reynolds number.....	32
1.10.7 Cavitations.....	32
Figures.....	34
CHAPTER 2: LITERATURE SURVEY OF FUEL PUMP.....	59
2.1 Fuel pump.....	59
2.2 Requirements for fuel pump in fuel injection system.....	60

23

24

25

26

27

Figure

CH

3.1

3.2

3.3

3.4

3.5

3.6

3.7

3.8

3.9

3.10

Fig-

CH

4.1

4.2

4.3

4.4

4.5

2.3	Returnless fuel delivery of fuel pump in the fuel system.....	65
2.3.1	Electronic returnless of fuel pump in the fuel system.....	66
2.3.2	Mechanical returnless of fuel pump in the fuel system.....	67
2.4	Mechanical fuel pump.....	68
2.4.1	AC-Delco and SU mechanical diaphragm positive displacement fuel-lift pump.....	68
2.4.2	Unitac mechanical diaphragm pump.....	71
2.4.3	AC mechanical diaphragm pump.....	72
2.4.4	AC Alpha mechanical pump.....	72
2.4.5	Bosch plunger-type pump.....	73
2.5	Electrical fuel pump.....	74
2.5.1	Electrical positive displacement fuel-lift pump.....	75
2.5.2	Roller-cell electrical positive displacement pump.....	77
2.5.3	Rotary electrical positive displacement pump.....	78
2.5.4	AC universal electronic solenoid fuel pump.....	81
2.5.5	SU electrical fuel-lift pump.....	82
2.6	Advantages and disadvantages of mechanical & electrical fuel pump	83
2.6.1	Mechanical fuel pump.....	83
2.6.2	Electrical fuel pump.....	84
2.7	Conclusions of mechanical fuel pump and electrical fuel pump.....	86
	Figures.....	88

CHAPTER 3: CONVENTIONAL CENTRIFUGAL PUMP DESIGN METHOD

3.1	Specific speed, suction specific speed, and suction diameter.....	112
3.2	Impeller discharge velocity triangle.....	113
3.3	Impeller discharge dimensions.....	116
3.4	Impeller inlet diameter.....	116
3.5	Impeller inlet vane angles.....	118
3.6	Impeller inlet velocity triangle.....	118
3.7	Flow areas between vanes.....	118
3.8	Volute casing.....	120
3.9	Vaned diffuser.....	121
3.10	Loss estimates, resultant efficiency, and shaft power.....	122
	Figures.....	125

CHAPTER 4: UNCONVENTIONAL CENTRIFUGAL PUMP DESIGN METHOD

4.1	Analysis of Un-Conventional Centrifugal Pump Design.....	142
4.2	Circulation Head.....	146
4.3	Impeller Friction Head Loss.....	148
4.4	Volute Head Loss.....	151
4.5	Power due to Disk Friction Loss, Power due to Leakage Loss, Entrance-Bend Loss.....	159
4.5.1	Power due to Disk Friction Loss.....	159
4.5.2	Power due to Leakage Loss.....	162

4.5.3	Entrance-Bend Loss.....	163
4.6	Optimizing Number of Blades and Blade Angle of A Logarithmic Vane Impeller.....	164
4.7	Derivation of Euler's Head Equation.....	168
4.8	Determination of Logarithmic Blade Length.....	172
	Figures.....	174
CHAPTER 5: DESIGN RECOMMENDATION.....		188
	Figures.....	194
CHAPTER 6: CONCLUSIONS.....		203
BIBLIOGRAPHY.....		210
APPENDIX A.....		218
	CALCULATION OF CONVENTIONAL CENTRIFUGAL PUMP DESIGN	
APPENDIX B.....		227
	CALCULATION OF PUMP GEOMETRICAL PARAMETERS FOR UN- CONVENTIONAL CENTRIFUGAL PUMP DESIGN	
APPENDIX C.....		232
	CALCULATION OF PUMP EFFICIENCY FOR UN-CONVENTIONAL CENTRIFUGAL PUMP DESIGN	
APPENDIX D.....		241
	SUMMARY OF UN-CONVENTIONAL CENTRIFUGAL PUMP DESIGN	
APPENDIX E.....		252
	INTEGRATION OF VOLUTE ENERGY LOSS RATE EQUATION	
APPENDIX F.....		271
	COMPUTER PROGRAMS OF PUMP GEOMETRY DETERMINATION & PUMP EFFICIENCY DETERMINATION	

Table

Table

Table

Table

Table

Table

Table

LIST OF TABLES

Table 5.1	Un-conventional Pump Efficiencies of twelve design cases at Design Point.....	189
Table 5.2	Rotational speed, flow rate, head, specific speed in fifteen design cases of pump geometry determination.....	191
Table 5.3	Necessary Impeller and Volute constants in determining the optimized pump geometrical parameters from fifteen design cases.....	191
Table 5.4	Impeller Geometry of Conventional Centrifugal Pump Design.....	199
Table 5.5	Impeller Geometry of Un-Conventional Centrifugal Pump Design....	200
Table A.1	Volute dimensions.....	224
Table A.2	Volute dimensions.....	225

LIST OF FIGURES

Figure 1.1	Alternative suction systems for an end suction centrifugal pump.....	35
Figure 1.2	Simple suction pipe.....	36
Figure 1.3	Ducted entry suction.....	36
Figure 1.4	Pressure changes on a stream surface in the suction of a centrifugal machine.....	36
Figure 1.5	Unstable flow in the suction region of a centrifugal pump under “part flow” operating conditions.....	37
Figure 1.6	Inducer.....	37
Figure 1.7	Effect on the $NPSH_R$ curve for a pump of adding an inducer.....	37
Figure 1.8	Transient flow patterns in the suction region of a pump at low flow rates.....	38
Figure 1.9	Frontal and cross-sectional view of pump impeller.....	39
Figure 1.10	Double-suction centrifugal impeller.....	39
Figure 1.11	Pump impeller.....	40
Figure 1.12	Relative and absolute flow velocity vectors in a rotating impeller.....	40
Figure 1.13	Velocity triangle with C = Absolute velocity, W = Relative velocity, U = Blade velocity.....	40
Figure 1.14	Impeller streamline locations for velocity and blade coordinate calculations.....	41
Figure 1.15	Velocity triangles at the impeller inlet (U_1 , C_1 , W_1) and exit (U_2 , C_2 , W_2).....	41
Figure 1.16	Actual and Ideal diagrams at exit from an impeller caused by slip.....	41
Figure 1.17	Velocity diagram at the impeller exit with slip.....	42
Figure 1.18	Fluid rotation relative to impeller and the resulting slip velocity.....	42
Figure 1.19	Velocity diagram at impeller exit.....	43
Figure 1.20	Conservation of energy equation and rothalpy in the rotating impeller.....	43
Figure 1.21	Nomenclature of impeller and diffuser geometry.....	44
Figure 1.22	Vaned diffuser.....	44
Figure 1.23	Vaned diffuser configurations.....	44
Figure 1.24	Arrangement of diffusers and impeller.....	45
Figure 1.25	Volute throat area.....	45
Figure 1.26	Volute throat velocity.....	46
Figure 1.27	Separated “Jet-Wake” flow in impeller.....	47
Figure 1.28	“Jet-Wake” flow pattern criterion.....	47
Figure 1.29	Fraction of streamline length.....	48
Figure 1.30	Pressure difference across the impeller blade: Blade Loading.....	48
Figure 1.31	Typical performance characteristics for a centrifugal pump of a given size operating at a constant impeller speed; Head Pump, Efficiency, Power-Flow Curve at constant speed.....	49
Figure 1.32	Head versus flow rate showing pump characteristics with unstable range.....	49

Figure 1.33	Head and flow coefficient diagram. The slip coefficient shown is for six blades.....	50
Figure 1.34	Effect of losses on the centrifugal pump head-flow rate curve.....	50
Figure 1.35	Flow velocity profiles in clearance between rotating impeller face and housing.....	51
Figure 1.36	Balancing of axial thrust on impeller: leakage flow.....	51
Figure 1.37	Inlet blade incidence: (a) increased flow rate, $Q > Q_o$; (b) reduced flow rate $Q < Q_o$ ($i = \beta_{1f} - \beta_{1b}$).....	51
Figure 1.38	Incidence and separation on slanted leading edge: leading-edge vortex.....	52
Figure 1.39	Friction factors for flow in pipes.....	53
Figure 1.40	Meridional view of a centrifugal pump.....	54
Figure 1.41	Diagram of a blade impeller when looking down the Leading Edge from the Shroud to the Hub.....	55
Figure 1.42	Meridional view of a return channel.....	56
Figure 1.43	Velocity triangle sign convention for both angle systems; meridional format of upper triangle and tangential format of lower triangle.....	56
Figure 1.44	Impeller inlet velocity triangles, using both angle systems.....	57
Figure 1.45	Impeller exit velocity triangles; showing meridional format on the left and the tangential format on the right, using both angle systems...	57
Figure 1.46	Efficiency as a function of specific speed and capacity.....	58
Figure 1.47	Comparison of pump profiles.....	58
Figure 2.1	Gasoline is drawn from the tank into the fuel pump. From the pump, gasoline flows to the carburetor as well as back to the fuel tank. This tends to cool the gasoline in the pump and reduces the change of vapor lock.....	89
Figure 2.2	Parallel routing of fuel return line and vapor line.....	89
Figure 2.3	Fuel and air system.....	90
Figure 2.4	Electronic fuel injector in the fuel delivery subsystem.....	90
Figure 2.5	Electronic fuel supply system.....	91
Figure 2.6	Fuel system installed in conjunction with heater units.....	91
Figure 2.7	Fuel tank vapor separator allows some of the fuel vapors to condense back into liquid and return to the tank. Only vapors can normally enter the higher main vent tube opening.....	92
Figure 2.8	Vapor separator attached to the fuel tank.....	92
Figure 2.9	Vapor separator in fuel vent lines.....	93
Figure 2.10	Vapor separator located near the fuel pump.....	93
Figure 2.11	Weber device for removing vapor from the warm return flow from fuel rail to tank; it could be used for solving a chronic vapor lock problem if no better remedy is practicable.....	94
Figure 2.12	Car and light trucks usually have an in-tank strainer and a gasoline filter.....	94
Figure 2.13	V-8 engines usually have pushrod between the camshaft eccentric and the fuel pump.....	95
Figure 2.14	Return fuel system.....	95
Figure 2.15	Electronic returnless system.....	96

Figure
Figure
Figure
Figure
Figure

Figure
Figure

Figure
Figure
Figure

Figure
Figure
Figure

Figure
Figure
Figure
Figure
Figure
Figure
Figure
Figure

Figure
Figure
Figure
Figure
Figure

Figure
Figure
Figure

Figure
Figure
Figure

Figure 2.16	Mechanical returnless system using in-tank regulation.....	96
Figure 2.17	Mechanical fuel pump.....	97
Figure 2.18	Mechanical fuel pump assembly.....	97
Figure 2.19	Section view of a mechanical diaphragm pump on the inlet and outlet strokes.....	98
Figure 2.20	The AC-Delco fuel lift pump, with the inlet valve on the right and the delivery valve sectioned on the left. It has a glass dome retained by a stirrup. Under the dome is the inlet stack pipe, capped by a fine mesh filter for trapping water.....	98
Figure 2.21	(a) SU AF700 fuel lift pump, and (b) SU AF800 fuel lift pump.....	99
Figure 2.22	Weber double diaphragm fuel lift pump. The inlet valve is on the left and the outlet on the right, above it, a domed accumulator to damp out pulsations.....	99
Figure 2.23	The AC lift pumps for diesel engines.....	100
Figure 2.24	Representation of the Bosch plunger type pump.....	101
Figure 2.25	An AC plunger type pump with, embodied on the right, a manual-priming pump.....	102
Figure 2.26	Common problems with a mechanical pump.....	102
Figure 2.27	Electric fuel pump components.....	103
Figure 2.28	Some models use an inertia switch to turn off the electric fuel pump in an accident.....	104
Figure 2.29	Electric fuel pump with impellers.....	104
Figure 2.30	Electric fuel pump system located inside the fuel tank.....	105
Figure 2.31	Electric fuel pump located outside the fuel tank.....	105
Figure 2.32	Bellows-type fuel pump.....	106
Figure 2.33	The SU electric pump.....	106
Figure 2.34	The SU electric fuel-lift pump.....	107
Figure 2.35	Weber plunger type electric fuel-lift pump.....	107
Figure 2.36	The Weber roller-cell type pump with a section through the roller chamber.....	108
Figure 2.37	Roller-cell positive displacement pump – electric pump.....	108
Figure 2.38	The AC in-tank fuel pump.....	108
Figure 2.39	Bosch two-stage low-pressure rotary electric fuel pump.....	109
Figure 2.40	The AC Universal Electronic solenoid type pump.....	109
Figure 2.41	In this AC medium pressure twin turbine fuel pump, the first stage impeller removes vapor by centrifuging the fuel outwards and thus leaving the vapor in the center, when it is returned to the tank. The delivery pressure is about 1 bar.....	109
Figure 2.42	Diagrammatic illustrations of five different fuel-pump Arrangements.....	110
Figure 3.1	Efficiency as a function of specific speed and capacity.....	126
Figure 3.2	Efficiency of centrifugal pumps versus specific speed, size, and shape.....	127
Figure 3.3	C_{m3}/U_2 versus specific speed.....	128
Figure 3.4	Impeller discharge angle versus specific speed.....	128
Figure 3.5	Hydraulic efficiency versus capacity.....	129

Figure 3.6	Vaned diffuser.....	129
Figure 3.7	Vaned diffuser with throat area.....	129
Figure 3.8	Impeller profile.....	130
Figure 3.9	Impeller inlet velocity triangles.....	130
Figure 3.10	Impeller velocity diagrams.....	131
Figure 3.11	Impeller outlet velocity diagram.....	131
Figure 3.12	Impeller discharge velocity triangles.....	132
Figure 3.13	C_{thr}/U_2 versus specific speed.....	132
Figure 3.14	A_{thr}/A_{II} versus specific speed.....	133
Figure 3.15	Volute casing.....	134
Figure 3.16	The plan view of the impeller and the volute casing with leading dimensions.....	135
Figure 3.17	Volute casing: a) Polar view; b) Meridional view including Section A-A of throat T.....	136
Figure 3.18	Volumetric efficiency as a function of specific speed and capacity.....	137
Figure 3.19	Ratio of mechanical power loss to water power as a function of specific speed and capacity.....	137
Figure 3.20	Impeller with vanes extended into axial inlet.....	138
Figure 3.21	Impeller with cylindrical vanes.....	138
Figure 3.22	Logarithmic spiral.....	139
Figure 3.23	Blade construction.....	140
Figure 3.24	Defining the geometry of a pump stage.....	141
Figure 3.25	Hub and shroud profiles of centrifugal pump impeller.....	141
Figure 4.1	Volute Constants.....	175
Figure 4.2	Impeller Constants.....	176
Figure 4.3	Pump Efficiency versus Specific Speed and Pump Size -Worthington.....	177
Figure 4.4	Secondary Flow in Bends.....	178
Figure 4.5	Bend Coefficients in Resistance of Bends Found by Various Investigators.....	178
Figure 4.6	Character of the Flow in a 90° Bend and the Associated Loss Coefficient.....	179
Figure 4.7	Resistance of 90° Bends.....	179
Figure 4.8	Variation of Resistance Coefficient $K (= f L/D)$ with Size.....	180
Figure 4.9	Ideal Impeller Velocities ($V_1, W_1; V_2, W_2$ Without Slip Effect) and Actual Impeller Velocities ($V_1', W_1'; V_2', W_2'$ With Slip Effect) at Inlet and Exit.....	181
Figure 4.10	Flow Through A Blade Passage.....	182
Figure 4.11	Determination of θ_0	183
Figure 4.12	Volute Element.....	184
Figure 4.13	Tangential Velocity of Fluid at any radius $V_{t(r)}$	185
Figure 4.14	Forces and Velocities in an Impeller.....	186
Figure 4.15	Logarithmic Profile.....	187
Figure 5.1	Pump Efficiency vs. Volume Flow Rate for P420 Blade Impeller.....	195
Figure 5.2	Pump Efficiency vs. Volume Flow Rate for P430 Blade Impeller.....	195
Figure 5.3	Pump Efficiency vs. Volume Flow Rate for P470 Blade Impeller.....	195

Figur

Figur

Figur

Figur

Figur

Figur

Figur

Figur

Figur

Figur

Figur

Figure 5.4	Pump Efficiency vs. Volume Flow Rate for P490 Blade Impeller.....	196
Figure 5.5	Pump Efficiency vs. Volume Flow Rate for P620 Blade Impeller.....	196
Figure 5.6	Pump Efficiency vs. Volume Flow Rate for P630 Blade Impeller.....	196
Figure 5.7	Pump Efficiency vs. Volume Flow Rate for P670 Blade Impeller.....	197
Figure 5.8	Pump Efficiency vs. Volume Flow Rate for P690 Blade Impeller.....	197
Figure 5.9	Pump Efficiency vs. Volume Flow Rate for P820 Blade Impeller.....	197
Figure 5.10	Pump Efficiency vs. Volume Flow Rate for P830 Blade Impeller.....	198
Figure 5.11	Pump Efficiency vs. Volume Flow Rate for P870 Blade Impeller.....	198
Figure 5.12	Pump Efficiency vs. Volume Flow Rate for P890 Blade Impeller.....	198
Figure 5.13	Un-conventional Centrifugal Pump Assembly Volute cover is removed, ($Z = 4$, $\beta_2 = 70^\circ$, $\eta = 65.0498\%$).....	201
Figure 5.14	Un-conventional Centrifugal Pump Assembly Cutting Section A-A ($Z = 4$, $\beta_2 = 70^\circ$, $\eta = 65.0498\%$).....	202

NOMI

ALPH

A

A₀

A_e

A_s

a

b

B

b_m

b₀

b_e

c

C

C_a

C_c

C_e

C_{is}

C_{ii}

C_s

C_Q

D

D_a

D₀

D_i

D_j

D_k

D_m

d

d_i

d_e

E

e

e_i

e_e

E_i

E_e

E_s

E_t

H

H_i

H_e

H_s

NOMENCLATURE

ALPHABETICAL

A	Cross-sectional area
A_0	Clearance area between the tip of the tongue and the impeller periphery; Volute cross-sectional area at tongue clearance
A_e	Volute cross-sectional area at exit
A_S	Shear area
a	Coefficient
b	Impeller Blade width
B	Blade width in the axial direction
b_m	Mean blade width
b_o	Housing inside axial width in the volute region
b_e	Housing axial width at exit
c	Clearance width
C	Absolute velocity
C_a	Volute area variation constant
C_d	Volute hydraulic diameter variation constant
C_{fr}	Friction coefficient
C_{dis}	Discharge coefficient
C_H	Head coefficient
C_q	Volute flow variation constant
C_Q	Capacity coefficient
D	Diameter
D_h	Hydraulic diameter
D_o	Volute hydraulic diameter at tongue clearance
D_e	Volute hydraulic diameter at exit
D_v	Volute hydraulic diameter
D_h	Hydraulic diameter
D_{mi}	Impeller mean hydraulic diameter
d	Impeller diameter
d_i	Pump Inlet diameter
d_m	Mean Impeller diameter
E	Rate of internal energy change
f	Volute friction factor
f_c	Friction coefficient
F	Weight at moment arm
F_t	Tare weight
g	Gravitational acceleration
g_c	Gravitational constant
h_c	Head drop across the wear ring
H_v	Volute head loss
H	Pump output head
H_e	Euler head
H_c	Circulation head

H_a
 H_{ab}
 H_i
 H_j
 H_m
 I

 k

 K_t
 K_s
 L
 L_{pass}
 m

 n
 m_a
 N
 N_s
 $NPSF$
 P
 p
 P_d
 P_L
 P_i
 P_o
 P_p
 P_s
 P_{total}
 q_o
 Q
 Q_L
 r
 R
 R_*
 Re
 Re_i
 Re_r
 S
 S_m
 t
 t_p
 t_r
 T
 U
 v

H_a	Head due to finite number of blades
H_{eb}	Head loss due to entrance bend
H_f	Friction head loss
H_{kj}	Output head for impeller with k number of blades and blade angle j
H_{th}	Theoretical head
I	Rothalpy
k	Hub-to-Shroud ratio, $k = 1 - \left(\frac{r_h}{r_s}\right)^2$
K_b	Bend coefficient
K_S	Stodola coefficient
L	Blade length, the length of the channel
L_{pass}	Passage length
m	Constant in disk friction loss
n	Constant in disk friction loss
m_h	Hydraulic radius of the channel section
N	Impeller rotational speed
N_s	Specific speed
$NPSH$	Net Positive Suction Head
P	Pressure in volute element; Power
p	Perimeter
P_d	Power loss due to disk friction
P_L	Power loss due to leakage
P_i	Pump input power (theoretical)
P_o	Pump output power (theoretical)
P_p	Pressure on pressure side
P_s	Pressure on suction side
P_{total}	Total pressure
q_o	Volume flow rate through A_o
Q	Volume flow rate/Pump capacity
Q_L	Leakage volume flow rate
r	Radial direction; Impeller radius
R	Impeller radius
R_w	Wearing radius
Re	Reynolds number
Re_i	Impeller Reynolds number
Re_v	Volute Reynolds number
S	Slip velocity
S_m	Mean slip velocity
t	Blade thickness
t_0	Tongue clearance between the impeller and the tongue
t_e	Volute radial clearance at exit
T	Torque
U	Peripheral velocity
v	Velocity at the section with the hydraulic radius (m_h)

V
V_r
V_t
V_a
V_m
W
W_u
W_b
Z
z

GRE

a
a₀
β
β_π
δ
θ
θ
θ₀
λ
ω
μ
ν
σ
π
ρ
τ
ψ
Δ

SUPE

SUBS

1
2
3
b
f
sh
m
id
R

V	Absolute velocity
V_r	Radial velocity
V_t	Tangential velocity
V_u	Tangential velocity
V_{mi}	Impeller mean velocity
W	Relative velocity
W_{out}	Pump output power
W_{in}	Pump input power
Z	Number of impeller blades
z	Axial direction

GREEK

α	Flow angle
α_o	Flow angle at tongue clearance
β	Blade angle
β_m	Mean blade angle
δ	Axial clearance between impeller and housing
ϕ	Volute angle
ϕ	Flow coefficient
θ	Impeller circular angle
θ_o	Imaginary angle subtended by fluid
λ	Impeller friction factor
ω	Angular velocity
μ	Dynamic viscosity; Slip coefficient
ν	Kinematic viscosity
σ	Slip coefficient
η	Pump efficiency
ρ	Density
τ	Shear stress
ψ	Head coefficient
Δ	Incremental

SUPERSCRIPTS

'	Ideal
---	-------

SUBSCRIPTS

1	Impeller inlet
2	Impeller exit
3	Impeller discharge
b	Blade
f	Fluid; Flow
th	Theoretical; Throat
m	Meridional
id	Ideal
R	Radial

T
H
S
S
u
x
w
θ

T	Tangential
H	Hub
S	Shroud
S	Suction
u	Tangential; Circumferential
x	Axial
w	Wall
θ	Tangential

1.1

inle

Wh

axis

vole

pun

imp

Tha

imp

fron

abs

of ti

A si

two

sect

de

Chapter 1

INTRODUCTION TO CENTRIFUGAL PUMP

1.1 Introduction

A single-stage centrifugal pump consists of the inlet without an inducer or the inlet with an inducer at its center, the impeller, the diffuser, and the volute (Figure 1.40). When the impeller rotates, the liquid is sucked in through the eye of the casing near the axis of a high-speed impeller and then the impeller will radially discharge liquid into the volute surrounding the impeller by the centrifugal force. The blades of the centrifugal pumps push the fluid in the direction of the blade motion. Therefore, the rotating impellers impart energy to the fluid, so work is done on the fluid by the rotating blades. This creates a large increase in kinetic energy of the fluid flow flowing through the impeller. This kinetic energy is transferred into an increase in pressure as the fluid flows from the impeller into the volute enclosing the impeller. As a result, both pressure and absolute velocity of the fluid are increased as the fluid flow from the eye to the periphery of the blades.

The centrifugal pump can be classified as the single-stage and multi-stage pump. A single-stage centrifugal pump has only one impeller. Multi-stage centrifugal pump has two or more impellers in a single volute. The impeller can be a single suction or double suction. A single-suction impeller admits the liquid on only one side of the impeller. A double-suction impeller has two suction inlets, one on each side of the impeller.

The a

•

•

•

1.2 B

with

the v

Figur

centr

centr

(Fig)

1.3 I

impe

Thes

partic

when

The advantages of the centrifugal pump are as follows:

- Compactness and low cost in large sizes
- Smooth flow through the pump and uniform pressure in the discharge pipe
- Power characteristics that make it an easy load for its driver. An increase in head reduces the power required, a characteristics that makes overloading of the motor by closing the discharger impossible.

1.2 Basic Components of A Centrifugal Pump

The single-stage centrifugal pump consists of four main components: the inlet with the inducer or the inlet without the inducer, the impeller attached to a rotating shaft, the vaneless and vaned diffuser, and the volute enclosing the impeller (Figure 1.9 and Figure 1.40).

Centrifugal pump can be single stage or multistage. For the single-stage centrifugal pumps, only one impeller is mounted on the rotor shaft. For the multi-stage centrifugal pumps, several impellers are mounted on the rotor shaft and a return channel (Figure 1.42) is used between the two single-stage centrifugal pumps.

1.3 Inlet and Flow Mechanism in the Inlet

The simplest inlet system in centrifugal pumps is the straight pipe coaxial with the impeller centerline. However, space and suction system layout requires a ducted inlet. These can cause undesirable inlet velocity profiles and strong three-dimensional flow patterns in the eye of the impeller. This is particularly true in double suction impeller, where the shaft passes through the flow on both sides of the impeller.

There are three alternatives of suction inlet system for an end suction pump.

- A coaxial cylindrical straight suction line (Figure 1.1 a)
- An inclined cone type suction (Figure 1.1 b)
- A flared inlet that may be used for vertical designs (Figure 1.1 c)

For the first alternative of the end suction design (Figure 1.1 a), the optimum inlet pipe is provided by a straight inlet pipe because this offers the best inlet flow patterns. The inlet line is often larger than the pump eye diameter, which is provided to reduce the suction line velocities and losses. For the second alternative (Figure 1.1 b), a conical reducer is provided for the inlet system because of installation reasons. This will give a more confused flow in the impeller eye. When there may be gas in the fluid, or solids are being carried, an offset reducer may be used. This assures that gas pockets do not form on shut down and also provides a route for solids to move away from the impeller when flow ceases.

For the third alternative (Figure 1.1 c), a flared inlet is used for the vertical designs. This illustrates a bell mouth intake used when liquid is taken from a tank or vessel. The diameter D_0 is empirically determined from the design chart (Stepanoff 1976) or the approach to limit cavitation. Inlet zero whirl is assumed at design flow. If the inlet diameter D_0 is too large, re-circulation can occur. The flow patterns can arise at part flow observed by Grist (1988) (Figure 1.5 and Figure 1.8). If the diameter D_0 is too large, this re-circulation can occur at a flow rate quite close to the design value, and can result in an increase in the NPSH required. The re-circulation can cause the flow loss for the flow pattern. Hence, it is only the solution when the margin between $NPSH_R$ (Net Positive Suction Head required) and $NPSH_A$ (Net Positive Suction Head available) allows.

1.4 Inducer

pr

av

ce

be

sn

th

Pe

er

in

De

Th

lo

le

inc

cro

int

for

to

Ho

In some pump applications, the centrifugal pump provides a very low suction pressure to the impeller, and so this results in the cavitations in the pump. In order to avoid or mitigate the cavitation, a simple axial pump upstream from the impeller of a centrifugal pump, called an inducer (Figure 1.6), is used in the suction immediately before the impeller. This small pump is a high specific speed machine and provides a small pressure rise to increase the fluid energy in the main impeller suction. Therefore, the inducer can reduce the risk of cavitation problems and provides the $NPSE_R$ (Net Positive Suction Energy required) of the centrifugal pump. In reality, the inducer tends to erode. However, it is cheaper to replace the inducer than the main impeller. Moreover, inducer allows bringing the fluid into the centrifugal pump more smoothly.

Inducer consists of axial flow rotors with spiral-shaped blades (Figure 1.6). Designers use only three or four blades inclined 7° to 14° to the circumferential direction. The leading edge must be as sharp as possible. The axial or meridional velocity is kept low. The slight positive incidence is preferred because the inducer should make the flow leaving the inducer to meet the leading edges of the impeller blades at a reasonable incidence to minimize the incidence losses. The low axial velocity requires larger inlet cross sections than the normal impeller inlet. Consequently, pumps using inducers are intended for very low suction heads. They need an exceptionally large inlet cross section for the inducer. The flow passage cross section decreases at the centrifugal impeller inlet to increase the meridional velocity and results in reasonable inlet blade angles.

The improvement in cavitation performance can be achieved (Figure 1.7). However, when comparing the performance between the impeller with inducer and the

impell

NPSH

1.5 Im

The im

The fl

the im

1.5.1 T

the shr

impelli

betwee

circula

•

•

•

•

•

•

impeller without inducer, the improvement is not uniform across the flow range. The NPSH (NPSE) curve rises dramatically at low flow rate and high flow rate.

1.5 Impeller

The impeller contains radial flow passages formed by rotating blades arranged in a circle. The flow enters axially near the center of rotation and turns in the radial direction inside the impeller (Figure 1.41).

1.5.1 Types of Impeller

There are two types of impeller such as open impeller and shrouded impeller. For the shrouded impeller, the blades are covered on both hub and shroud ends.

In the open impeller, the liquid enters the eye of the impeller where turning impellers add energy to the fluid and direct the liquid to the volute. A narrow clearance between the impellers and the casing is necessary to prevent most of the fluid from re-circulating back to the eye of the impeller.

There are some characteristics of the open impeller as follows:

- The efficiency can be maintained through impeller clearance adjustment.
- The impeller can be easily adjusted for wear and so the pump can remain close to its best efficiency. The centrifugal pump doesn't necessarily have to disassemble for the best efficiency.
- The open impeller is less probable to clog with solids, and it is trouble-free to clean.
- The pump is less expensive to manufacture with a simple open impeller design.
- The open impeller has all the visible parts.
- The open impeller can easily be cut or filed to increase the capacity.

- The

rate

In t

the impell

between th

The

- It is

- The

effi

- The

disa

- The

shre

- The

diff

- The

imp

- It is

- The

Pur

For the sin

impeller. F

- The open impeller can provide a greater range of specific speed choices and flow rate.

In the shrouded (closed) impeller, the liquid enters the eye of the impeller where the impellers add energy to the fluid and direct it to the volute. There is clearance between the impellers and the pump volute.

There are some characteristics of the shrouded impeller as follows:

- It is good for volatile liquids.
- The shrouded impeller is very efficient at the beginning, but later it loses the efficiency as the shrouded impeller clearance increases because of wear.
- The shrouded impeller adjustment is impossible. Therefore, the pump had to be disassembled to check the status of the wear.
- The shrouded impeller can clog. It is difficult to clean out the solids between the shroud and the shrouded impellers.
- The shrouded impeller is difficult to cast because the internal parts are hidden and difficult to inspect for flaws.
- The closed impeller is a more complicated and expensive design because the impeller shape is required and the additional wear rings are needed.
- It is difficult to modify the shrouded impeller to improve its performance.
- The specific speed and flow rate ranges are limited because of the shape.

Pump impellers can be categorized as the single suction and the double suction. For the single-suction impeller, the fluid enters through the eye on only one side of the impeller. For the double suction impeller, the fluid enters the impeller along its axis from

both si

net inle

1.5.2 F

determ

it oper

must b

impelli

assume

to zero

turbule

differs

studied

second

a. A "J

of diffe

perpend

energy

energy

(Figure

either s

both sides. The double suction impeller can reduce the end thrust on the shaft, and so the net inlet flow area is larger, inlet velocities are reduced.

1.5.2 Flow Mechanism in the Impeller

The shape of the impeller blades and the resulting flow pattern in the impeller determine how much the energy is transferred by a given impeller size and how efficient it operates. In order to evaluate the values of the exit angular momentum, the velocities must be examined at the inlet of the impeller (the leading edge of the blades), and at the impeller exit (the trailing edge of the blades). The flow entering the impeller is usually assumed to have no pre-whirl, and so the circumferential velocity component C_{t1} is equal to zero. This assumption is valid for fluid flow on one particular streamline.

The flow in a centrifugal impeller is highly complex. It is three-dimensional, turbulent, viscous, and unsteady. The flow at the impeller exit is highly non-uniform and differs from the one-dimensional calculation. The flow mechanism in the impeller was studied from three different areas: (1) “Jet-Wake” flow pattern, (2) Boundary layers and secondary-flows region, (3) Flow separation in the impeller.

a. A “Jet-Wake” flow pattern

In the impeller, a shear layer, or separation streamline, between two flow regions of different fluid energy is stabilized if the acceleration and corresponding pressure rise perpendicular to the shear layer are directed from the low-energy region toward the high-energy region. When separation appears in the impeller, two flow regions of different energy can be distinguished: the separated region and the main stream flow region (Figure 1.27). The relative velocity (W) remains constant, but the values are different on either side of the streamline separating the two regions. The acceleration, and

corresp

low-ene

region.

migrate

of a sta

near th

angle (

sense o

expecte

b. A bo

"bound

enters

(blade-

fluid o

Separ

and a "

veiocit

passag

differe

corresponding pressure increase, is directed from the suction side to the pressure side. A low-energy separated region on the suction side will be stable. A low-energy separated region, a boundary layer on the pressure side, would be unstable and would tend to migrate along the hub and shroud surfaces to the suction side. The flow pattern consisting of a stable separated region or “wake” on the suction side and a mainstream flow or “jet” near the pressure side of the blades is called “a jet-wake” flow pattern (Figure 1.27).

The blades in most centrifugal pumps lean strongly backward, and so the flow angle (β) of the separation streamline from the radial in the direction opposite to the sense of rotation is relatively large. Consequently, “a jet-wake flow pattern” would not be expected in centrifugal pumps (Figure 1.28).

b. A boundary-layers and secondary-flows region

Moreover, the flow then enters the region of axial-to-radial bend. In this region, “boundary layers” and “secondary flows” will be developed in impellers after the liquid enters the blade impeller. In the radial part of the impeller, the balance between the local (blade-to-blade) pressure gradient sets up a secondary flow, which drives low-momentum fluid onto the blade suction side. This creates a separation zone towards the impeller tip. Separation in both the meridional plane and the blade-to-blade plane produces a “jet ” and a “wake” region at the impeller tip. The fluid in the “wake” region has very low fluid velocity relative to the flow elsewhere.

High friction losses will happen as the “boundary layers” develop along the blade passages. “Secondary flows” contribute to the deterioration of the pump performance by different means. They contribute to the destabilization of the flow; hence eventually this

promote

the turn

c. Flow

(W), al

measure

defined

and the

suction

between

"blade

different

loading

separati

by appl

volume

radial d

pressure

promotes the separation of the flow near the shroud-suction side region. They also affect the turning of the flow and the associated pressure rise in the centrifugal pump.

c. Flow separation in the impeller

To illustrate the flow condition in the impeller, the plot of the relative velocity (W), along the pressure and the suction side of the blade, against the streamline length, measured from the leading edge, is constructed (Figure 1.29). The “blade loading” is defined by the relative velocity difference in the impeller. Because of the blade loading and the pressure difference across the blade, the pressure side velocity is lower than the suction side compared at the same fraction of the streamline length. The difference between the velocities on either side of the blade illustrates the pressure difference or “blade loading”, but only qualitatively. For a quantitative measure of the pressure difference, the squares of the velocities need to be plotted. From the plot, if the blade loading becomes too large, the velocity on the pressure side approaches zero. The flow separation must be avoided.

An approximate estimation for the appearance of the separated flow is obtained by applying the principle of the angular momentum change to a very narrow annular volume (Figure 1.30). If the incremental increase in the angular momentum over a small radial distance of Δr is $\rho(\Delta C_t r_1)$, the pressure difference across the blade is

$$P_p - P_s = \frac{\Delta T}{Z(\Delta r)(B r_1)} = \frac{Q}{2\pi(B r_1)} \frac{2\pi \rho(\Delta C_t r_1)}{(\Delta r)} \quad (1.1)$$

$$P_p - P_s = \frac{2\pi}{Z} C_r \frac{\rho(\Delta C_t r_1)}{(\Delta r)} \quad (1.2)$$

From the above equation, the energy added to the fluid is proportional to the pressure difference across the blade, which is the blade loading. In the flow passage

b

a

re

fr

th

ve

fin

th

re

pi.

for

we

sep

bl.

de.

to

cor

gro

between two blades, the pressure decreases in the circumferential direction, approximately linear, from the “pressure side” of the blade facing in the direction of rotation to the “suction side”. As a result, there is a corresponding increase in the velocity from the “pressure side” to the “suction side” in the impeller. If the blade loading and the pressure difference across the impeller blade (**Figure 1.29**) become very high, the velocity at the pressure side of the blade can become very small or vanish. This results in flow separation or losses. Generally speaking, the “blade loading” provides a measure of the likelihood of the flow separation.

In centrifugal pumps, the inlet relative velocity (W_1) is usually larger than the exit relative velocity (W_2). Therefore, certain diffusion, slowing of the velocity, must take place in the impeller and this diffusion should not be excessive. A tolerate velocity ratio for this required diffusion is $W_2/W_1 = 0.7$. “Separation losses” and increasing flow losses would then present when the velocity ratios are beyond this value. The first flow separation in the impeller usually appears on the shroud and on the suction side of the blades. The highest inlet velocity occurs at this location, and the greatest diffusion deceleration takes place. A sharp curvature of the shroud in the radial plane contributes to the likelihood of separation and this should be avoided.

The good centrifugal pump design demands that the “blade loading” and the corresponding velocity difference between the pressure sides and suction sides gradually grow at the inlet and taper off at the exit.

equ

rota

The

equa

The si

The th

The pu

the pur

The follo

C

C

1.5.3 Governing Equations

The torque, the power and the theoretical head are determined by the Euler's equation when the principle of conservation of angular momentum is applied. For a rotating shaft, the power transferred, \dot{W}_{shaft} , is given by

$$T = T_{\text{shaft}} = Q(\rho C_{t2}r_2 - \rho C_{t1}r_1) = Q\rho (C_{t2}r_2 - C_{t1}r_1) = \dot{m} (C_{t2}r_2 - C_{t1}r_1) \quad (1.3)$$

$$\dot{W}_{\text{shaft}} = P = T \omega = Q\rho (C_{t2}r_2 - C_{t1}r_1)\omega = \rho Q H_{\text{th}} g \quad (1.4)$$

The power supplied to the shaft of the pump is transferred to the fluid by the following equation

$$U_1 = r_1 \omega, U_2 = r_2 \omega \quad (1.5)$$

$$\dot{W}_{\text{shaft}} = T_{\text{shaft}} \omega = Q\rho (C_{t2}r_2 - C_{t1}r_1)\omega = Q\rho (C_{t2}U_2 - C_{t1}U_1) \quad (1.6)$$

The shaft power per unit mass of flowing fluid is

$$w_{\text{shaft}} = \frac{\dot{W}_{\text{shaft}}}{Q\rho} = C_{t2}U_2 - C_{t1}U_1 \quad (1.7)$$

The theoretical head in the Euler's equation is described by

$$H_{\text{th}} = \frac{(C_{t2}r_2 - C_{t1}r_1)\omega}{g} = \frac{C_{t2}U_2 - C_{t1}U_1}{g} \quad (1.8)$$

The pump ideal (theoretical) head rise is the work per unit weight added to the fluid by the pump. This ideal head rise can be presented by a different way.

$$w_{\text{shaft}} = \frac{\dot{W}_{\text{shaft}}}{Q\rho} = C_{t2}U_2 - C_{t1}U_1 \quad (1.9)$$

The following relation is established from the velocity triangle (Figure 1.12)

$$C^2 = C_t^2 + C_x^2 \quad (1.10)$$

$$C_x^2 + (C_t - U)^2 = W^2 \quad (1.11)$$

The re

(the c

$(U_2^2 -$

centrif

the rot

centrif

differen

diamete

almost

exit dia

$(W_1^2 -$

words, t

velocity

N

(no Inlet

$$C_x^2 + C_t^2 - 2C_t U + U^2 = W^2 \quad (1.12)$$

$$C_t U = \frac{C_x^2 + C_t^2 + U^2 - W^2}{2} = \frac{C^2 + U^2 - W^2}{2} \quad (1.13)$$

$$w_{\text{shaft}} = \frac{\dot{W}_{\text{shaft}}}{Q\rho} = C_{t2} U_2 - C_{t1} U_1 = \frac{(C_2^2 - C_1^2) + (U_2^2 - U_1^2) - (W_2^2 - W_1^2)}{2} \quad (1.14)$$

The result of the theoretical head is

$$H_{\text{th}} = \frac{C_{t2} U_2 - C_{t1} U_1}{g} = \frac{1}{2g} \left[(C_2^2 - C_1^2) + (U_2^2 - U_1^2) + (W_1^2 - W_2^2) \right] \quad (1.15)$$

The first term, $(C_2^2 - C_1^2)$, represents the increase in the kinetic energy of the fluid (the change in absolute kinetic energy occurring in the impeller). The second term, $(U_2^2 - U_1^2)$, represents the pressure head rise that develops across the impeller due to the centrifugal force. In other words, this represents the change of energy due to movement of the rotating air from one radius of rotation to another. This change of energy is the centrifugal energy, which raises the static pressure in the impeller. This term makes a difference between the centrifugal pump and the axial pump. The inlet (r_i) and exit diameter (r_e) of the axial pump has the same value, and so “ $U_2 = r_e \omega$ ” and “ $U_1 = r_i \omega$ ” are almost the same. However, The inlet diameter of the centrifugal pump is smaller than the exit diameter of the centrifugal pump, and so U_2 and U_1 are different. The third term, $(W_1^2 - W_2^2)$, represents the diffusion of the relative flow in the blade passage. In other words, this term expresses the change in kinetic energy due to the change of the relative velocity, and this results in a further change of static pressure within the rotor.

Normally, the fluid has no tangential component of velocity C_{t1} , or “no pre-swirl” (no Inlet Guide Vane, IGV), when the fluid enters the impeller. This means that the angle

between the absolute velocity and the tangential direction is 90° ($\alpha_1 = 90^\circ$). As a result, the centrifugal pump is usually designed for no angular momentum at the inlet, $C_{t1}r = 0$. Hence, the theoretical head in Euler's head equation is simplified by

$$H_{th} = \frac{C_{t2}(r_2\omega)}{g} = \frac{C_{t2}(U_2)}{g} = \frac{C_{t2}(U)}{g} \quad (1.16)$$

1.5.4 Velocity Triangles of the Impeller

The flow conditions, the velocities and the pressures in the impeller are described in terms of cylindrical coordinates: r , θ , z . In the cylindrical coordinates, the three absolute velocity components are designated C_r , C_t , and C_z . In the cylindrical coordinates, the three relative velocity components are designated W_r , W_t , and W_z . The sign convention of velocity triangle has the absolute angle (α) and the relative angle (β) with respect to meridional direction (radial direction); or the absolute angle (α) and the relative angle (β) with respect to the tangential direction (Figure 1.43). The impeller inlet velocity triangles (Figure 1.44) and the impeller exit velocity triangles (Figure 1.45) are defined with both systems of sign convention of absolute angle (α) and relative angle (β).

The components C_{t2} and C_{r2} in the circumferential and radial directions construct the resultant absolute velocity C_2 .

$$C_2^2 = C_{t2}^2 + C_{r2}^2 \quad (1.17)$$

$$C_{t2} = U_2 - W_{t2} = U_2 - W_{r2}\tan\beta_{F2} \quad (1.18)$$

The theoretical head, the energy added to a unit mass of fluid by the pump, can be written

$$H_{th} = \frac{U_2 C_{t2}}{g} = \frac{U_2^2 - U_2 W_{r2}\tan\beta_{F2}}{g} \quad (1.19)$$

The expression of the theoretical head is very important for calculating pump performance and for designing new centrifugal pumps.

1.5.5 Slip Factor and Various Slip Factor Equations

The fluid entering the impeller can be considered to be irrotational. When the flow is viewed in the rotating frame of reference, a relative eddy rotating in a direction opposite to the impeller is required to maintain the flow irrotational in the absolute frame. More clearly, the flow will not be perfectly guided by the blades due to the presence of this relative eddy. Because of these phenomena, the fluid that flows through a radially bladed centrifugal impeller leaves the impeller tip with a fluid velocity component in the tangential direction that is less than the blade tangential velocity of the impeller tip. Therefore, the fluid must “slip” with respect to the impeller during its passage through the impeller. In other words, the relative flow leaving the impeller of a centrifugal pump will receive less perfect guidance from the vanes under the frictionless conditions. As a result, the flow is said to slip.

Because of the slip, the actual flow does not follow the blade exactly. The flow angle β_{F2} is not identical to the blade angle β_2 , because the relative exit velocity W_2 is slightly more inclined opposite to the direction of rotation. This deviation takes place because the fluid, which retains its orientation in the absolute frame of reference, appears to rotate with respect to the rotating impeller in the opposite direction. This results in a tangential velocity component at the impeller exit opposed to the direction of rotation.

A slip factor is defined by the ratio of the flow tangential absolute velocity $C_{\theta 2}$ to the blade tangential absolute velocity $C'_{\theta 2}$ (Figure 1.16). In general, the slip factor is

described as a function of the impeller geometry and the number of blades on the impeller.

$$\sigma = \mu = \frac{C_{\theta 2}}{C'_{\theta 2}} \quad (1.20)$$

The slip factor can be defined as

$$\sigma = \frac{C_{\theta 2}}{C'_{\theta 2}} = \frac{C'_{\theta 2} - C_{\theta s}}{C'_{\theta 2}} = 1 - \frac{C_{\theta s}}{C'_{\theta 2}} \quad (1.21)$$

To compensate for this deviation of slip, a correction applied to the equation of the theoretical head is the slip coefficient σ .

$$H_{th} = \frac{U_2 C_{t2}}{g} = \frac{U_2^2 \sigma - U_2 W_{r2} \tan \beta_{F2}}{g} \quad (1.22)$$

The slip factor is distinguished between the radial vaned impeller (no back sweep and no forward sweep) ($\beta_{2b} = 90^\circ$), and backward vaned impeller (impeller with back sweep, backward-curved blade) ($\beta_{2b} < 90^\circ$) or forward vaned impeller (impeller with forward sweep, forward-curved blade) ($\beta_{2b} > 90^\circ$).

- The slip factor for radial vane ($\beta_{2b} = 90^\circ$) is $\sigma = \frac{C_{\theta 2}}{U_2} \quad (1.23)$

- The slip factor for backward vane ($\beta_{2b} < 90^\circ$) or forward vane ($\beta_{2b} > 90^\circ$) is

$$\sigma = \frac{C_{\theta 2}}{C'_{\theta 2}} = \frac{C_{\theta 2}}{C_{\theta 2\text{-Theory}}} = \frac{C_{\theta 2}}{C_{\theta 2\text{-Ideal}}} \quad (1.24)$$

The flow coefficient is defined by

$$\phi_2 = \frac{C_{m2}}{U_2} = \frac{C_{r2}}{U_2} = \frac{\dot{m}}{A_2 \rho_2 U_2} \quad (1.25)$$

There are several different definitions for slip coefficients used for centrifugal pump design as follows:

1. Eck slip correlation: ($\beta_{2b} \neq 90^0$)

$$\sigma = \frac{C_{\theta 2}}{C'_{\theta 2}} = \frac{C_{\theta 2}}{C_{\theta 2 \cdot \text{Theory}}} = \frac{C_{\theta 2}}{C_{\theta 2 \cdot \text{Ideal}}} = \frac{1}{1 + \frac{\sin(\beta_{2b})}{2Z \left(1 - \frac{d_{s1}}{d_2}\right)}} \quad (1.26)$$

2. Stodola slip correlation: ($\beta_{2b} \neq 90^0$)

$$\sigma = \frac{C_{\theta 2}}{C_{\theta 2 \cdot \text{Ideal}}} = 1 - \frac{(\pi/Z) \cos(\beta_{2b})}{1 - \phi_2 \tan(\beta_{2b})} = 1 - \frac{(\pi/Z) \cos(\beta_{2b})}{1 - (C_{r2}/U_2) \tan(\beta_{2b})} \quad (1.27)$$

$$\text{Or: } \sigma = 1 - \frac{\pi}{Z} \sin \beta_{2b} \quad (1.28)$$

For straight radial bladed impellers: ($\beta_{2b} = 90^0$)

$$\sigma = \frac{C_{\theta 2}}{U_2} = 1 - \frac{1}{2} \sin\left(\frac{2\pi}{Z}\right) \quad (1.29)$$

If a large number of impeller blades are assumed, the approximation $\sin(2\pi/Z) \cong 2\pi/Z$ is valid and the slip factor equation becomes

$$\sigma = 1 - \frac{1}{2} \frac{2\pi}{Z} = 1 - \frac{\pi}{Z} \quad (1.30)$$

3. Stanitz slip correlation: ($\beta_{2b} \neq 90^0$)

$$\sigma = \frac{C_{\theta 2}}{C'_{\theta 2}} = \frac{C_{\theta 2}}{C_{\theta 2 \cdot \text{Theory}}} = \frac{C_{\theta 2}}{C_{\theta 2 \cdot \text{Ideal}}} = 1 - \frac{\left(0.63 \frac{\pi}{Z}\right)}{1 - \phi_2 \tan(\beta_{2b})} \quad (1.31)$$

For straight radial bladed impellers: ($\beta_{2b} = 90^0$)

$$\sigma = \frac{C_{\theta 2}}{U_2} = 1 - 0.315 \left(\frac{2\pi}{Z}\right) \sin \phi_2 = 1 - 0.63 \left(\frac{\pi}{Z}\right) \sin \phi_2 \quad (1.32)$$

$$\text{Or: } \sigma = \frac{C_{\theta 2}}{C_{\theta 2}} = \frac{C_{\theta 2}}{C_{\theta 2\text{-Theory}}} = \frac{C_{\theta 2}}{C_{\theta 2\text{-Ideal}}} = 1 - 0.63 \frac{\pi}{Z} \cong 1 - \frac{2}{Z} \quad (1.33)$$

4. Wiesner slip coefficient (Wiesner 1967): ($\beta_{2b} \neq 90^0$)

$$\sigma = \frac{C_{\theta 2}}{C_{\theta 2\text{-Ideal}}} = 1 - \frac{\sqrt{\cos(\beta_{2b})/Z^{0.7}}}{1 - \phi_2 \tan(\beta_{2b})} \quad (1.34)$$

5. Coppage slip correlation (Tom Sawyer): ($\beta_{2b} \neq 90^0$)

$$\sigma = \frac{C_{\theta 2}}{C_{\theta 2\text{-Ideal}}} = 1 - \frac{1}{1 + \frac{\pi \sin \beta_{2b}}{2Z \left(1 - \frac{\bar{d}_1}{d_2}\right)}}, \quad \bar{d}_1 = \frac{d_{s1} + d_{h1}}{2} \quad (1.35)$$

6. Balje slip correlation for radial bladed impellers: ($\beta_{2b} = 90^0$)

$$\sigma = \frac{C_{\theta 2}}{U_2} \cong \frac{Z}{Z + 6.2 \left(\frac{r_1}{r_2}\right)^{2/3}} \quad (1.36)$$

7. Busemann slip correlation: ($\beta_{2b} \neq 90^0$)

$$\sigma = \frac{C_{\theta 2}}{C_{\theta 2\text{-Ideal}}} = 1 - \frac{\sqrt{\sin \beta_{2b}}}{Z^{0.7}} \quad (1.37)$$

Busemann analyzed the flow in impellers with “logarithmic spiral vanes” to obtain a somewhat accurate model for slip factor.

8. Pfleiderer slip correlation for radial bladed impellers: ($\beta_{2b} = 90^0$)

$$\sigma = \frac{C_{\theta 2}}{U_2} = \frac{1}{1 + \frac{3.6}{Z[1 - (r_1/r_2)^2]}} \quad (1.38)$$

A more general form of Pfleiderer slip correlation ($\beta_{2b} \neq 90^0$)

$$\sigma = \frac{C_{\theta 2}}{C_{\theta 2-\text{Ideal}}} = \frac{1}{1 + \frac{a}{Z} \left(1 + \frac{\beta_{2b}}{60} \right) \frac{2}{1 - (r_1/r_2)^2}} \quad (1.39)$$

For a volute: $a = 0.65$ to 0.85 ; For a vaned diffuser: $a = 0.6$;

For a vaneless diffuser: $a = 0.85$ to 1.0

9. Stechkin slip correlation for radial bladed impellers: ($\beta_{2b} = 90^\circ$)

$$\sigma = \frac{C_{\theta 2}}{U_2} = \frac{1}{1 + \frac{2}{3} \frac{\pi}{Z} \frac{1}{1 - (r_{1m}/r_2)^2}} \quad (1.40)$$

10. Amsler slip correlation for radial bladed impellers: ($\beta_{2b} = 90^\circ$)

$$\sigma = \frac{C_{\theta 2}}{U_2} = 1 - 1.25 \frac{C_{m2}}{U_2} \pi^2 \frac{b_2}{2r_2} \quad (1.41)$$

11. Yadav and Misra slip correlation for radial bladed impellers: ($\beta_{2b} = 90^\circ$)

$$\sigma = \frac{C_{\theta 2}}{U_2} = 1 - \frac{0.855 \pi^2}{Z} \frac{C_{m2}}{U_2} \quad (1.42)$$

The slip coefficient does not represent an energy loss. It only affects the magnitude of the head produced by a given size impeller. For operation at low flow rates, the slip factor is affected by suction side flow separation, which generally begins near the shroud. The velocity on the suction surface near the leading edge increases rapidly with increasing incidence ($i = \beta_{1f} - \beta_{1b}$).

1.5.6 Relative Velocity in the Impeller and Rothalpy

The inlet relative velocity is defined by

$$W_1^2 = U_1^2 + C_1^2 = \omega^2 r_1^2 + C_1^2 \quad (1.43)$$

The total enthalpy is found by applying the Bernoulli's equation to the inlet

Ber

The :

1.6 E

energ

1.6.1 l

space

diffuse

the suc

If the l

impose

the exi

the var

"vanele

allows

diffuse

diffuse

$$h_0 = h_1 + \frac{C_1^2}{2g} = h_1 + \frac{W_1^2 - \omega^2 r_1^2}{2g} = h_1 + \frac{W_1^2}{2g} - \frac{\omega^2 r_1^2}{2g} \quad (1.44)$$

The rothalpy equation, which represents the relationship equivalent to the Bernoulli's equation, applies in the rotating impeller in terms of the relative velocity W

$$I = h + \frac{W^2}{2g} - \frac{\omega^2 r^2}{2g} - \text{losses} \quad (1.45)$$

The rothalpy is also called the relative energy (Wislicenus 1965).

1.6 Diffuser

The diffuser, following the impeller, can transform kinetic energy into pressure energy but cannot increase the total energy of the fluid.

1.6.1 Flow Mechanism in Vaneless and Vaned Diffusers

The vaned diffuser follows the impeller exit. A short radial distance, a vaneless space or a vaneless diffuser, precedes the vaned diffuser. The diameter of the vaned diffuser inlet is usually about 5% to 10% greater than the impeller diameter.

The pressure and the relative velocity vary from the pressure side of the blades to the suction side at the impeller exit. As a result, a fluctuating flow comes off the impeller. If the leading edge of the diffuser vane is too close to the impeller, the flow fluctuations impose on the diffuser vanes and can produce undesirable noise and pressure pulsation at the exit. In order to preclude this noise and vibration of pressure pulsation, the vanes of the vaned diffuser are located at certain distance from the impeller tip, which creates the “vaneless space” between the impeller tip and the vaned impeller. The “vaneless space” allows the flow to mix, becomes more uniform, and adjusts to the inlet of the vaned diffuser. The pressure pulsations can be reduced by slating the leading edge of the diffuser vanes in the circumferential direction with respect to the trailing edge of the

0

1

f

f

c

1

th

1.

st

de

an

pre

int

1.7

inc

and

from

diffuser vanes. Instead of overlapping exactly at a certain moment, the trailing edge of the impeller blades sweeps gradually across the leading edge of the diffuser vanes.

The flow accelerating into the diffuser throat will result in less head loss than the flow slowing down. Theoretically, the diffuser should be correctly matched at design flow conditions. This happens because the flow can accelerate at flow rates above the design flow rate and can slow down at flow rates below the design flow rate.

1.6.2 Governing equations

The diffuser throat velocity, assuming straight vanes and sidewalls, is given by the expression

$$C_{Q3} = \frac{Q}{A_s} = \frac{Q}{2 \pi R_3 B_3 \cos \beta_3} = C_3 = C_2 \frac{R_2}{R_3} \quad (1.46)$$

1.7 Volute

The liquid leaves the impeller at a high velocity. Hence, the volute-shaped casing shape is designed to gradually reduce the velocity as the fluid leaves the impeller. This decrease in kinetic energy of the velocity head created by the impeller is converted into an increase in pressure head needed in the discharge pipe.

The volute-shaped casing, with its increasing area in the direction flow, is used to produce an essentially uniform velocity distribution as the fluid moves around the casing into the discharge opening.

1.7.1 Flow Mechanism in Volute

The impeller often discharges the fluid directly into the volute. Its cross section increases gradually around the impeller periphery, starting from the volute tongue and ending at the volute throat. The volute tongue directs the total flow, which is collected from around the impeller, through the throat to the pump exit flange. The diffuser may or

o

f

a

te

st

1.

av

th

co

18

the

Wj

may not exist between the volute throat and the exit flange. This depends on the available space and the flow velocities.

When the flow rate is greater than the design flow rate, the flow generally accelerates in the volute, and the pressure tends to decrease in the circumferential direction. When the flow rate is less than the design flow rate, the volute velocity tends to decrease, and the pressure increase circumferentially around the impeller. Because of this pressure increase or decrease, a transverse pressure force appears on the impeller at off-design conditions, which must be resisted by the pump bearings.

At flow rates less than the design flow rate, the volute tongue deflects some of the flow approaching the volute throat, which passes between the tongue and the impeller, and return into the volute. If the space between the tongue and the impeller is very large, too much flow return unnecessarily, and losses will increase. If the space is too small, strong pressure fluctuations at the blade frequency can occur.

1.7.2 Governing Equations

The volute throat cross-sections are calculated from the flow rate and from an average tangential velocity at the volute cross-section center. The flow model assumes that the impeller exit tangential velocity decreases in proportion to the radius to maintain constant angular momentum. The volute throat cross-sections is defined by

$$A = \frac{[\theta/(2\pi)]Q}{C_2 R_2/r} \quad (1.47)$$

1.8 Design Considerations and Sixteen Principal Design Variables

From the hydraulic standpoint, the ideal blade thickness will be zero. In reality, the hydraulic load must be taken, and the blades and shrouds must be thick enough to withstand them and also give the stable structure to the impeller. As a result, the normal

casting thickness needed for good casting ability with cast iron or the other common materials give a good margin against failure. Minimum casting thicknesses are based on good foundry practice. There are some important assumptions of casting ability in centrifugal pump design.

- Blade thickness: The minimum blade thickness = Impeller Diameter/100 but not less than 4 mm.
- Outlet passage width: The minimum outlet passage width = 3-4 (Impeller outside diameter)/100 but not less than 12 mm or larger than 10 times blade thickness.
- Fillet radii – Vane to Shroud and to back plate: These should not usually be less than half of the sections being joined.
- Thickness of central dividing rib in a double suction impeller: The minimum thickness should be at least 4mm and the radius therefore at 2 mm or half the thickness of the dividing rib.

Sixteen Principal Design Variables

1. Impeller rotational speed.
2. Impeller Vane outlet diameter.
3. Impeller eye (shroud) and hub diameter.
4. Impeller number of vanes.
5. Impeller vane inlet tip positions.
6. Impeller vane inlet tip angles.
7. Impeller profile width.
8. Impeller vane outlet angles.
9. Impeller vane shape between inlet and outlet.

10. Impeller vane length.
11. Impeller symmetry and concentricity.
12. Collector throat shape and area.
13. Collector vane inlet tip radius.
14. Collector vane inlet tip angles.
15. Collector diffuser passage shapes.
16. Impeller and collector surface finish.

1.9 Pump Performance Parameters and Dimensionless Design Coefficients

1.9.1 Overall Performance Parameters

The centrifugal pump uses shaft power to increase the energy, pressure, or head of the fluid. The flow rate (Q), head (H), and efficiency (η) define the overall performance parameters of a pump. The pump head (H) corresponds to the increase in total pressure, from inlet flange to exit flange, divided by the specific weight of the fluid. The pump overall efficiency is the ratio of power actually gained by the fluid to the shaft power supplied.

$$\eta = \frac{\text{Net hydraulic power gained by the fluid}}{\text{Shaft power driving the pump}} \quad (1.48)$$

$$H = \frac{P_{02} - P_{01}}{\rho g} \quad (1.49)$$

In the English system of units (lbf, ft, sec, and psi), (assuming water $\rho g = 62.4 \text{ lbf/ft}^3$)

$$H(\text{ft}) = \frac{P(\text{psi}) (144 \text{ in}^2/\text{ft}^2)}{62.4 \text{ lbf/ft}^3} \quad (1.50)$$

$$Q(\text{ft}^3/\text{sec}) = \frac{Q(\text{gpm}) (231 \text{ in}^3/\text{gal})}{(60 \text{ sec/min}) (1728 \text{ in}^3/\text{ft}^3)} \quad (1.51)$$

The net hydraulic power P delivered by the pump can be calculated from

$$P(\text{hp}) = P(\text{kW}) (1.333\text{hp/kW})$$

$$P(\text{hp}) = \frac{\rho g (\text{lbf/ft}^3) H(\text{ft}) Q(\text{ft}^3/\text{sec})}{550 (\text{ft} \cdot \text{lbf/sec})/\text{hp}} \quad (1.52)$$

In the SI system of units (N, m, sec, and PA), (assuming water $\rho g = 9806 \text{ N/m}^3$)

$$H(\text{m}) = \frac{P(\text{N/m}^2)}{9806 \text{ N/m}^3} \quad (1.53)$$

$$P(\text{hp}) = P(\text{kW}) (1.333\text{hp/kW})$$

$$P(\text{hp}) = \rho g (\text{N/m}^3) H(\text{m}) Q(\text{m}^3/\text{sec}) (0.001333 \text{ hp/W}) \quad (1.54)$$

$$\text{Shaft power} = \frac{P(\text{hp})}{\eta} \quad (1.55)$$

The overall pump efficiency consists of three sources: the hydraulic efficiency (η_h), the mechanical efficiency (η_m), and the volumetric efficiency (η_v).

$$\eta = (\eta_h)(\eta_m)(\eta_v) \quad (1.56)$$

The overall pump efficiency is defined as a function of specific speed and capacity (Figure 1.46). From the given specific speed and capacity, there are some selection for profiles of pump blade impeller (Figure 1.47).

The overall pump efficiency is affected by the “hydraulic losses” in the pump and by the “mechanical losses” in the bearing and seals. There may also be some power loss due to leakage of the fluid between the back surface of the impeller hub plate and the casing, or through other pump components. This leakage contribution to the overall efficiency is called the “volumetric losses”. The “hydraulic losses” are caused by: (1) “skin friction” and (2) “eddy and separation losses” due to changes in direction and magnitude of the velocity of flow. The “eddy losses” and “separation losses” include the

so-called “shock losses” and “diffusion losses”. Losses at the impeller entrance and exit are usually called “shock losses”. The nature of the hydraulic losses at the impeller entrance is caused by a sudden expansion or diffusion after separation when liquid approaches at a high angle of attack. “Shock losses” occur at the cutwater of a volute pump and at the entrance of diffusion vanes when a diffusion vane casing is used. These losses are of the same nature as “shock losses” at the entrance to the impeller. They are called “diffusion losses”.

Performance characteristics for a centrifugal pump and operating speed are usually given in the plot of head, efficiency, and power (Figure 1.31). The pump efficiency is a function of the flow rate and reaches a maximum value at the normal flow rate or design flow rate or capacity for the centrifugal pump. The points on the various curves corresponding to the maximum efficiency are call “best efficiency points” (BEP). At the pump's best efficiency point, the power going into the pump is the closest power to the power coming out of the pump. The pump's best efficiency point allows the pump shaft to experience the least amount of vibration.

The pump head varies as the flow rate changes. The pump performance is shown by a plot of the head as a function of the flow rate for a certain shaft speed (Figure 1.31). The efficiency – the ratio of the output power and the input power, is also a function of the flow rate. To select a centrifugal pump for a particular application, it is necessary to utilize both the “system curve”, as determined by the system equation, and the “pump performance curve”. If both curves are plotted on the same graph (Figure 1.31), the intersection (point A) of the “pump performance curve” and the “system curve” represents the “operating point” for the system. This point gives the head and the flow

rate that satisfies both the system equation and the pump equation. Ideally, the “operating point” should be near the Best Efficiency Point (BEP) for the centrifugal pump.

The stability of an operating point can be determined by slightly moving the operating point and observing where the centrifugal pump comes back to its steady operating point (Figure 1.32). The operating point at the lower flow rate is unstable, and the operating point at the higher flow rate is stable.

1.9.2 Dimensionless design coefficients

There are some dimensionless design coefficients, which are also used to evaluate the pump performance. They are Head coefficient and Flow coefficient (Capacity coefficient).

$$\text{Head coefficient } \psi = \frac{C_{t2}}{U_2} = \frac{C_{u2}}{U_2} = \frac{C_{\theta 2}}{U_2} = \frac{g H}{\eta U_2^2} \quad (1.57)$$

$$\text{Flow coefficient } \phi = \frac{C_{m2}}{U_2} = \frac{C_{r2}}{U_2} = \frac{Q}{\pi D_2 B_2 U_2} \quad (1.58)$$

The plot (Figure 1.33) reproduces the velocity diagram at the impeller exit in a dimensionless form. The tangential direction is along the vertical axis, and the meridional direction along the horizontal. As the flow rate changes, the operating point of the pump moves along the straight line of constant angle β_2 . The velocities, C_{t2} , proportional to the theoretical head, and C_{m2} proportional to the flow rate, fully determine the pump performance.

$$\text{Head coefficient from the velocity triangle: } \psi = \sigma - \tan\beta_2 \quad (1.59)$$

Due to the general complexity of flow through the centrifugal pump, the actual performance of the centrifugal pump cannot be accurately predicted on a completely theoretical basis as indicated by the data (Figure 1.34). The losses, which make the actual

head small

The external

internal loc

Moreover,

"Reynolds

1.10 Some

1.10.1 Disk

The

impeller. T

absorb shaf

between the

centrifugal p

a disk that is

with the circ

accelerate th

wall tends to

impeller fac

circumferent

substantially

The c

disk, perpend

exists on the

head smaller than the theoretical head, include the external losses and the internal losses. The external losses are “disk friction losses” on the impeller, “leakage losses”. The internal losses are “incidence losses”, “friction losses”, and “separation losses”. Moreover, the actual performance of the centrifugal pump is also affected by “viscosity”, “Reynolds number”, and “cavitations”.

1.10 Some loss factors influencing the pump performance

1.10.1 Disk friction losses on the impeller– External losses

The practical hydraulic centrifugal pump must consider all hydraulic forces on the impeller. The circumferential, fluid frictional force on the impeller, and disk friction absorb shaft power and affect the overall pump efficiency. Clearance spaces must exist between the stationary housing and the rotating hub and shroud faces of the impeller. In centrifugal pump, the external faces of the impeller on the hub and shroud side resemble a disk that is rotating in a stagnant fluid (Figure 1.35). The fluid at the disk surface rotates with the circumferential velocity of the disk. The fluid shear at the rotating disk tends to accelerate the fluid volume in the clearance and the fluid shear at the stationary housing wall tends to slow it down. Consequently, the fluid volume in the clearance between the impeller face and the housing will rotate with a velocity about half that of the circumferential velocity of the impeller. The outer periphery of the disk contributes substantially to the total frictional forces.

The circumferential velocity of the fluid in the clearance changes rapidly near the disk, perpendicular to the surface, over a certain small distance. A similar boundary layer exists on the housing wall. If the clearance between the impeller and the housing is much

er than the thickness of these boundary layers, the clearance width does not
nce the magnitude of the friction force, the disk friction, on the impeller.

The boundary layer thickness, and more generally the flow pattern in the
nce space, can be affected by the leakage flow rate through the clearance space; an
ximate value of the boundary layer thickness can be obtained. In general, the disk
n losses of the pump will be minimized if the clearance width, between the impeller
and the housing walls is made much larger than the boundary layer thickness.
fore, the overall pump efficiency can be increased.

Leakage losses – External losses

The flow pattern in the front clearance space of the pump, between the shroud and
housing, is complicated. On the outer periphery, it connects with the fluid at the
er exit, and at the inner periphery, with the pump inlet (Figure 1.36). A sleeve with
clearance, a wear ring at the pump inlet, restricts the leakage flow from the pump
ack to the inlet. In general, the leakage of fluid through the annular space due to the
re difference between entrance and exit section. Furthermore, leakage is not
ed by rotation, as long as turbulent flow in the clearance space persists. Leakage
e affected by rotation whenever rotation changes the state of the flow from laminar
ulent in the ring space.

This leakage flow is a drain on the high-energy flow delivered by the pump, and
ore reduces the pump efficiency. The leakage flow rate must be deducted from the
ate through the impeller to arrive at the actual net flow rate delivered by the pump.
ge flow is usually kept to 1% to 2% of the total flow to minimize leakage losses.

Leak

gover

the le

equat

exit v

runnin

place

stages

1.10.3

relativ

design

inlet at

the me

Leakage calculations assume that the pressure drop across the wear ring clearance alone governs the leakage flow rate q . A simple orifice flow equation will suffice to estimate the leakage flow rate:

$$q = C_{dis} 2\pi R_w c \sqrt{2g h_w} \quad (1.60)$$

$$h_w = (h_2 - h_1) - \frac{\left(\frac{1}{8}\right) \omega^2 (R_2^2 - R_w^2)}{2g} \quad (1.61)$$

The static head rise (h_1-h_2) across the impeller is calculated by using Bernoulli's equation from the theoretical head (H_{th}) and the velocity heads of the absolute inlet and exit velocities, C_1 and C_2 .

$$h_2 - h_1 = H_{th} - \frac{C_2^2}{2g} + \frac{C_1^2}{2g} \quad (1.62)$$

Leakage losses represent the head loss due to the flow passing through the running clearance between the rotating element and the stationary casing part. It takes place between the casing and the impeller at the impeller eye, between two consecutive stages in a multistage pump.

1.10.3 Incidence Losses– Internal losses

The flow separates at the leading edge of the impeller blade if the direction of the relative velocity W_1 does not align with the leading edge (Figure 1.37). Correct pump design usually assures correct alignment between the velocity vector and the blade at the inlet at the best efficiency flow rate.

At flow rates greater than design flow rate, the flow angle (β_{F1}) measured from the meridional or radial direction is smaller than the blade angle at the inlet ($\beta_{1b} = \beta_1$).

This

The

"suct

incid

the b

beco

devel

incid

section

separ

This

comp

meets

the le

centri

veloc

circu

merid

of the

indica

This produces a “separated flow region” on the “pressure side” of the blade ($\beta_{1b} > \beta_{F1}$). The incidence ($i = \beta_{1f} - \beta_{1b}$) becomes “negative incidence”.

At flow rates lower than design flow rate, “separated flow region” occurs on the “suction side” of the blade ($\beta_{F1} > \beta_{1b}$). The incidence ($i = \beta_{1f} - \beta_{1b}$) becomes “positive incidence”. The term “incidence” designates the difference between the flow angle and the blade angle: $\beta_{F1} - \beta_{1b}$. The “separated flow region” on the “pressure side” of the blade becomes unstable with “negative incidence”. Flow oscillation and rapid mixing will develop. “Separated flow region” on the “suction side” remains stable with “positive incidence” and persists far into the impeller.

The blockage from leading-edge separation restricts the flow passage across the section and therefore increases the local velocity. The head loss incurred when the separated region mixing with the main stream can be considered a sudden expansion loss. This will adversely affect the overall pump performance.

The real flow conditions at the impeller inlet at incidence are often much more complicated than those of the two-dimensional separation model. If the flow velocity meets the leading edge at a slant, a tip vortex can develop in the separated region along the leading edge, which trails away toward the hub (Figure 1.38). High-specific-speed centrifugal pumps are particularly sensitive to inlet conditions because the through-flow velocities are relatively high and the inlet diameter is also relatively large. The circumferential velocity on the shroud exceeds the circumferential velocity at the hub. meridional velocities are high on the shroud and low on the hub because of the curvature of the streamlines. Since flow losses vary with the square of the velocity, high velocities indicate high losses, which also reduce the overall pump performance.

1.10.4 Friction losses – Internal losses

The viscous boundary layers are responsible for the friction losses. The expression developed for pipe flow is used to estimate the loss in total pressure due to friction.

$$\frac{\Delta P_{\text{total}}}{\rho} = 4C_{\text{fr}} \frac{L_{\text{pass}}}{2D_h} W^2 \quad (1.63)$$

$$h_f = f_c \frac{L}{4m_h} \frac{v^2}{2g}$$

$$f_c = \frac{(\Delta P_o / \rho)}{\frac{1}{2} C^2 \left(\frac{L}{D} \right)} = \frac{4 \tau_w}{\frac{1}{2} \rho C^2}$$

(1.64)

$$\text{Re} = \frac{\rho C D}{\mu} \quad (1.65)$$

For pipe flow, the Moody chart (Figure 1.39) is used to find the friction coefficient as a function of the Reynolds number and the relative roughness.

1.10.5 Viscosity

The viscosity results in the resistance to the ability of pumping liquid of the centrifugal pump. Therefore, an increase in the viscosity of the pumped liquid changes the performance characteristic's curves for a centrifugal pump. The higher the viscosity of the pumped liquid is, the thicker the fluid enters the pump. A centrifugal pump used for higher viscous fluids will be impinged on by the following elements:

- The brake horsepower requirement will increase.
- A reduction in the head the pump will produce.
- Some reduction in the flow rate will occur with moderate and high viscosities.

- The pump's efficiency will decrease.

With more viscous fluids, the “hydraulic losses” is definitely applied to the so-called “through-flow” losses. These losses are directly the result of skin friction and eddy systems along the primary path of the fluid passing through the centrifugal pump.

1.10.6 Reynolds number

The general trend of the Reynolds number characteristics indicates three different zones, within which the influence of the major losses is changing in weight.

1. For the range of water and air performance above Reynolds numbers $Re > 10^6$, the efficiency losses are essential due to the hydraulic “through-flow” losses. These “through-flow” losses are produced by disk friction and leakage.
2. For the Reynolds numbers $10^6 > Re > 10^4$, the increase in power input is caused mainly by rapidly growing “disk and ring friction” losses, while “through-flow” losses increase at a comparative low rate. The “through-flow” losses are indicated by the relatively small decrease in head and capacity, which proves that turbulent flow persists essentially throughout the pump. “Leakage” losses have assumed a negligible part.
3. For the Reynolds numbers $Re < 10^4$, the “through-flow” losses increase more rapidly as indicated by a downward trend in head and capacity. Laminar-flow conditions are gradually established for the main flow. “Disk and ring friction” losses become less dominant and due to the large dissipation of power into heat on account of the laminar-flow conditions, the pump efficiency losses cannot increase more by “disk and ring friction” losses.

1.10.7 Cavitations

The cavitations can occur when the high local velocity corresponding to low static pressure happens near the blade leading edge. Under cavitating conditions, the absolute local static pressure falls below the vapor pressure of the fluid, and steam or gas bubbles appear. The evolving gas corresponding to the volume increase can choke down the flow and prevent further increase of the flow rate. This will decrease the overall pump efficiency. Moreover, the cavitation bubbles and the re-entering fluid jet on the blade surface can generate very high local pressures and destroy the blade material.

In order to specify a centrifugal pump to a certain application, the Net Positive Suction Head Available (NPSHA) from the system is calculated by estimating the total absolute pressure available from the system at the pump inlet, P_{01} .

$$\text{NPSHA} = \frac{P_{01} - P_{vp}}{\rho g} = h_{01} - h_{vp} \quad (1.66)$$

The NPSHA must be greater than the NPSHR (Net Positive Suction Head Required) in order that the centrifugal pump performance can't significantly reduce. The temperature of the fluid affects the vapor pressure and may also lead to premature cavitations. Hot or boiling fluids may require pressurization of the pump inlet.

FIGURES

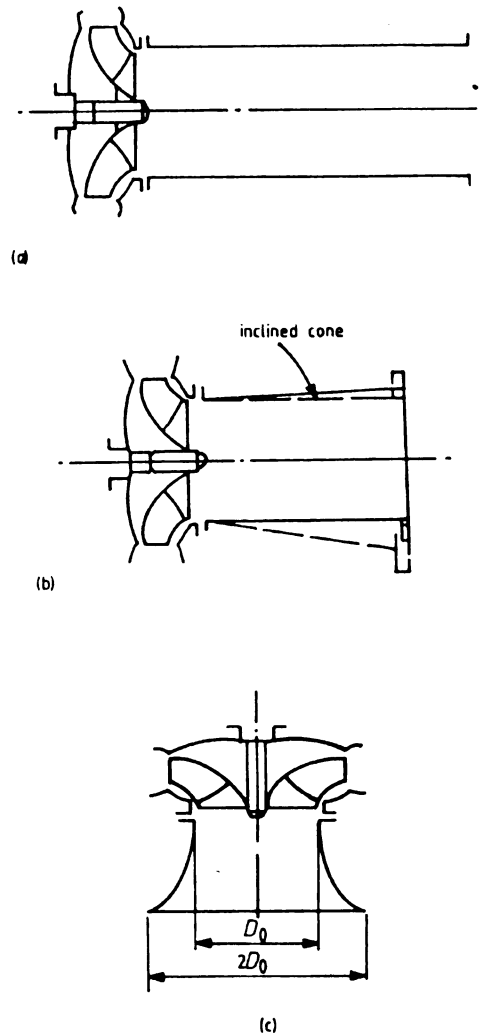


Figure 1.1 Alternative suction systems for an end suction centrifugal pump
 (a) A co-axial cylindrical straight suction line
 (b) An inclined cone type suction
 (c) A flared inlet that may be used for vertical design
 (after Turton, R. K., 1994)

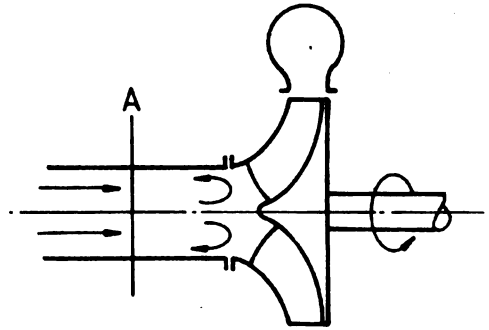


Figure 1.2 Simple suction pipe (after Turton, R. K., 1984)

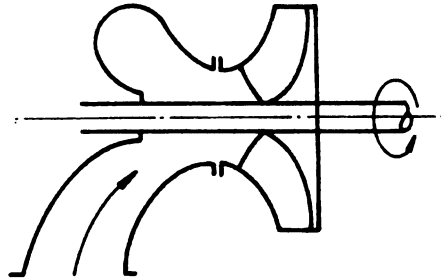


Figure 1.3 Ducted entry suction (after Turton, R. K., 1984)

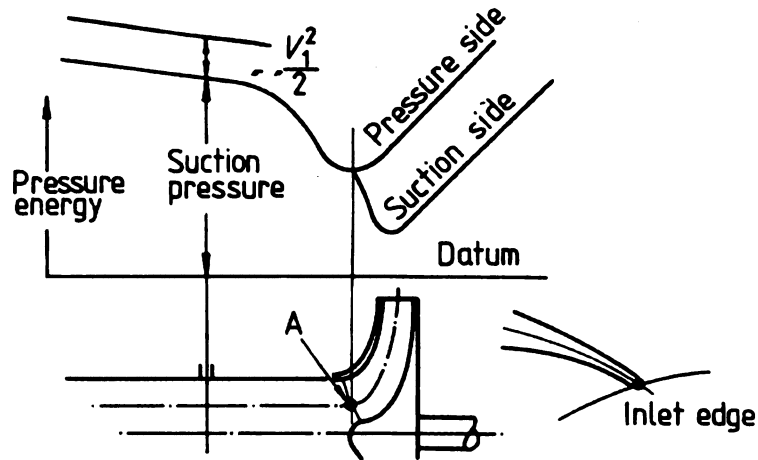


Figure 1.4 Pressure changes on a stream surface in the suction of a centrifugal Machine (after Turton, R. K., 1984)

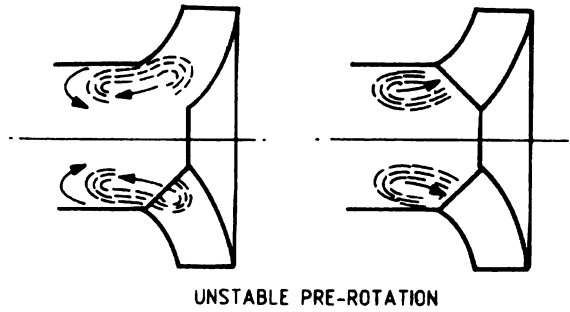


Figure 1.5 Unstable flow in the suction region of a centrifugal pump under “part flow” operating conditions (after Grist, 1988, Courtesy of the Institution of Mechanical Engineers)

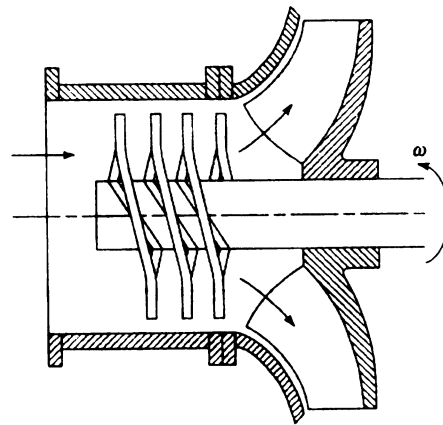


Figure 1.6 Inducer (after John Tuzson, 2000)

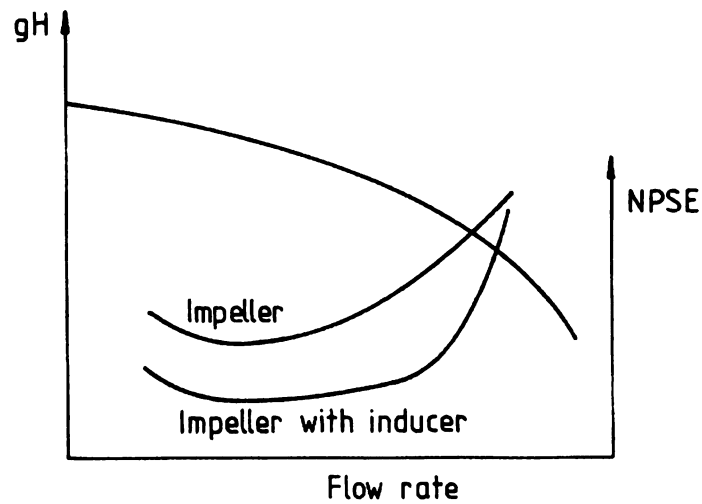
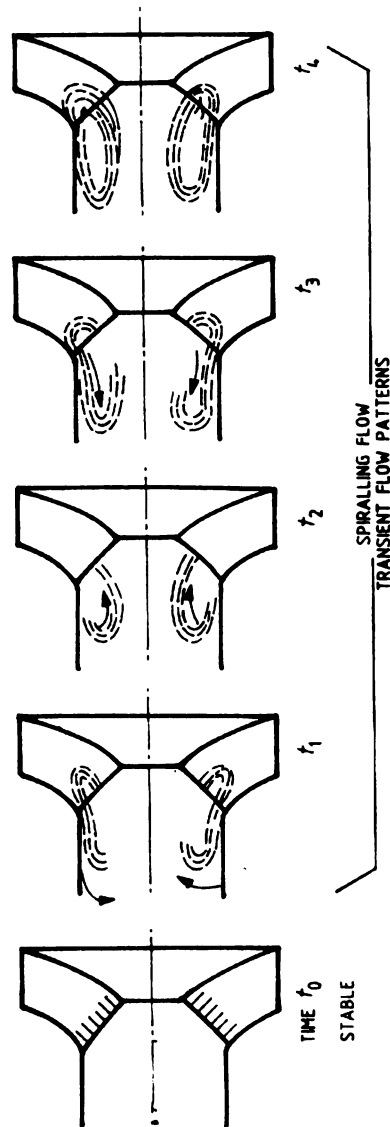


Figure 1.7 Effect on the $NPSH_R$ curve for a pump of adding an inducer (after Turton, R. K., 1984)



**Figure 1.8 Transient flow patterns in the suction region of a pump at low flow rates
(after Grist, 1988, Courtesy of the Institution of Mechanical Engineers)**

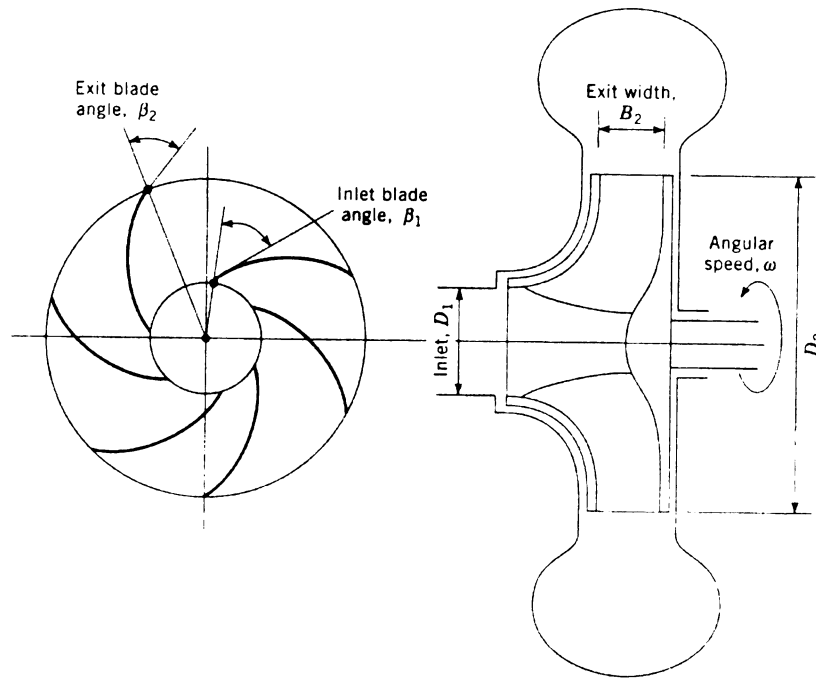


Figure 1.9 Frontal and cross-sectional view of pump impeller (after John Tuzson, 2000)

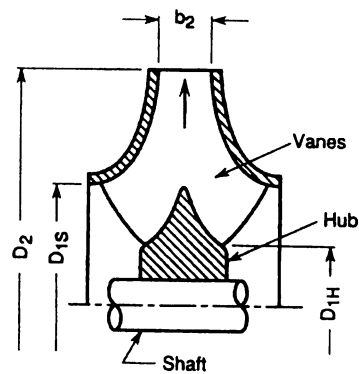


Figure 1.10 Double-suction centrifugal impeller (after Earl Logan, 1993)

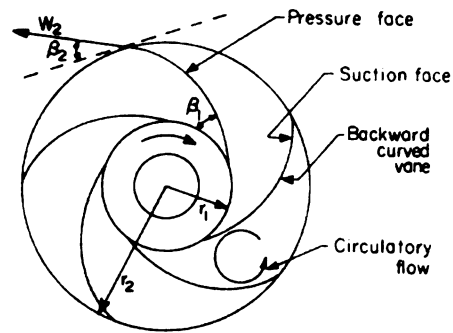


Figure 1.11 Pump impeller (after Earl Logan, 1993)

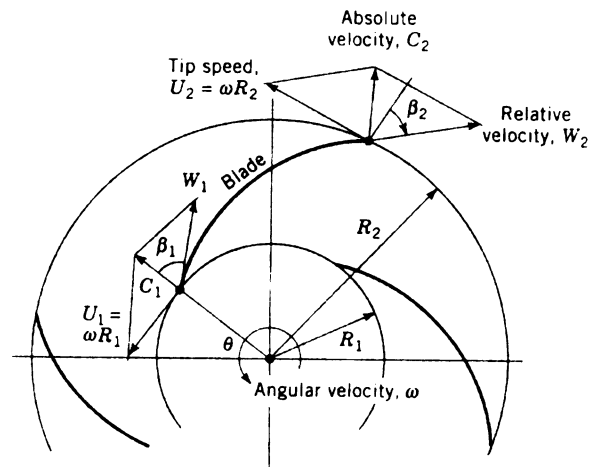


Figure 1.12 Relative and absolute flow velocity vectors in a rotating impeller (after John Tuzson, 2000)

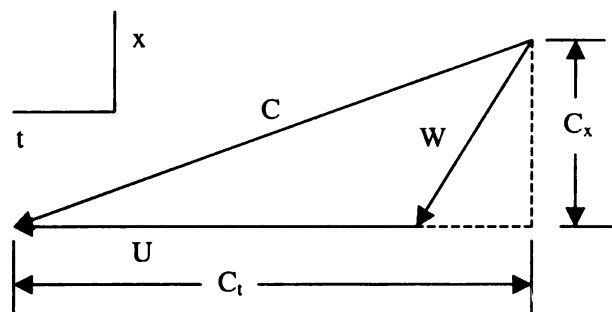


Figure 1.13 Velocity triangle with C = Absolute velocity, W = Relative velocity, U = Blade velocity

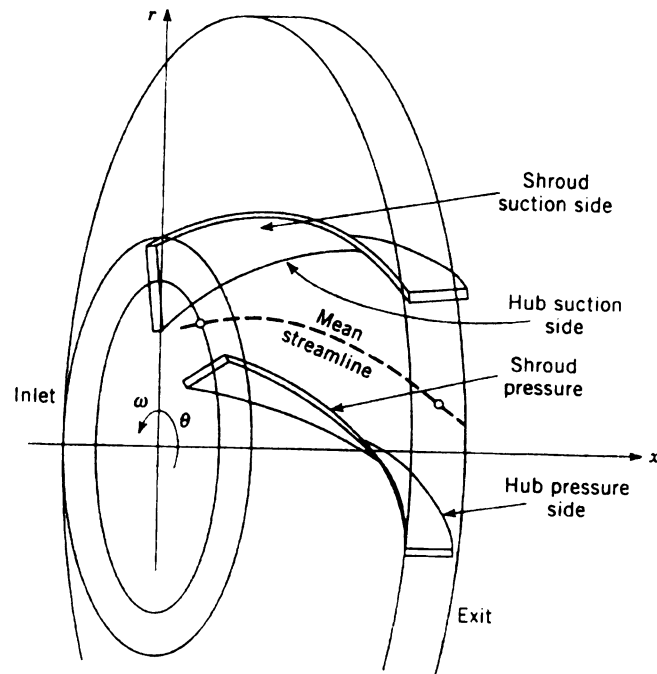


Figure 1.14 Impeller streamline locations for velocity and blade coordinate calculations (after John Tuzson, 2000)

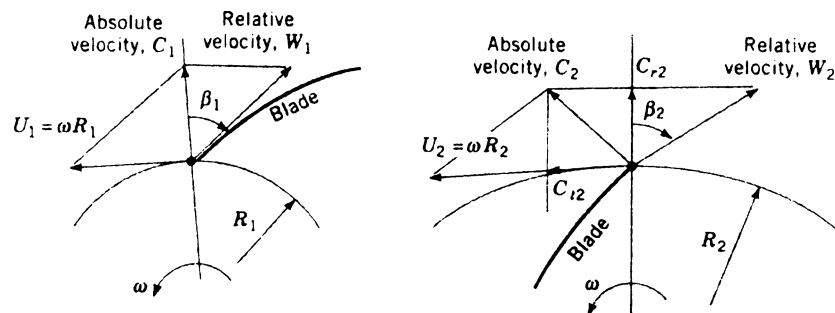


Figure 1.15 Velocity triangles at the impeller inlet (U_1, C_1, W_1) and exit (U_2, C_2, W_2) (after John Tuzson, 2000)

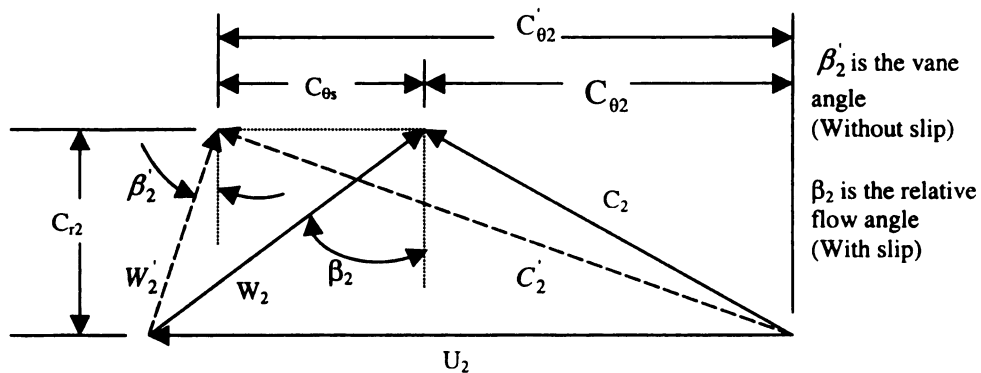
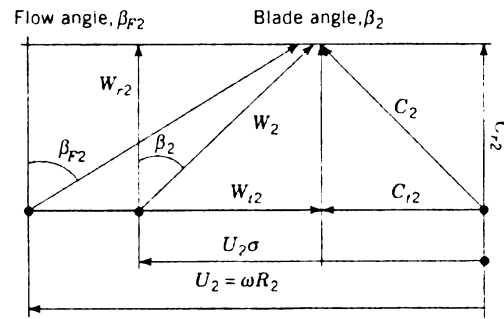


Figure 1.16 Actual and Ideal diagrams at exit from an impeller caused by slip



Absolute tangential velocity, C_{t2}
 $C_{t2} = U_2 - W_{r2} \tan \beta_{F2} = U_2 \sigma - W_{r2} \tan \beta_2$
 Radial velocity, $W_{r2} = C_{r2} = Q/\pi D_2 B_2$

Figure 1.17 Velocity diagram at the impeller exit with slip (after John Tuzson, 2000)

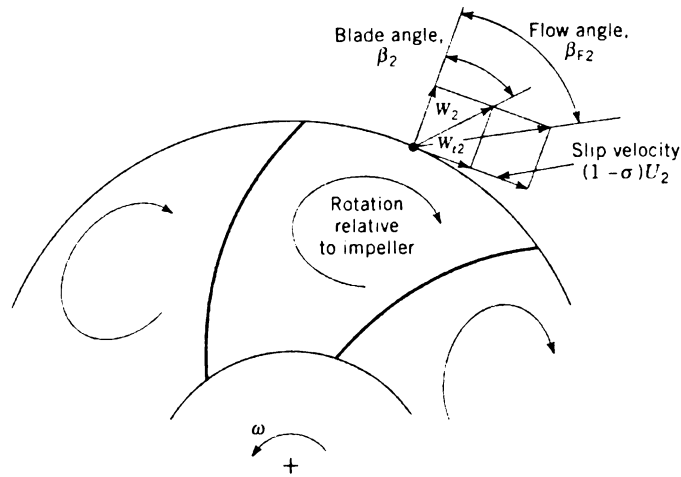


Figure 1.18 Fluid rotation relative to impeller and the resulting slip velocity (after John Tuzson, 2000)

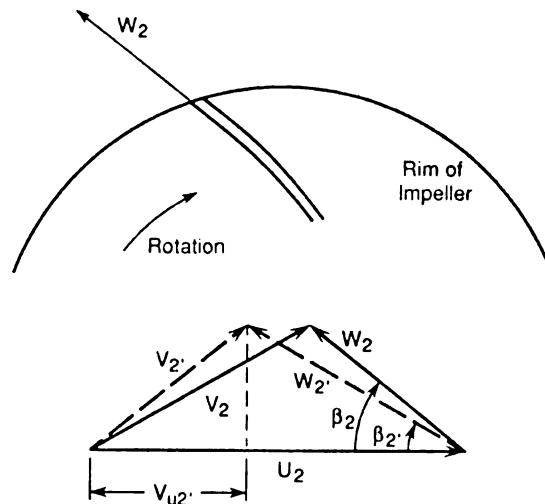


Figure 1.19 Velocity diagram at impeller exit (after Earl Logan, 1993)

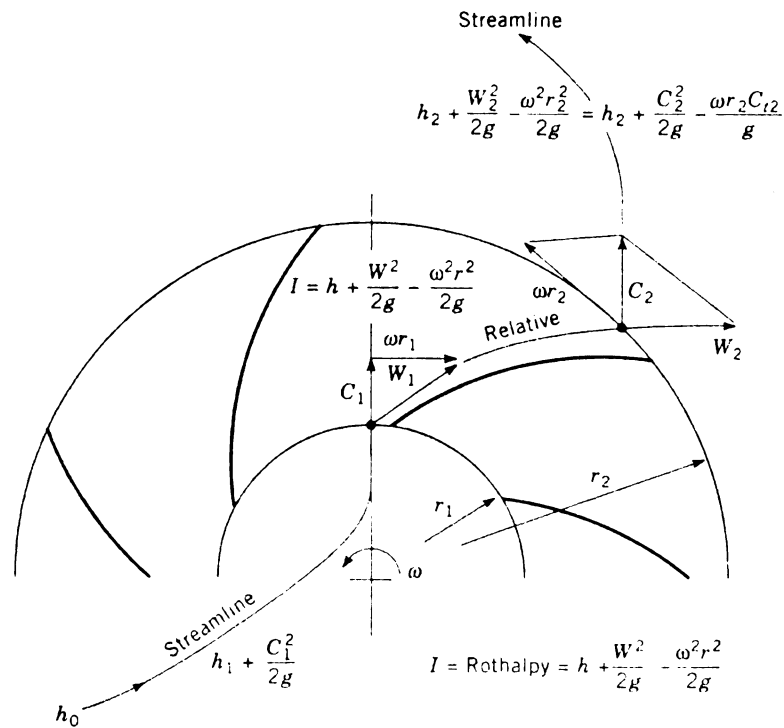


Figure 1. 20 Conservation of energy equation and rothalpy in the rotating impeller (after John Tuzson, 2000)

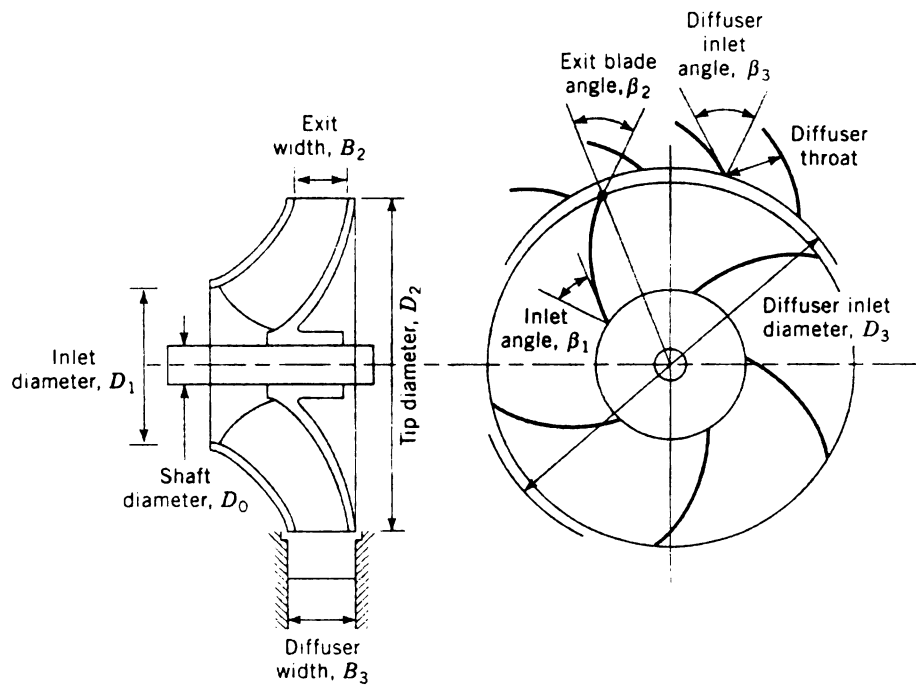


Figure 1.21 Nomenclature of impeller and diffuser geometry (after John Tuzson, 2000)

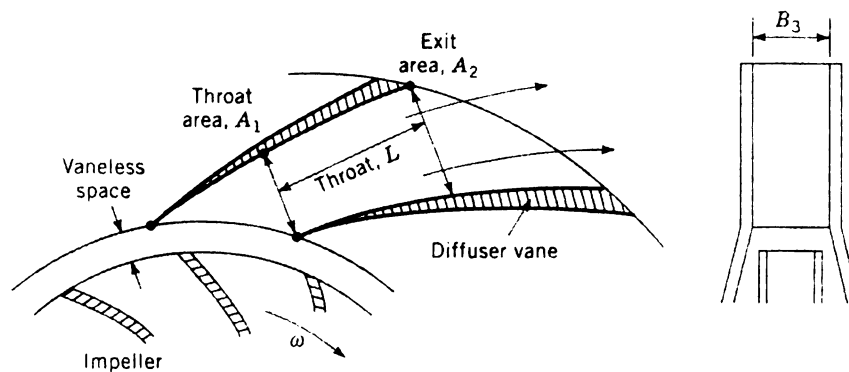


Figure 1.22 Vaned diffuser (after Earl Logan, 1993)

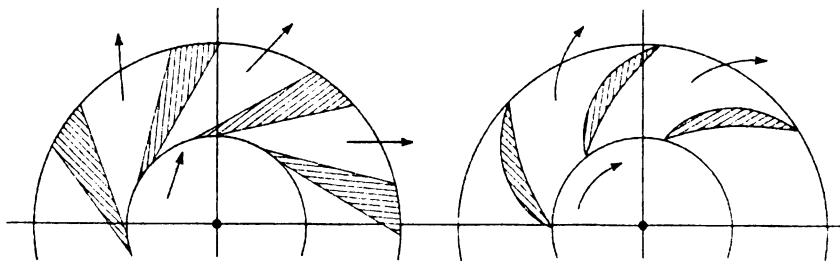


Figure 1.23 Vaned diffuser configurations (after Earl Logan, 1993)

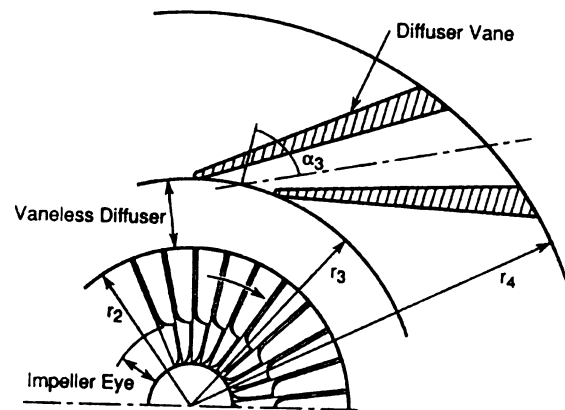


Figure 1.24 Arrangement of diffusers and impeller (after Earl Logan, 1993)

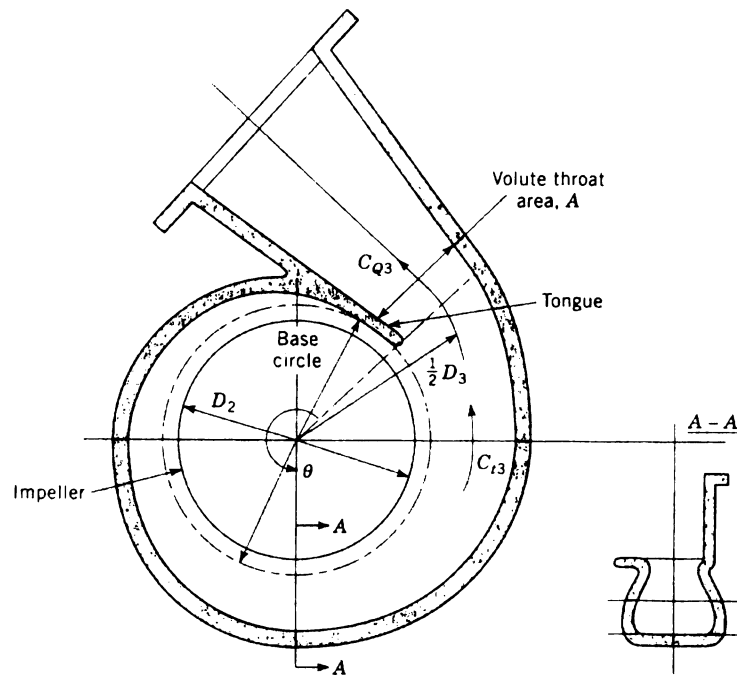


Figure 1.25 Volute throat area (after John Tuzson, 2000)

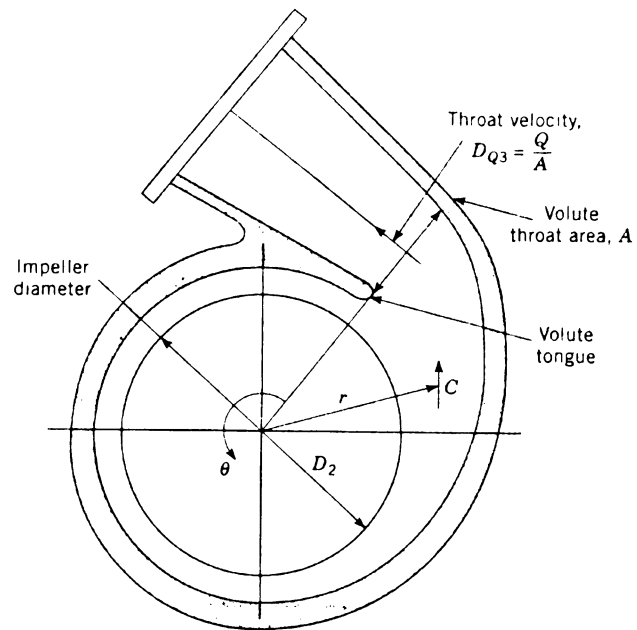


Figure 1.26 Volute throat velocity (after John Tuzson, 2000)

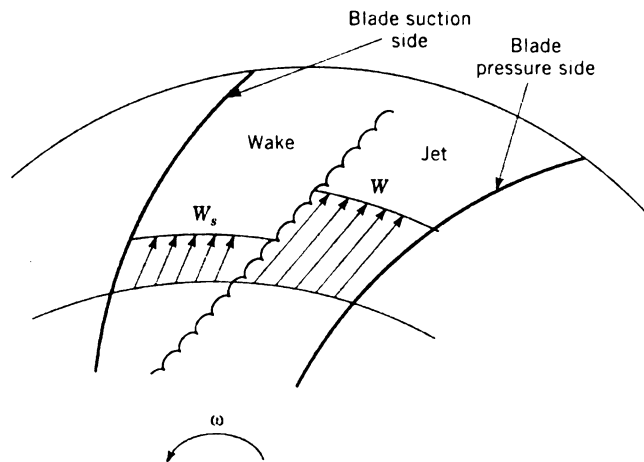


Figure 1.27 Separated “Jet-Wake” flow in impeller (after John Tuzson, 2000)

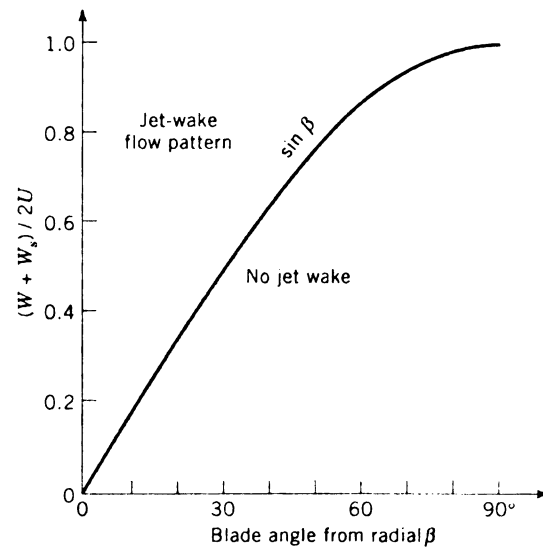
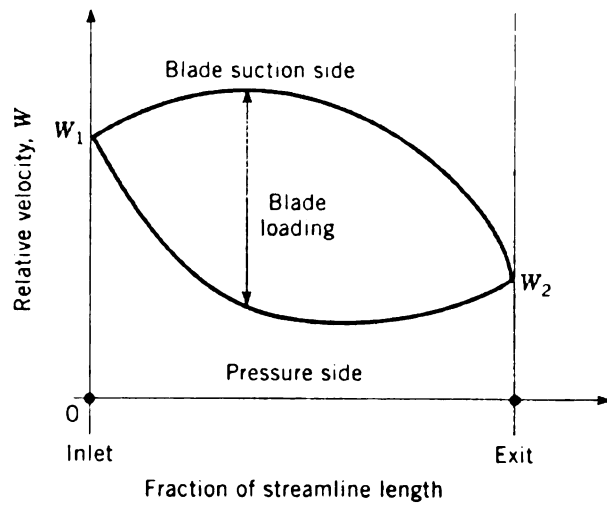
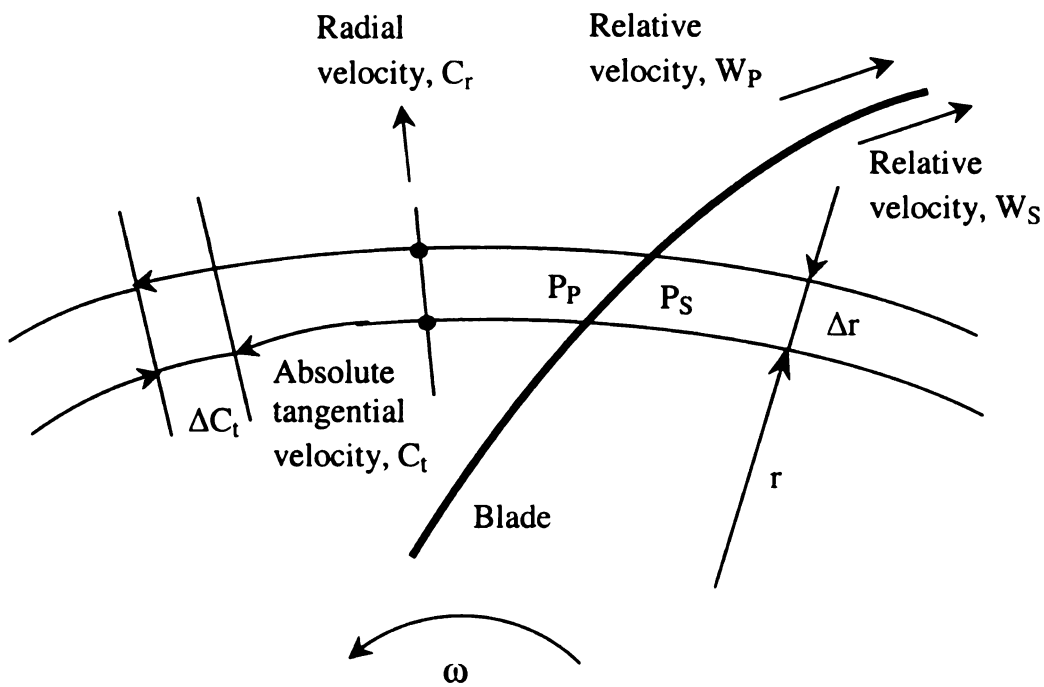


Figure 1.28 “Jet-Wake” flow pattern criterion (after John Tuzson, 2000)



re 1.29 Fraction of streamline length (after John Tuzson, 2000)



$$P_P - P_S = \frac{2\pi}{Z} C_r \frac{\rho \Delta C_t r_1}{2g} = \rho \left(\frac{W_S^2 - W_P^2}{2} \right)$$

re 1.30 Pressure difference across the impeller blade: Blade Loading

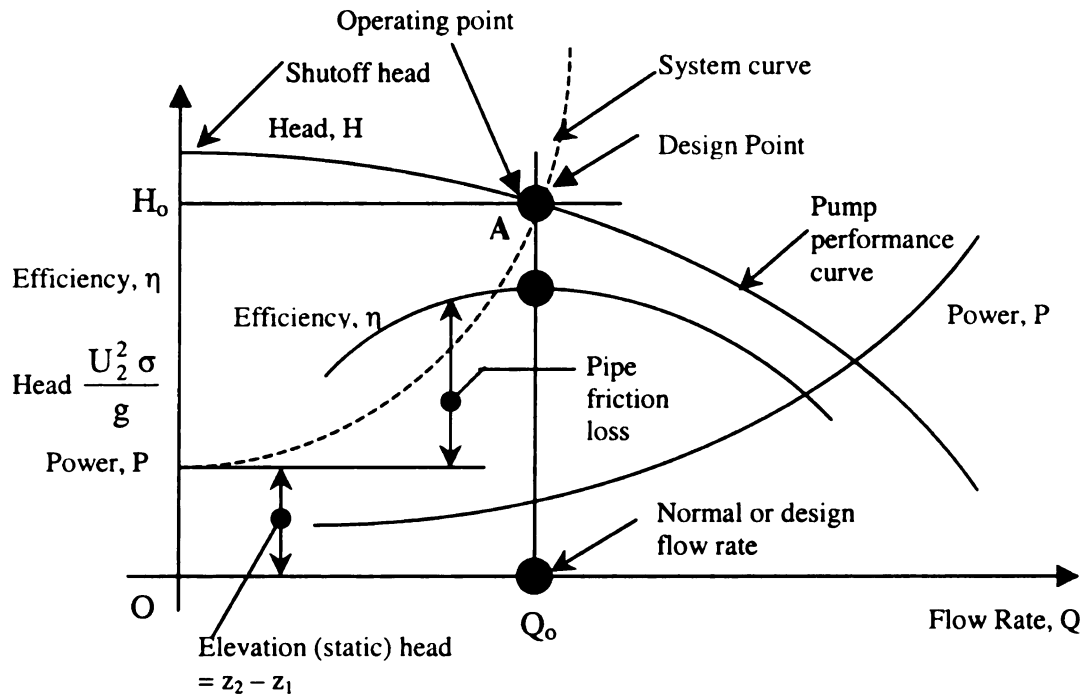


Figure 1.31 Typical performance characteristics for a centrifugal pump of a given size operating at a constant impeller speed; Head Pump, Efficiency, Power-Flow Curve at constant speed

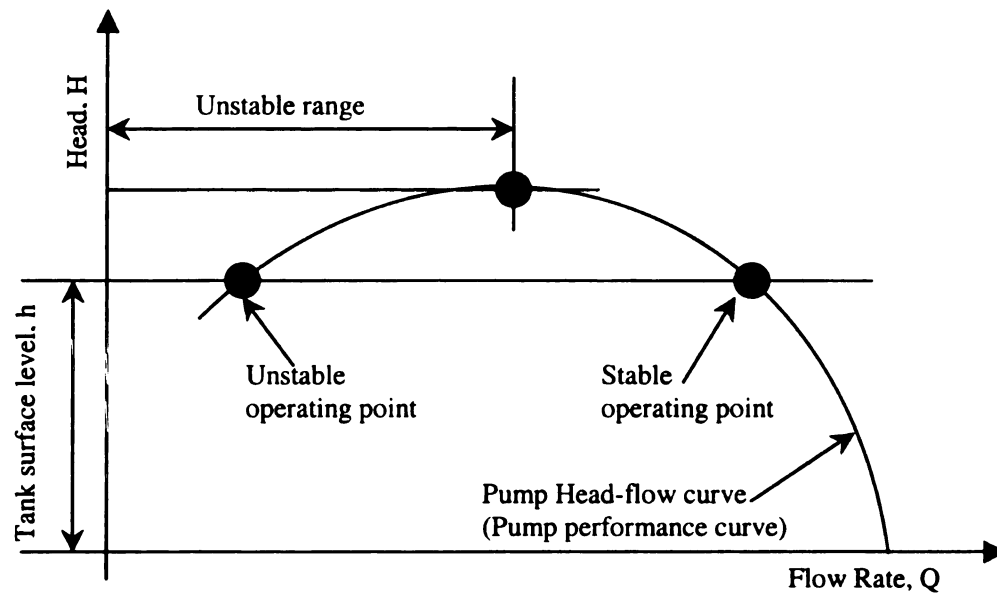


Figure 1.32 Head versus flow rate showing pump characteristics with unstable range

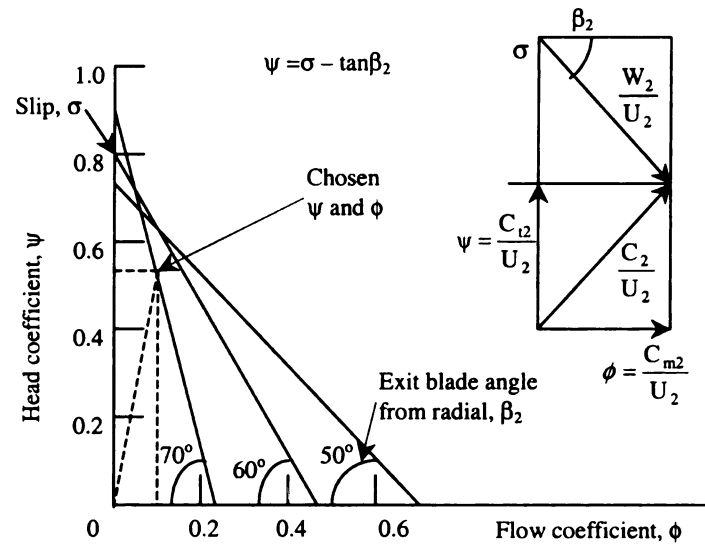


Figure 1.33 Head and flow coefficient diagram. The slip coefficient shown is for six blades

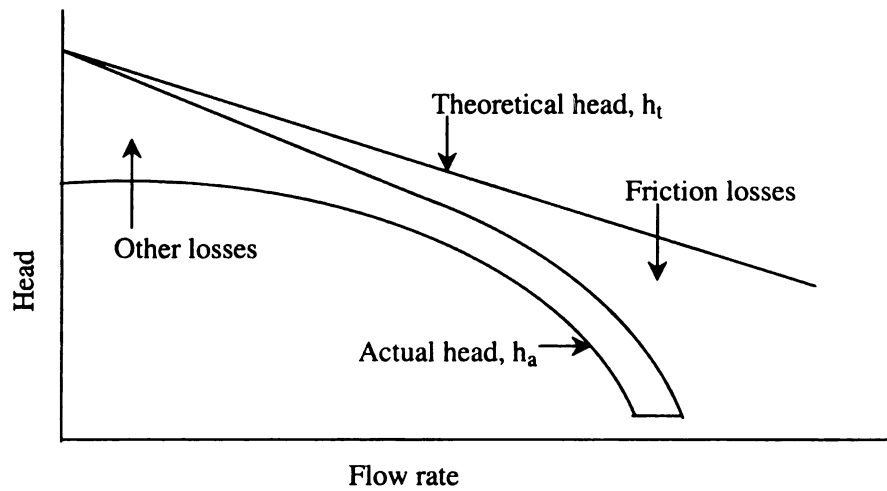


Figure 1.34 Effect of losses on the centrifugal pump head-flow rate curve

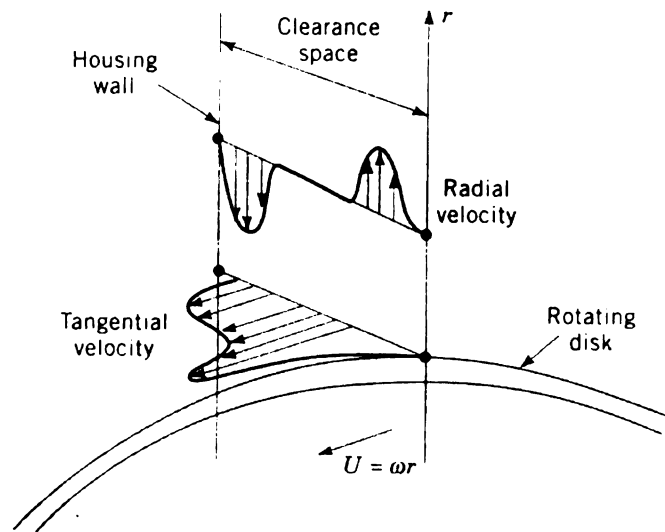


Figure 1.35 Flow velocity profiles in clearance between rotating impeller face and housing (after John Tuzson, 2000)

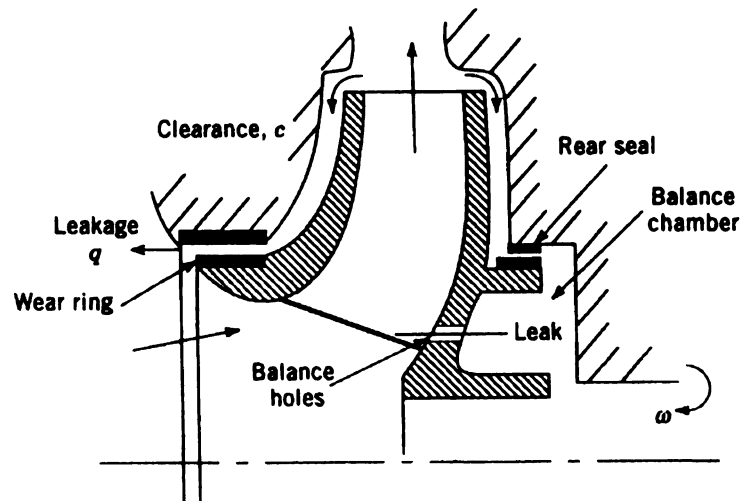


Figure 1.36 Balancing of axial thrust on impeller: leakage flow (after John Tuzson, 2000)

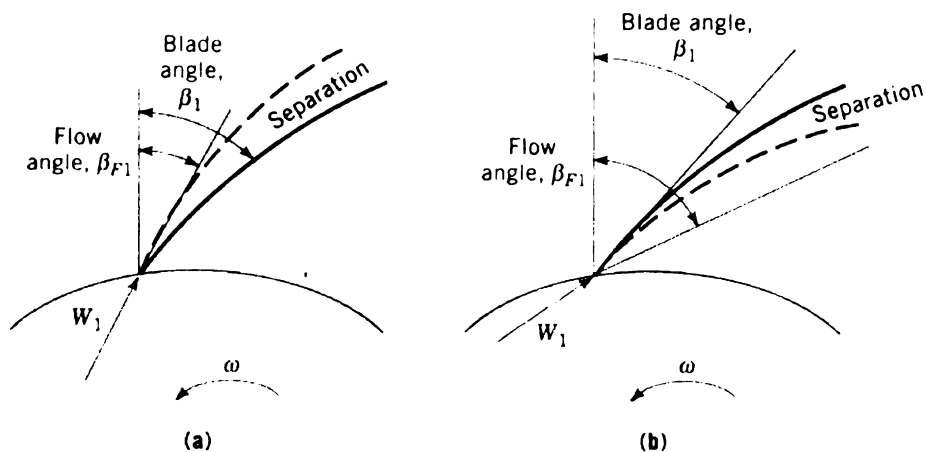
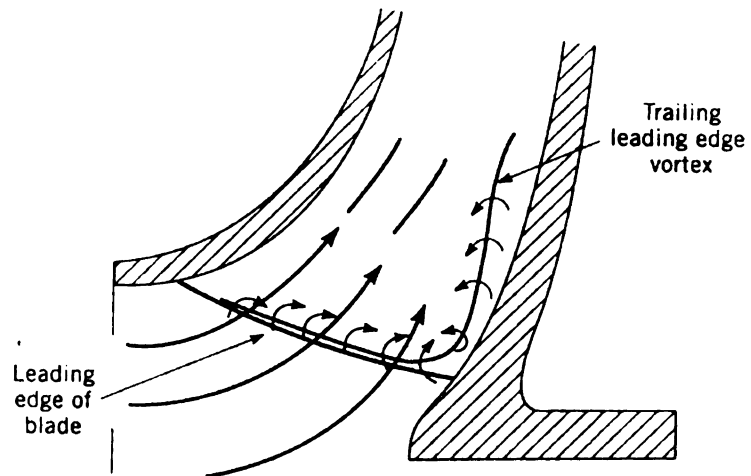


Figure 1.37 Inlet blade incidence: (a) increased flow rate, $Q > Q_0$; (b) reduced flow rate $Q < Q_0$ ($i = \beta_{1f} - \beta_{1b}$) (after John Tuzson, 2000)



**Figure 1.38 Incidence and separation on slanted leading edge: leading-edge vortex
(after John Tuzson, 2000)**

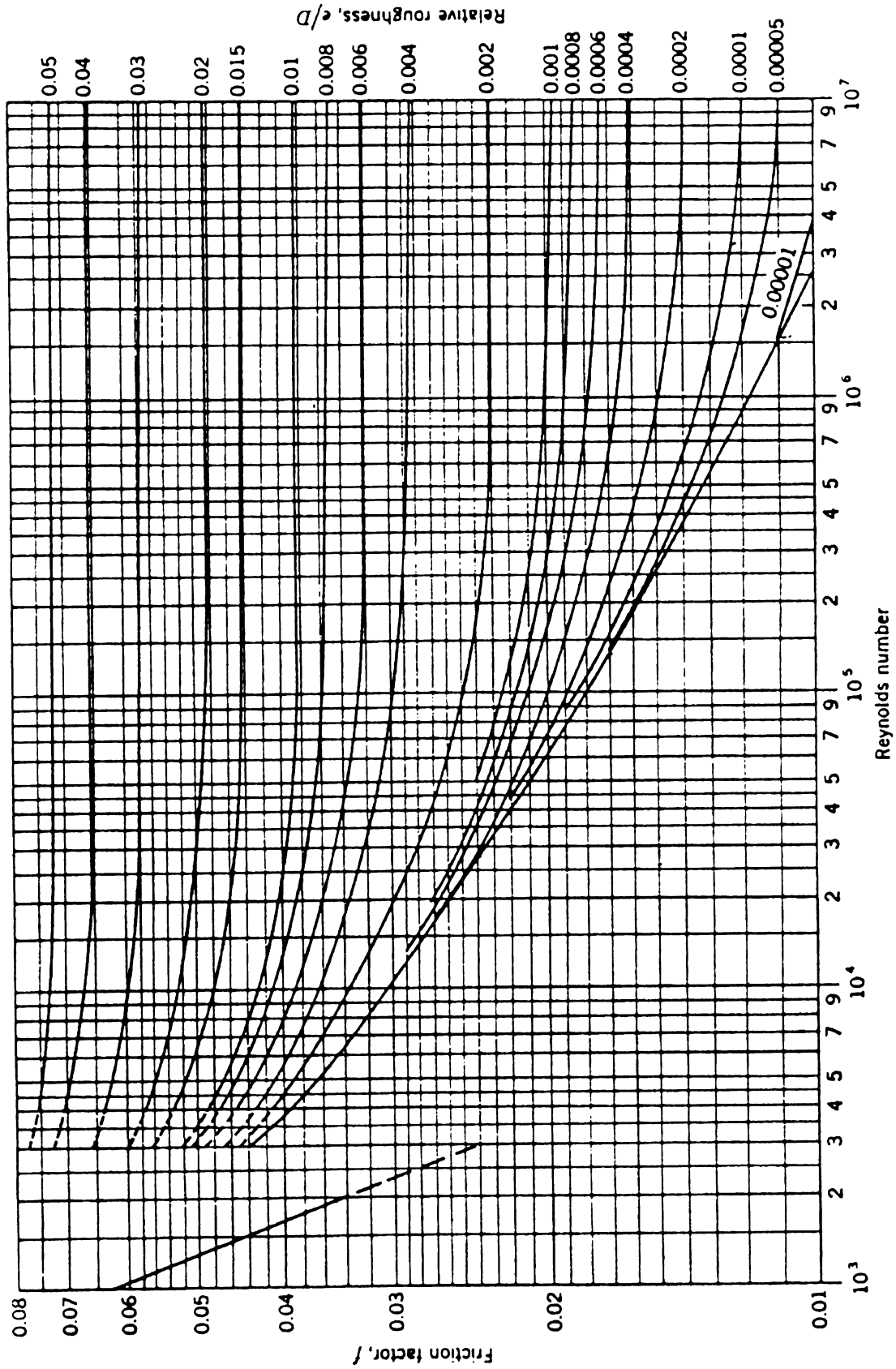


Figure 1.39 Friction factors for flow in pipes (after Japikse, D., Marscher, W. D., and Furst, R. B., 1997)

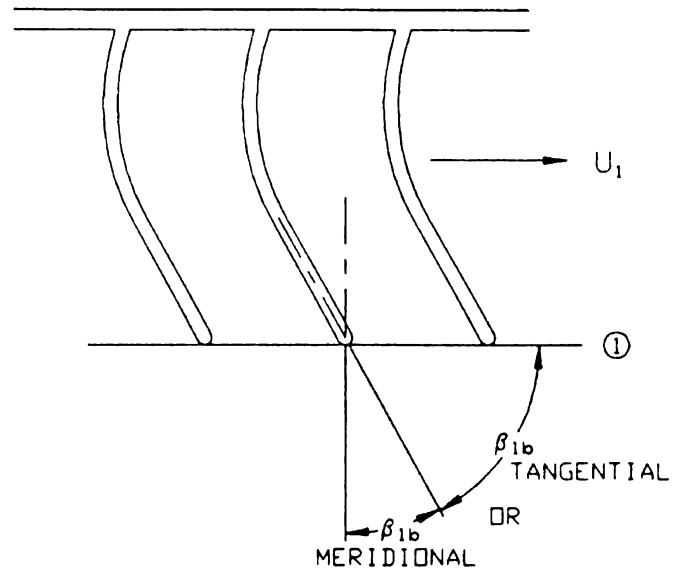


Figure 1.41 Diagram of a blade impeller when looking down the Leading Edge from the Shroud to the Hub (after Japikse, D., Marscher, W. D., Furst, R. B., 1997)

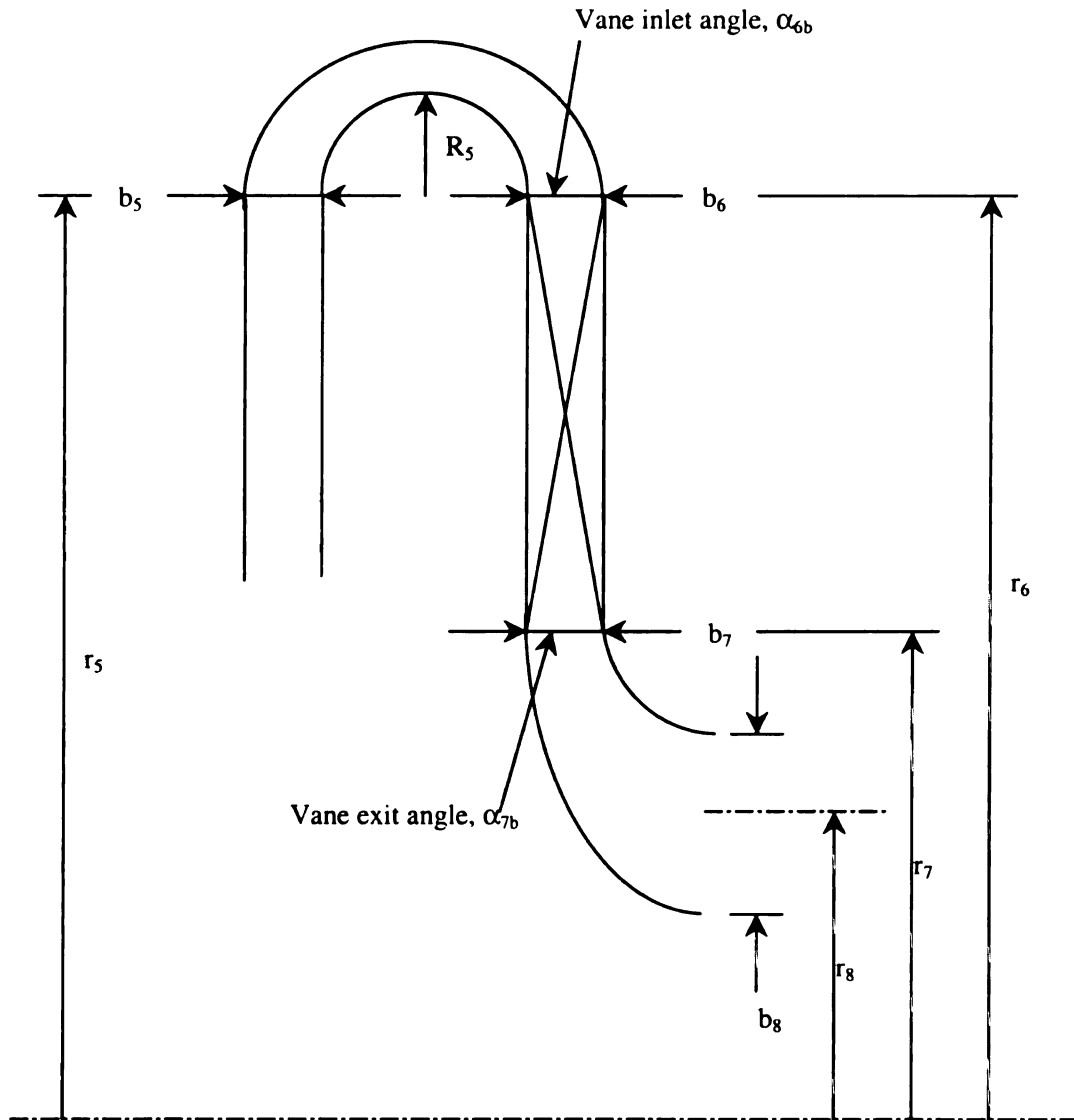


Figure 1.42 Meridional view of a return channel

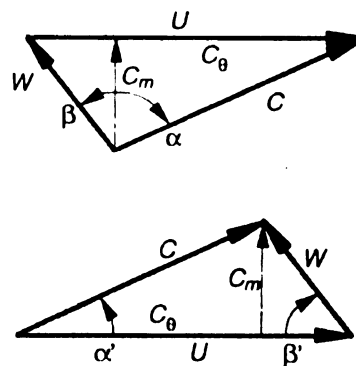


Figure 1.43 Velocity triangle sign convention for both angle systems; meridional format of upper triangle and tangential format of lower triangle (after Japikse, D., Marscher, W. D., and Furst, R. B., 1997)

The relative velocity + wheel speed =
the absolute velocity

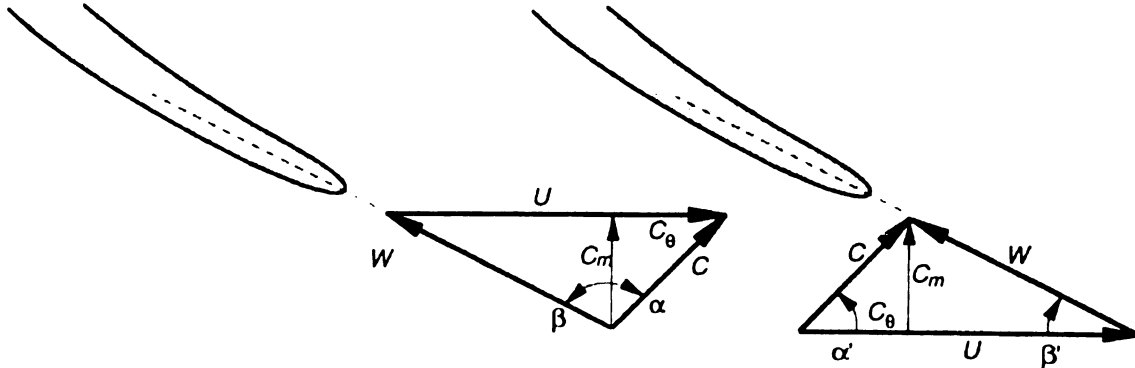


Figure 1.44 Impeller inlet velocity triangles, using both angle systems (after Japikse, D., Marscher, W. D., and Furst, R. B., 1997)

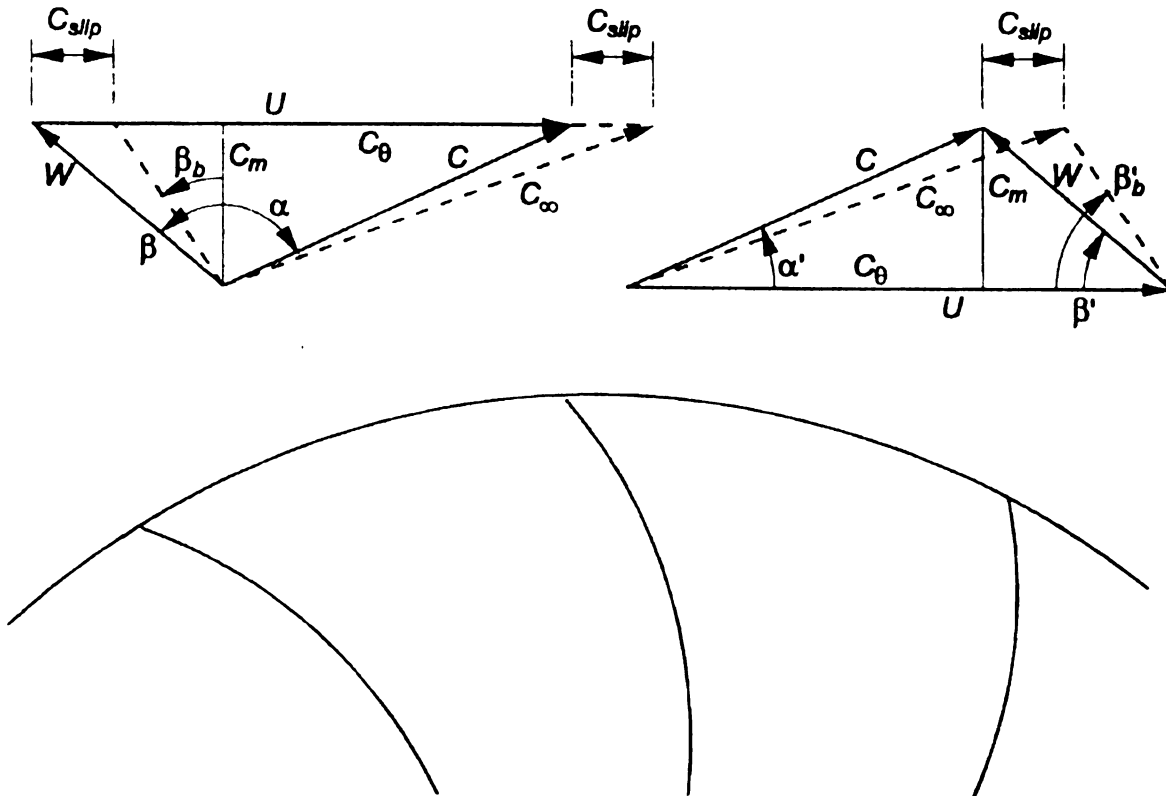


Figure 1.45 Impeller exit velocity triangles; showing meridional format on the left and the tangential format on the right, using both angle systems (after Japikse, D., Marscher, W. D., and Furst, R. B., 1997)

Figure

NOTE
high scale

Figure

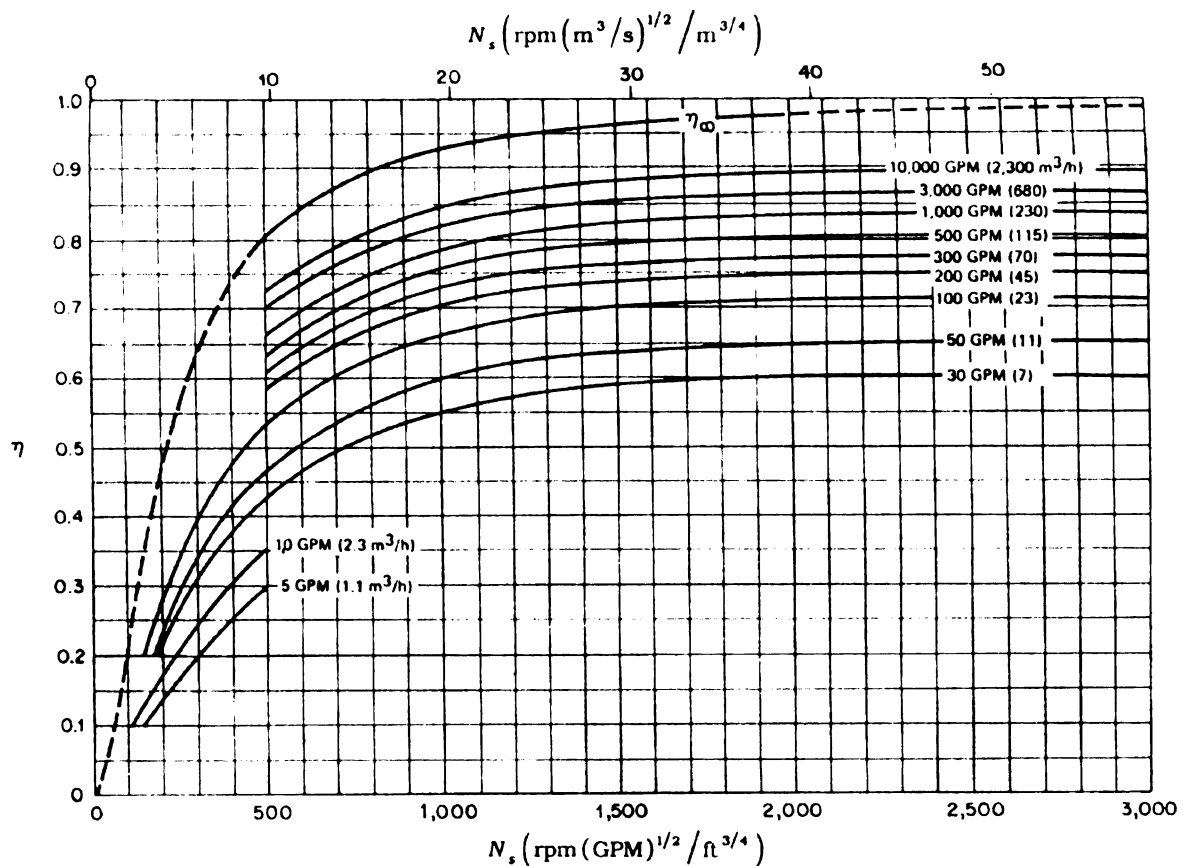
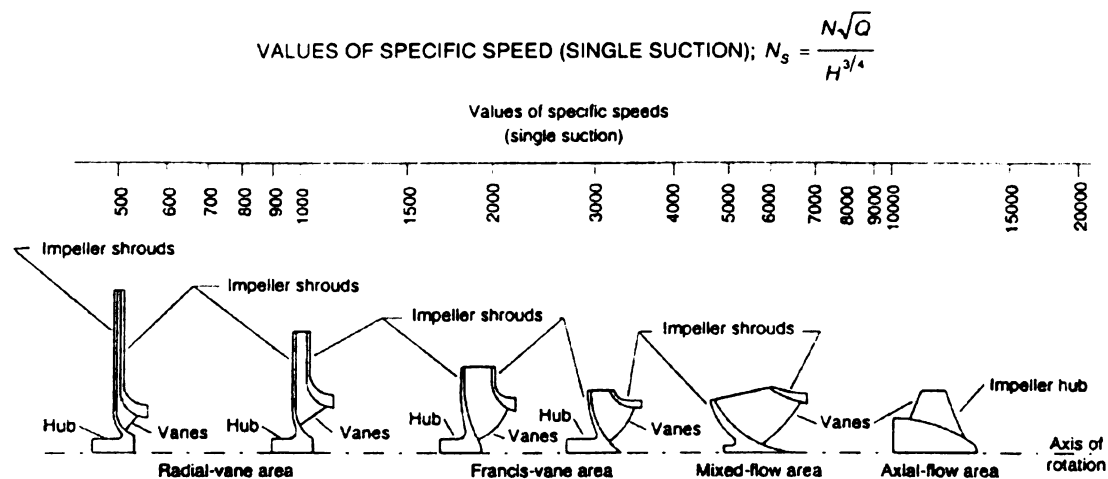


Figure 1.46 Efficiency as a function of specific speed and capacity (after Japikse, D., Marscher, W. D., and Furst, R. B., 1997)



NOTE – Profiles of several pump impeller designs ranging from low specific speed radial flow on the left to a high specific speed axial flow on the right, placed according to where each design fits on the specific speed scale.

Figure 1.47 Comparison of pump profiles (after Japikse, D., Marscher, W. D., and Furst, R. B., 1997)

Chapter 2

LITERATURE SURVEY OF FUEL PUMP

2.1 Fuel pump

The automotive fuel system (Figure 2.1) consists of the gasoline tank, the fuel pump, fuel filter, and connecting lines. The fuel pump is the device that draws the fuel in the fuel tank through the fuel lines to the engine's carburetor or injectors. Basically, there are two types of fuel pumps: mechanical and electrical (Figure 2.4). The electrical fuel pump is commonly used nowadays (Figure 2.5).

Gasoline is stored in the tank under the rear floor in the front-engine automobiles. To function correctly, the fuel pump must move the gasoline in the fuel system from the tank to the carburetor or fuel injection system in sufficient volume and pressure. The sufficient pressure of gasoline in the line between the carburetor and the pump can keep the fuel from boiling and prevent the vapor lock. This gasoline transfer keeps the carburetor bowl full of clean gasoline, regardless of vehicle speed or maneuvering. The fuel pump has to lift the fuel against a head of 0.6 m from the tank or more to the carburetor or fuel injection.

The fuel metering and atomization system is located higher in the vehicle than the fuel tank. A mechanical or electrical pump is employed to draw the fuel from the tank and deliver it to the carburetor or fuel injectors. It must have sufficient capacity to supply the engine with fuel under all operating conditions. The pump should also maintain sufficient pressure in the line to the carburetor to keep the fuel from boiling and causing vapor block due to high engine temperature under the hood (Figure 2.2).

Modern fuel tanks include devices that prevent vapors from leaving the tank. The fuel tank has a separate air chamber dome at the top (Figure 2.3). This will contain vapors and allow for expansion, contraction, and overflow that results from changes in the temperature. Another way to contain vapors is to use a separate internal expansion tank within the main tank. From the fuel tank, the vapors travel through a line, or continuous tube, to a charcoal-filled canister. When the engine starts, fresh air is drawn through the charcoal canister where it mixes with the vapors from the fuel tank. From these, these vapors then pass through the intake manifold and into the cylinders, where they are burned along with the normal air-fuel mixture.

The fuel feed pump for the diesel engine is the equivalent of a fuel lift-pump for the gasoline engine. It draws the fuel from the tank and delivers it to the injection pump. Delivery of fuel both continuously and at a reasonable pressure is necessary because, if the extremely rapidly moving injection pumping plungers have to suck the fuel in, the lighter fraction of the fuel could form vapor bubbles in the pump and cavitation could occur. Of course, this would lead to uncontrolled variations in the rate of delivery of fuel to the cylinders, and therefore rough running and possibly even mechanical damage to the engine. The cavitation could also cause mechanical damage in the injection pump.

2.2 Requirements for fuel pump in fuel injection system

It is important that neither air nor vapor is sucked into the systems for gasoline injection system. When the vehicle climbs up a mountain road, the heat from the engine is conducted and radiated into an already warm fuel system and this, together with the low atmospheric pressure at altitude causes a proportion of the fuel in the system to

vaporize. This vapor can be large enough to drive all the fuel back down the pipe into the tank, leaving the pump full of vapor. This cannot make the engine to restart.

Some forms of liquid vapor separator are incorporated into most modern vehicles to stop liquid fuel or bubbles from reaching the vapor storage canister or the engine crankcase (Figure 2.7). It can be located inside the tank, or on the tank (Figure 2.8) or in fuel vent lines (Figure 2.9). It can also be located near the fuel pump (Figure 2.10).

The first solution of solving the vapor lock is illustrated in Figure 2.11. The fuel is delivered down into the top of a float chamber; the needle valve is mounted on top of the float chamber. A branch back to the tank is installed from the delivery pipe immediately above the inlet port to the needle valve. A restrictor in the branch pipe ensures that only a small proportion of the fuel delivered passes into it to be returned, but any vapor that it contains passes much more freely. In any case, the fuel naturally tends to drop down into the unit and the vapor to rise up the branch pipe. The vapor flow temporarily exceed the capacity of the restrictor to allow it to pass and this vapor accumulates in the float chamber, but continuously returns to the tank so long as the needle valve is open. The delivery passes through a second, but larger, restrictor to ensure that there is always a backpressure in the float chamber to drive the vapor out.

In the second solution of solving vapor lock, an external low-level pump fed by gravity from the tank can obviate the vapor problem. This ensures that even if the whole pipeline and pump system contained only vapor, fuel under the influence of gravity, quickly dropped back into the pump when it was switched on.

In the third solution of solving vapor lock, a pressure relief valve in the venting system opened only when the pressure due to evaporation of the fuel in the tank attained

the va

alway

implos

the tan

pump s

way be

always

restarte

to be re

then the

tend to b

S

the cold

at. How

build up

be starte

first sol

element

extremel

started.

mesh str

disintegr

the value necessary for ensuring that, in the vent of vapor blowback, the pump would always be ready. This valve was of the two-way type for the prevention also of implosion. The pump is installed at a level about mid-way between those of the fuel when the tank is full and empty, instead of lower than the tank.

In the fourth solution of solving vapor lock, the pumps have a low pressure lift-pump submerged in the tank, serving an external main delivery pump set at a height mid-way between the full and empty tank fuel levels. The function of the submerged pump is always to deliver at a positive pressure to the main pump. Before the engine can be restarted, first all the vapor and air has to be cleared from the system, then the pump has to be ready, next the pressure must be built up to its normal operational level, and only then the engine can be started. Another point is that all fuel pumps generate noise and tend to become noisier as their temperature rise.

Small crystals of wax, which is formed in very cold weather, can adversely affect the cold operation of the engine. Under extreme conditions, the engine may not even start at. However, it starts and runs for perhaps five or ten minutes, while the wax crystals build up until they block the pipeline or clog the filter. Then, the engine stalls and cannot be started again until the fuel temperature rises above the wax precipitation point. **The first solution of disintegrating small crystals of wax** is to incorporate a fuel heater element (Figure 2.6), either in stream or upstream of the filter, for the location with extremely low temperatures. This enables the driver to warm the fuel before the engine is started. Because of the risk of blockage by wax crystals, it is necessary to have a wire mesh strainer on the lower end of the fuel pick-up in the tank. **In the second solution of disintegrating small crystals of wax**, the heat exchanger coil assembly is inserted into

the tank. A 5-kW heater warms water pipe from the engine coolant system. It has its own circulation pump, and therefore can be set in operation long before the engine is started. The advantage of such a system is that it is energy efficient. Moreover, the whole tank full of fuel is brought up to the required operating temperature and since the quantity of heat it contains is such that it takes a fairly long time to be dissipated, wax is less likely to form in the tank while the vehicle initially igniting the heater, there is no drain on the battery. This system can be adapted for keeping the engine running at optimum temperature or during operation at light load in extremely cold ambient temperature. The disadvantages are high initial cost, long lengths of water.

The fuel pump should eliminate the noise generation. There are three main excitation mechanisms occurring in fuel pumps.

- According to the pump principle, the fuel flow has various flow-pressure characteristics. These pulsations are radiated to the fuel lines on both suction and pressure side. This propagates with sound velocity. The sound waves in the pipes create alternating forces, which are transmitted as solid-born sound into the car structure.
- Fuel pumps always vibrate due to pressure pulsation. The pressure pulsation occurs due to the compression of the fuel after having interrupted the connection of the pump chamber to the inlet port before connecting it to the outlet. These vibrations are transferred by the fuel lines as well as by the pump-mounting bracket.
- Vapor bubbles are formed on the suction side of the pump, especially with increasing fuel temperature. When pressure rises in the pump, these cavitation

bubbles collapse. This produces shock waves with high frequency components and creating corresponding body vibrations.

The delivery system in a fuel injected Internal-Combustion engine must be able to precisely meter fuel to the engine for drivability, emissions, and economy. The function of its delivery system is to transport fuel to the fuel injection system at the desired pressure and quantity as demanded by engine consumption under anticipated operating conditions. Desirable standards of a fuel delivery system includes

- Providing the function at the lower cost, with reliable fuel supply and pressure control from the fuel tank to the fuel injector under all temperature conditions, using all anticipated formulations of fuel in the field, and over the life of the vehicle.
- Efficient power conversion, it can minimize electrical power consumption.
- The system can minimize delays to engine fuel demand transients to maintain constant pressure for accurate metering.
- Damping of fuel rail pressure pulsation caused by the injector and the inertia of the fuel.
- The system can provide a means for consistent rail pressure regulation accommodating dynamic line friction and filtration pressure losses in the supply system. Moreover, the system can regulate rail pressure either referenced to intake manifold pressure, or to atmospheric.
- The system can minimize the formation of evaporative hydrocarbon vapor in the fuel delivery system.

The modern fuel pump is a sealed unit that cannot be repaired. If the pump leaks from either the vent hole or from a seam, it must be replaced. If the engine performance indicates inadequate fuel, the pump should be tested at normal operating temperature and at idle speed for pressure and volume while mounted on the engine. In fact, incorrect fuel pump pressure and low volume (capacity of flow rate) are the most likely fuel pump troubles that will affect engine performance as follows:

- Low pressure will cause a lean mixture and fuel starvation at high speeds.
- Excessive pressure will cause high fuel consumption and carburetor flooding.
- Low volume will cause fuel starvation at high speeds.

2.3 Returnless fuel delivery of fuel pump in the fuel system

The returnless fuel delivery systems (Figure 2.14) are being developed to assist the vehicle to meet lower emissions requirements for evaporative hydrocarbons from the vehicle. Because the fuel return line contributes to this vapor formation, its elimination is desirable. Existing returnless fuel delivery includes mechanical and electronic means for pressure regulation. The returnless fuel systems have the following differences compared to return type systems as follows:

- No return line is associated with the rail. Rail operates deadheaded.
- No bypass regulator exists on the rail. A bypass regulator must function with a return line.
- Only engine consumption fuel flows in the supply line to the rail. Average flow rate is reduced considerably. As a corollary, all fuel flow through the supply line and rail must pass through the injectors, including vapor.

- Rails and injectors operate at higher temperature. As average flow rate in the supply line is reduced, supply fuel spends more time in transit to absorb heat of the engine compartment.
- Higher rail pressure may be required to meet hot fuel handling criteria. Vapor formation in the rail must be prevented through adequate pressure.

2.3.1 Electronic returnless of fuel pump in the fuel system

A typical electronic returnless system consists of three components (Figure 2.15). Fuel pressure at the rail is sensed by a pressure transducer (first component), which delivers a low level signal to an electronic controller (second component). The controller contains logic to calculate a signal for the pump power driver (third component). The power driver incorporates a high current transistor, which controls the pump speed using pulsation-width modulation of pump current. This transducer, which can be differentially referenced to manifold pressure, provides closed-loop feedback correcting and maintaining the pump's output to a desired rail set pressure. The electronics can be stand-alone or integrated into existing on-board vehicle controllers such as the engine computer.

This system is capable of continuously varying rail operating pressure as functions of engine vacuum, engine fuel demand, and rail temperature (as sensed by an external temperature transducer, if necessary). To accommodate fuel trapped in the supply line between the dead-headed rail and the check-valve located at the fuel sender, a pressure vent valve is employed to relieve over-pressure during transient 'tip-outs' and hot soaks (accommodating the thermal expansion of fuel). In addition, a supply line bleed

is normally facilitated by a jet-pump in-tank reservoir. This supply bleed is necessary for proper pump operation.

The electronic returnless fuel system has some characteristics. The system reduces the vapor generation and lowers the average pump current. The cost is higher. The system has the control flexibility and increases the injector dynamic range. There is no rail pulsation damping. The system can have slower transient response.

2.3.2 Mechanical returnless of fuel pump in the fuel system

The mechanical returnless of fuel pump in the fuel system (Figure 2.16) employs a bypass regulator to control rail pressure located in close proximity to the fuel tank. Fuel pressure regulators, employing a spring, diaphragm, and valve, are reliable and cost-effective. These regulators have been downsized for weight and cost.

The fuel is sent by the in-tank fuel sender to a chassis mounted in-line filter, with excess fuel returning to the tank through a short return line. Supply pressure is therefore maintained to the deadhead rail through the supply line. Moreover, the in-line filter is mounted directly on the tank completely eliminating the shortened return line. Supply pressure is regulated on the downstream side of the in-line filter to accommodate changing restriction throughout the filter's service life.

The mechanical returnless fuel system has some characteristics. The system has the higher pump current and lower cost. There is no pulsation damping and the fuel sender is flexible. It is impractical to have the regulator of mechanical returnless fuel system in the tank referencing to the manifold pressure on the engine. Hence, the mechanical returnless fuel system is limited to constant rail pressure system calibration. The system can have slower transient response.

2.4 Mechanical fuel pump

The most common type of fuel pump is the mechanical diaphragm-type pump (Figure 2.17). The rocker arm of mechanical fuel pump rides against an eccentric lobe on the camshaft (Figure 2.18). The amount of fuel pumped increases as the camshaft rotates faster. The force of the diaphragm spring establishes the maximum working pressure of the fuel pump. It limits the amount of fuel according to engine requirements.

Mechanical fuel pump have a synthetic rubber diaphragm inside the unit that is actuated by an eccentric located on the engine's camshaft (Figure 2.19). As the camshaft rotates during engine operation, a shaft or a rocker arm in the pump is moved up and down or back and forth, depending on the fuel pump's position on the engine. This causes the diaphragm to move back and forth, drawing fuel from the fuel tank, through the fuel lines, and to the carburetor or injectors. On some V-8 engines, a pushrod, which is located between the camshaft eccentric and fuel pump, actuates the fuel pump rocker arm.

The mechanical fuel pump is located on the engine block near the front of the engine (Figure 2.13). This pump is influenced by the engine heat. Further, during fuel intake, a low-pressure area is developed in the fuel line. High temperatures and low pressure can lead to a vapor lock condition. To overcome this condition, most modern mechanical fuel pump systems contain a fuel vapor separator and vapor return line to the fuel tank.

2.4.1 AC-Delco and SU mechanical diaphragm positive-displacement fuel-lift pump

(For Gasoline engine)

The mechanical diaphragm fuel pump is operated by an eccentric lobe on the camshaft (Figure 2.19). A spring-loaded arm is held against the eccentric lobe, contacting it at all times. In some systems, a short push rod is fitted between the eccentric lobe and the spring-loaded arm. The cam-actuated lever arm pulls the diaphragm from the fuel chamber side, increasing its volume and thereby drawing fuel from the gasoline tank. A spring on the lever side of the diaphragm pushes against the diaphragm as the cam eccentric lobe movement relaxes its pull on the arm lever and diaphragm. The force of this spring pressure on the diaphragm puts pressure on the fuel. This force transfers the fuel toward the carburetor or fuel injector. The fuel pump is fitted with two check valves. The inlet-check valve on the tank side of the pump allows the fuel to go into the pump. The outlet-check valve on the engine side of the pump allows the fuel to leave the pump. As the pump fuel chamber is made to increase in volume by the linkage, the gasoline is drawn into the pump from the tank through the inlet-check valve. As the pump fuel chamber is made to decrease in volume by the spring, the gasoline is pushed toward the engine through the outlet-check valve.

The two more illustrations of mechanical positive displacement fuel lift pumps with diaphragm are a modern AC-Delco mechanical pump (Figure 2.20) and two SU mechanical units (Figure 2.21). All three pumps are diaphragm type, positive displacement pumps.

Fuel lift pumps of the reciprocating type may reciprocate about 100 million times throughout the lives of the vehicles, on which they are lifted. Modern diaphragms reinforced with very strong and fatigue resistant fabrics are extremely reliable.

Diaphragms are preferred to pitons because they are simpler, lighter, less costly, more easily sealed and do not call for close clearances or machining to tight tolerances.

These pumps are mostly actuated by an eccentric on the engine camshaft with a rocker follower, the end of the other arm of which has a slotted connection to a pull-rod attached to the center of a diaphragm. The slot serves as a lost motion device. This lost motion extends between the lowest and uppermost ends of stroke, the rocker arm being returned upwards by a small diameter spring installed horizontally to keep the follower in contact with the eccentric. The rocker pulls the diaphragm downwards, drawing fuel into the chamber above it. Then the diaphragm is returned upwards by a large diameter spring installed coaxially beneath it, but its stroke is determined by the quantity of the fuel that has been delivered from the chamber above it to the engine. If the engine were being motored on a dynamometer, the rocker could reciprocate with the limits of the slot indefinitely without actually doing any pumping.

Arrangements of valves differ from make-to-make, but they are almost invariably in the roof of the diaphragm chamber. In the SU AUF700 unit (Figure 2.21), a single hollow valve is employed. Around its lower end is a mushroom head and, inside its upper end, a reed type delivery valve. Both valves are flexible and centered directly above the diaphragm. In each of diaphragms of the other two pumps, the inlet valve is on the right and the delivery valve to the left of center. One has flexible mushroom and the other disc type valves. Most pumps of the diaphragm type have a filter over the inlet valve. In the AC-Delco unit, it is a slightly domed gauze on top of what amounts to a stack pipe that forms a water trap inside the large domed glass top cover. This cover is retained by a spring-clip, part of which can be seen on top of the dome. In the SU AUF800 unit (Figure

2.21), a thimble type filter can be inserted in the small dome into which the inlet pipe is fitted, and on the SU AUF700 unit, it is a gauze disc clamped between the washer that seals the rim of the top cover and the upper half of the diaphragm housing.

Another version of the diaphragm pump is the Weber unit (Figure 2.22). This pump functions in much the same way, but it has a double diaphragm. The lower diaphragm ensures that the fuel will not leak into the engine if the fuel leaks past the upper diaphragm, which does the pumping. The ingoing fuel passes up into the domed chamber and then down through the inlet valve, passing twice through the filter as it does so. Above the delivery valve is a thimble, a grooved metal ring, containing air for attenuating the pulsations.

2.4.2 Unitac mechanical diaphragm pump (For Diesel engine)

The Unitac pump has a cam-and-lever actuation mechanism (Figure 2.23a). When the outer end of the cam follower lever rides up the cam profile, its inner end, bearing down on a saddle at the lower end of the rod, pulls the diaphragm down, compressing its return spring. The pressure differential across the two valves above the diaphragm closes the delivery valve on the left, and opens the inlet valve on the right. Thus, this allows the fuel to enter the chamber above the diaphragm. On the return stroke, because the inner end is divided to extend around the rod, it rises freely and independently of the rod. This leaves the diaphragm to be pushed upwards by its return spring. Again, the pressure differential actuates the valves, but this time, the inlet valve is closed and the delivery valve opened. The upward motion of the diaphragm is limited to supply the demand for fuel from the engine, which varies considerably from idling to maximum power output.

The function of the large chamber above the inlet valve is to ensure that the pump remains ready even if its feed pipe drains back to the tank.

2.4.3 AC mechanical diaphragm pump (For Diesel engine)

The AC pump is similar to Unitac pump (Figure 2.23b). Except that it is designed for direct cam actuation, without a lever type follower, so the rod connected to the diaphragm is pushed up instead of being pulled down by the cam mechanism. The return spring for the diaphragm is weaker than the spring for the push rod. Consequently, as the cam nose rotates past its top dead center, the push rod is pulled down by its return spring until the head formed at its upper end stands against the seating in the diaphragm carrier. This allows the head to pull the diaphragm down with it. The inlet valve is opened by the pressure differential in the chamber above the diaphragm, which is therefore filled with the fuel. On the return stroke, the inlet valve closes and the delivery valve opens, allowing fuel to be delivered by the action of the diaphragm return spring, but only at the rate required to satisfy the demands of the engine. Therefore, the cam rotates clear of the end of the push rod until it again lifts the diaphragm to fill the chamber above for the continuing round.

2.4.4 AC Alpha mechanical pump (For Diesel engine)

Fuel enters at the top and leaves at the side (Figure 2.25). The piston on the left is push rod actuated, while the plunger on the right, which has a flexible top cover to prevent the entry of dirt and water, is used solely for manual preparedness.

When the cam lift the piston, the inlet valve in the upper end of its cylinders closes and the fuel in the chamber above the piston passes through the transfer valve at its lower end into the chamber below. As the cam rotates past its top dead center, the piston

is moved down again by the two return spring above it, forcing fuel out through the delivery valve on the left, but at only the rate needed to satisfy the demand of the engine. Consequently, the push rod falls clear of the piston until the cam lifts it again. The spring that returns the piston is considerably stronger than the spring of the plunger on the right. Because the effective area of the latter is much smaller, it is not sucked downwards as the piston is lifted by its push rod.

2.4.5 Bosch plunger-type pump (For Diesel engine)

Bosch makes two plunger pumps, single plunger pumps and double plunger pumps. The single plunger pump suffers the disadvantage that its delivery pressure can fall to zero in extreme conditions between pumping strokes. The double plunger pump does not suffer this disadvantage. On the other hand, the plunger pump must have a pressure relief valve, and either a bypass back to the inlet or a return line to the tank, because the double plunger pump delivers continuously. Both bypass and return line are extremely compact so much that they can even be flange-mounted on the Bosch injection pumps, in which the cams are situated for actuating them.

From Figure 2.24, it can be seen that the single plunger pumps comprise a cam-actuated piston in a cylinder flanked by non-return valves. As viewed in the illustration, the piston is lifted by its return spring, drawing fuel through the port on the right and a filter and non-return valve, into the pressure chamber. When the cam, acting on a roller-follower and push rod, forces it down again, the non-return valve on the inlet side closes and the non-return valve over the transfer port on the other side opens. This allows the fuel to pass up into the chamber above the piston.

As the cam follower and the push rod rise, the piston is pushed upwards by its return spring. This time, it displaces the fuel above it through the outlet port to the injection pump at the rate demanded by the engine. This happens because the pressure generated by return spring closes the non-return valve over the transfer port. Since the piston lift varies with demand for fuel, its stroke can vary from the almost zero strokes at idling to the required stroke for sustaining maximum power output.

The double plunger pump has no transfer valve. Instead, it has two inlet valves and two delivery valves. With each stroke, fuel is drawn directly through the filter into the chamber on one side of the piston. On the other side, the fuel is delivered to the injection pump. This is why fuel in excess of the demand from the engine must be diverted through a pressure relief valve as indicated previously.

2.5 Electrical fuel pump

Electrical fuel pumps (Figure 2.27) have four basic types.

1. **Diaphragm pump:** This type works the same way as a mechanical pump, with the exception that an electromagnet moves the diaphragm.
2. **Plunger pump:** An electromagnetic switch controls a plunger or piston that moves up and down in this type.
3. **Impeller pump:** This pump has no input and outlet valves. Instead, it has a revolving armature that works much the same way as a fan blow air. The impeller creates suction that draws fuel into the pump and pushes it out to the carburetor (Figure 2.29).
4. **Bellows pump:** This pump is similar to the diaphragm type. However, a metal bellows is used instead of a diaphragm (Figure 2.32).

The electric fuel pump can be located inside or outside the fuel tank (Figure 2.30 and Figure 2.31). The in-tank electric pump is usually a rotary type. The diaphragm, the plunger, and bellows type are usually the styles requested. That is the pump begins operation when the ignition is turned on. It shuts off automatically when the carburetor bowl is full and the fuel line is pressurized. When the carburetor demands more fuel, the electrical pump pumps more. When demand is lower, it pumps less. Therefore, proper fuel flow and pressure are constantly maintained. In most installations, the rotary electric fuel pump is considered to be a continuous operated type.

The electrical fuel pump is usually installed in an accessible position in the boot, just above the tank, so that it pumped against both a pressure and a suction head, each of modest proportions, the suction head being nowhere near as large as that beneath a pump mounted on the engine. In consequence, the likelihood of the occurrence of vapor lock was greatly reduced, and these pumps tended to remain primed for longer periods than the engine-actuated type.

When gasoline injection was commonly developed and the pulse-free pumps became essential, the electrical pump really became installed much more in the greatest majority of cars and commercial vehicle.

2.5.1 Electrical positive displacement fuel-lift pump (For Gasoline engine)

The Electrical positive displacement fuel lift pumps comprise a valve unit, a solenoid-actuated diaphragm, and a flick-over make-and-break switch (Figure 2.34). Fuel entering the chamber passes through the filter, and on up past a disc-valve into a second chamber. Each time, the diaphragm is pulled to the left by the solenoid and the fuel is drawn into the diaphragm chamber. When the solenoid is moved to the right again, by its

return spring, the previously mentioned disc-valve closes and the above disc-valve opens to allow the fuel to pass out to the carburetor as the diaphragm is forced back again by its return spring.

An armature disc with a large peripheral groove is attached to the center of the diaphragm. A number of discs and the edges, which are carried in this groove, are rounded. These discs have three functions. The first function is to center the armature in the magnetic pot, in which the solenoid winding is housed. Secondly, they back up the diaphragm, helping to prevent it from ballooning under the pressure generated in the fuel by its return spring. Thirdly, by virtue of the profiles of their rounded edges and of the counter-bore, in which they seat in the magnet pot, they regulate the density of the magnetic flux passing through them, to maintain an approximately constant axial pull on the armature throughout its stroke. A fiber disc in a counter-bore in the center of the armature prevents metal-to-metal contact between it and the tubular core of the solenoid. This tubular core for the winding houses a push rod interconnecting the center of the armature and a flick-over switch at the opposite end of the unit. The left-hand end of the rod is connected to one of two rocker arms, pivoted scissors fashion at their lower ends. Carried on the upper end of one of these arms is the earth contact of the switch for energizing the solenoid, the positive contact being mounted on the switch base-plate, which is of insulating material. Interconnecting the upper ends of both arms is a floating spring of the coiled type. This spring flicks alternately back and forth. This movement serves the dual function of holding the contacts closed while the rod is at one end of its stroke and open while it is at the other end.

In the Weber plunger type electric fuel-lift pump, the cast iron armature serves as the pump plunger, which reciprocates in a non-magnetic tubular core around which the solenoid is wound. The inlet valve seats on a port in the base of a thimble shape chamber, surrounded by a filter sleeve beneath the plunger, while the delivery valve in the lower end of the hollow plunger is above it.

When the current to the solenoid is cut off, the plunger is forced upwards by the return spring seating in the thimble below. This opens the inlet valve and fills the chamber beneath the plunger with fuel. At the same time, it forces the fuel above it into the delivery chamber and then out to the carburetor. Above the separation diaphragm, the space in the domed top of the delivery chamber is filled with air to attenuate the pulsations. As the iron plunger approaches the top of its stroke, the magnet is attracted to it. Thus, this actuates the rocker that closes the contacts for the solenoid. This energizes the solenoid to pull the plunger down again, appropriately closing the inlet and opening the delivery valve.

2.5.2 Roller-cell electrical positive displacement pump (For Gasoline engine)

The pump and its electric motor are located in a common housing and are subject to a constant flow of fuel. This means that lubrication problems and seals, which are susceptible to breakdown, can be avoided. At the same time, the electric motor is effectively cooled. The electric fuel pump is maintenance-free and can be mounted underneath the vehicle in the direct vicinity of the fuel tank or inside the tank. A non-return valve is installed in the outlet fitting. Pressure pulsations on the outlet and inlet side can cause noise. For reduction of suction side pressure pulsations, a plastic pressure damper is incorporated in the pump. For achieving extended product life, a carbon

bearing bushing is used for the pump wheel and a plastic driver connects the armature with the pump wheel. Delivery of hot fuel could become a problem if clearances between pump rotor and the intermediate plate are too great. The pump design with a fixed axle and an armature with hollow shaft allow the pump parts to be assembled with minimal radial clearance. This results in reliable fuel delivery under hot conditions and with all types of present fuels.

The roller-cell pump is a high-pressure fuel pump driven by a permanent d.c. electric motor. Its pumping element is in the armature housing and the fuel flows right through, from one end to the other, to cool and lubricate all the rotating parts (Figure 2.37). A permanent magnet of the d.c. electric motor drives a radially slotted disc rotating in a housing. The inner cylindrical wall is eccentric relative to the disc and shaft. There are five radial slots, each containing a roller. As the disc rotates, the slots revolve past an outlet port and the eccentricity of the housing simultaneously forcing the roller to move radially inwards, against centrifugal force. During further rotation, the rollers move out again, while their slots revolve past an inlet port. Therefore, the fuel is alternately forced out to one side and drawn in from the opposite side of the pump. A relief valve between the armature housing and the fuel inlet limits the pressure to 5 bars. At the opposite end, the main fuel delivery port houses a check valve to ensure that the pump remains prepared after it is switched off.

2.5.3 Rotary electrical positive displacement pump (For Gasoline engine)

There are three different types of rotary electric fuel-lift pumps:

- Weber Roller-cell positive displacement pump.
- AC in-tank fuel pump.

- Bosch low-pressure electric fuel pump.

The Weber Roller-cell positive displacement pump is used in the gasoline injection systems (Figure 2.36). This pump has all the advantages as being attributable to electric drive. This pump can be installed actually inside the fuel tank, where it is well protected from damage, leakage and fire risk, and is constantly cooled by the fuel flowing through and around it. This pump can avoid the fire risk because its electrical components cannot come into contact with a combustible mixture of air and fuel. When the tank becomes empty, the pump cannot deliver air against the head of fuel remaining in the system upstream of it.

The Weber Roller-cell positive displacement pump comprises two sub-assemblies within a common cylindrical housing. One is a power unit and the other mounted axially in line with it is the pump. The power unit is a permanent magnet of the d.c. electric motor. It drives a radially slotted disc in the pump unit. This disc rotates in a short cylindrical housing, the bore of which is eccentric relative to the disc and shaft. Contained in each of five slots, machined radially inwards from the periphery of the disc, is a metal roller.

As the disc of Weber Roller-cell pump rotates, the slots revolve past an outlet port, the eccentricity of the housing simultaneously moving each roller in turn, as it approaches the port, radially inwards against centrifugal force. Thus, the fuel beneath it is displaced out through the port, past the motor and away through the main delivery port at the far end of the pump. Further rotation causes the rollers to move out again, while the slots, or cells, in which they are contained, revolve past an inlet port, drawing fuel in from the opposite end of the pump. Since, fuel is always delivered in excess of the

requirements of the engine, a relief valve in the wall between the armature housing and the fuel inlet chamber limits the pressure to 5 bars. At the opposite end of the unit, the main fuel delivery port accommodates a check-valve to ensure that the pump remains ready after it is switched off. The motor is wired through the ignition switch, and there is a safety override switch to cut the pump out of operation if the engine should be stalled, for example in an accident.

The AC in-tank fuel pump is illustrated in Figure 2.38. Fuel from the inlet is passed by a radial vane impeller axially through the motor housing to the outlet. In Figure 2.41, there are two stages driven. The first stage is for freeing the fuel from any vapor that might be present and the second stage is for handling the liquid gasoline. The first stage has a radial impeller, the vapor being drawn off from its center. Fuel leaving at the periphery of this first stage is then passed on through the motor housing and out at the other end by an eccentric rotor type pump, in the second stage. The need for separation arises in some American limousines, in which the tanks are so large that even when nearly empty, there is still a lot of fuel swilling around on the bottom, from which the pump may continue for drawing a mixture of air and fuel.

The Bosch two-stage rotary electric fuel pump has a two-stage rotor (Figure 2.39). The first stage, which comprises radial vanes in the disc, is a side-channel pump, in which the fuel enters on the left-hand side. In this stage, its pressure is increased sufficiently to avoid vapor formation as it enters the second stage, where peripheral vanes boost its pressure to 1 bar. In this stage, the fuel is radially transferred to the second stage by radial vanes, which ensure that the fuel is under pressure. The fuel is vapor-free when it passes to the second stage. The radial vanes on the periphery comprise the second stage

of the pump. In this stage, the energy content of the flow is further boosted before the fuel is delivered into the armature housing at a higher pressure. Then, the fuel passes into the housing of the permanent magnet rotor. Here, the fuel cools the armature before the fuel leaves through a check valve in the outlet port. The check valve prevents fuel from flowing back through the pump into the tank when the engine is stopped.

The output from a rotary electric fuel pump is relatively independent from pulsations. This happens because there are low amplitude and high frequency periodic disturbances due to the passage of vanes, the passage of the rotor past the ports. In general, the overall layouts of the electrically driven rotor type pumps are nearly all similar to that of the positive displacement pump.

The advantages are similar to the electrically driven pump and the electrically actuated diaphragm pump. The disadvantage is that the pump might fail to deliver when the vapor is formed in its inlet because this pump is fairly sensitive to vapor.

2.5.4 AC universal electronic solenoid fuel pump (For Diesel engine)

This pump has few moving parts and none that wear out (Figure 2.40). It has been designed for operation at high temperatures, is quiet and reliable by its solid-state circuits. Since the fuel is confined to a central tubular core, the coil assembly and electronics components around it are kept dry.

When the coil is energized, it pulls the piston down against the resistance offered by the return spring. At the same time, the outlet valve in the delivery closes, and the inlet valve in the piston crown opens and, as the piston moves downward, fuel enters the chamber above it.

When the piston reaches the bottom of its stroke, the electronic system switches off the current to the coil and return stroke of the piston is powered by its spring, forcing the fuel above it up through the outlet valve. This sequence occurs many times per second. The quantity of fuel actually delivered depends on the engine, so the piston stroke is rarely its maximum. To cater for reverse polarity voltage being inadvertently applied, the circuit is protected against electro-magnetic interference and alternator dump loads.

2.5.5 SU electrical fuel-lift pump (For Gasoline engine)

The SU electrical pump is the electrically actuated diaphragm pump. The diaphragm comprises several layers of fabrics, and its center is clamped to the armature (Figure 2.34). The discs having rounded-faced peripheries instead of square-faced peripheries are interposed between the groove periphery of the armature and the counter bore in the end of the magnet pot M. These discs not only center the armature as it reciprocates axially, but also back up the diaphragm, helping to prevent it from ballooning under the load due to the pressure it generates in the gasoline. The shoulders in the counter bore in the end of magnet pot are so balanced that as the lines of force can find the shortest path. So, the axial pull on the armature remains approximately constant throughout the travel.

The magnetic circuit is completed through the core C, over which is threaded by the winding spool W (Figure 2.33). A fiber disc is inserted in the center of the armature to prevent metal-to-metal contact of armature and core. The residual magnetism might prevent the return of the armature under the action of the delivery spring. The suction stroke occurs when the armature and diaphragm are moved to the left by the magnetic

pull, and the fuel then enters the pump chamber through the filter F and the lower of the two plate valves V. On the breaking of the circuit by the flick-over mechanism, the diaphragm is returned by the compression spring, and the fuel is delivered to the float chamber of the carburetor through the upper plate valve. The float chamber of the carburetor should be so full as to close the needle valve. The float mechanism of the carburetor must be matched with the spring of the pump so that flooding cannot occur. When the electric circuit is switched off, the diaphragm will remain at rest until further delivery is required.

The advantages and disadvantage of electrically actuated diaphragm pump are similar to the electrically driven pump.

2.6 Advantages and disadvantages of mechanical & electrical fuel pump

2.6.1 Mechanical fuel pump

a. Advantage

- The main benefits of the mechanical diaphragm pump are the simplicity, the low cost, and extremely reliable. This pump can operate in very wet and dirty ambient conditions.
- It is more reliable than an electrical pump because the mechanical pump allows the presence of water or dirt.

b. Disadvantage

- In order to provide the fuel economically with a mechanical drive, the pump has to be mounted on the engine because of the pulsating nature of its output.
- The pump not only has to pump against a large suction head, but also may be affected by conducted and radiated heat, especially from the exhaust manifold. Both the suction head and the heat tend to cause vapor lock on the suction side of the pump.

- Mechanical pumps in the engine compartment are subject to heat. A low-pressure area is also created in the fuel line during the fuel intake. Both of these conditions can lead to vapor lock.
- A cam-actuated pump on a vehicle that had been standing for a long time might not begin to deliver until after the engine had been cranked for several revolutions. As a result, starting the engine in the cold weather could be a difficult operation and impose a heavy load on the battery.
- A pulsating output requires putting the pump on the engine to obtain a mechanical drive. It is easy to have a vapor lock. This occurs not only to the large suction head between the pump and the tank, but also to their proximity of sources of radiated and conducted heat.

2.6.2 Electrical fuel pump

a. Advantage

- Electrical fuel pumps offer important advantages over mechanical fuel pumps. Because the electrical fuel pumps maintain constant fuel pressure, they aid starting and reduce vapor lock problems. Since they are not mechanically attached to the engine, fixing problems are eliminated. This makes them especially useful when an exact replacement mechanical fuel pump is unavailable.
- Unlike mechanical fuel pumps, the operation of electrical fuel pump is not affected by worn cams. It is also easy to install a hidden on-off switch for the electric pumps as an antitheft precaution. An inertia switch is sometimes installed in the electric fuel pump circuit to turn it off in case of accident (Figure 2.28).

- The electrical fuel pump can be mounted anywhere between the fuel tank and the carburetor because it does not depend on an engine-driven cam for its drive. When installed close to the fuel tank or in the fuel tank. It eliminates vapor block because with fuel under pressure, it is difficult for vapor to form even if the fuel lines get hot.
- The pump motor could be wired through the ignition switch and therefore could begin to function immediately when the ignition was switched on.
- The pump can be located anywhere, including where the suction head is small and the temperature is low. Hence, the vapor lock inside the pump can be avoided.
- The pump is wired into the ignition circuit, so it supplies the fuel immediately after the engine is switched on. Thus, the pump facilitates starting, and it ceases to do so when the engine is switched off.

A summary of the advantages of the electromagnetic drive with outside guidance-members for the armature is

- **No** complicated mechanical drive of the pump is needed. Only a control of the energizing of the magnets is required.
- **The** moving-speed of the plunger-element is independent of the engine-speed. As a result, an excellent atomization of the fuel is obtained even during starting.
- **By** increasing plunger-speed during the pressure-stroke, a good atomization of the fuel by a relatively low injection-pressure is achieved.
- **It is** possible for applying a simple interruption of injection by deceleration or by a closed throttle valve.
- **A** multiple injection per engine-cycle is practicable in a simple way when a separate starting-injector becomes superfluous. The pump itself functions as a starting injector.

- Temporary eliminating of combustion in some engine-cylinders can simply be executed.

The energizing circuits contain moments, during which no force is executed on the contacting elements. A very small force for variation of the governing-mechanism is necessary.

- The reliability and the cost price of these construction-elements are well predictable and favorable.

b. Disadvantage

- Some major areas in electrical fuel pump can be dead or inoperative pump, too much fuel pressure, and too little fuel pressure.

- This pump could become a fire hazard following an accident by continuing to supply the fuel even though the engine had stalled.

- Rust and corrosion can prevent a good ground for electrical fuel pump.

- Failure of the pump relay or computer driver signal can cause slow starting because the fuel pump will not come on until the engine cranks long enough to build up sufficient oil pressure to trip the pressure switch.

- If an oil pressure switch or relay sticks in the closed position, the pump can run continuously whether the key is on or off depending on how the circuit is wired.

2.7 Conclusions of mechanical fuel pump and electrical fuel pump

Diaphragms represent a potential weakness, owing to their repeated flexure, though this type of mechanical pump has been in use for over a century and has been developed to an extremely high degree of reliability. Electrically actuated pumps are relatively advantageous to engine-driven mechanical pumps. The outputs of electrically actuated pumps are high under starting conditions when a steady supply of fuel to the

injection pump is especially desirable, and during idling when a pulsating supply of fuel cause unstable running.

Both mechanical fuel pump and electric fuel pump have advantages and disadvantages in the operation process. In general, the electric fuel pump can provide more precise amount of fuel than mechanical fuel pump. Moreover, the ability of avoiding the vapor lock in the fuel from electric fuel pump is better than the mechanical pump. However, the mechanical fuel pump has more reliable operation than the electric fuel pump because of allowing the presence of the water or dirt in the fuel. In mechanical fuel pump, the manufacturing cost is lower and the design is simpler. Furthermore, the mechanical fuel pump does not have a fire hazard when the engine stops.

Having based on these analyses of the current fuel pumps, the automobile industry would like to investigate a new generation of fuel pump, which can combine most of advantages from electric fuel pump and mechanical fuel pump. One suggestion of a new generation of fuel pump is the centrifugal pump, which was studied in this Thesis.

FIGURES

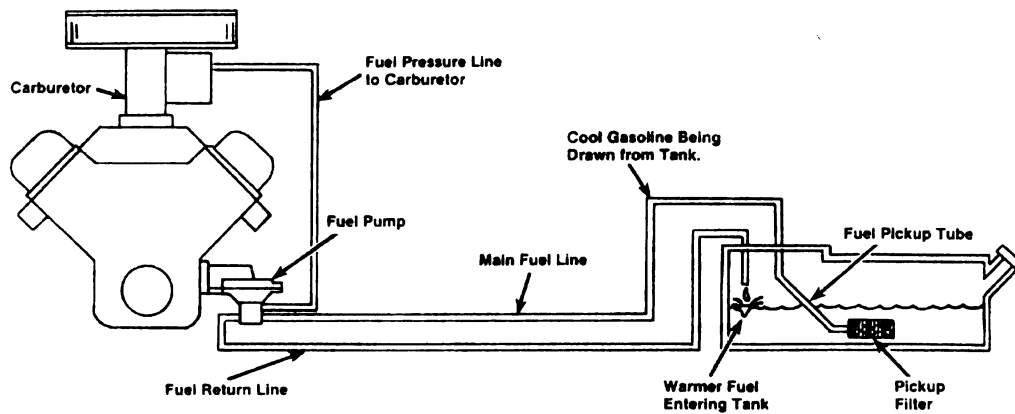


Figure 2.1 Gasoline is drawn from the tank into the fuel pump. From the pump, gasoline flows to the carburetor as well as back to the fuel tank. This tends to cool the gasoline in the pump and reduces the change of vapor lock (after Robert Scharff, 1989)

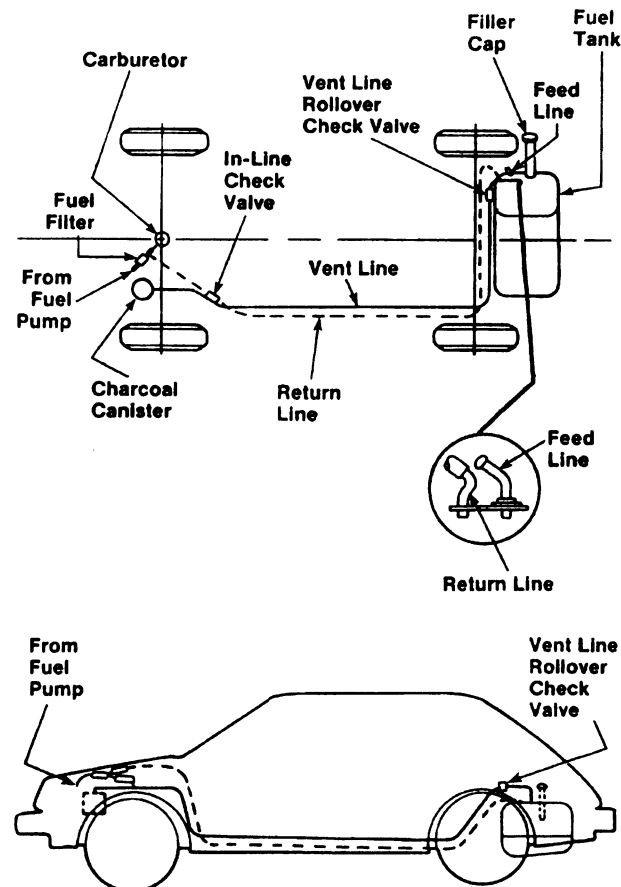


Figure 2.2 Parallel routing of fuel return line and vapor line (after Robert Scharff, 1989)

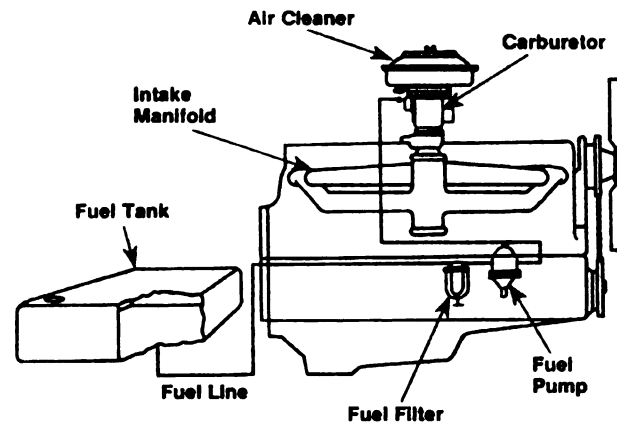


Figure 2.3 Fuel and air system (after Robert Scharff, 1989)

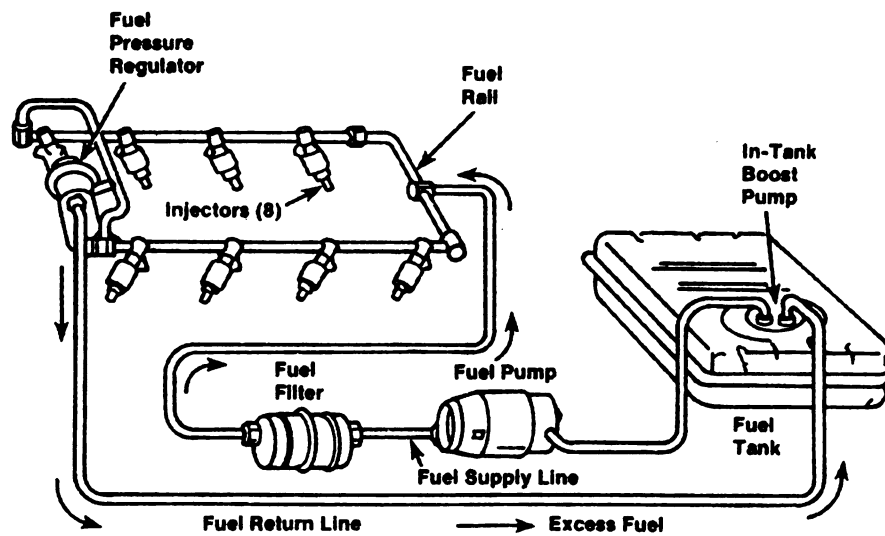


Figure 2.4 Electronic fuel injector in the fuel delivery subsystem (after Robert Scharff, 1989)

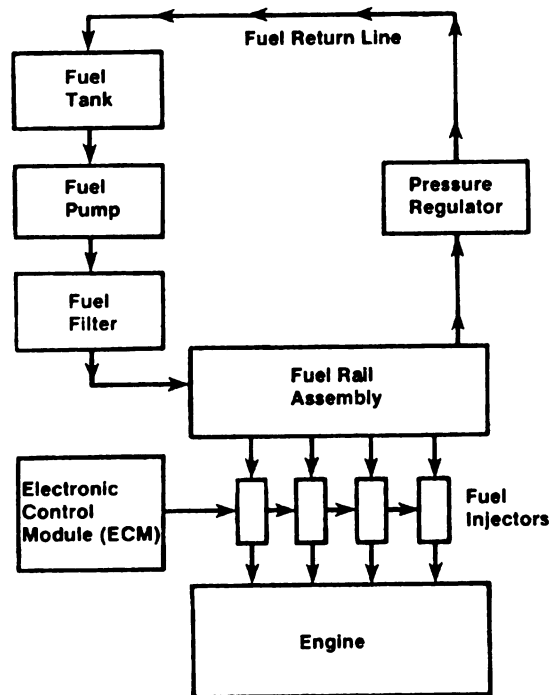


Figure 2.5 Electronic fuel supply system (after Robert Scharff, 1989)

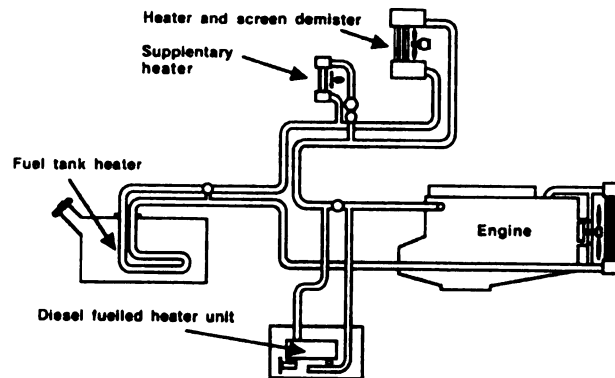


Figure 2.6 Fuel system installed in conjunction with heater units (after Garrett, T. K., 1991)

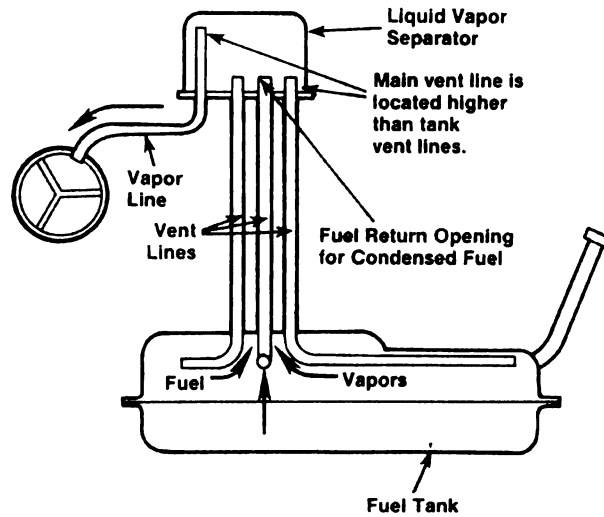


Figure 2.7 Fuel tank vapor separator allows some of the fuel vapors to condense back into liquid and return to the tank. Only vapors can normally enter the higher main vent tube opening (after Robert Scharff, 1989)

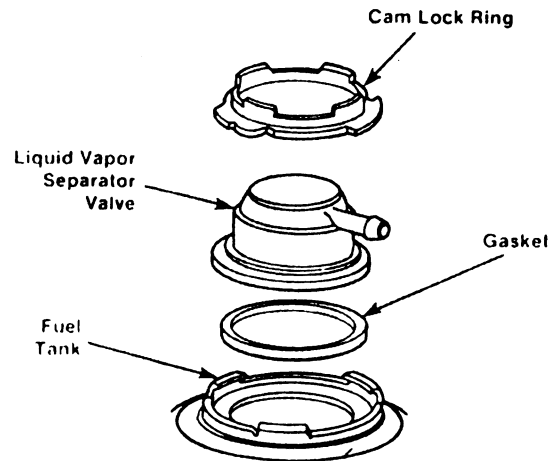


Figure 2.8 Vapor separator attached to the fuel tank (after Robert Scharff, 1989)

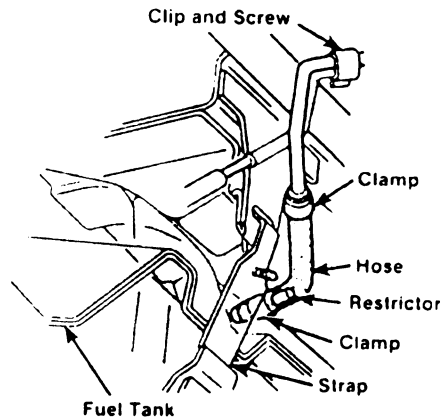


Figure 2.9 Vapor separator in fuel vent lines (after Robert Scharff, 1989)

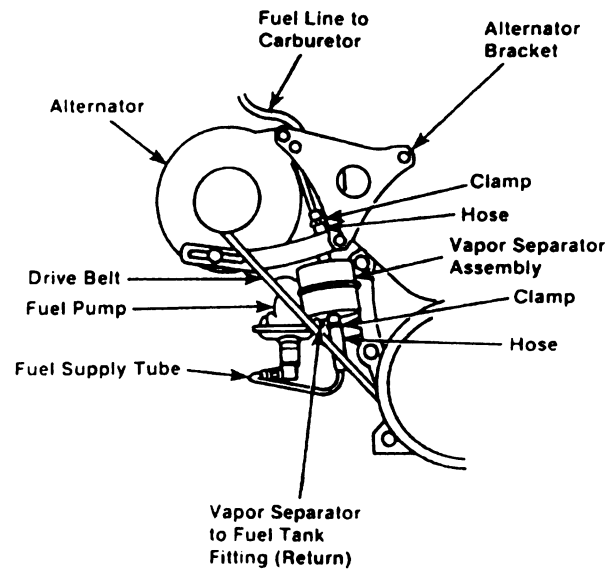


Figure 2.10 Vapor separator located near the fuel pump (after Robert Scharff, 1989)

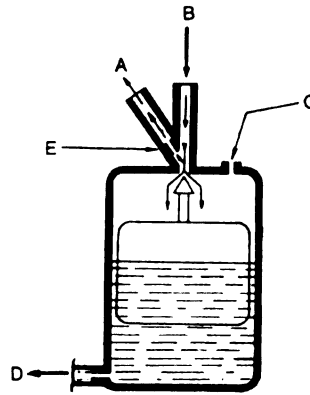


Figure 2.11 Weber device for removing vapor from the warm return flow from fuel rail to tank; it could be used for solving a chronic vapor lock problem if no better remedy is practicable
 A: Vapor return to tank, B: Fuel in, C: Float chamber vent, D: Fuel out, E: Restrictor (after Garrett, T. K., 1991)

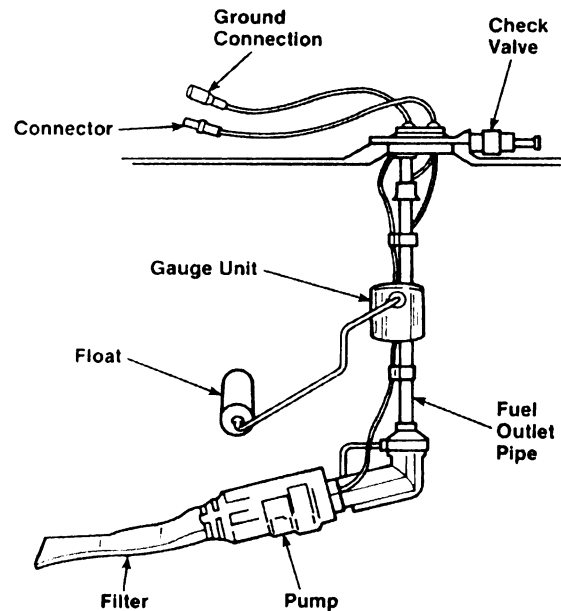


Figure 2.12 Car and light trucks usually have an in-tank strainer and a gasoline filter (after Robert Scharff, 1989)

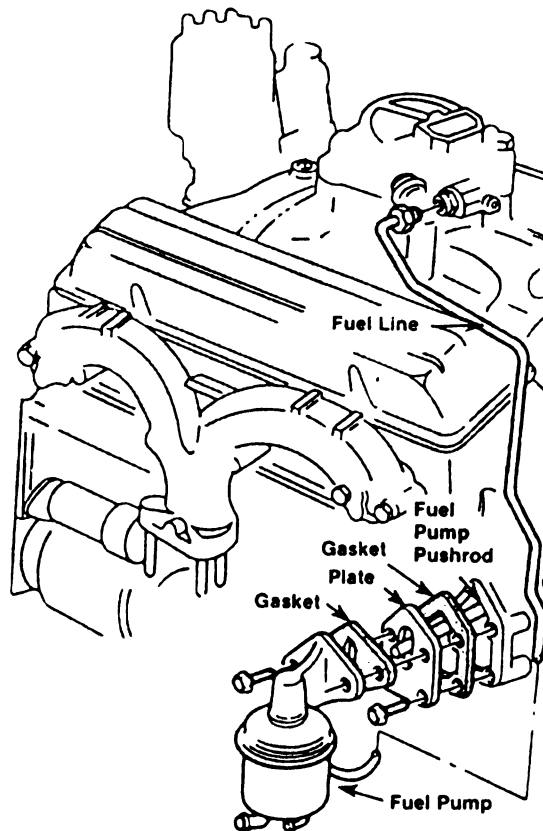


Figure 2.13 V-8 engines usually have pushrod between the camshaft eccentric and the fuel pump (after Robert Scharff, 1989)

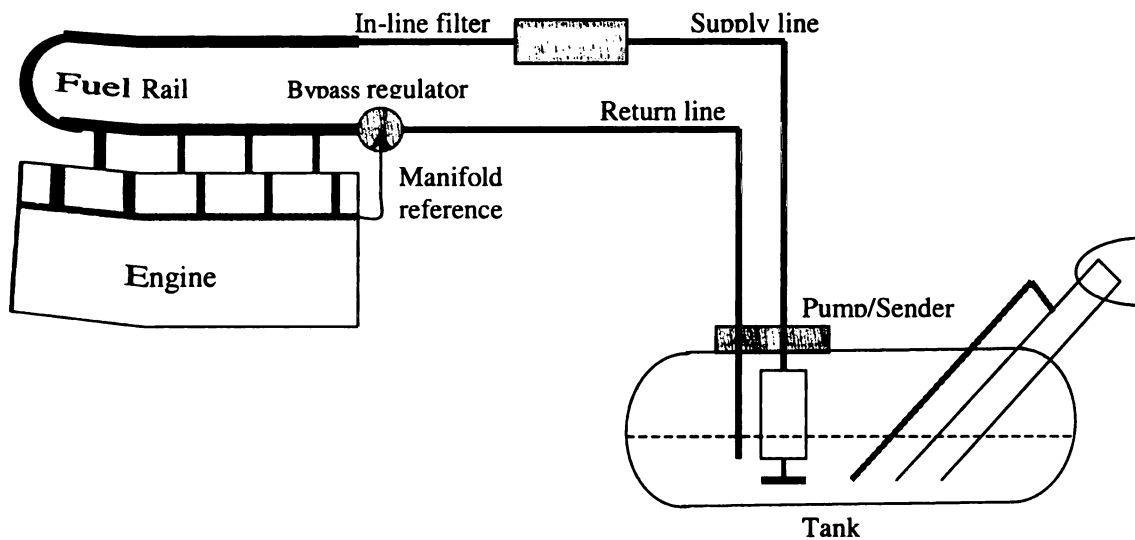


Figure 2.14 Return fuel system

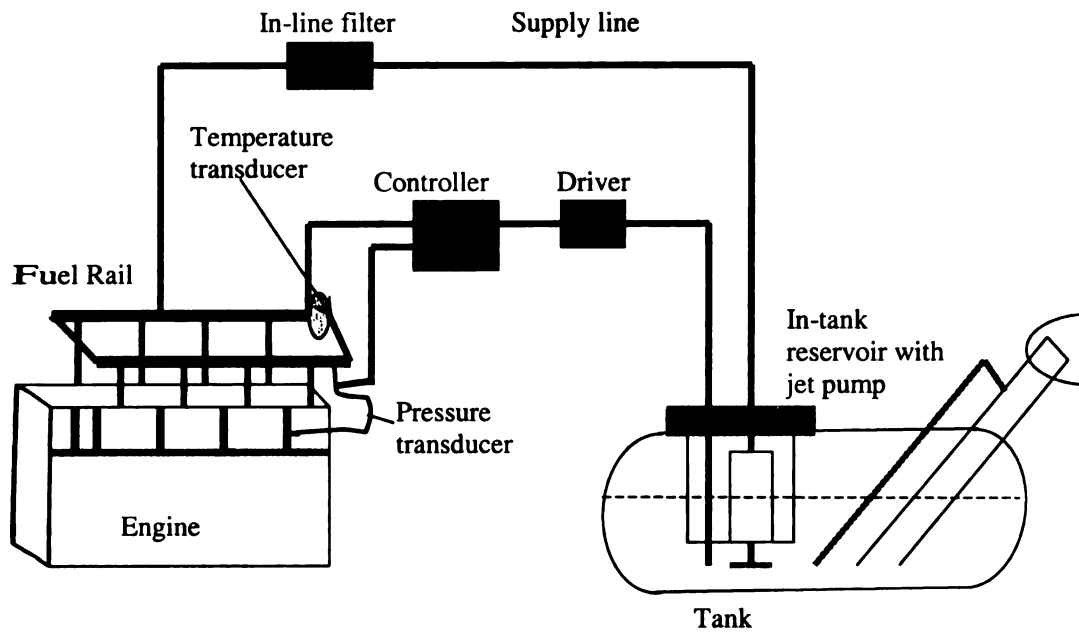


Figure 2.15 Electronic returnless system

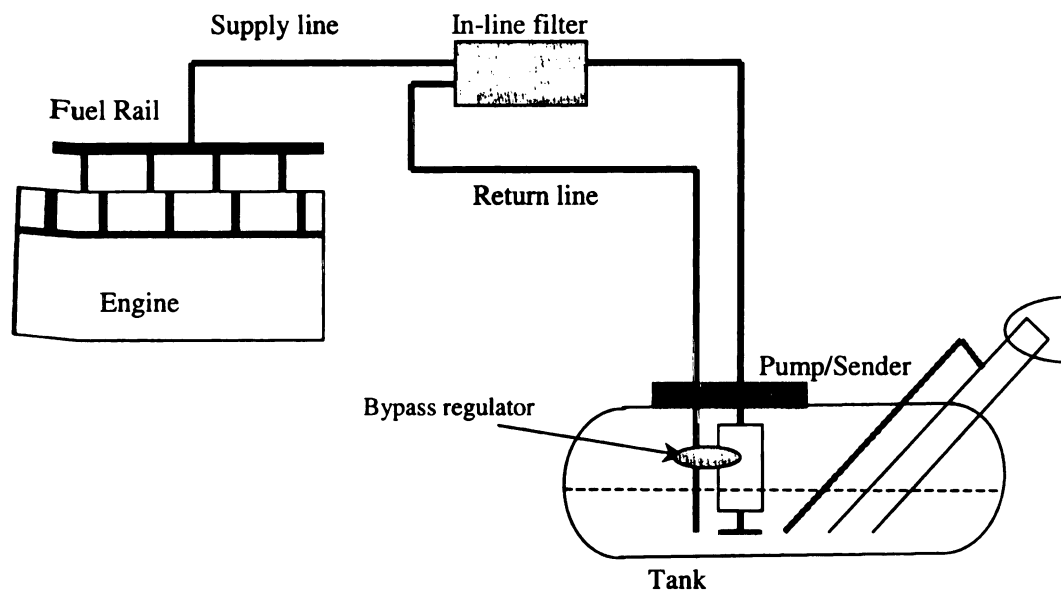


Figure 2.16 Mechanical returnless system using in-tank regulation

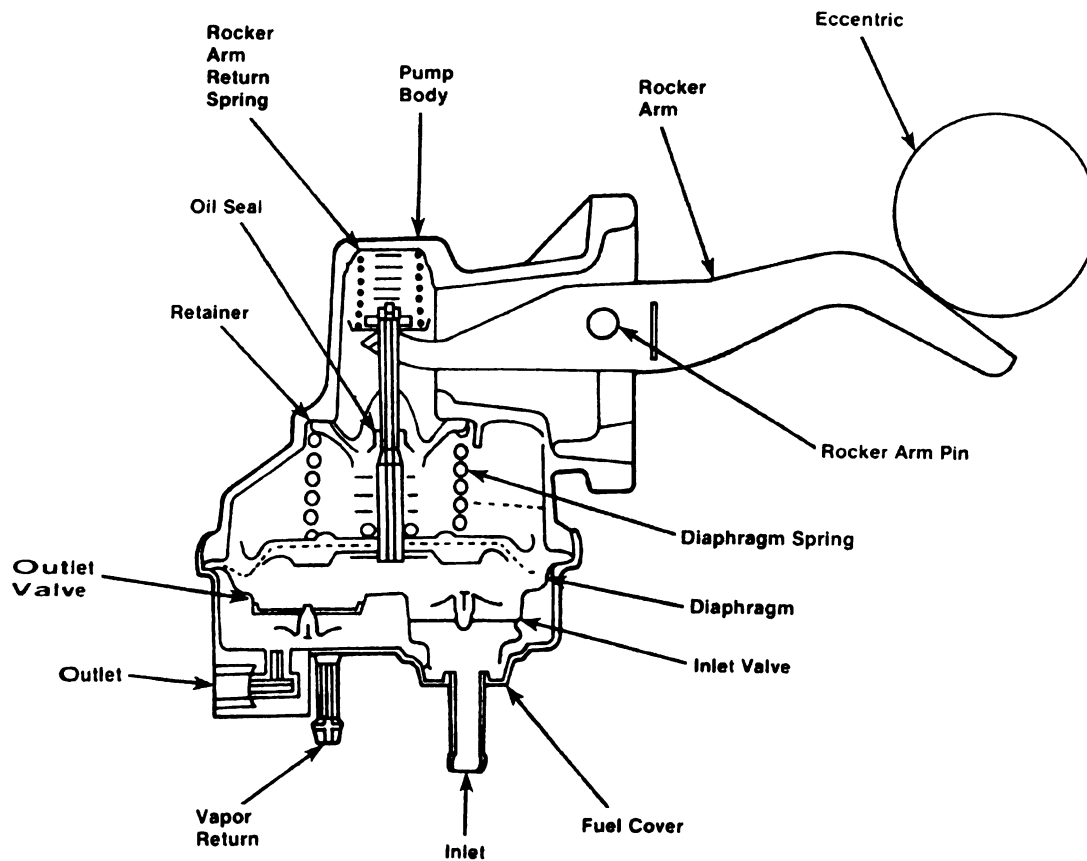


Figure 2.17 Mechanical fuel pump (after Robert Scharff, 1989)

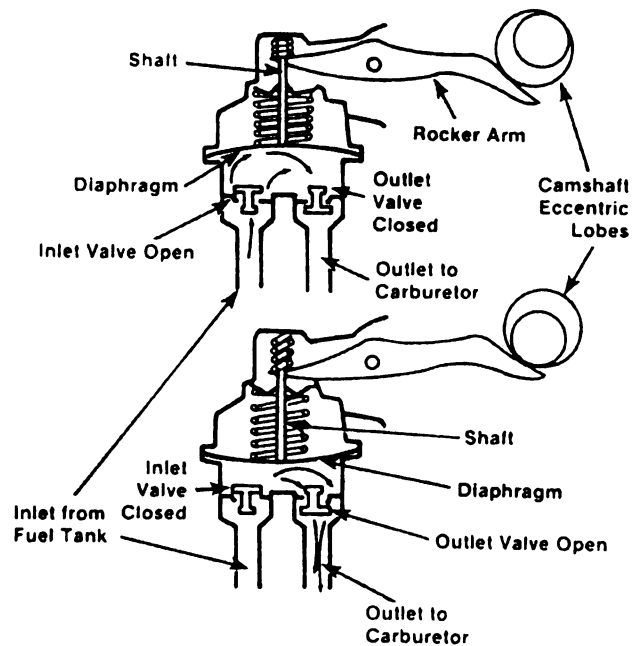


Figure 2.18 Mechanical fuel pump assembly (after Robert Scharff, 1989)

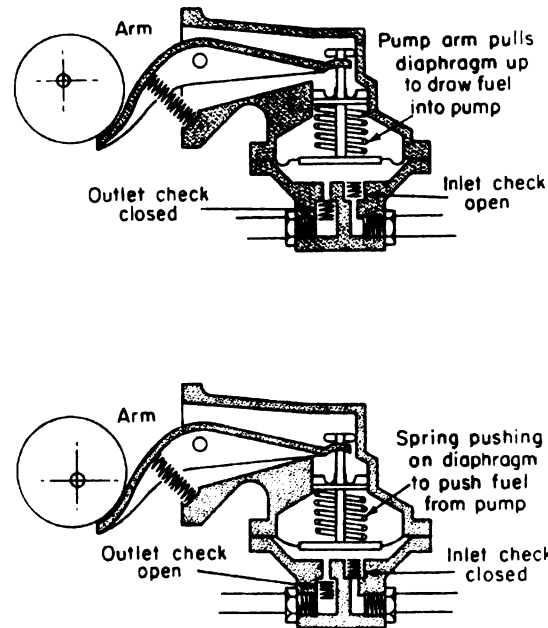


Figure 2.19 Section view of a mechanical diaphragm pump on the inlet and outlet strokes (after Ellinger, H. E., 1976)

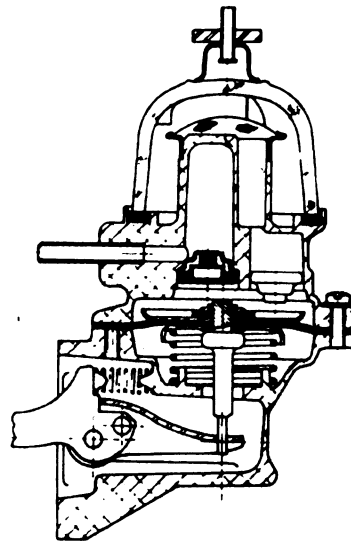


Figure 2.20 The AC-Delco fuel lift pump, with the inlet valve on the right and the delivery valve sectioned on the left. It has a glass dome retained by a stirrup. Under the dome is the inlet stack pipe, capped by a fine mesh filter for trapping water (after Garrett, T. K., 1991)

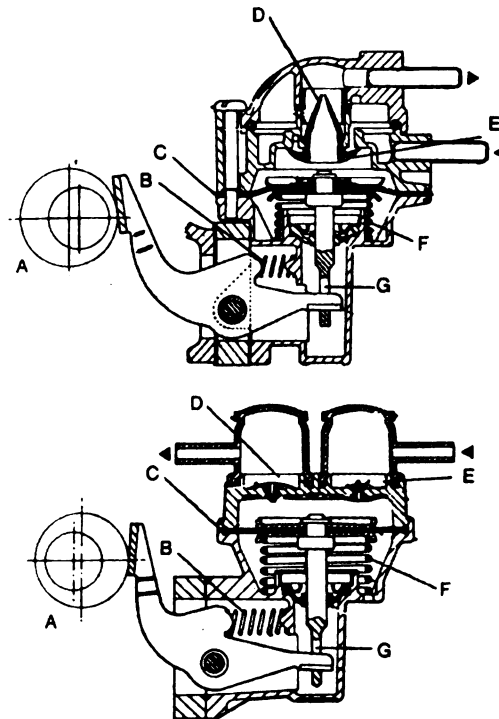


Figure 2.21 (a) SU AF700 fuel lift pump, and (b) SU AF800 fuel lift pump
A: Eccentric on camshaft, B: Follower rocker return spring,
C: Diaphragm, D: Delivery valve, E: Inlet valve, F: Diaphragm return
spring, G: Lost motion slot (after Garrett, T. K., 1991)

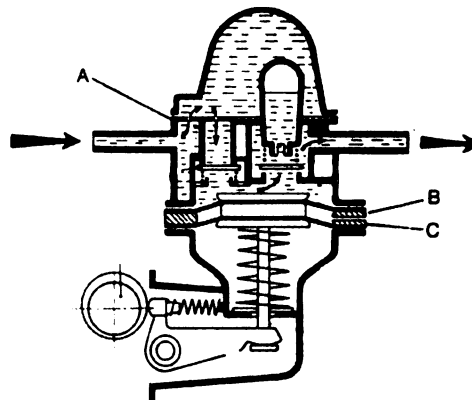


Figure 2.22 Weber double diaphragm fuel lift pump. The inlet valve is on the left
and the outlet on the right, above it, a domed accumulator to damp out
pulsations; A: Filter, B: Pumping diaphragm, C: Sealing diaphragm
(after Garrett, T. K., 1991)

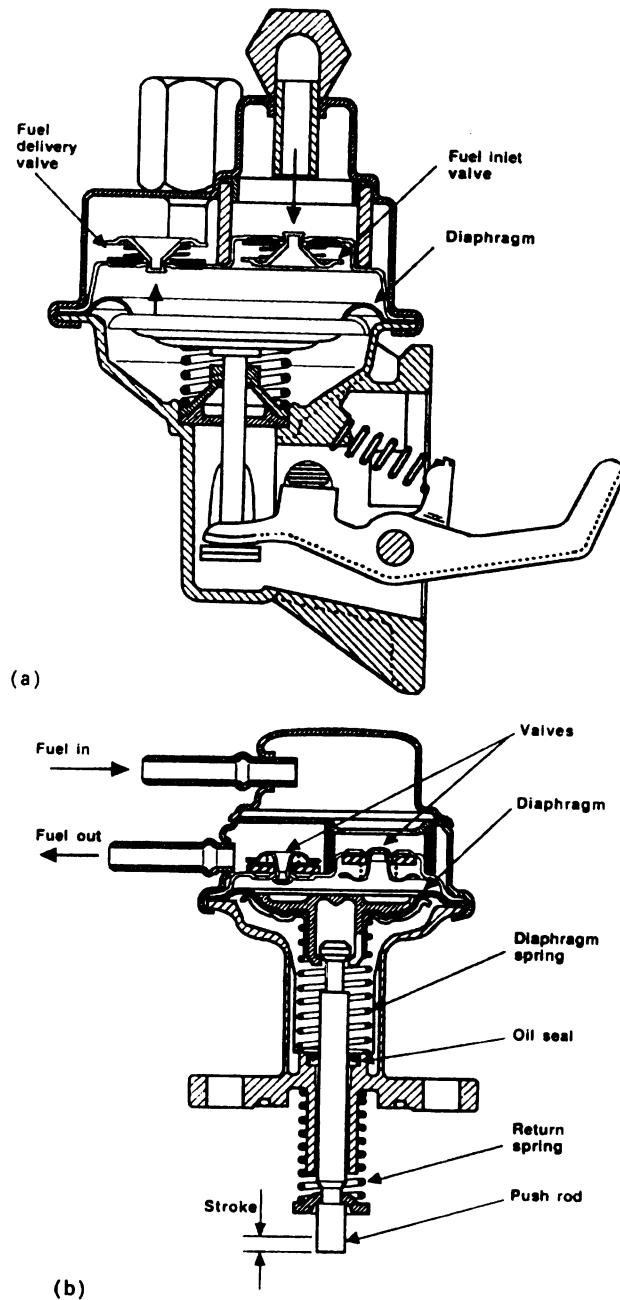
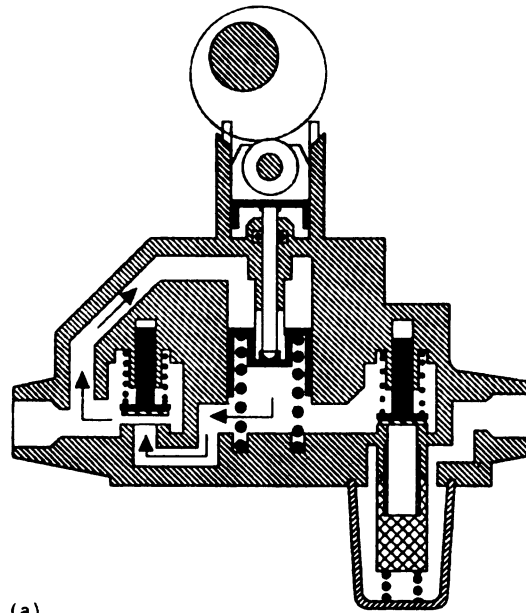
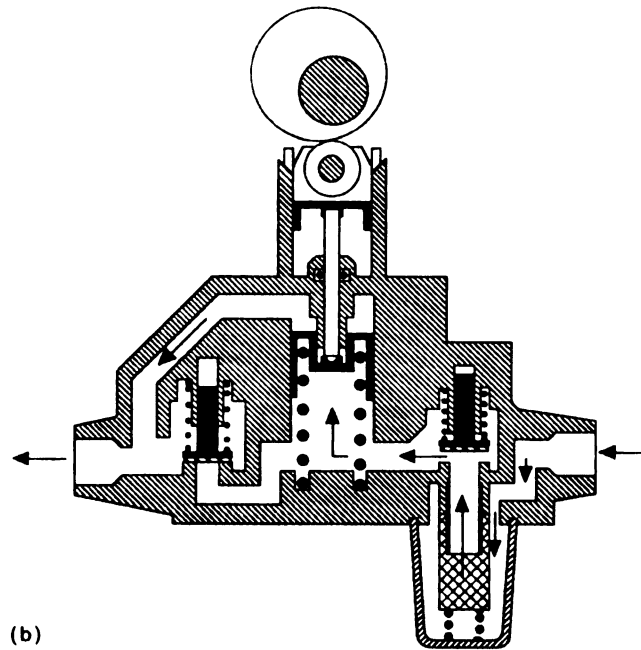


Figure 2.23 The AC lift pumps for diesel engines; (a) The Unitac unit is actuated by lever arm (b) The Unitac unit is directly actuated by an eccentric on

the camshaft (after Garrett, T. K., 1991)



(a)



(b)

Figure 2.24 Representation of the Bosch plunger type pump;
(a) In the fuel transfer; (b) In the fuel delivery condition (after Garrett,
T. K., 1991)

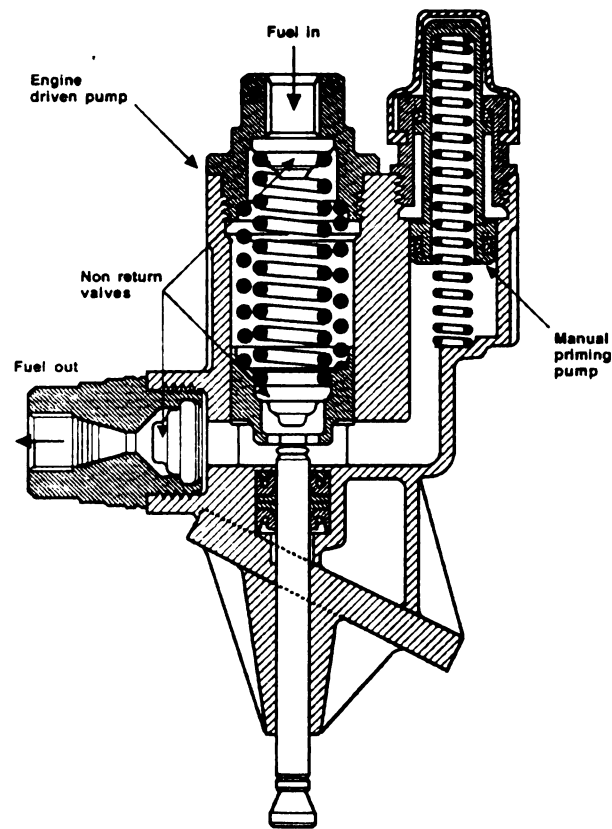


Figure 2.25 An AC plunger type pump with, embodied on the right, a manual-priming pump (after Garrett, T. K., 1991)

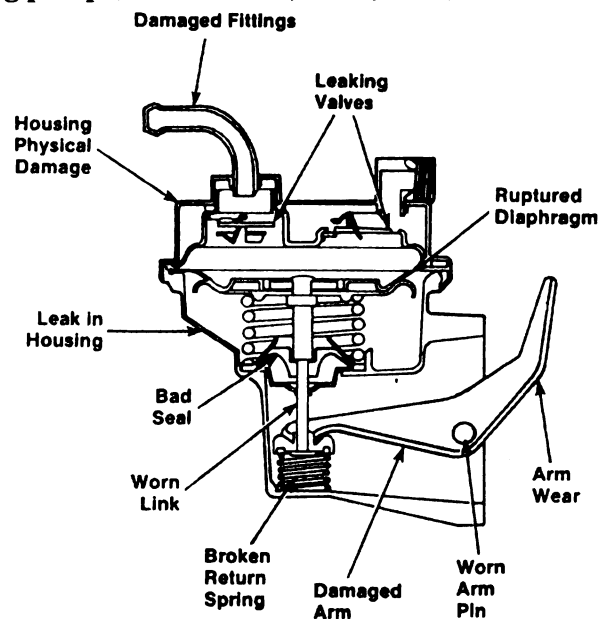


Figure 2.26 Common problems with a mechanical pump (after Robert Scharff, 1989)

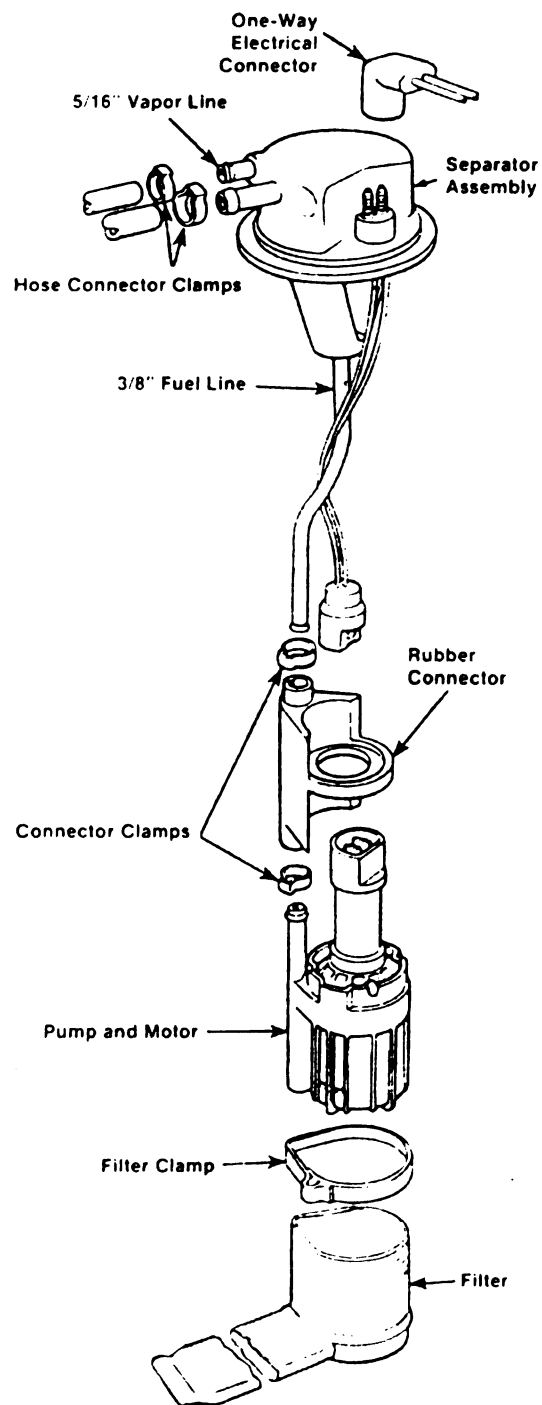


Figure 2.27 Electric fuel pump components (after Robert Scharff, 1989)

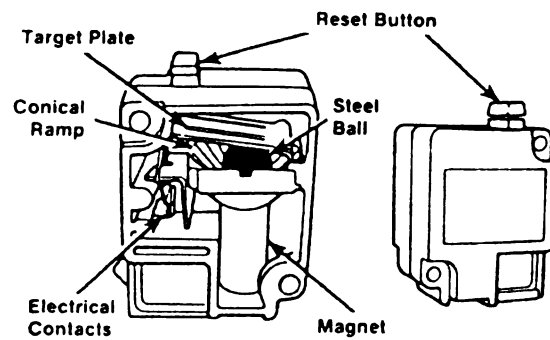


Figure 2.28 Some models use an inertia switch to turn off the electric fuel pump in an accident (after Robert Scharff, 1989)

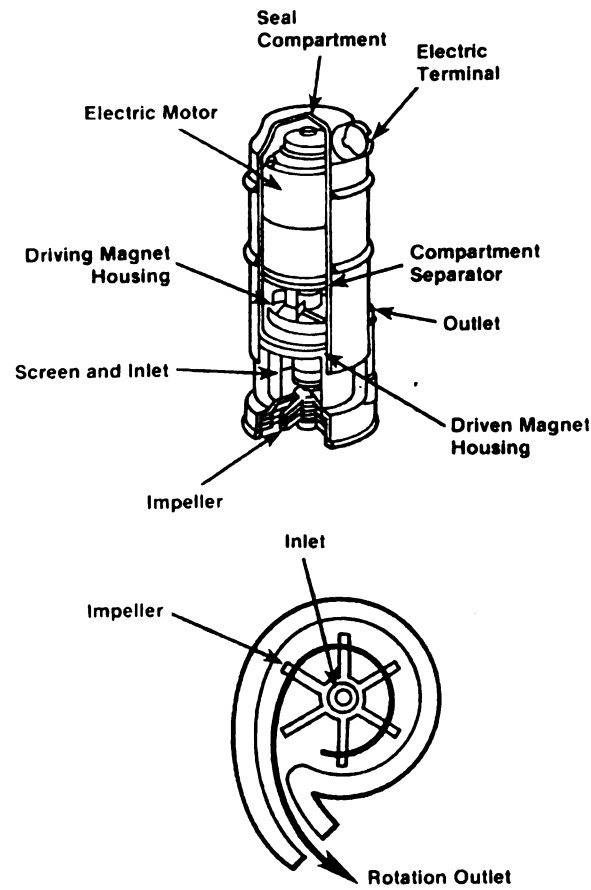


Figure 2.29 Electric fuel pump with impellers (after Robert Scharff, 1989)

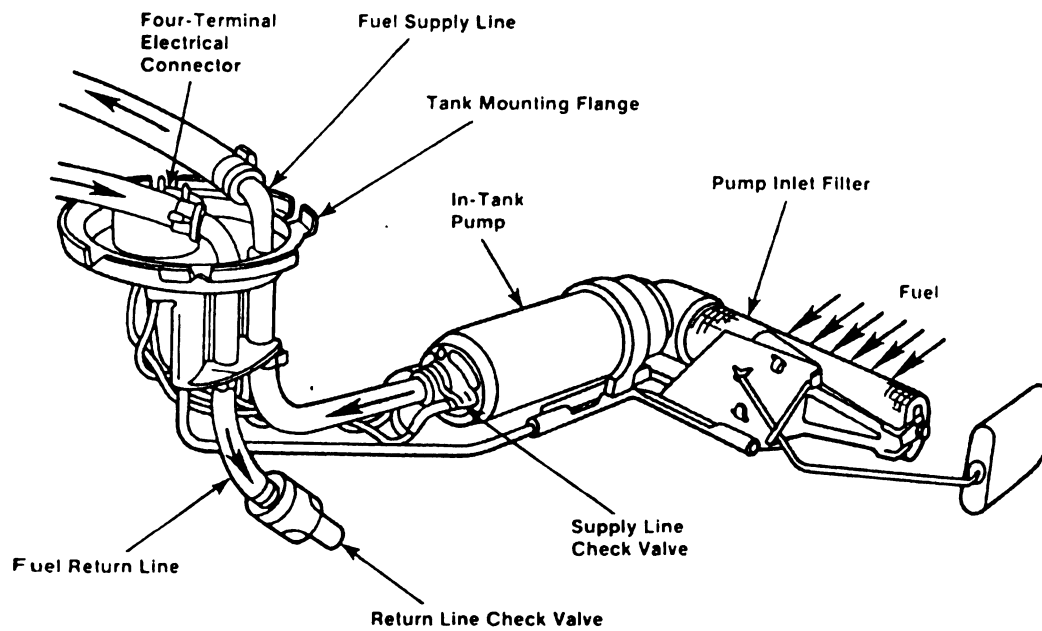


Figure 2.30 Electric fuel pump system located inside the fuel tank (after Robert Scharff, 1989)

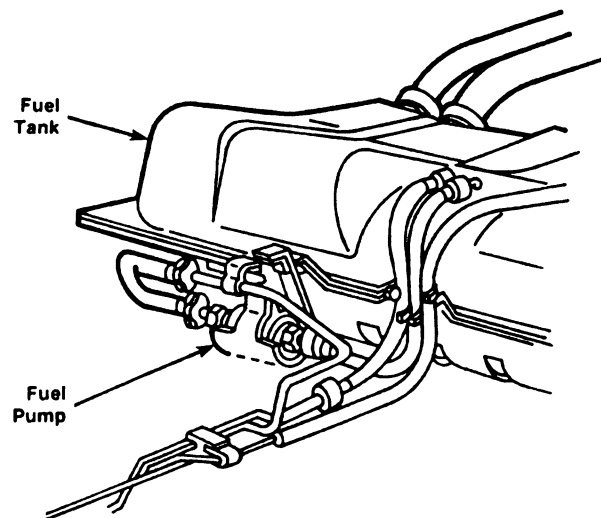


Figure 2.31 Electric fuel pump located outside the fuel tank (after Robert Scharff, 1989)

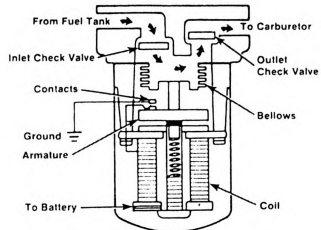


Figure 2.32 Bellows-type fuel pump (after Robert Scharff, 1989)

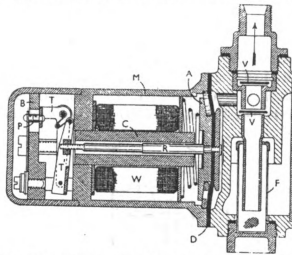


Figure 2.33 The SU electric pump (after Newton, K., Steeds, W. and, Garrett, T. K., 1996)

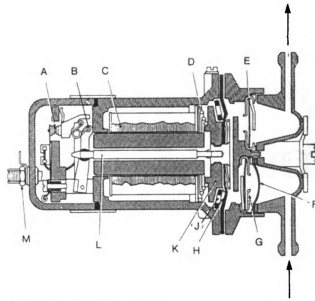


Figure 2.34 The SU electric fuel-lift pump

A: Contacts, B: Scissors type lick-over mechanism, with hairpin spring, C: Winding, D: Diaphragm return spring, E: Delivery valve, F: Fine mesh filter, G: Inlet valve, H: Diaphragm, J: Rollers, K: Armature, L: Push rod, M: Electrical connections (after Garrett, T. K., 1991)

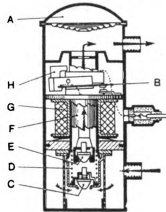


Figure 2.35 Weber plunger type electric fuel-lift pump

A: Air space with separator diaphragm below it, B: Contacts, C: Inlet valve, D: Plunger return spring, E: Delivery valve, F: Plunger, G: Winding, H: Permanent magnet (after Garrett, T. K., 1991)

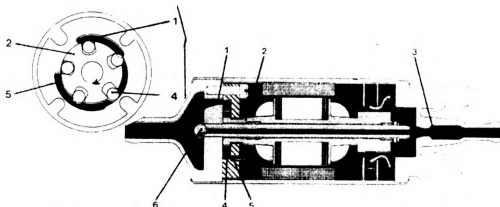


Figure 2.36 The Weber roller-cell type pump with a section through the roller chamber; 1. Inlet port; 2. Pump rotor; 3. Non-return valve; 4. Rollers; 5. Delivery port; 6. Pressure relief valve (after Garrett, T. K., 1991)

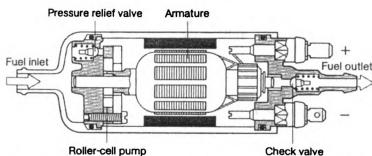


Figure 2.37 Roller-cell positive displacement pump – electric pump (after Newton, K., Steeds, W. and, Garrett, T. K., 1996)

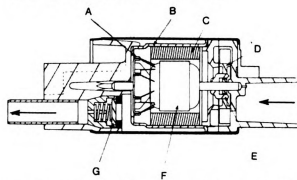


Figure 2.38 The AC in-tank fuel pump; A: Commutator, B: Flux carrier, C: Magnet, D: Impeller, E: Drive spigot, F: Armature, G: Check valve (after Garrett, T. K., 1991)

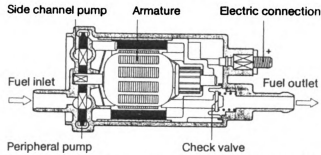


Figure 2.39 Bosch two-stage low-pressure rotary electric fuel pump (after Newton, K., Steeds, W. and, Garrett, T. K., 1996)

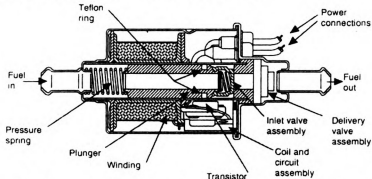


Figure 2.40 The AC Universal Electronic solenoid type pump (after Garrett, T. K., 1991)

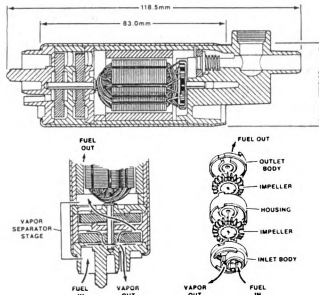


Figure 2.41 In this AC medium pressure twin turbine fuel pump, the first stage impeller removes vapor by centrifuging the fuel outwards and thus leaving the vapor in the center, when it is returned to the tank. The delivery pressure is about 1 bar. (after Garrett, T. K., 1991)

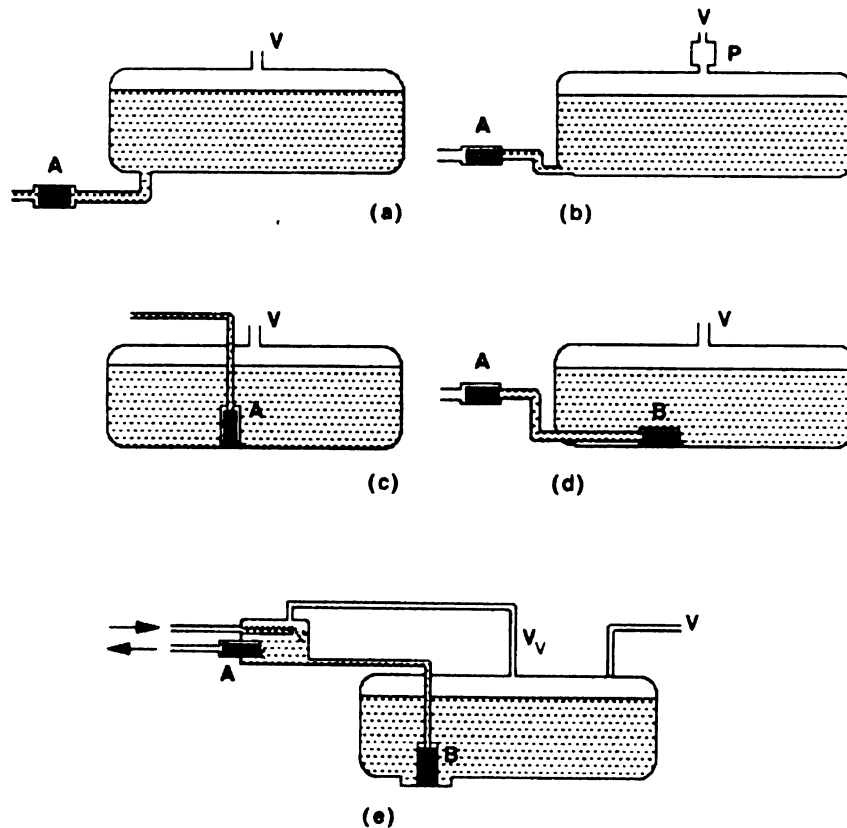


Figure 2.42 Diagrammatic illustrations of five different fuel-pump arrangements

(a) Gravity feed to pump

(b) Pressurized tank

(c) The common arrangement of an in-tank pump

(d) Lift pump in tank, pressure pump outside at mean level of fuel

(e) In-tank lift pump, and a combined vapor separator and priming reservoir outside the tank; A filter and pressure relief valve were mounted on pressure pump. The return flow from the fuel rail is discharged into the small reservoir, vapor from which is vented back to the tank.

A: Pressure pump, B: Lift pump, V: Vent, P: Pressure regulating valve
(after Garrett, T. K., 1991)

Chapter 3

CONVENTIONAL CENTRIFUGAL PUMP DESIGN METHOD

This chapter describes the conventional design method from Karassik, Krutzsch, Fraser, and Messina (1986). One-Dimensional design parameters of conventional design method of centrifugal pump will include the geometrical parameters and the fluid parameters.

The main geometrical parameters defining the impeller are:

- **H**ub radius R_H
- **S**hroud (or Tip) radius R_S
- **B**lade angle distribution from inlet to exit and from hub to shroud
- **I**nlet absolute flow angle (α_{f1}) and exit absolute flow angle (α_{f2})
- **I**nlet relative blade angle (β_{b1}) and exit relative blade angle (β_{b2})
- **I**mpeller exit radius R_2
- **I**mpeller exit width b_2
- **B**lade thickness t
- **T**he number of Blade Z
- **I**mpeller axial length L_{ax}

The main fluid parameters are:

- **I**nlet absolute velocity C_1 , inlet relative velocity W_1 , inlet tip speed U_1
- **E**xit absolute velocity C_2 , exit relative velocity W_2 , exit tip speed U_2
- **R**elative velocity ratio W_2/W_1

- Inlet absolute flow angle (α_{f1}) and exit absolute flow angle (α_{f2})
- Inlet relative blade angle (β_{b1}) and exit relative blade angle (β_{b2})
- Choice of slip factor for performance prediction

The absolute angle and the relative angle are defined by the following rules of American method and European method.

The American method defines by

- The absolute angle from the axial direction (at rotor inlet) or from radial (meridional) direction (at rotor exit) to the absolute velocity is α .
- The relative angle from the axial direction (at rotor inlet) or from radial (meridional) direction (at rotor exit) to the relative velocity is β .

The European method defines by (Figure 3.11)

- The absolute angle from the tangential direction to the absolute velocity is α .
- The relative angle from the tangential direction to the relative velocity is β .

3.1 Specific speed, suction specific speed, and suction diameter

The specific rotation speed is defined by

$$N_s = \frac{N\sqrt{Q}}{g H^{0.75}} \quad (3.1)$$

Normally, the gravitational acceleration is dropped because the gravity is very nearly constant over the surface of the earth. As a result, the gravity “g” is combined with the specific speed. Finally, the specific speed is written

$$N_s = \frac{N\sqrt{Q}}{H^{0.75}} \quad (3.2)$$

The expected pump efficiency is estimated from Figure 3.1. Figure 3.2 shows the efficiency of centrifugal pumps versus specific speed, size, and shape. When the value of NPSH is provided, the suction specific speed is defined by

$$S_m = \frac{N\sqrt{Q}}{NPSH^{0.75}} \quad (3.3)$$

The suction diameter is defined by

$$D_s = 2897 \left(\frac{Q}{k N \tan(\beta_0)} \right) \quad (3.4)$$

The hub ratio is $k = 1 - \left(\frac{D_H}{D_s} \right)^2$ (3.5)

The impeller inlet design is based on the inlet flow angle β_0 (taken at the outer diameter of the inlet) (Figure 3.9). The station “0” is located right in front of the vane inlet tip. The flow angle β_0 is selected between 10° and 25° , independent of specific speed. The flow angle is often used $\beta_0 = 17^\circ$, which is a compromise between the efficiency and the capitation. For best efficiency, the flow angle β_0 should be larger and for lower NPSH, the flow angle β_0 should be smaller. There are two types of configuration for vane impeller. Figure 3.20 shows the impeller with vanes extended into axial inlet and Figure 3.21 shows the impeller with cylindrical vanes

3.2 Impeller discharge velocity triangle

The slip factor by Stodola’s formula is

$$\mu = 1 - \frac{\pi \sin \beta_2}{Z} \quad (3.6)$$

The angle β_2 is determined from Figure 3.4, the number of vanes Z is assumed to be “ $Z = 7$ ”, and the velocity ratio of “ C_{m3}/U_2 ” is determined from Figure 3.3.

Figure 3.3 gives the band of commonly used values of " C_{m3}/U_2 ". This parameter decreases with smaller specific speed and it tends toward zero at zero specific speed. If values higher than those shown in Figure 3.3 are utilized at low specific speed, the usual manufacture of the impellers by casting will be difficult for such small vane discharge widths. The velocity ratio of " C_{m3}/U_2 " relates the meridional velocity (taken right after the impeller discharge) to the impeller peripheral speed. In addition, if one angle is known, the whole impeller discharge velocity triangle can be drawn. It is usually to specify the blade discharge angle (β_{2b}), instead of a flow angle (α), because the vane discharge angle (β_2) is one of the design parameters, which must be selected. The range of the commonly used values of the vane discharge angle (β_2) is given in Figure 3.4.

Since the vane discharge angle (β_2) is not a flow angle, it is important to determine the slip factor in order to complete the velocity triangle diagram. This slip factor is implicitly calculated by using the usual number of vanes (Z), which is four to eight for specific speeds up to 4000. The three design parameters " C_{m3}/U_2 ", " β_2 ", and " Z " are sufficient to describe the impeller-discharge velocity triangle in an approximate manner. The values plotted in Figure 3.3 and Figure 3.4 originated from the experiment in pump industry. Therefore, the experimental values form bands rather than arrange the design values inside these bands. Besides the influence of three design parameters upon the design point efficiency, the three design parameters have an effect upon the shape of the head capacity curve. It rises toward the shutoff if smaller values of " β_2 ", " Z ", and larger values of " C_{m3}/U_2 " are selected. These extreme values within the bands can be seen from Figure 3.3 and Figure 3.4.

The slip factor by Pfleiderer's formula is

$$\mu = \frac{1}{1 + \frac{a}{Z} \left(1 + \frac{\beta_2}{60} \right) \frac{2}{1 - (r_1^2/r_2^2)}} \quad (3.7)$$

For the radius ration $r_1/r_2 < 1$, the slip factor does not increase any more. For such small radius ratio, the slip factor for $r_1/r_2 = 1$ should be used. The slip factor is affected not only by the impeller configuration but also by the interaction of the diffusing system with the impeller. These effects are taken into account by the coefficient “a” as follows:

Volute: $a = 0.65$ to 0.85

Vaned diffuser: $a = 0.6$

Vaneless diffuser: $a = 0.85$ to 1.0

The hydraulic efficiency depends very much on the design and the execution of the flow passages. The specific speed has only a small influence on the hydraulic efficiency. The hydraulic efficiency is estimated from Figure 3.5.

$$\eta_H \approx 1 - \frac{0.071}{Q^{0.25}} \quad (3.8)$$

The head coefficient is computed by

$$\psi = 2 \mu \eta_H \left(1 - \frac{C_{m3}}{U_2} \cot(\beta_2) \right) = \frac{H}{U_2^2/(2g)} \quad (3.9)$$

The necessary impeller peripheral (tangential) speed is

$$U_2 = \sqrt{\frac{2gH}{\psi}} \quad (3.10)$$

The meridional velocity C_{m3} is calculated right after the impeller discharge width

$$C_{m3} = \frac{Q \cdot 10^6}{2 \pi r_2 b_3} = \frac{Q \cdot 10^6}{2 \pi r_2 b_2} \quad (3.11)$$

The meridional right after the impeller discharge is

$$C_{m3} = \left(\frac{C_{m3}}{U_2} \right) U_2 \quad (3.12)$$

The peripheral component of the absolute impeller-discharge velocity without slip is calculated with geometric relationships, which can be seen from Figure 3.8, Figure 3.9, Figure 3.12, Figure 3.20, and Figure 3.21.

$$C_{u3} = U_2 - C_{m3} \cot(\beta_2) \quad (3.13)$$

With slip, the peripheral component of the absolute impeller-discharge velocity is calculated with definition of slip factor ($\beta_{2b} \neq 90^\circ$). Figure 3.11 and Figure 3.12 show the actual and ideal tangential velocities in the impeller discharge velocity triangle, which are produced by slip effect.

$$\mu = \sigma = \frac{C_{u3}}{C'_{u3}} = \frac{C_{u2}}{C'_{u2}} = \frac{C_{\theta 2}}{C'_{\theta 2}} = \frac{C_{u2\text{-actual}}}{C_{u2\text{-ideal}}} = \frac{C_{\theta 2\text{-actual}}}{C_{\theta 2\text{-ideal}}} \quad (3.14)$$

3.3 Impeller discharge dimensions

The geometry of a pump stage and the impeller discharge dimensions are defined in Figure 3.24. The impeller discharge diameter is

$$D_2 = \frac{60 U_2 (1000)}{\pi N} \quad (3.15)$$

$$\text{The impeller discharge radius (Figure 3.8) is } r_2 = \frac{D_2}{2} \quad (3.16)$$

The meridional velocity C_{m3} is calculated right after the impeller discharge width

$$C_{m3} = \frac{Q \cdot 10^6}{2 \pi r_2 b_3} = \frac{Q \cdot 10^6}{2 \pi r_2 b_2} \quad (3.17)$$

$$\text{The impeller discharge width is calculated from } b_3 = \frac{Q (10^6)}{2 \pi r_2 C_{m3}} \quad (3.18)$$

3.4 Impeller inlet diameter

The impeller inlet design is based on the inlet flow angle β_0 (taken at the outer diameter of the inlet). Figure 3.10 and Figure 3.11 illustrate the blade angle (β_{b1} , β_{b2}) and the flow angle (β_{f1} , β_{f2}) in impeller velocity diagrams. The flow angle is selected between 10° and 25° and this flow angle is independent of the specific speed. The flow angle is a compromise between efficiency and cavitations. For best impeller efficiency, the flow angle β_0 should be larger, for lower NPSH, the flow angle β_0 should be smaller. Since NPSH requirements are not critical, the normal flow angle is $\beta_0 = 17^\circ$

Hub and shroud profiles of centrifugal pump impeller are shown in Figure 3.25. An axial inlet will be assumed with a small hub, which does not protrude far enough to block the inlet flow. Therefore, the hub diameter equals zero ($D_H = 0$). The hub-tip ratio is defined by

$$k = 1 - \left(\frac{D_H}{D_s} \right)^2 \quad (3.19)$$

Since the hub diameter equals zero, the hub-tip ratio is $k = 1$

The suction diameter is $D_s = 2897 \left(\frac{Q}{k N \tan \beta_0} \right)^{1/3} = 2897 \left(\frac{Q}{k N \tan \beta_{is}} \right)^{1/3} \quad (3.20)$

The inlet radius is $r_i = r_s = \frac{D_s}{2} \quad (3.21)$

The mean inlet radius is $r_{im} = \left(\frac{r_s^2 + r_H^2}{2} \right)^{1/2} \quad (3.22)$

The calculated ratio of radius r_{im}/r_2 should be smaller than the initially assumed radius ratio r_1/r_2 . The hub-tip ratio is selected by the designer and can have value from zero to more than 0.5. The constant k approaches unity as the hub-tip ratio decreases to

zero and can be taken as unity to approximate the shroud diameter. The hub diameter must exceed the shaft diameter if the shaft needs to pass through the eye. In such cases, the ratio may be taken as 0.5.

3.5 Impeller inlet vane angles

The minimum vane thickness will equal the impeller diameter divided by 100, but the vane thickness cannot be less than 4 mm. The inlet vane thickness will be assumed to be $s_1 = 4.8$ mm. The inlet vane angle at outer radius is calculated by

$$\tan\beta_{1(r)} = \frac{\tan\beta_{0(r)}}{1 - \frac{Z s_1}{2 \pi r_1 \sin\beta_{1(r)}}} \quad (3.23)$$

The Mean inlet vane angle at the Mean radius is calculated by

$$\tan\beta_{1m} = \frac{\tan\beta_{0(r)}}{1 - \frac{Z s_1}{2 \pi r_{1m} \sin\beta_{1m}}} \quad (3.24)$$

$$r_{1m} = \left(\frac{r_1^2 + r_H^2}{2} \right)^{1/2}$$

3.6 Impeller inlet velocity triangle

The meridional velocity ahead of the vanes is

$$C_{m0} = \frac{Q (10^6)}{\pi r_1^2} \quad (3.25)$$

The peripheral vane velocity at the eye is

$$U_1 = \frac{\pi r_1 N}{30 (1000)} \quad (3.26)$$

3.7 Flow areas between vanes (Impeller vane layout)

Vane thickness creates blockage, in which the space taken up by vanes, is not available for flow. Therefore, the local velocities are increased and this yields the flow

disturbance created by the blade edges at the inlet and outlet the blade impeller. As a result, the total inlet blockage area and the total exit blockage area should be indicated in computing the actual inlet and exit areas between vanes.

$$\text{The actual inlet area between vanes is } A_1 = \pi (r_{s1}^2 - r_{h1}^2) - \frac{Z t (r_{s1} - r_{h1})}{\sin(\beta_1)} \quad (3.27)$$

$$\text{The actual exit area between vanes is } A_1 = \pi d_2 b_2 - \frac{Z t b_2}{\sin(\beta_{b2})} \quad (3.28)$$

For Francis-type vanes with mixed flow in the vane inlet area and small hub, the inlet area between vanes is approximately

$$A_I = Z a_I \approx \pi r_1^2 \sin \beta_{1m} \quad (3.29)$$

The Mean inlet vane angle at the Mean radius is calculated from equation 3.24. The outlet vane thickness will be assumed to be “ $s_2 = 4.8\text{-mm}$ ”. If the front shroud in the discharge region is inclined for Francis-type impellers, the discharge area between vanes is approximately

$$A_{II} = Z a_{II} \approx b_2 (2 \pi r_2 \sin \beta_2 - Z s_2) \quad (3.30)$$

If the front shroud in the discharge region is not inclined area, about 25% should be subtracted from equation 3.30. The area ratio of A_{II}/A_I should be from “1.0” to “1.3” for high hydraulic efficiency and the avoidance of flow separation. The areas between vanes must be checked by the actual vane layout. The vane layout depends mainly upon the selected angles “ β_1 ” and “ β_2 ” (Figure 3.22). The recommended ranges for these two angles overlap. Therefore, the outlet vane angle is occasionally equal to the inlet vane angle. In such a case, the vane takes the shape of a logarithmic spiral vane impeller (Figure 3.22). The blade construction is built up from logarithmic spiral vane impeller (Figure 3.23).

3.8 Volute casing

The throat area (A_{thr}) and the throat distance r_4 can be calculated from the initially assumed throat velocity (C_{thr}) and the tongue clearance (t). A single volute shall be used because of its simplicity (Figure 3.17). The plan view of the impeller and the volute casing with leading dimensions are presented in Figure 3.16. The throat velocity is tentatively selected from the ratio of C_{thr}/U_2 (Figure 3.13) for the calculated specific speed N_s . The throat velocity (C_{thr}) is calculated from

$$C_{thr} = \left(\frac{C_{thr}}{U_2} \right) U_2 \quad (3.31)$$

The tentative throat area is

$$A_{thr} = \frac{Q (10^6)}{C_{thr}} \quad (3.32)$$

Assuming a circular throat section, the throat radius is

$$r_{thr} = \sqrt{\frac{A_{thr}}{\pi}} \quad (3.33)$$

The tongue distance is selected to be 7% of the impeller radius: $t = 0.07 (r_2)$

The distance of the throat center from the axis is $r_4 \approx r_2 + t + r_{thr}$ (3.34)

The average throat velocity C (the flow factor) should be checked by

$$C = \frac{C_{thr} r_4}{C_{u3} r_2} \quad (3.35)$$

The value of $C = 1$ is a good design value for volutes of large pumps or very smooth volutes of medium-size pump. For commercially cast volutes of medium size and small pumps, the value $C = 0.9$ gives a reasonable approximation. If the flow factor C had been larger than 1.0 or smaller than 0.9, then the calculation would have to repeat

with an improved choice for C_{thr} . The area ratio of A_{thr}/A_{II} should be verified at the calculated specific speed N_s (by using the data from Figure 3.14). This ratio should fall into the region of high efficiency. The intermediate volute areas are approximated by Stepanoff's equation

$$A_v = A_{thr} \frac{\phi_v}{360} \quad (3.36)$$

The intermediate volute areas are assumed to be circular, and their radii and distances from the areas are calculated. All the results are tabulated for the central angle ϕ_v from 0° to 360° . The previously calculated flow factor C should be used in calculating C_v and A_v . The intermediate volute velocities are calculated on the basis of constant angular momentum:

$$C_v = \frac{r_2}{r_v} C(C_{u3}) \quad (3.37)$$

The intermediate volute areas are

$$A_v = \frac{Q(10^6)}{C_v} \frac{\phi_v}{360} \quad (3.38)$$

The newly calculated intermediate areas result in new center distances r_v , which are then compared with the assumed values. These results are then tabulated. The calculated center distances r_v should be close to the assumed value. The volute can be drawn using the section radii " r " and distance " r_v " of the volute centers from the axis (Figure 3.15).

3.9 Vaned diffuser

A vaned diffuser consists of a number of vanes set around the impeller. The flow from the vaned diffuser is collected in a volute and discharged through the outlet pipe. The throat velocity is calculated by

$$\frac{C_{thr}}{C_{u3}} = \frac{r_2}{r_4} C \quad (3.39)$$

The distance “ r_4 ” (Figure 3.6 and Figure 3.7) of the center of the throat from the axis is smaller than for the volute pump of equal specific speed. Therefore, the throat velocity is expected to be larger. The typical value of the factor “ C ” is “ $C = 0.8$ ”. The number of diffuser vanes in the vaned diffuser should be more than the number of impeller vanes. In this way, circulation around the diffuser vanes, which is resulted from the uneven impeller channel discharge, is minimized.

3.10 Loss estimates, resultant efficiency, and shaft power

The hydraulic efficiency is defined by

$$\begin{aligned} \eta_H &\approx 1 - \frac{0.8}{[Q(\text{gpm})]^{0.25}} \\ \eta_H &\approx 1 - \frac{0.071}{[Q(\text{m}^3/\text{s})]^{0.25}} \end{aligned} \quad (3.40)$$

The volumetric efficiency η_v should be calculated from the calculated specific speed N_s and flow rate Q (using the data of Figure 3.18). The volumetric efficiency takes into account flow rate Q and leakage flow rate Q_L .

$$\eta_v = \frac{Q}{Q + Q_L} \approx \frac{1}{1 + 5 \left[\frac{\frac{\delta}{r_R} \left(\frac{r_e}{r_2} \right)^2}{\Omega_s^2 \psi} \right]} \quad (3.41)$$

The clearance ratio δ/r_R is typically 0.001 to 0.002.

The mechanical efficiency is defined by

$$\eta_m = 1 - \frac{(C_m/2)\eta_p}{\Omega_s^2 \psi^{5/2}}$$

$$C_m \approx \frac{0.085}{\left(\frac{\Omega r_{t,2}^2}{\nu}\right)^{0.2}} \quad (3.42)$$

The typical value of C_m is $C_m = 0.004$ (at $Re = 4.3 \cdot 10^6$).

To calculate the leakage flow, the details of the individual design pump must be known. Standard methods can be found in Pfleiderer (1961) and Stepanoff (1957). The ratio of mechanical losses power to waterpower P_M/P_w must be determined from the calculated specific speed N_s and flow rate Q (using the data of Figure 3.19). The ratio of impeller disk friction power to waterpower P_{DF}/P_w is determined by

$$\frac{P_{DF}}{P_w} = \frac{10.89}{N_s^{5/3}} \quad (3.43)$$

The equation 3.43 is reliable only from $N_s = 500$ to $N_s = 2000$. If the specific speed is above 2000, the disk friction power is relatively small and can be approximated by

$$\frac{P_{DF}}{P_w} \approx 0.02 \quad (3.44)$$

The impeller disk friction (equation 3.43), which was derived from the maximum efficiency and indirectly from the performance of actual pump, does include those effects of pump design and the operation. These effects are not represented in the usual rotating disk experiments: partial recovery of impeller disk friction energy in the casing, reduction of outer shroud friction due to impeller swirl, and wearing-ring flow. Equation 3.43 gives

a more realistic estimate of the effective disk friction loss of centrifugal pump than the formulas based only on rotating disk experiment. Furthermore, equation 3.43 is limited to water at room temperature and those fluids, which have similar kinematic viscosity. For other viscosities, the rotating disk experiment suggests a correction made by multiplying equation 3.43 by $(\nu/\nu_{\text{water}})^{0.2}$.

The pump overall efficiency is calculated from

$$\eta = \frac{1}{\frac{1}{\eta_H \eta_v} + \frac{P_{DF}}{P_w} + \frac{P_M}{P_w}} \quad (3.45)$$

The calculated pump efficiency from the estimated losses should be close to the experimental data of pump efficiency (using the data of Figure 3.1). The pump overall efficiency is the ratio of waterpower P_w to shaft power P_s . From the calculated pump efficiency, the power necessary to operate the pump is (specific gravity = 1) (see Appendix A).

$$P_s = \frac{(9.8) Q H (\text{specific_gravity})}{\eta} = \frac{P_w}{\eta} \quad (3.46)$$

FIGURES

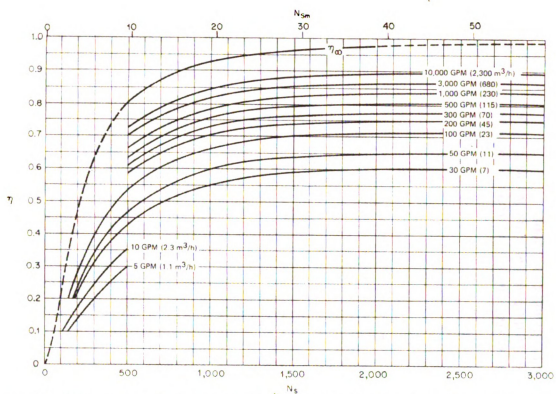


Figure 3.1 Efficiency as a function of specific speed and capacity (after Karassik, I., Krutzsch, W., Fraser, W., and Messina, J., C, 1986)

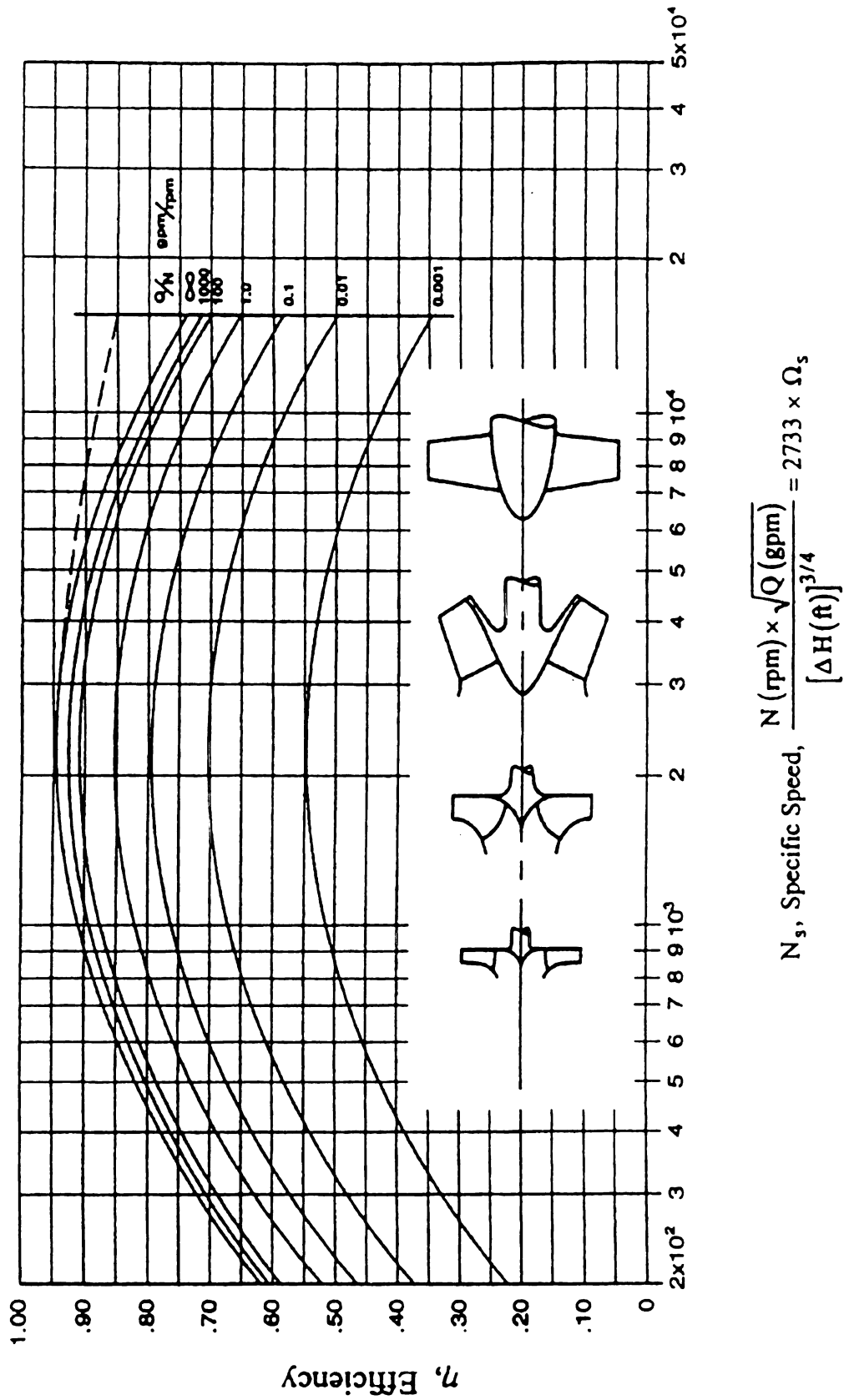


Figure 3.2 Efficiency of centrifugal pumps versus specific speed, size, and shape; Actual experience for $N_s > 2286$ shows higher efficiency, as indicated by the dashed line (after Karassik, I. J., Krutzsch, W., Fraser, W., Messina, J. P., Cooper, P., Heald, C. C., 2001)

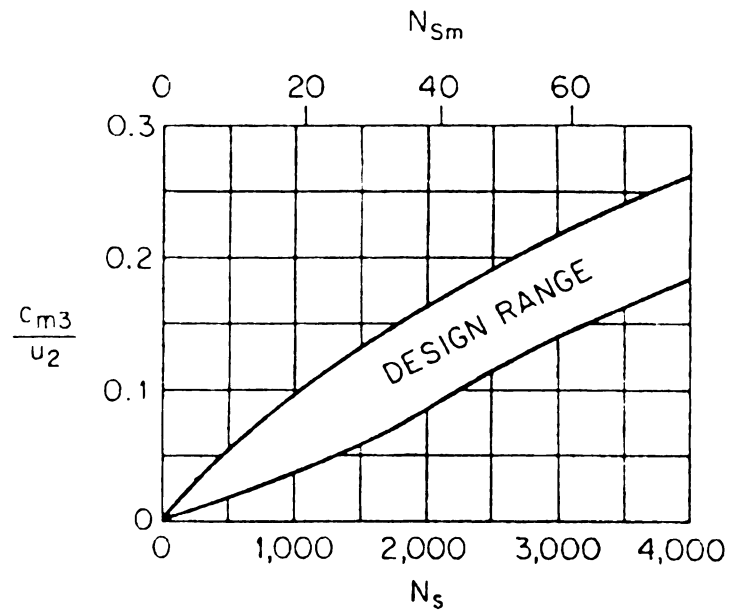


Figure 3.3 C_{m3}/U_2 versus specific speed (after Karassik, I., Krutzsch, W., Fraser, W., and Messina, J., C, 1986)

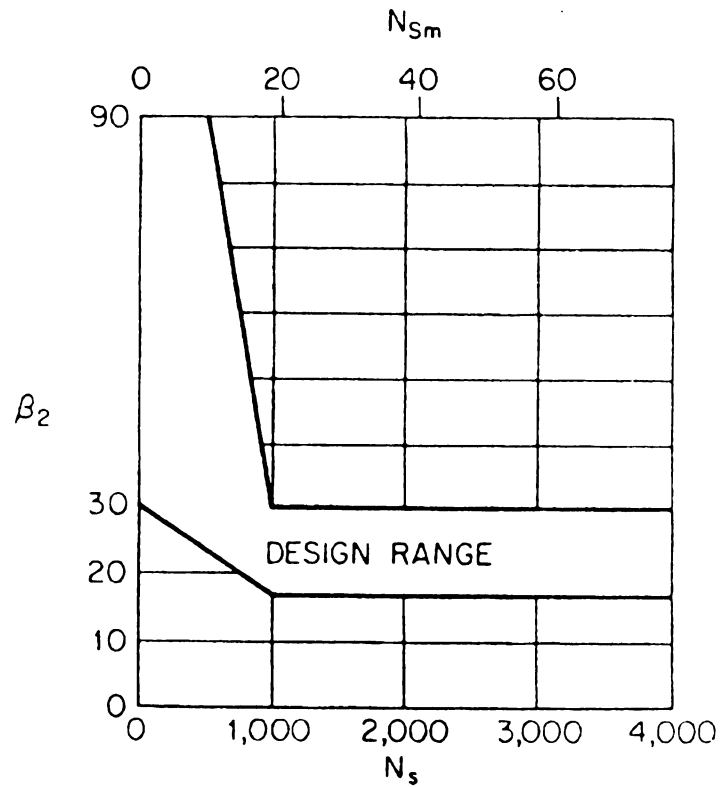


Figure 3.4 Impeller discharge angle versus specific speed (after Karassik, I., Krutzsch, W., Fraser, W., and Messina, J., C, 1986)

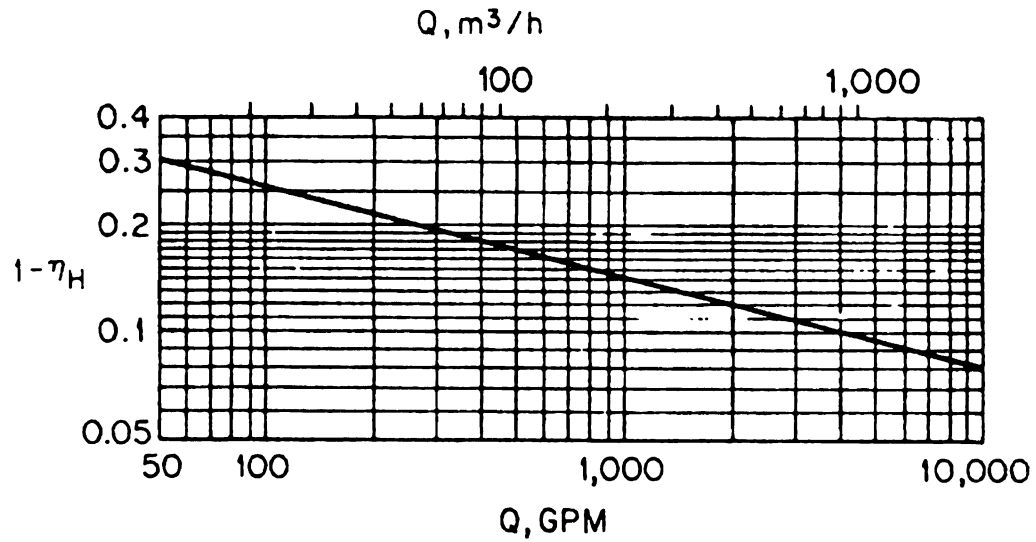


Figure 3.5 Hydraulic efficiency versus capacity (after Karassik, I., Krutzsch, W., Fraser, W., and Messina, J., C, 1986)

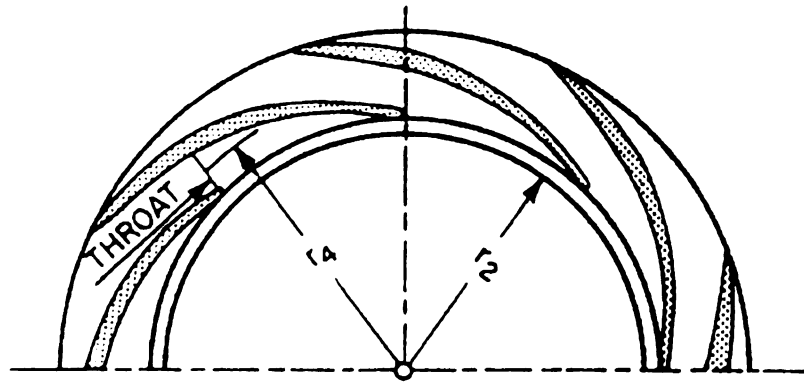


Figure 3.6 Vaned diffuser (after Karassik, I., Krutzsch, W., Fraser, W., and Messina, J., C, 1986)

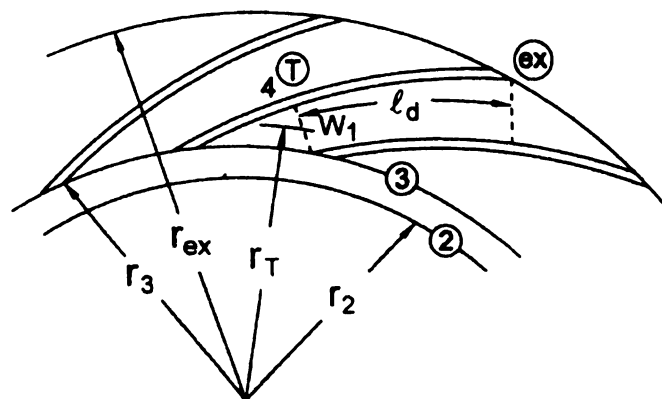


Figure 3.7 Vaned diffuser with throat area (after Karassik, I. J., Krutzsch, W., Fraser, W., Messina, J. P., Cooper, P., and Heald, C. C., 2001)

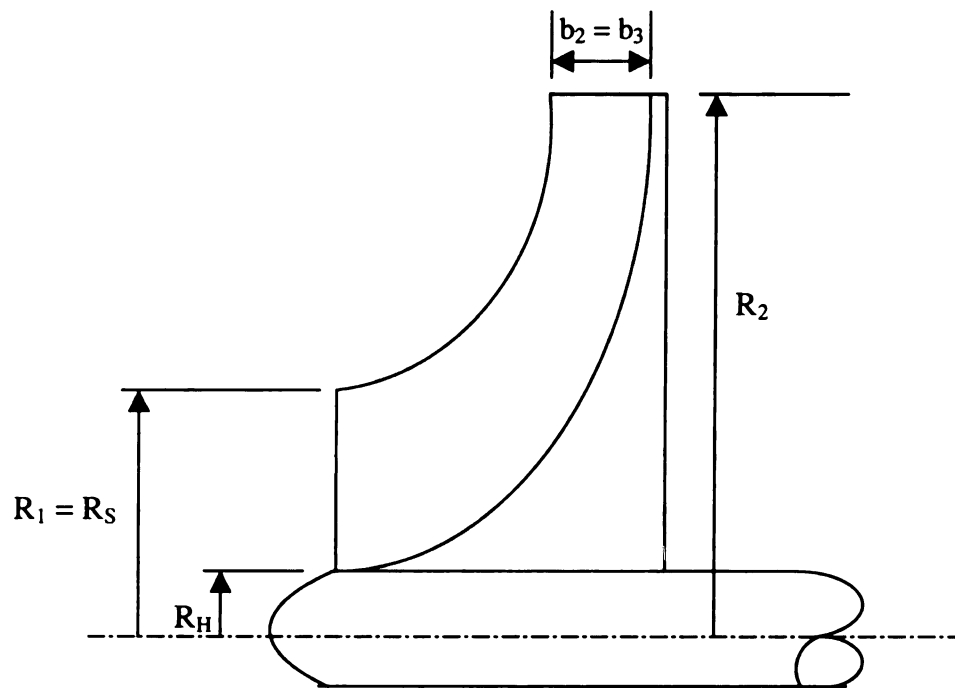


Figure 3.8 Impeller profile

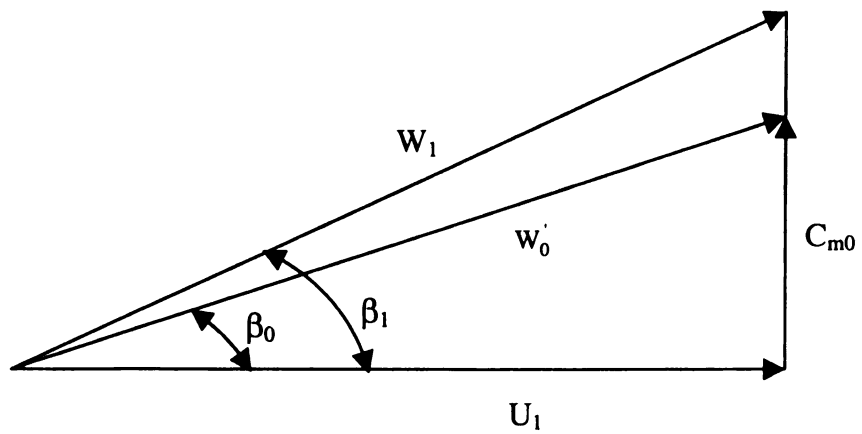


Figure 3.9 Impeller inlet velocity triangles

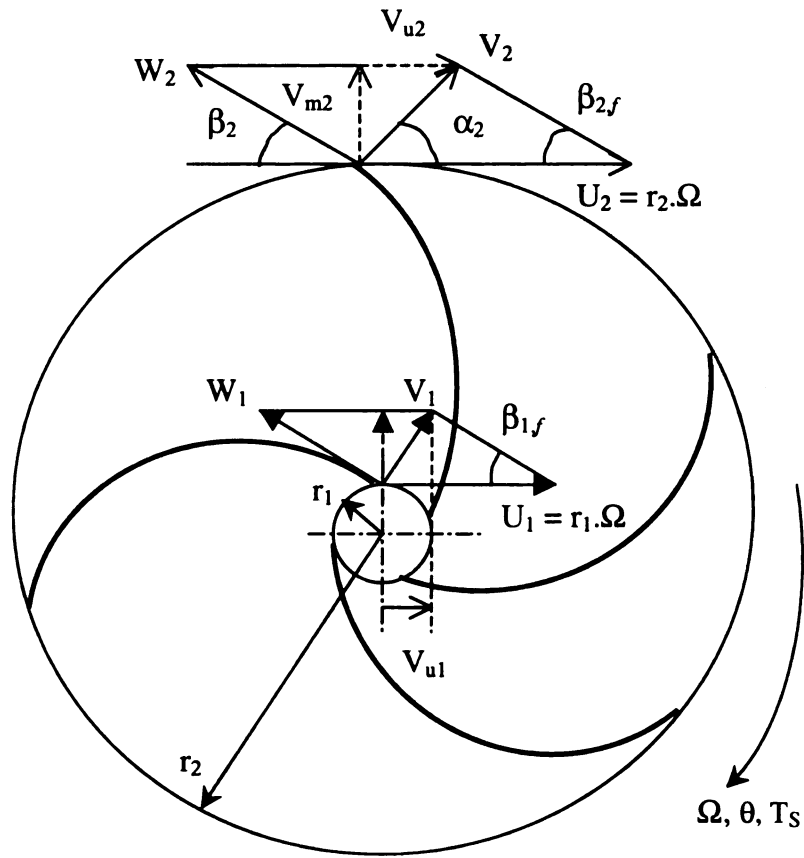


Figure 3.10 Impeller velocity diagrams (1 = inlet; 2 = outlet)

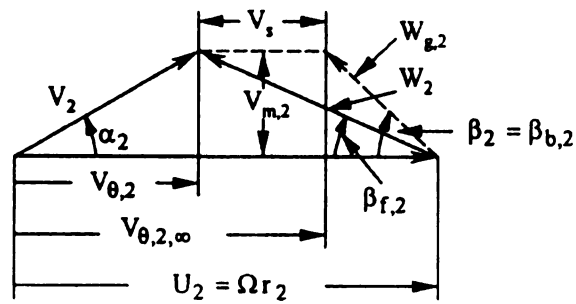


Figure 3.11 Impeller outlet velocity diagram (after Karassik, I. J., Krutzsch, W., Fraser, W., Messina, J. P., Cooper, P., and Heald, C. C., 2001)

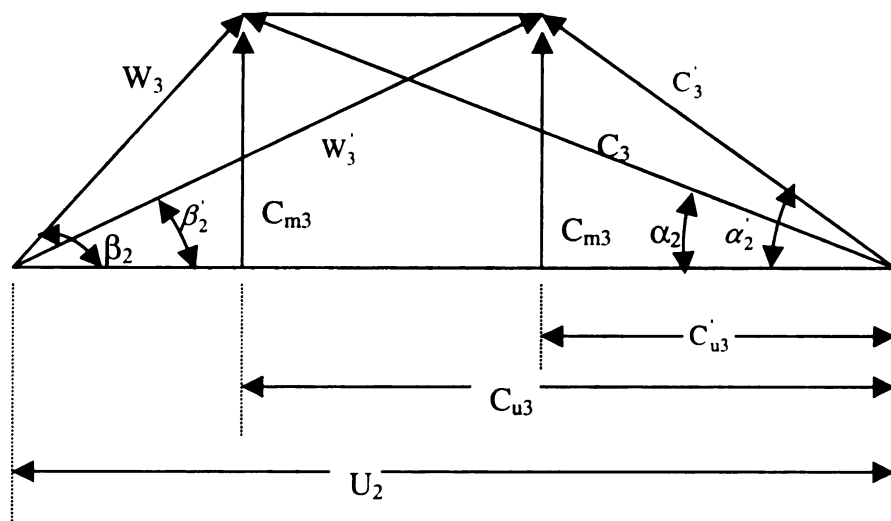


Figure 3.12 Impeller discharge velocity triangles

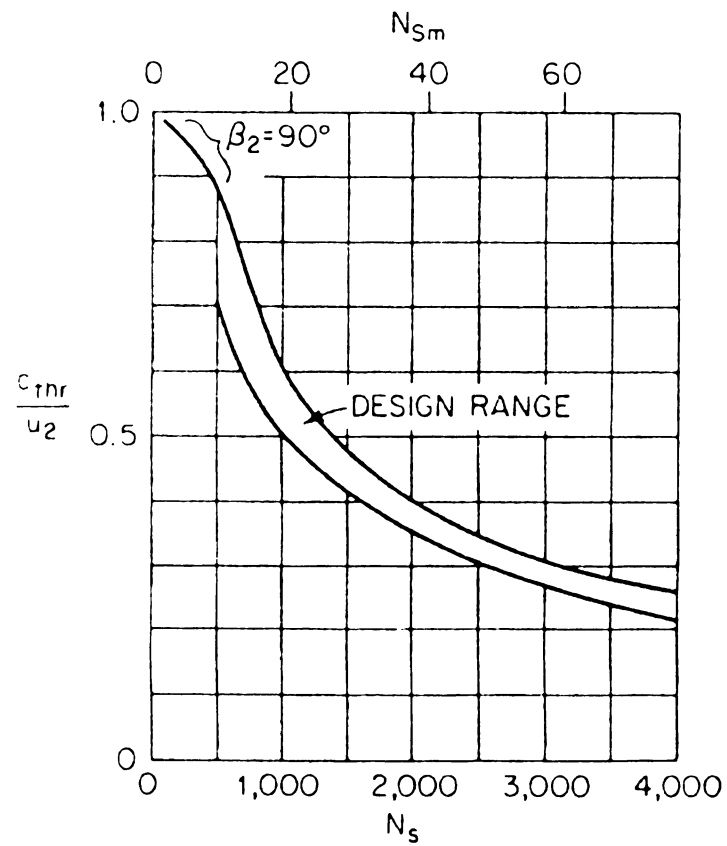


Figure 3.13 C_{thr}/U_2 versus specific speed (after Karassik, I., Krutzsch, W., Fraser, W., and Messina, J., C, 1986)

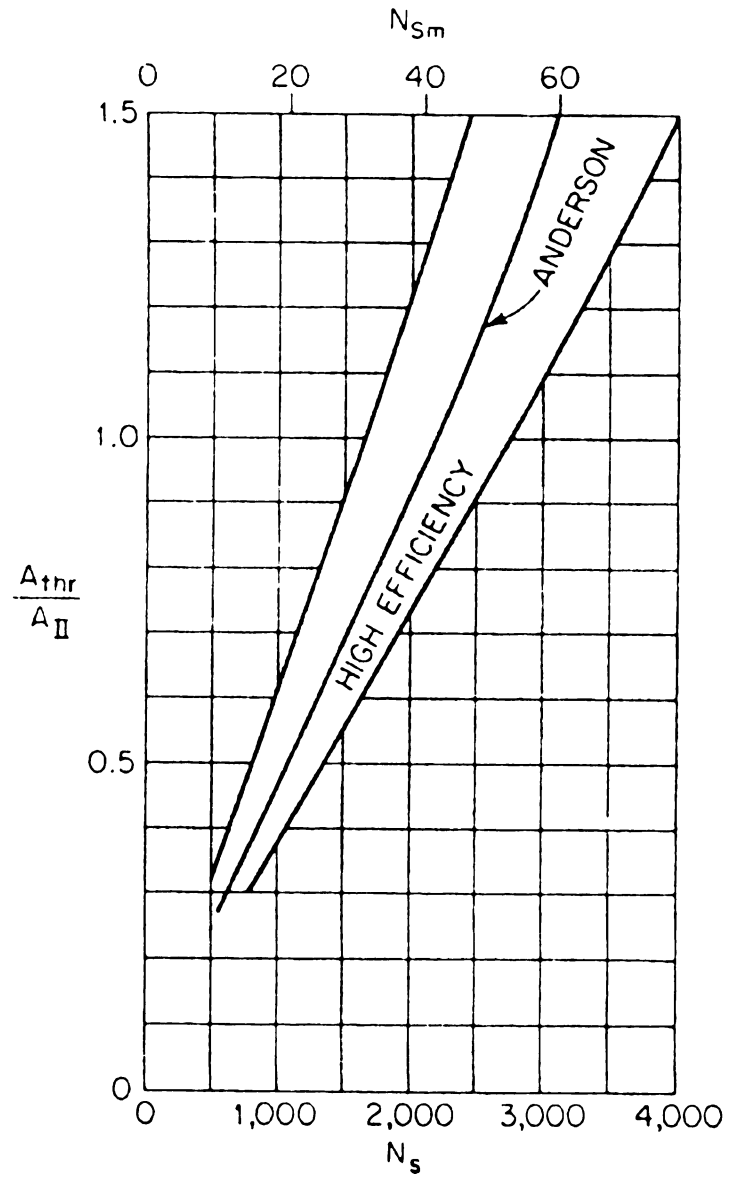


Figure 3.14 A_{thr}/A_{II} versus specific speed (after Karassik, I., Krutzsch, W., Fraser, W., and Messina, J., C, 1986)

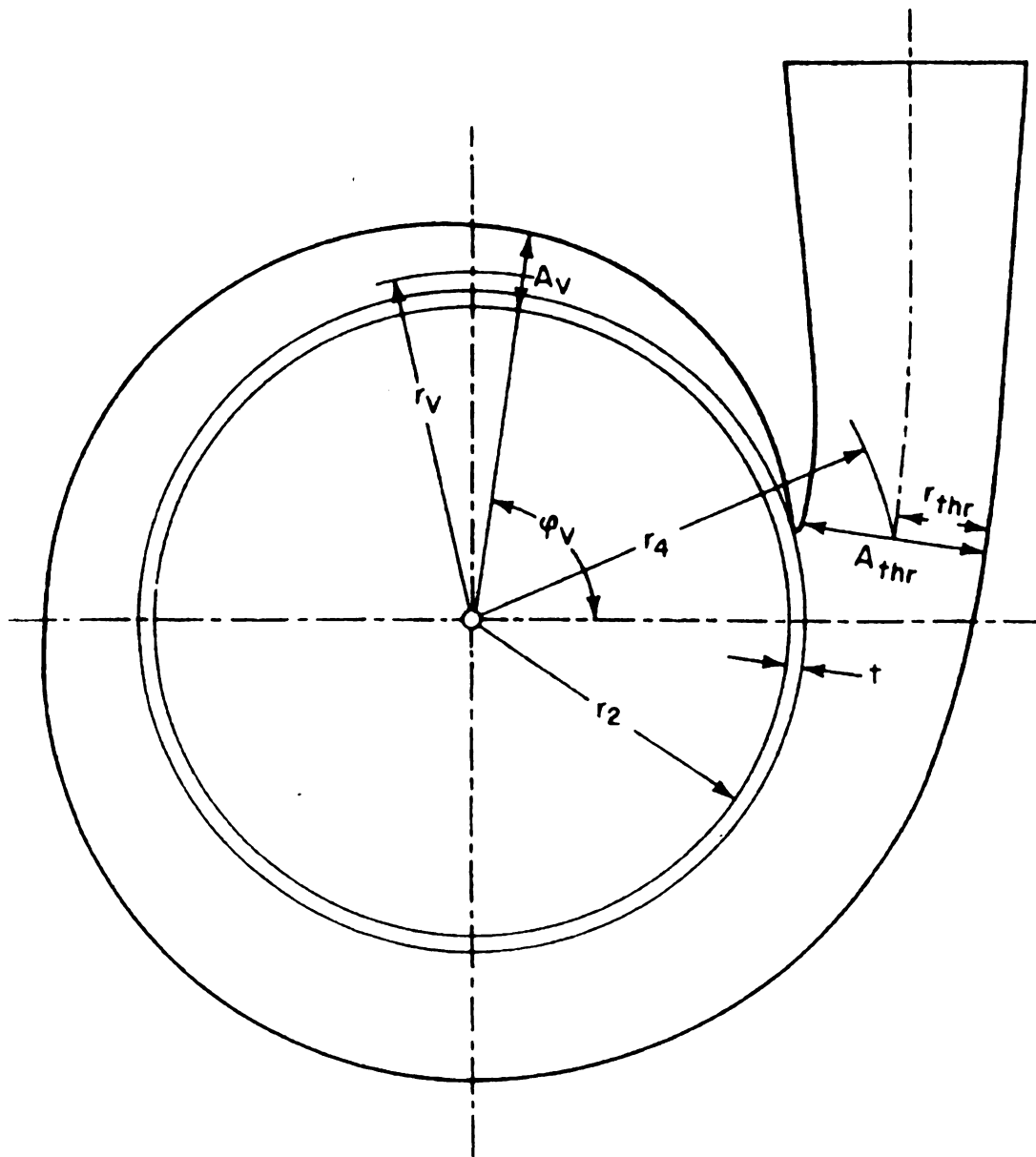


Figure 3.15 Volute casing (after Karassik, I., Krutzsch, W., Fraser, W., and Messina, J., C, 1986)

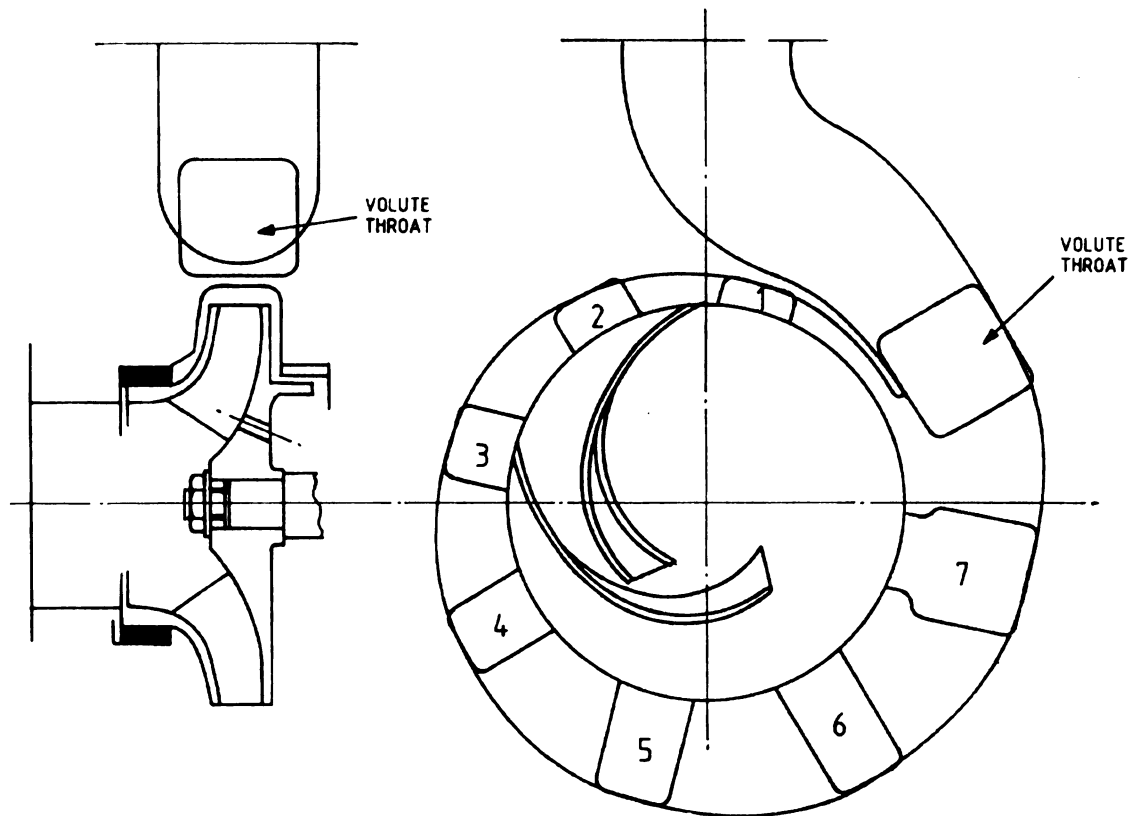


Figure 3.16 The plan view of the impeller and the volute casing with leading dimensions (after Turton, R. K., 1994)

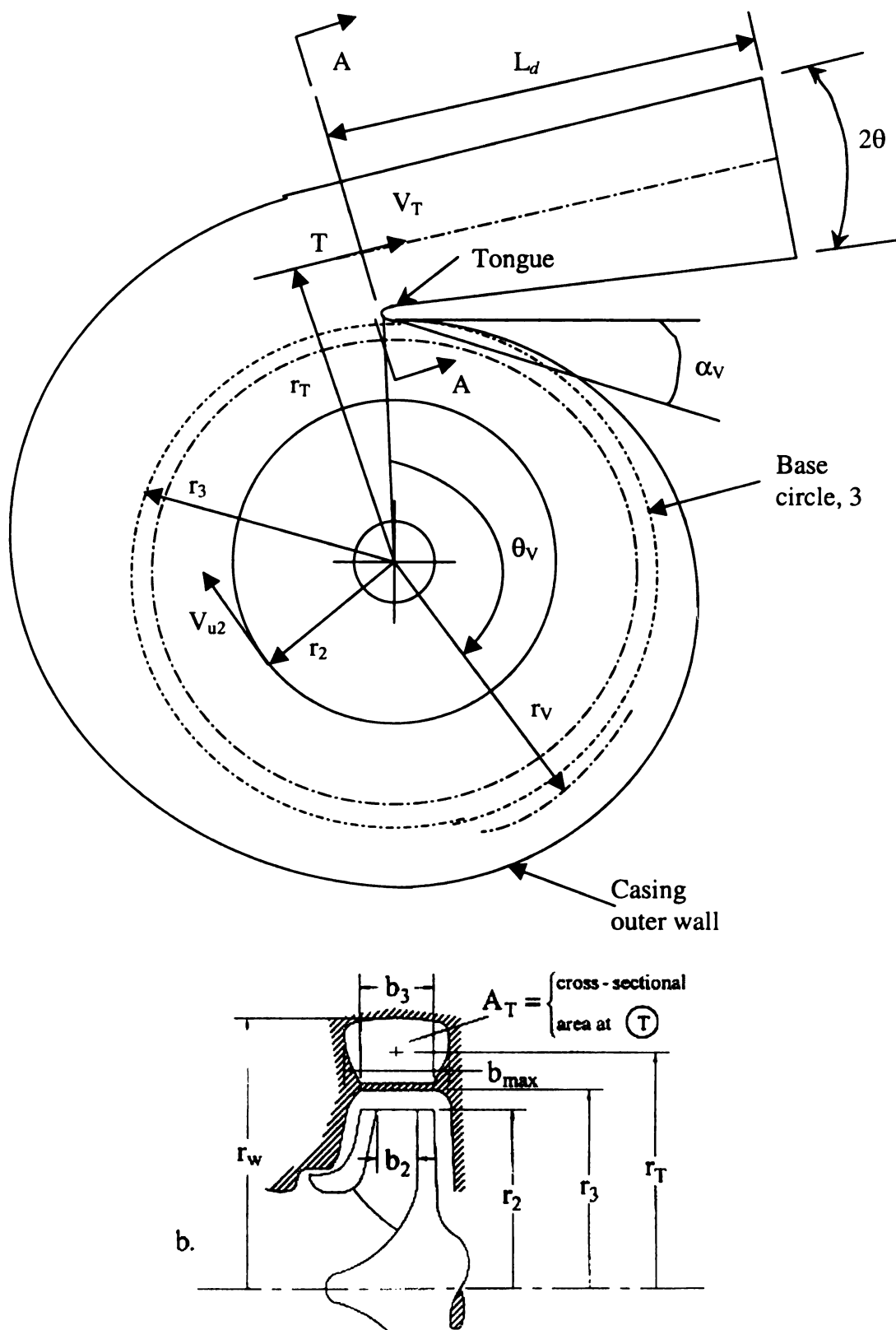


Figure 3.17 Volute casing: a) Polar view; b) Meridional view including Section A-A of throat T

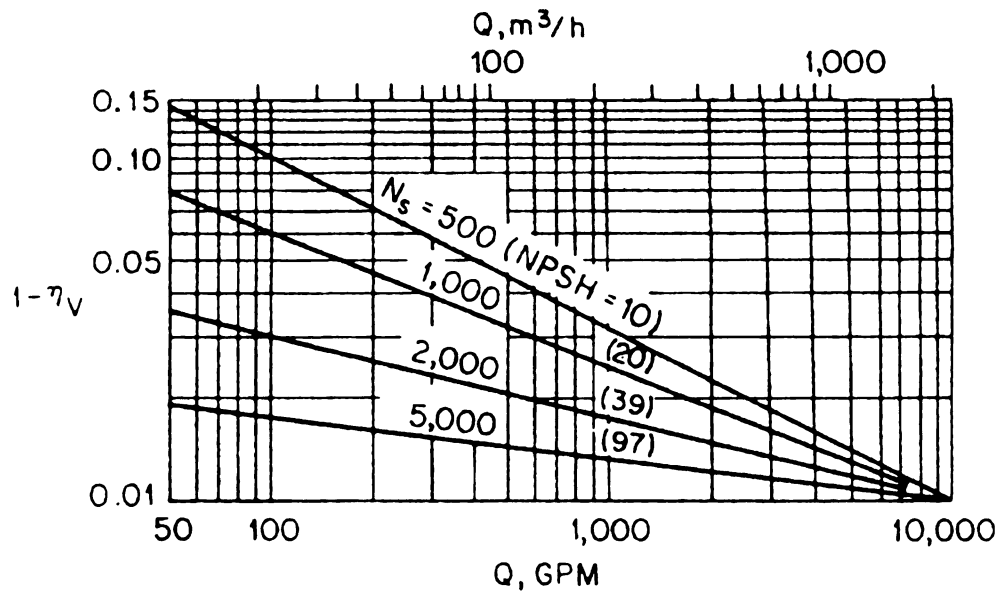


Figure 3.18 Volumetric efficiency as a function of specific speed and capacity (after Karassik, I., Krutzsch, W., Fraser, W., and Messina, J., C, 1986)

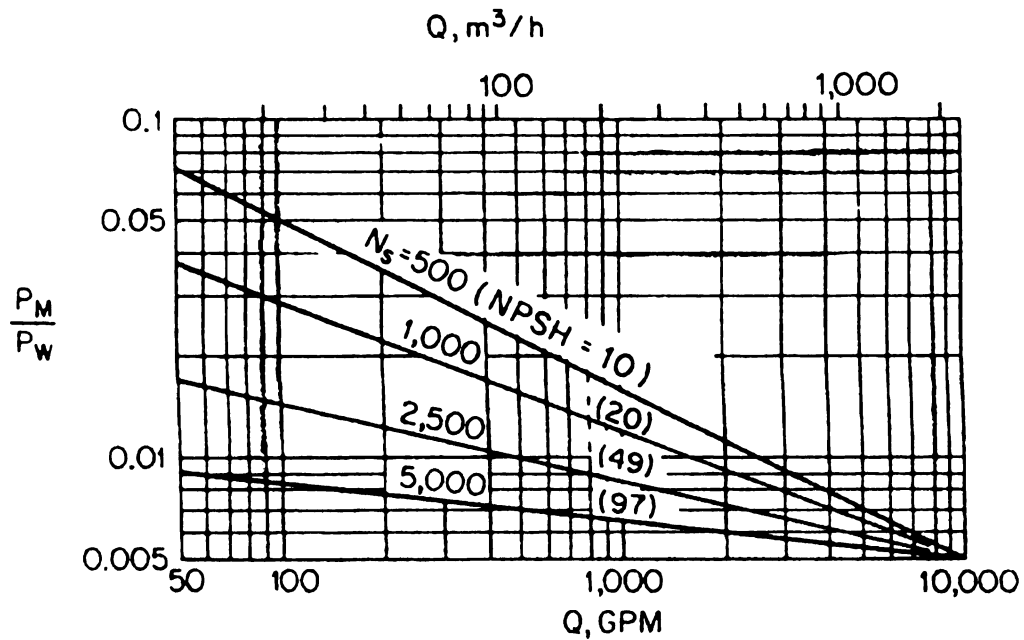


Figure 3.19 Ratio of mechanical power loss to water-power as a function of specific speed and capacity (after Karassik, I., Krutzsch, W., Fraser, W., and Messina, J., C, 1986)

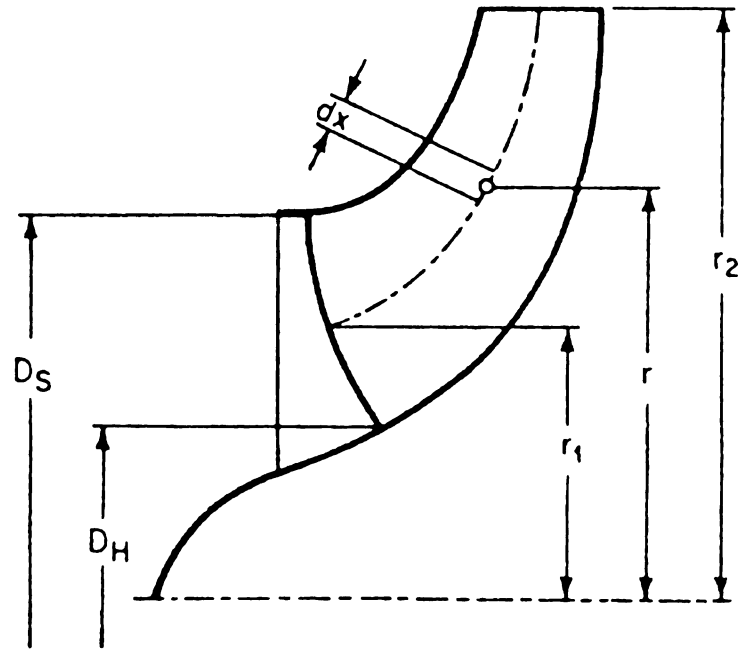


Figure 3.20 Impeller with vanes extended into axial inlet (after Karassik, I., Krutzsch, W., Fraser, W., and Messina, J., C, 1986)

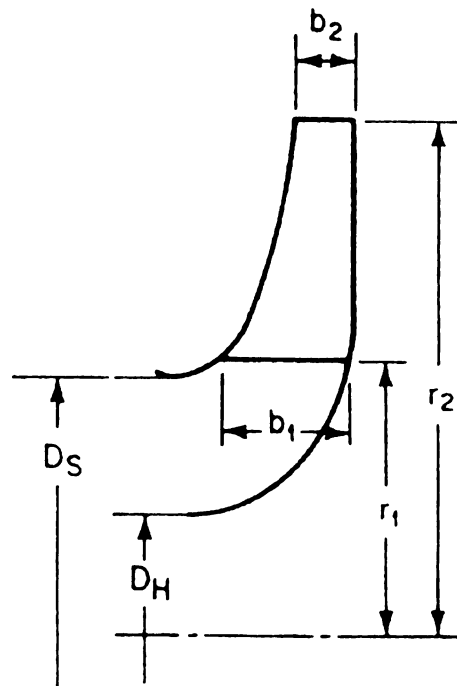


Figure 3.21 Impeller with cylindrical vanes (after Karassik, I., Krutzsch, W., Fraser, W., and Messina, J., C, 1986)

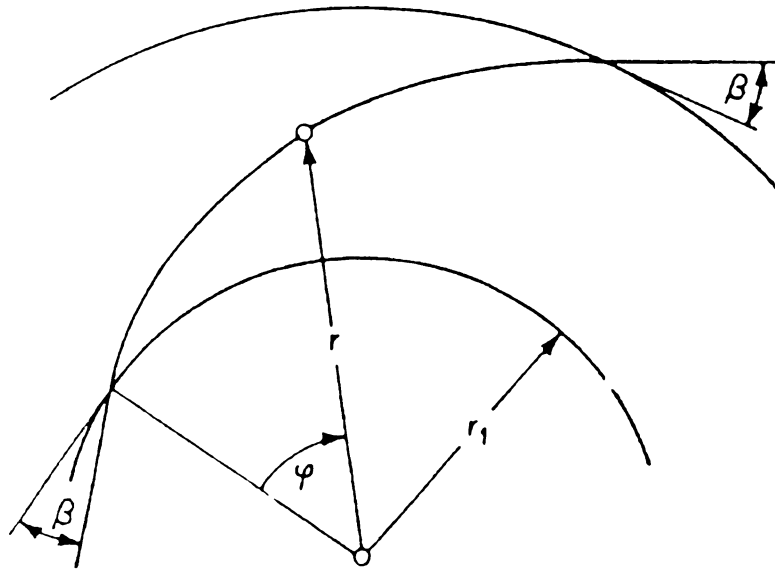


Figure 3.22 Logarithmic spiral (after Karassik, I., Kruttsch, W., Fraser, W., and Messina, J., C, 1986)

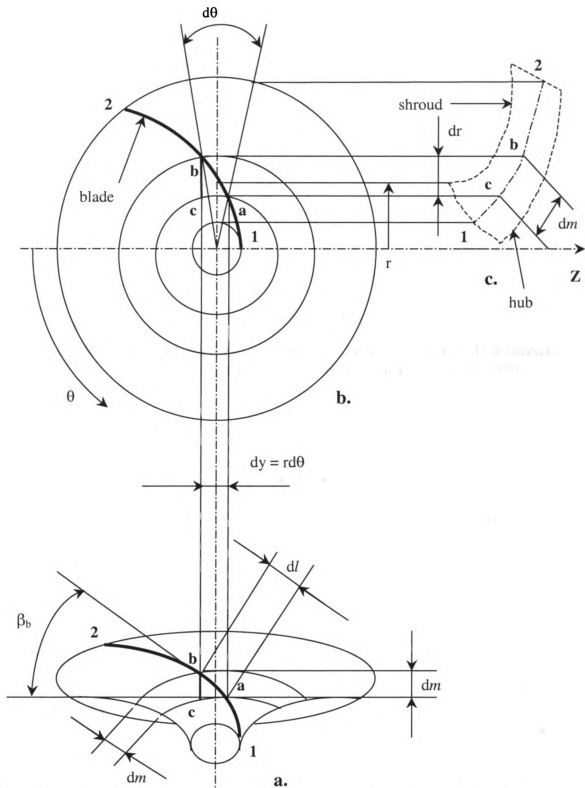


Figure 3.23 Blade construction: a) View of construction surface of revolution; b) Polar view; c) Meridional view

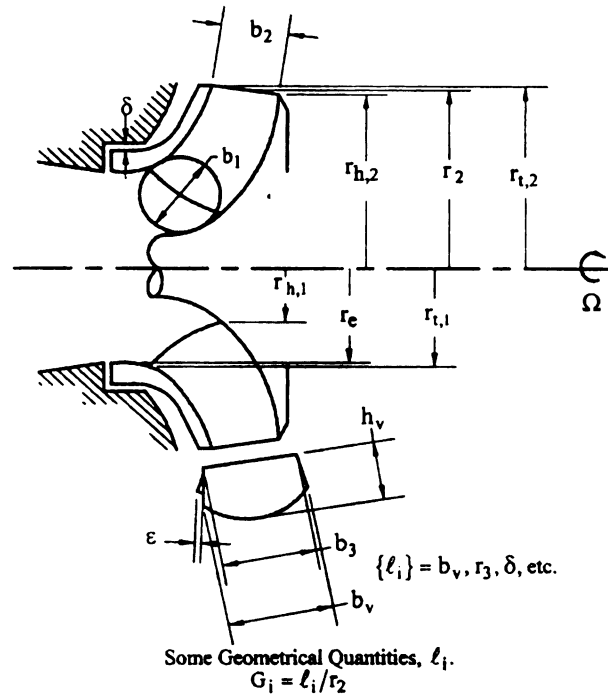


Figure 3.24 Defining the geometry of a pump stage (after Karassik, I. J., Krutzsch, W., Fraser, W., Messina, J. P., Cooper, P., and Heald, C. C., 2001)

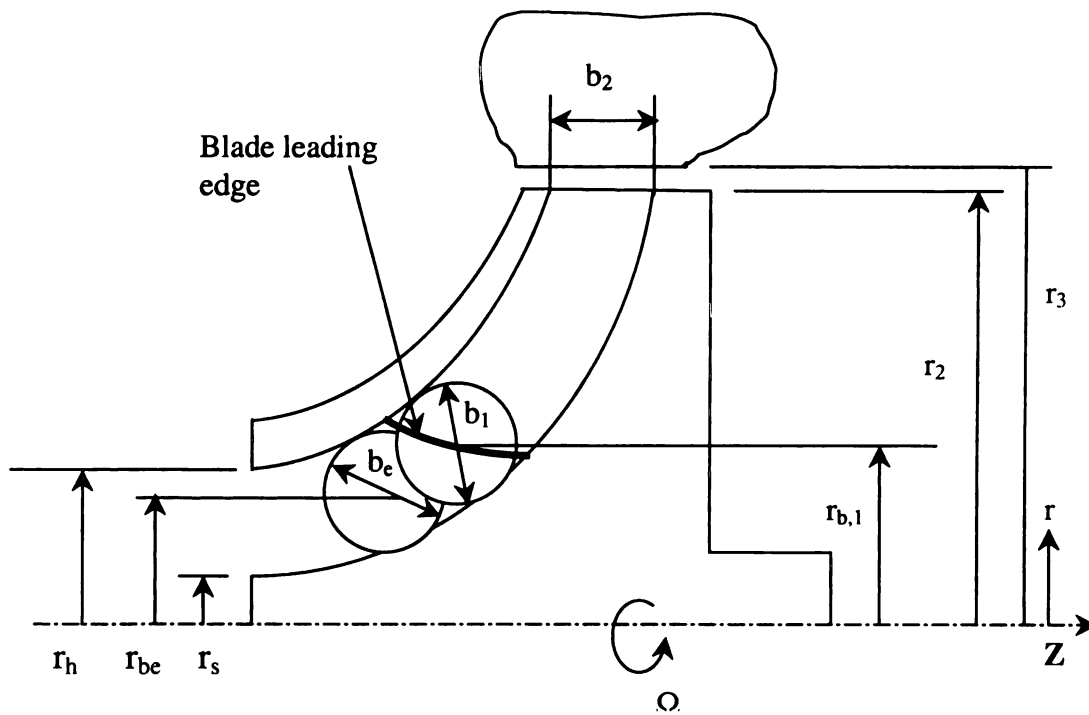


Figure 3.25 Hub and shroud profiles of centrifugal pump impeller

Chapter 4

UNCONVENTIONAL CENTRIFUGAL PUMP DESIGN METHOD

4.1 Analysis of Un-Conventional Centrifugal Pump Design

The flow of fluid through a centrifugal pump is considered as a superposition of a free-vortex flow over a radial through-flow. The path of the incompressible fluid under this condition is a logarithmic or equiangular spiral with a constant angle between the tangents to the path of the fluid at any point and the radius at that point.

A logarithmic vane impeller would not force the fluid to follow any particular path. Hence, this kind of impeller would let the fluid follow its own path and would not create adverse pressure gradients.

The energy received by the liquid as it follows through the inter-vane passage can be expressed as the difference in the moment of momentum of the peripheral and relative velocities at the inlet and outlet circumference of the impeller vane. Figure 4.9 shows the velocity triangles at the inlet and outlet.

The analysis of un-conventional centrifugal pump design includes the following sections:

- (1) Circulation head (H_c)
- (2) Impeller friction head loss (H_f)
- (3) Volute head loss (H_v)
- (4) Power due to disk friction loss (P_d), power due to leakage loss (P_L), and entrance-bend loss (H_{eb})

the

ce

1.1

$\frac{d}{dt}$

For

ce

For

2.

con

$\frac{d}{dt}$

For

\int
cs

(5) Optimization with respect to number of blades and blade angle of a logarithmic vane impeller.

(6) Derivation of Euler's Head (H_e)

(7) Determination of Logarithmic blade length (L)

The three equations of integral conservation laws in fluid mechanics are used for the arbitrary non-deformable control volume over the fluid body in un-conventional centrifugal pump design method.

1. Integral continuity equation (Mass conservation)

$$\frac{d}{dt} \left[\int_{\text{Control-Volume}} \rho dV \right] + \int_{\text{Control-Surface}} \rho (\vec{U} - \vec{U}_b) \cdot \vec{n} dS = \frac{d}{dt} \left[\int_{\text{C.V.}} \rho dV \right] + \int_{\text{C.S.}} d\dot{m} = 0 \quad (4.1)$$

$$\text{For the steady flow: } \frac{d}{dt} \left[\int_{\text{Control-Volume}} \rho dV \right] = 0 \quad (4.2)$$

$$\int_{\text{Control-Surface}} \rho (\vec{U} - \vec{U}_b) \cdot \vec{n} dS = \int_{\text{C.S.}} d\dot{m} = 0 \quad (4.3)$$

$$\text{For the steady uniform flow: } \dot{m} = \rho_1 A_1 V_1 = \rho_2 A_2 V_2 \quad (4.4)$$

2. Integral linear momentum equation, "Navier-Stokes equation" (Linear momentum conservation)

$$\frac{d}{dt} \left[\int_{\text{C.V.}} \rho \vec{U} dV \right] + \int_{\text{C.S.}} \rho (\vec{U} - \vec{U}_b) (\vec{U} \cdot \vec{n}) dS = \frac{d}{dt} \left[\int_{\text{C.V.}} \rho \vec{U} dV \right] + \int_{\text{C.S.}} \vec{U} d\dot{m} = \Sigma \vec{F} \quad (4.5)$$

$$\text{For the steady flow: } \frac{d}{dt} \left[\int_{\text{C.V.}} \rho \vec{U} dV \right] = 0 \quad (4.6)$$

$$\int_{\text{C.S.}} \rho (\vec{U} - \vec{U}_b) (\vec{U} \cdot \vec{n}) dS = \int_{\text{C.S.}} \vec{U} d\dot{m} = \Sigma \vec{F} \quad (4.7)$$

For

Fr

In

gi

p

Δ

inc

It

Th

bo

eq

en

an

cha

fro

eith

circ

stre

For the steady uniform flow: $\Sigma F = (\rho_1 A_1 V_1) V_1 - (\rho_2 A_2 V_2) V_2$
 $\Sigma F = \dot{m}(V_1 - V_2)$ (4.8)

From the differential linear momentum equation, the Euler's equation was derived as:

$$dP = -\rho V dV \quad (4.9)$$

Integrating the Euler's equation between two points "1" and "2" along the streamline gives:

$$\frac{\rho V_2^2}{2} + P_2 = \frac{\rho V_1^2}{2} + P_1 = \text{Constant} \quad (\text{Along a streamline or throughout the flow}) \quad (4.10)$$

$$\Delta P = \frac{\rho (\Delta V^2)}{2}$$

The above equation is Bernoulli's equation. From this equation, when the velocity increases, the pressure decreases, and when the velocity decreases, the pressure increases. It is important to see that Bernoulli's equation was derived from the momentum equation. This is a statement of Newton's second law for an inviscid, incompressible flow with no body forces. The term, $\rho V^2/2$, is the kinetic energy per unit volume. The Bernoulli's equation states that the pressure gradient (boost), ΔP , is proportional to the kinetic energy, " $\rho V^2/2$ ". Hence, Bernoulli's equation is also a relation for mechanical energy in an incompressible flow, and the work done on a fluid by pressure forces is equal to the change in kinetic energy of the flow. Furthermore, Bernoulli's equation can be derived from the integral energy equation. In general, Bernoulli's equation can be interpreted as either Newton's second law or an energy equation.

In applying the differential linear momentum equations, when there is additional circulation and so the rotational speed " ω " is equal to zero, Bernoulli's equation across streamlines can be used over the fluid particles. When there is no additional circulation

and

across

3. In

$$\frac{d}{dt} \left[\frac{1}{2} \rho \int_C \right]$$

For the

$$\int_{CS} \rho$$

$$\int_{CS} \rho$$

For the

$$\left(\frac{V_z^2}{2} \right)$$

$$\left(\frac{V_z^2}{2} \right)$$

$$Q \left(\frac{1}{2} \right)$$

equation

stream

and so the rotational speed “ ω ” is not equal to zero, the full Navier Stokes equation across streamlines must be used over the fluid particles.

3. Integral energy equation (Energy conservation)

$$\frac{d}{dt} \left[\int_{C.V.} \rho \left(\tilde{u} + \frac{V^2}{2} + g z \right) dV \right] + \int_{C.S.} \rho \left(\tilde{u} + \frac{V^2}{2} + g z + \frac{P}{\rho} \right) (\tilde{U} \cdot \tilde{n}) dS = \dot{Q} - \Sigma \dot{W} \quad (4.10)$$

$$\text{For the steady flow: } \frac{d}{dt} \left[\int_{C.V.} \rho \left(\tilde{u} + \frac{V^2}{2} + g z \right) dV \right] = 0 \quad (4.11)$$

$$\int_{C.S.} \rho \left(\tilde{u} + \frac{V^2}{2} + g z + \frac{P}{\rho} \right) (\tilde{U} \cdot \tilde{n}) dS = \dot{Q} - \Sigma \dot{W} \quad (4.12)$$

$$\int_{C.S.} \rho \left(\frac{V^2}{2} + g z + \frac{P}{\rho} \right) (\tilde{U} \cdot \tilde{n}) dS + \text{losses} = \Sigma \dot{W}$$

For the steady uniform flow:

$$\begin{aligned} \left(\frac{V_2^2}{2} + \frac{P_2}{\rho_2} + g z_2 + \tilde{u}_2 \right) - \left(\frac{V_1^2}{2} + \frac{P_1}{\rho_1} + g z_1 + \tilde{u}_1 \right) &= \frac{\dot{Q} - \dot{W}_s}{\dot{m}} = \frac{\dot{Q} - \dot{W}_s}{\rho Q} \\ \left(\frac{V_2^2}{2} + \frac{P_2}{\rho_2} + g z_2 \right) - \left(\frac{V_1^2}{2} + \frac{P_1}{\rho_1} + g z_1 \right) + \text{losses} &= \frac{-\dot{W}_s}{\dot{m}} = \frac{-\dot{W}_s}{\rho Q} = \frac{-(\text{Shaft work})}{\rho Q} \\ Q \left(\frac{\rho V_2^2}{2} + P_2 + \rho g z_2 \right) - Q \left(\frac{\rho V_1^2}{2} + P_1 + \rho g z_1 \right) + \text{losses} &= -\dot{W}_s = \text{Energy} \end{aligned} \quad (4.13)$$

The Bernoulli equation (a simplified form of conservation of the integral energy equation) of inviscid flow, steady flow, incompressible flow ($\rho = \text{constant}$), flow along a streamline is written between two point “1” and “2” along the streamline as follows:

$$\frac{\rho V_2^2}{2} + P_2 + \rho g z_2 = \frac{\rho V_1^2}{2} + P_1 + \rho g z_1 = \text{Constant} \quad (4.14)$$

$$Q \left(\frac{\rho V_2^2}{2} + P_2 + \rho g z_2 \right) = Q \left(\frac{\rho V_1^2}{2} + P_1 + \rho g z_1 \right) = \text{Constant Energy} \quad (4.15)$$

and t

If z_1

Or: Q

4.2 C

Euler

and h

the re

relativ

circul

veloci

the di

outlet

impell

The sh

Substit

In the above equation, the term, “ $\rho V^2/2$ ”, is the “kinetic energy per unit volume”, and the term, “ $\rho g z$ ”, is the “potential energy per unit volume”.

$$\text{If } z_1 = z_2 = \text{Constant: } \frac{\rho V_2^2}{2} + P_2 = \frac{\rho V_1^2}{2} + P_1 = \text{Constant} \quad (4.16)$$

$$\text{Or: } Q \left(\frac{\rho V_2^2}{2} + P_2 \right) = Q \left(\frac{\rho V_1^2}{2} + P_1 \right) = \text{Constant Energy} \quad (4.17)$$

4.2 Circulation Head (H_c)

Euler’s head equation for an infinite number of blades (see Section 4.7) is:

$$H_e = \frac{U_2 V_2 \cos(\alpha_2) - U_1 V_1 \cos(\alpha_1)}{g} \quad (4.18)$$

This expression does not include the effect of a finite number of impeller vanes and head losses in the impeller. Besides this, channel circulation in the impeller reduces the relative velocity, W , at the leading surface of the impeller vane and increases the relative velocity, W , at the trailing surface of the vane (Figure 4.10 c). The channel circulation of the fluid contributes a slip velocity, S_1 , in the direction of the peripheral velocity, U_1 , to the absolute velocity, V_1 , at the impeller inlet, and a slip velocity, S_2 , in the direction opposite to the peripheral velocity, U_2 , to the absolute velocity, V_2 , at the outlet circumference of the impeller. As a result, the actual head, H_a , developed by the impeller with a finite number of blades and the slip factor effect is:

$$H_a = \frac{U_2 V_2' \cos(\alpha_2') - U_1 V_1' \cos(\alpha_1')}{g} \quad (4.19)$$

The slip head due to channel circulation is:

$$H_c = H_e - H_a \quad (4.20)$$

Substituting H_e and H_a gives:

in

nu

th

Th

Ac

Th

"S.

are

The

App

$$H_c = \frac{U_2(V_2 \cos(\alpha_2) - V_2' \cos(\alpha_2')) + U_1(V_1' \cos(\alpha_1') - V_1 \cos(\alpha_1))}{g} \quad (4.21)$$

The circulation head, H_c , will approach to zero if there are an infinite number of impeller blades. The value of circulation head, H_c , may be considerable for a small number of blades in an impeller. The slip velocities, S_1 , and, S_2 , at the inlet and outlet of the impeller blades are defined as:

$$S_1 = V_1' \cos(\alpha_1') - V_1 \cos(\alpha_1) \quad (4.22)$$

$$S_2 = V_2 \cos(\alpha_2) - V_2' \cos(\alpha_2') \quad (4.23)$$

The circulation head is written as follows:

$$H_c = \frac{U_2 S_2 + U_1 S_1}{g} \quad (4.24)$$

According to Stodola, the slip velocities, S_1 , and, S_2 , are given by:

$$S_1 = U_1 K_s (\pi/Z) \sin(\beta_1) \quad (4.25)$$

$$S_2 = U_2 K_s (\pi/Z) \sin(\beta_2) \quad (4.26)$$

The logarithmic vane impeller has an equiangular spiral with a constant angle. Therefore, the blade inlet and exit angles are equal, $\beta_1 = \beta_2 = \beta$. Substituting “ S_1 ” and “ S_2 ” into the equation of circulation head, H_c , gives:

$$H_c = \frac{\pi K_s \sin(\beta)(U_2^2 + U_1^2)}{g Z} \quad (4.27)$$

The centrifugal pump geometrical parameters used for the following calculations are determined from volute constants (Figure 4.1) and impeller constants (Figure 4.2). The calculation procedure of centrifugal pump geometrical parameters can be found from Appendix B.

T

R

fa

th

he

tr

4

gi

the

bla

to t

The peripheral velocities, U_1 , and, U_2 , are given by:

$$U_1 = \frac{\omega d_1}{2} \quad (4.28)$$

$$U_2 = \frac{\omega d_2}{2} \quad (4.29)$$

Rewriting the circulation head equation due to a finite number of impeller blades and slip factor effect gives:

$$H_c = \frac{\pi K_s \omega^2 \sin(\beta)(d_2^2 + d_1^2)}{4 g Z} \quad (4.30)$$

The circulation head, H_c , is inversely proportional to the number of vanes, Z , in the impeller. This circulation head is not an energy loss. Nevertheless, this circulation head can constitute a reduction in the effectiveness of the blade impeller when transferring energy from the shaft to the fluid.

4.3 Impeller Friction Head Loss (H_f)

The impeller friction head loss, H_f , due to fluid friction in non-circular ducts is given by Darcy's equation.

$$H_f = \frac{\lambda L V^2}{2 g D} \quad (4.31)$$

From Darcy's equation, the friction head loss, H_f , is proportional to the square of the velocity, V^2 , and inversely proportional to the hydraulic diameter, D . The logarithmic blade length (see Section 4.8) is given by

$$L = \frac{d_2 - d_1}{2 \sin(\beta)} \quad (4.32)$$

From the equation of friction head loss, the friction head loss, H_f , is proportional to the square of the velocity, V^2 . As a result, the following method is used to obtain,

v

bl

in

the

pas

The

exp

relat

V^2/D , in Darcy's equation. The relative velocities on the leading and trailing sides of the blade are $(W-S)$ and $(W+S)$ due to channel circulation (Figure 4.10 c). The mean velocity in the section behind the blade is $(W+S/2)$ and the mean velocity in the section in front of the blade is $(W-S/2)$. Because of the consideration for the mean velocity, the whole blade passage is split into two halves. The term of " V^2/D " is written as:

$$\frac{V^2}{D} = \frac{1}{2} \left[\frac{\bar{V}_{\text{behind}}^2}{D} + \frac{\bar{V}_{\text{front}}^2}{D} \right] = \frac{1}{2} \left[\frac{(W + 0.5S)^2 + (W - 0.5S)^2}{D} \right] \quad (4.33)$$

$$\frac{V^2}{D} = \frac{W^2 + 0.25S^2}{D} \quad (4.34)$$

The average of " V^2/D " between the blade inlet and blade exit is:

$$\frac{V^2}{D} = \frac{1}{2} \left[\frac{W_1^2 + 0.25S_1^2}{D_1} + \frac{W_2^2 + 0.25S_2^2}{D_2} \right] \quad (4.35)$$

Substituting " V^2/D " and " L " into the friction head loss equation, H_f , the new expression for the friction head loss due to friction in the impeller is:

$$H_f = \frac{\lambda L V^2}{2 g D} = \frac{\lambda (d_2 - d_1)}{8 g \sin(\beta)} \left[\frac{W_1^2 + 0.25 S_1^2}{D_1} + \frac{W_2^2 + 0.25 S_2^2}{D_2} \right] \quad (4.36)$$

$$H_f = \frac{\lambda (d_2 - d_1)}{8 g \sin(\beta)} \left[\frac{W_1^2}{D_1} + \frac{W_2^2}{D_2} + \frac{0.25 S_1^2}{D_1} + \frac{0.25 S_2^2}{D_2} \right]$$

By including the total blockage area at inlet and outlet of vane impeller, the relative velocities at the inlet and exit of the impeller blade are given by:

$$W_1 = \frac{Q}{b_1 (\pi d_1 \sin(\beta) - Z t)} \quad (4.37)$$

$$W_2 = \frac{Q}{b_2 (\pi d_2 \sin(\beta) - Z t)} \quad (4.38)$$

peri

The

Sub

Sub

imp

was

The hydraulic diameter, D , is calculated from the wetted parameter, P , (the perimeter of the cross-section) by:

$$D = \frac{4 A}{P} \quad (4.39)$$

The inlet and exit hydraulic diameters of the blade impeller are:

$$D_1 = \frac{2 b_1 (\pi d_1 \sin(\beta) - Z t)}{(\pi d_1 \sin(\beta) - Z t + Z b_1)} \quad (4.40)$$

$$D_2 = \frac{2 b_2 (\pi d_2 \sin(\beta) - Z t)}{(\pi d_2 \sin(\beta) - Z t + Z b_2)} \quad (4.41)$$

Substituting S_1 , S_2 , W_1 , W_2 , D_1 , and D_2 into the friction head loss equation gives

$$\begin{aligned} H_f = & \frac{\lambda (d_2 - d_1) Q^2}{16 g \sin(\beta)} \left[\frac{\pi d_1 \sin(\beta) - Z t + Z b_1}{b_1^3 (\pi d_1 \sin(\beta) - Z t)^3} + \frac{\pi d_2 \sin(\beta) - Z t + Z b_2}{b_2^3 (\pi d_2 \sin(\beta) - Z t)^3} \right] + \\ & + \frac{\lambda (d_2 - d_1) K_s^2 \pi^2 \sin(\beta)}{16 g Z^2} \left[\frac{U_1^2 (\pi d_1 \sin(\beta) - Z t + Z b_1)}{b_1 (\pi d_1 \sin(\beta) - Z t)} + \right. \\ & \left. + \frac{U_2^2 (\pi d_2 \sin(\beta) - Z t + Z b_2)}{b_2 (\pi d_2 \sin(\beta) - Z t)} \right] \end{aligned} \quad (4.42)$$

Substituting $U_1 = \frac{\omega d_1}{2}$ and $U_2 = \frac{\omega d_2}{2}$, the equation of friction head loss in the blade

impeller becomes:

$$\begin{aligned} H_f = & \frac{\lambda (d_2 - d_1) Q^2}{16 g \sin(\beta)} \left[\frac{\pi d_1 \sin(\beta) - Z t + Z b_1}{b_1^3 (\pi d_1 \sin(\beta) - Z t)^3} + \frac{\pi d_2 \sin(\beta) - Z t + Z b_2}{b_2^3 (\pi d_2 \sin(\beta) - Z t)^3} \right] + \\ & + \frac{\lambda (d_2 - d_1) K_s^2 \pi^2 \omega^2 \sin(\beta)}{64 g Z^2} \left[\frac{d_1^2 (\pi d_1 \sin(\beta) - Z t + Z b_1)}{b_1 (\pi d_1 \sin(\beta) - Z t)} + \right. \\ & \left. + \frac{d_2^2 (\pi d_2 \sin(\beta) - Z t + Z b_2)}{b_2 (\pi d_2 \sin(\beta) - Z t)} \right] \end{aligned} \quad (4.43)$$

The first part of the above equation is related to the average flow because this part was derived from relative velocities, W_1 , and W_2 . The second part is related to the

circ

hec

vis

4.4

tar

wl

di

ar

ar

fo

A

ce

circulation because this part was resulted from slip velocities, S_1 , and S_2 . This friction head loss represents an energy loss since the shaft work is being dissipated by the fluid viscous forces.

4.4 Volute Head Loss (H_v)

The volute is a collection chamber for the flow from the vane impeller. Each tangential section of the vane impeller discharges a portion of the total flow into the flow, which is already in the volute. A moment balance of a volute element gives the pressure distribution, and energy balance gives the head loss in the volute.

A volute element “a-b-c-d” is considered from a linear volute (Figure 4.12). The angle, θ , is measured from the starting point of the volute and the angle, ϕ , is the volute angle. By ignoring the pressure and velocity distributions in the radial direction, the following assumptions are made:

- (i) The pressure P represents an average pressure over the cross-sectional area, A .
- (ii) The velocity V represents an average velocity over the cross-sectional area, A .
- (iii) The discharge flow rate, q , is uniform over the width of the impeller, and also over the circumference of the blade impeller.
- (iv) The volute radial width is small compared to the impeller exit radius so that the moment arm, r , about the central axis may be taken as the impeller radius.
- (v) The fluid is incompressible.

A moment balance of a volute element “a-b-c-d” in the θ -direction is taken about the central axis:

$$P A r + \left(P + \frac{1}{2} \Delta P \right) \Delta A_s \sin(\phi) r - (P + \Delta P)(A + \Delta A) r - \tau \Delta A_s \cos(\phi) r = (\rho/g_c) [(q + \Delta q)(V + \Delta V) r - q V r - V_t \Delta q r] \quad (4.44)$$

Th

Di

ba

-

T

T

V

T

S

S

T

The second and high order terms are neglected:

$$\begin{aligned} P \Delta A_s \sin(\phi) r - P \Delta A r - \Delta P A r - \tau \Delta A_s \cos(\phi) r = \\ = (\rho/g_c)(V \Delta q + q \Delta V - V_t \Delta q) r \end{aligned} \quad (4.45)$$

Dividing the above equation by “ $rA\Delta\theta$ ” and taking the limits of the equation of a moment balance $\Delta A \rightarrow 0$, $\Delta A_s \rightarrow 0$, $\Delta q \rightarrow 0$, $\Delta V \rightarrow 0$, $\Delta P \rightarrow 0$, as $\Delta\theta \rightarrow 0$ gives:

$$-\frac{dP}{d\theta} - \frac{P}{A} \left[\frac{dA}{d\theta} - \frac{dA_s}{d\theta} \sin(\phi) \right] = \frac{\tau}{A} \cos(\phi) \frac{dA_s}{d\theta} + \frac{\rho}{g_c} \left[\frac{q}{A} \frac{dV}{d\theta} + \frac{V}{A} \frac{dq}{d\theta} - \frac{V_t}{A} \frac{dq}{d\theta} \right] \quad (4.46)$$

The wall shear stress, τ_w , with the presence of the friction factor, f , is:

$$\tau_w = f \left(\frac{1}{2} \rho V^2 \right)$$

The shear stress, τ , including the elemental friction surface area, A_s , is:

$$\tau dA_s = \frac{1}{4} f \left[\left(\frac{\rho}{g_c} \right) \frac{1}{2} V^2 \right] \left(p r \frac{d\theta}{\cos(\phi)} \right) \quad (4.47)$$

Where f and p represent the volute friction factor and the wetted perimeter.

The wetted perimeter is given in terms of the volute hydraulic diameter, D_v , by:

$$p = \frac{4 A}{D_v} \quad (4.48)$$

Substituting the wetted perimeter, p , and the shear stress is:

$$\tau dA_s = \frac{1}{2} \frac{f \rho V^2 A r d\theta}{g_c D_v \cos(\phi)} \quad (4.49)$$

Substituting τdA_s into the equation taking the limits of a moment balance gives:

$$-\frac{dP}{d\theta} - \frac{P}{A} \left[\frac{dA}{d\theta} - \frac{dA_s}{d\theta} \sin(\phi) \right] = \frac{f \rho V^2 r}{2 g_c D_v} + \frac{\rho}{g_c} \left[\frac{q}{A} \frac{dV}{d\theta} + \frac{V}{A} \frac{dq}{d\theta} - \frac{V_t}{A} \frac{dq}{d\theta} \right] \quad (4.50)$$

The shear area is related to the volute angle as:

$$\sin(\phi) = \frac{dA}{dA_s} \quad (4.51)$$

The velocity is defined from the volume flow rate, q , by:

$$V = \frac{q}{A} \quad (4.52)$$

$$\frac{dV}{d\theta} = \frac{1}{A} \frac{dq}{d\theta} - \frac{q}{A^2} \frac{dA}{d\theta} \quad (4.53)$$

Substituting $\sin(\phi)$, V , $dV/d\theta$ into the equation of a moment balance in the θ -direction,

which already substitutes τdA_s , provides:

$$-\frac{dP}{d\theta} - \frac{P}{A} \left[\frac{dA}{d\theta} - \frac{dA_s}{d\theta} \sin(\phi) \right] = \frac{f \rho V^2 r}{2 g_c D_v} + \frac{\rho}{g_c} \left[\frac{q}{A} \frac{dV}{d\theta} + \frac{V}{A} \frac{dq}{d\theta} - \frac{V_t}{A} \frac{dq}{d\theta} \right] \quad (4.54)$$

$$-\frac{dP}{d\theta} = \frac{\rho}{g_c} \left[\frac{f q^2 r}{2 D_v A^2} + \frac{2q}{A^2} \frac{dq}{d\theta} - \frac{V_t}{A} \frac{dq}{d\theta} - \frac{q^2}{A^3} \frac{dA}{d\theta} \right] \quad (4.55)$$

The variation of P with respect to θ can be obtained if the variations of A , D_v , and q with respect to θ are known. Iversen studied the variation of q with respect to θ and found a linear relationship of the linear volute geometry. The following linear relationships at the tongue are taken as:

$$A = A_0 + C_1 \theta \quad (4.56)$$

$$q = q_0 + C_2 \theta \quad (4.57)$$

$$D_v = D_0 + C_3 \theta \quad (4.58)$$

When A_0 is included, then the flow rate at any section of the volute will be the combination of the flow in impeller discharging from the tongue to the position θ , and the flow discharging through the area A_0 . The constants are given by:

$$C_1 = A_e / (2 \pi) \quad (4.59)$$

Su

θ (

is c

flo

d"

rate

of

The

$$C_2 = Q/(2\pi) \quad (4.60)$$

$$C_3 = D_e/(2\pi) \quad (4.61)$$

Substituting A, q, D_v into the previous equation of a moment balance presents:

$$-\frac{dP}{d\theta} = \frac{\rho}{g_c} \left[\frac{f q^2 r}{2 D_v A^2} + \frac{2q}{A^2} \frac{dq}{d\theta} - \frac{V_t}{A} \frac{dq}{d\theta} - \frac{q^2}{A^3} \frac{dA}{d\theta} \right] \quad (4.62)$$

$$-\frac{dP}{d\theta} = \frac{\rho}{g_c} \left[\frac{f (q_0 + C_2 \theta)^2 r}{2 (D_0 + C_3 \theta) (A_0 + C_1 \theta)^2} + \frac{2C_2 (q_0 + C_2 \theta)}{(A_0 + C_1 \theta)^2} - \frac{C_2 V_t}{(A_0 + C_1 \theta)} - \frac{C_1 (q_0 + C_2 \theta)^2}{(A_0 + C_1 \theta)^3} \right] \quad (4.63)$$

The above equation gives the variation of elemental fluid pressure with respect to θ ($dP/d\theta$). With the presence of the volute friction factor, f , the first term of the equation is due to friction, and the rest are due to mixing in the volute.

The rate of conversion of mechanical energy to internal energy during the fluid flow in the volute can be calculated from an energy balance of the volute element “a-b-c-d” (Figure 4.12). This rate of internal energy change is the difference between the energy rate input and the energy rate output of the volute element “a-b-c-d”. In addition, the rate of conversion of mechanical energy can be construed from Bernoulli’s equation:

$$\Delta E = q \Delta P = q \left(\frac{\rho}{g_c} \right) \frac{(\Delta V^2)}{2} \quad (4.64)$$

$$\Delta E = q \left[P + \frac{1}{2} \left(\frac{\rho}{g_c} \right) V^2 \right] + \Delta q \left[\left(P + \frac{1}{2} \Delta P \right) + \frac{1}{2} \left(\frac{\rho}{g_c} \right) (V_t^2 + V_r^2) \right] - (q + \Delta q) \left[(P + \Delta P) + \frac{1}{2} \left(\frac{\rho}{g_c} \right) (V + \Delta V)^2 \right] \quad (4.65)$$

The second and high order terms are neglected:

Dis

$\Delta\theta$

Su

Su

Int

Th

$$\Delta E = \frac{1}{2} \Delta q \left(\frac{\rho}{g_c} \right) (V_t^2 + V_r^2 - V^2) - q \Delta P - q \left(\frac{\rho}{g_c} \right) V \Delta V \quad (4.66)$$

Dividing both sides of equation by $\Delta\theta$ and taking the limits $\Delta q \rightarrow 0$, $\Delta V \rightarrow 0$, $\Delta P \rightarrow 0$, as $\Delta\theta \rightarrow 0$ gives:

$$\frac{dE}{d\theta} = \frac{\rho (V_t^2 + V_r^2 - V^2)}{2 g_c} \frac{dq}{d\theta} - q \frac{dP}{d\theta} - \frac{q \rho V}{g_c} \frac{dV}{d\theta} \quad (4.67)$$

Substituting V and $dV/d\theta$ into the above equation gives:

$$\frac{dE}{d\theta} = \left[\frac{\rho (V_t^2 + V_r^2)}{2 g_c} - \frac{3 \rho q^2}{2 g_c A^2} \right] \frac{dq}{d\theta} + \frac{\rho q^3}{g_c A^3} \frac{dA}{d\theta} - q \frac{dP}{d\theta} \quad (4.68)$$

Substituting q , A , $(dq/d\theta)$, $(dA/d\theta)$, $(-dP/d\theta)$ and simplifying gives:

$$\begin{aligned} \frac{dE}{d\theta} = & \frac{\rho C_2 (V_t^2 + V_r^2)}{2 g_c} - \frac{\rho C_2 (q_0 + C_2 \theta) V_t}{g_c (A_0 + C_1 \theta)} + \frac{\rho C_2 (q_0 + C_2 \theta)^2}{2 g_c (A_0 + C_1 \theta)^2} + \\ & + \frac{\rho f r (q_0 + C_2 \theta)^3}{2 g_c (D_0 + C_3 \theta) (A_0 + C_1 \theta)^2} \end{aligned} \quad (4.69)$$

Integrating this equation with respect to θ over the integral interval $(0, 2\pi)$ gives:

$$\begin{aligned} \int_0^{2\pi} \frac{dE}{d\theta} d\theta = & \int_0^{2\pi} \frac{\rho C_2 (V_t^2 + V_r^2)}{2 g_c} d\theta - \int_0^{2\pi} \frac{\rho C_2 (q_0 + C_2 \theta) V_t}{g_c (A_0 + C_1 \theta)} d\theta + \\ & + \int_0^{2\pi} \frac{\rho C_2 (q_0 + C_2 \theta)^2}{2 g_c (A_0 + C_1 \theta)^2} d\theta + \int_0^{2\pi} \frac{\rho f r (q_0 + C_2 \theta)^3}{2 g_c (D_0 + C_3 \theta) (A_0 + C_1 \theta)^2} d\theta \end{aligned} \quad (4.70)$$

The above equation is integrated as (See Appendix E)

$$\begin{aligned}
E = & \frac{\rho Q}{2 g_c} \left[V_r^2 + \left(V_t - \frac{Q}{A_e} \right)^2 + \frac{2Q}{A_e} \left(V_t - \frac{Q}{A_e} \right) \left(\frac{A_0}{A_e} - \frac{q_0}{Q} \right) \ln \left(1 + \frac{A_e}{A_0} \right) + \right. \\
& \left. + \left(\frac{Q}{A_e} \right)^2 \left(\frac{A_0}{A_e} - \frac{q_0}{Q} \right)^2 \left(\frac{A_0}{A_e} \right)^{-1} \left(1 + \frac{A_0}{A_e} \right)^{-1} \right] + \\
& + \frac{\rho Q 2 \pi f r}{2 g_c D_e} \left(\frac{Q}{A_e} \right)^2 \left[1 + \left(\frac{A_0}{A_e} - \frac{q_0}{Q} \right)^3 \left(\frac{A_0}{A_e} \right)^{-1} \left(1 + \frac{A_0}{A_e} \right)^{-1} \left(\frac{A_0}{A_e} - \frac{D_0}{D_e} \right)^{-1} \right. \\
& - \left(\frac{D_0}{D_e} - \frac{q_0}{Q} \right)^3 \left(\frac{A_0}{A_e} - \frac{D_0}{D_e} \right)^{-2} \ln \left(1 + \frac{D_e}{D_0} \right) + \\
& \left. + \left(\frac{A_0}{A_e} - \frac{q_0}{Q} \right)^2 \left(\frac{3 D_0}{D_e} - \frac{2 A_0}{A_e} - \frac{q_0}{Q} \right) \left(\frac{A_0}{A_e} - \frac{D_0}{D_e} \right)^{-2} \ln \left(1 + \frac{A_e}{A_0} \right) \right] \quad (4.71)
\end{aligned}$$

From the above equation, the second part of this equation is related to the volute friction factor, f , in the volute. Bernoulli's equation is written as follows:

$$Q \left(\frac{\rho V_2^2}{2} + P_2 + \rho g z_2 \right) = Q \left(\frac{\rho V_1^2}{2} + P_1 + \rho g z_1 \right) = \text{Constant Energy} \quad (4.72)$$

From Bernoulli's equation, the volute head loss, H_v , is related to the internal energy change, E , as:

$$E = \frac{\rho Q H_v g}{g_c} \quad (4.73)$$

Rewriting the equation with the internal energy change, E , and this provides the volute head loss:

H

ang

wh

The

and

The

meth

$$\begin{aligned}
H_v = \frac{1}{2g} & \left[V_r^2 + \left(V_t - \frac{Q}{A_e} \right)^2 + \frac{2Q}{A_e} \left(V_t - \frac{Q}{A_e} \right) \left(\frac{A_0}{A_e} - \frac{q_0}{Q} \right) \ln \left(1 + \frac{A_e}{A_0} \right) + \right. \\
& \left. + \left(\frac{Q}{A_e} \right)^2 \left(\frac{A_0}{A_e} - \frac{q_0}{Q} \right)^2 \left(\frac{A_0}{A_e} \right)^{-1} \left(1 + \frac{A_0}{A_e} \right)^{-1} \right] + \\
& + \frac{\pi f r}{g D_e} \left(\frac{Q}{A_e} \right)^2 \left[1 + \left(\frac{A_0}{A_e} - \frac{q_0}{Q} \right)^3 \left(\frac{A_0}{A_e} \right)^{-1} \left(1 + \frac{A_0}{A_e} \right)^{-1} \left(\frac{A_0}{A_e} - \frac{D_0}{D_e} \right)^{-1} - \right. \\
& - \left(\frac{D_0}{D_e} - \frac{q_0}{Q} \right)^3 \left(\frac{A_0}{A_e} - \frac{D_0}{D_e} \right)^{-2} \ln \left(1 + \frac{D_e}{D_0} \right) + \\
& \left. + \left(\frac{A_0}{A_e} - \frac{q_0}{Q} \right)^2 \left(\frac{3D_0}{D_e} - \frac{2A_0}{A_e} - \frac{q_0}{Q} \right) \left(\frac{A_0}{A_e} - \frac{D_0}{D_e} \right)^{-2} \ln \left(1 + \frac{A_e}{A_0} \right) \right] \quad (4.74)
\end{aligned}$$

This equation gives the volute head loss, H_v . The absolute and relative fluid angles are measured from the tangential direction of the velocity triangle (Figure 4.14) when taking into account of the total blockage area at inlet and outlet of blade impeller. The radial and tangential velocities of the fluid including the total blockage area at inlet and outlet of blade impeller and slip effect are given by:

$$V_r = V_{r2} = \frac{Q}{b_2 \left(\pi d_2 - \frac{Z t}{\sin(\beta)} \right)} \quad (4.75)$$

$$V_t = V_{t2} = U_2 - S_2 - \frac{V_{r2}}{\tan(\beta)} = U_2 - S_2 - V_{r2} \cot(\beta) \quad (4.76)$$

The volume flow rate, q_o , through the area, A_o , at the tongue is:

$$q_o = \frac{Q \theta_o}{2 \pi} \quad (4.77)$$

The angle, θ_o , is measured up to the tongue and determined from the following method. The parameter “ t_o ” the geometry of triangle OAB (Figure 4.11) is called the

cle

ang

Fro

Us

O.

clearance between the tongue and the impeller. The parameter “ α_o ” of the actual fluid angle being tangent to the impeller is:

$$\tan(\alpha_o) = \frac{V_r}{V_t} \quad (4.78)$$

From the geometry of triangle OAB (Figure 4.11), the sine law is used as:

$$\frac{r_2 + t_o}{\sin(90 + \alpha_o)} = \frac{r_2}{\sin(180 - \theta_o - 90 - \alpha_o)} \quad (4.79)$$

Using the trigonometrical identities gives:

$$\begin{aligned} (r_2 + t_o) \cos(\theta_o + \alpha_o) &= r_2 \cos(\alpha_o) \\ \cos(\theta_o) \cos(\alpha_o) - \sin(\theta_o) \sin(\alpha_o) &= \frac{r_2}{(r_2 + t_o)} \cos(\alpha_o) \end{aligned} \quad (4.80)$$

$$\begin{aligned} \left[\sin(\theta_o) \sin(\alpha_o) + \frac{r_2}{(r_2 + t_o)} \cos(\alpha_o) \right]^2 &= [\cos(\theta_o) \cos(\alpha_o)]^2 \\ [\sin(\theta_o) \sin(\alpha_o)]^2 + \frac{2 r_2}{(r_2 + t_o)} \sin(\alpha_o) \cos(\alpha_o) \sin(\theta_o) + \\ + \left[\frac{(r_2)^2}{(r_2 + t_o)^2} \right] \cos^2(\alpha_o) &= [\cos(\theta_o) \cos(\alpha_o)]^2 \end{aligned} \quad (4.81)$$

$$\begin{aligned} \sin^2(\theta_o) (1 - \cos^2(\alpha_o)) + \frac{2 r_2}{(r_2 + t_o)} \sin(\alpha_o) \cos(\alpha_o) \sin(\theta_o) + \\ + \left[\frac{(r_2)^2}{(r_2 + t_o)^2} \right] \cos^2(\alpha_o) &= (1 - \sin^2(\theta_o)) \cos^2(\alpha_o) \end{aligned} \quad (4.82)$$

$$\sin^2(\theta_o) + \frac{2 r_2}{(r_2 + t_o)} \sin(\alpha_o) \cos(\alpha_o) \sin(\theta_o) - \left[1 - \frac{(r_2)^2}{(r_2 + t_o)^2} \right] \cos^2(\alpha_o) = 0 \quad (4.83)$$

This equation is a quadratic equation with the variable $\sin(\theta_o)$. The positive root of this equation gives:

$$\sin(\theta_o) = \frac{1}{2} \left\{ \frac{-2r_2}{(r_2 + t_o)} \sin(\alpha_o) \cos(\alpha_o) + \left[\left(\frac{2r_2}{(r_2 + t_o)} \sin(\alpha_o) \cos(\alpha_o) \right)^2 + 4 \left[1 - \frac{(r_2)^2}{(r_2 + t_o)^2} \right] \cos^2(\alpha_o) \right]^{1/2} \right\} \quad (4.84)$$

$$\sin(\theta_o) = \cos(\alpha_o) \left\{ \left[1 - \cos^2(\alpha_o) \frac{(d_2)^2}{(d_2 + 2t_o)^2} \right]^{1/2} - \sin(\alpha_o) \frac{(d_2)}{(d_2 + 2t_o)} \right\} \quad (4.85)$$

The angle, θ_o , will be found from the calculated angle, α_o . Then, the volume flow rate, q_o , through the clearance can be found from the calculated angles, α_o , and, θ_o .

4.5 Power due to Disk Friction Loss (P_d), Power due to Leakage Loss (P_L),

Entrance-Bend Loss (H_{eb})

4.5.1 Power due to Disk Friction Loss (P_d)

The disk friction loss is the loss of energy arising from friction between the impeller disk and the fluid, which fills the clearance between the impeller and the housing. This does not constitute an impeller energy conversion loss, but this constitutes a loss, which is independent of the internal work of the impeller. This must be considered as an additional mechanical loss like friction in the bearing. This loss is usually less than 3% of the total energy. This loss depends on the surfaces, impeller speed, fluid properties, and the clearance. The disk friction phenomena can be considered as a two-dimensional axisymmetric flow. In the case of un-shrouded impeller, the tangential velocity of fluid at any radius, r , can be assumed as (Figure 4.13):

$$V_t = V_{t1} + \frac{(r - r_1)(V_{t2} - V_{t1})}{(r_2 - r_1)} = \left[\frac{(V_{t2} - V_{t1})}{(r_2 - r_1)} \right] r + \left[V_{t1} - \frac{r_1 (V_{t2} - V_{t1})}{(r_2 - r_1)} \right] \quad (4.86)$$

$$V_t = m_1 r + m_2$$

a

C:

$$V_{t1} = U_1 + S_1 - \frac{V_{r1}}{\tan(\beta)} = U_1 + S_1 - V_{r1} \cot(\beta) \quad (4.87)$$

$$V_{t2} = U_2 - S_2 - \frac{V_{r2}}{\tan(\beta)} = U_2 - S_2 - V_{r2} \cot(\beta) \quad (4.88)$$

$$S_1 = U_1 K_s (\pi/Z) \sin(\beta_1); S_2 = U_2 K_s (\pi/Z) \sin(\beta_2) \quad (4.89)$$

$$U_1 = \frac{\omega d_1}{2}; U_2 = \frac{\omega d_2}{2} \quad (4.90)$$

$$V_{r1} = \frac{Q}{b_1 \left(\pi d_1 - \frac{Z t}{\sin(\beta)} \right)}; V_{r2} = \frac{Q}{b_2 \left(\pi d_2 - \frac{Z t}{\sin(\beta)} \right)} \quad (4.91)$$

Substituting the tangential velocities V_{t1} , V_{t2} into V_t and simplifying gives:

$$\begin{aligned} V_t = r \omega - r \left[\frac{\omega K_s \pi (d_1 + d_2) \sin(\beta)}{Z (d_2 - d_1)} - \frac{2 Q (d_2 b_2 - d_1 b_1)}{\pi d_1 d_2 b_1 b_2 (d_2 - d_1) \tan(\beta)} \right] + \\ + \frac{\omega K_s \pi d_1 d_2 \sin(\beta)}{Z (d_2 - d_1)} - \frac{Q ((d_2)^2 b_2 - (d_1)^2 b_1)}{\pi d_1 d_2 b_1 b_2 (d_2 - d_1) \tan(\beta)} \end{aligned} \quad (4.92)$$

In the case of a shrouded impeller, the first term of the equation must be retained and the rest is dropped. The equation of tangential velocity for an un-shrouded impeller can be simplified as:

$$V_t = m_1 r + m_2 \quad (4.93)$$

$$\begin{aligned} m_1 &= (V_{t2} - V_{t1}) / (r_2 - r_1) \\ &= \omega \left[1 - \frac{K_s \pi (d_1 + d_2) \sin(\beta)}{Z (d_2 - d_1)} \right] + \frac{2 Q (d_2 b_2 - d_1 b_1)}{\pi d_1 d_2 b_1 b_2 (d_2 - d_1) \tan(\beta)} \end{aligned} \quad (4.94)$$

$$\begin{aligned} m_2 &= V_{t1} - r_1 (V_{t2} - V_{t1}) / (r_2 - r_1) \\ &= \frac{\omega K_s \pi d_1 d_2 \sin(\beta)}{Z (d_2 - d_1)} - \frac{Q ((d_2)^2 b_2 - (d_1)^2 b_1)}{\pi d_1 d_2 b_1 b_2 (d_2 - d_1) \tan(\beta)} \end{aligned} \quad (4.95)$$

The parameters of m_1 and m_2 have the units of angular and linear velocities. It can be assumed that the fluid particles adjacent to the impeller acquire the tangential velocity, V_t , and adjacent to the housing are stationary. As a result of centrifugal forces, the fluid particles start moving outward in the immediate neighborhood of the rotating disk and the new particles approach the disk near the center. Thus, a circulation would be established according to Stepanoff. If the path of this circulation is short and if the volume of the liquid surrounding the rotating disk is small, the particles approaching the disk will retain the part of their rotary motion. Thus, in theory, the volume of the liquid requires less power from the disk. However, in experiment, the power to drive the disk increases as the clearance between the disk and the housing is increased. As a result, this clearance must be kept as small as possible. When δ is the thickness of the region, in which velocity, V , varies from 0 at the wall to V_t (U_∞ , free stream velocity) in the free stream, the shear stress at any radius, r , by the flow friction is given with the assumption of a linear velocity gradient in the clearance as follows:

$$\tau = \mu \frac{U_\infty}{\delta} = \frac{\mu V_t}{g_c \delta} \quad (4.96)$$

The friction force at a radius, r , exerted on a ring having radial width, dr , can be expressed as:

$$\begin{aligned} dF &= 2 \tau dA \\ dA &= 2 \pi r dr \end{aligned} \quad (4.97)$$

Substituting V_t , τ , and simplifying give

$$dF = 4 \pi \mu \left(m_1 r^2 + m_2 r \right) \frac{dr}{g_c \delta} = 4 \pi \frac{\nu}{\rho} \left(m_1 r^2 + m_2 r \right) \frac{dr}{g_c \delta} \quad (4.98)$$

Th
flu

4.

va
o
in
c

c
ta
is
p

A

ap

The power due to Disk Friction Loss, P_d , required overcoming the resisting force of the fluid filling the clearance between the blade impeller and the housing is:

$$P_d = \int_{r_1}^{r_2} V_t dF \quad (4.99)$$

$$P_d = \frac{\pi v \rho}{2 g_c \delta} \left[\frac{(m_1)^2 ((d_2)^4 - (d_1)^4)}{8} + \frac{2m_1 m_2 ((d_2)^3 - (d_1)^3)}{3} + (m_2)^2 ((d_2)^2 - (d_1)^2) \right] \quad (4.100)$$

4.5.2 Power due to Leakage Loss (P_L)

Leakage occurs in open impellers from the leading side to the trailing side of the vanes, across the vane edge at the clearance between the vane and the housing. The vane of the impeller gives a velocity to the fluid in the clearance. This is dissipated in the fluid in the form of dynamic head loss, eddies and turbulence. This power loss can be calculated as follows:

An elemental volume in the clearance having a radial width, dr , at radius, r , is considered when evaluating the leakage loss. It is assumed that a dynamic pressure loss takes place in the clearance of each blade. The pressure gradient in Bernoulli's equation is defined as follows:

$$\frac{\rho V_2^2}{2} + P_2 = \frac{\rho V_1^2}{2} + P_1 = \text{Constant} \quad (\text{Along a streamline or throughout the flow}) \quad (4.101)$$

$$\Delta P = \frac{\rho (\Delta V^2)}{2}$$

The dynamic pressure loss, P_L , is normal to the blade profile and is given by applying Bernoulli's equation:

$$P_L = \frac{1}{2} \frac{\rho}{g_c} [r \omega \sin(\beta)]^2 \quad (4.102)$$

Moreover, it is assumed that the fluid adjacent to the housing has no velocity, the fluid adjacent to the blade acquires the blade velocity, and the velocity variation is linear in the clearance. The elemental leakage volume flow rate, dQ_L , through the elemental area, $dA = \delta dr$, on each side of the blade is given by:

$$dQ_L = V dA = \frac{1}{2} r \omega \delta dr \quad (4.103)$$

The loss of power, P_L , due to leakage by Z number of blades is:

$$P_L = \int_{r_1}^{r_2} 2 Z P_L dQ_L \quad (4.104)$$

Substituting P_L and dQ_L , and integrating give the equation for power loss due to the leakage:

$$P_L = Z \rho \delta \omega^3 \left((d_2)^4 - (d_1)^4 \right) \frac{\sin^2(\beta)}{128 g_c} \quad (4.105)$$

4.5.3 Entrance-Bend Loss (H_{eb})

The fluid enters the centrifugal pump axially and makes a right angle with sudden enlargement of the section (Figure 4.4). The character of the flow in a 90° -bend and the resistance of 90° -bend are shown in Figure 4.6 and Figure 4.7. This causes a secondary flow in bend and results in a loss of head, which can be significantly considerable. The head loss for the entrance-bend is given by:

$$H_{eb} = \frac{K_b V^2}{2 g} \quad (4.106)$$

The bend-resistance coefficient, K_b , is a function of bend angle and shape. Figure 4.5 illustrates the bend coefficients in resistance of bends. The parameter, K_b , is unity for a right bend angle. The velocity, V , at the pump inlet is:

Th

4.

op

di

di

oc

se

lo

w

op

Ti

m

is.

$$V = \frac{Q}{A} = \frac{Q}{\frac{1}{4} \pi (d_i)^2} \quad (4.107)$$

The head loss for the entrance-bend is:

$$H_{eb} = \frac{8 K_b Q^2}{\pi^2 g (d_i)^4} \quad (4.108)$$

4.6 Optimizing Number of Blades and Blade Angle of A Logarithmic Vane Impeller

It is important to select the proper number of blades and blade angle for efficient operation. If the number of blades is small, each vane is overloaded. Hence, the pressure difference between the two sides of the blades is high. Consequently, the velocity distribution in the blade channel is non-uniform, and very high local velocities may occur. This results in cavitations during operation. Too few blades may lead to flow separation. Too many blades may result in narrow blade channels and high friction losses. The optimum blade number, with optimum blade angle of a logarithmic blade, which gives the best efficiency, can be predetermined from the experiment. But the optimum blade number and the optimum blade angle vary from the design to the design. The most efficient pump is identified by varying the blade angle and number of blades mathematically. The pump ideal head for a finite number of blades and slip factor effect is:

$$H_a = H_e - H_c \quad (4.109)$$

$$H_e = \frac{U_2 V_{u2} - U_1 V_{u1}}{g} = \frac{U_2 (U_2 - V_{r2} \cot(\beta)) - U_1 (U_1 - V_{r1} \cot(\beta))}{g} \quad (4.110)$$

$$H_e = \frac{U_2 (U_2 - V_{r2}/\tan(\beta)) - U_1 (U_1 - V_{r1}/\tan(\beta))}{g}$$

$$H_c = \frac{\pi K_s \sin(\beta)(U_2^2 + U_1^2)}{g Z} = \frac{K_s \pi \omega^2 \sin(\beta)((d_1)^2 + (d_2)^2)}{4 g Z} \quad (4.111)$$

Assuming that there are no pre-rotation (no Inlet Guide Vane, no pre-whirl) and no tangential velocities of the liquid at the impeller entrance ($V_{u1} = 0$). The Euler head, H_e , and the circulation head, H_c , are simplified as:

$$H_e = \frac{(d_2)^2 \omega^2}{4 g} - \frac{d_2 \omega Q}{2 g b_2 \left(\pi d_2 - \frac{Z t}{\sin(\beta)} \right) \tan(\beta)} \quad (4.112)$$

$$H_c = K_s \pi \omega^2 (d_2)^2 \frac{\sin(\beta)}{4 g Z} \quad (4.113)$$

$$H_a = H_e - H_c$$

$$H_a = \frac{(d_2)^2 \omega^2}{4 g} - \frac{d_2 \omega Q}{2 g b_2 \left(\pi d_2 - \frac{Z t}{\sin(\beta)} \right) \tan(\beta)} - K_s \pi \omega^2 (d_2)^2 \frac{\sin(\beta)}{4 g Z} \quad (4.114)$$

It is worthy to note that as $Z \rightarrow \infty$ and $t \rightarrow 0$, $H_a \rightarrow H_e$

The pump output head is given by:

$$H = H_a - H_{eb} - H_f - H_v \quad (4.115)$$

The output head is a function of volume flow rate “Q”, impeller rotational speed “ ω ”, Stodola coefficient “ K_s ”, impeller and volute friction factors “ λ , f ”, and pump geometries “ b_1 , b_2 , d_1 , d_2 , t , A_0 , A_e ”.

The pump output power, W_{out} , is given by:

$$W_{out} = Q H \quad (4.116)$$

The input power, W_{in} , is given by:

$$W_{in} = Q H_a + P_d + P_L \quad (4.117)$$

The pump efficiency is given by:

$$\eta = \frac{W_{out}}{W_{in}} * 100 \quad (4.118)$$

For a given impeller exit width, surface roughness, and the Reynolds number, the impeller friction factor can be calculated from using Hagen-Poiseuille relation for laminar flow ($Re \leq 2300$) as:

$$\text{Friction factor: } \lambda = 64/Re \quad (4.119)$$

The impeller friction factor can be calculated from using Blasius relation for turbulent flow ($Re > 2300$) as:

$$\text{Friction factor: } \lambda = 0.3164/Re^{1/4} \quad (4.120)$$

The impeller Reynolds number is:

$$Re_i = \frac{V_{mi} D_{mi}}{\nu} \quad (4.121)$$

To obtain this Reynolds number, two open channels between two blades are assumed. The open channel at the trailing side of the blade has an average velocity of $(W_m + 0.5 S_m)$ and at the leading site $(W_m - 0.5 S_m)$. The velocity, S_m , and, W_m , are given by:

$$S_m = \frac{S_1 + S_2}{2} \quad (4.122)$$

$$W_m = \frac{Q}{b_m (\pi d_m \sin(\beta) - Z t)} \quad (4.123)$$

$$d_m = \frac{d_1 + d_2}{2} \quad (4.124)$$

$$b_m = \frac{b_1 + b_2}{2} \quad (4.125)$$

The hydraulic diameter of each channel is given by:

$$D_{mi} = \frac{2 b_m (\pi d_m \sin(\beta) - Z t)}{(\pi d_m \sin(\beta) - Z t + Z b_m)} \quad (4.126)$$

The Reynolds numbers of channels at the trailing (back) and leading (front) surfaces are given by:

$$Re_b = \frac{D_{mi} |W_m + 0.5 S_m|}{\nu} \quad (4.127)$$

$$Re_f = \frac{D_{mi} |W_m - 0.5 S_m|}{\nu} \quad (4.128)$$

The impeller Reynolds number is the mean of these two Reynolds numbers:

$$Re_i = \frac{D_{mi} [|W_m + 0.5 S_m| + |W_m - 0.5 S_m|]}{2 \nu} \quad (4.129)$$

This equation implies that at low volume flow rate ($W_m < 0.5 S_m$), the circulation determines the impeller Reynolds number. At higher volume flow rate ($W_m \geq 0.5 S_m$), the volume flow rate determines the impeller Reynolds number.

The volute Reynolds number, Re_v , is given by:

$$Re_v = \frac{V_{mv} D_{mv}}{\nu} \quad (4.130)$$

$$D_{mv} = \frac{1}{2} (D_0 + D_e) \quad (4.131)$$

$$V_{mv} = \frac{1}{2} \left[\left(\frac{q_0}{A_0} \right) + \left(\frac{Q}{A_e} \right) \right] \quad (4.132)$$

$$Re_v = \frac{D_0 + D_e}{4 \nu} \left[\frac{q_0}{A_0} + \frac{Q}{A_e} \right] \quad (4.133)$$

To optimize the pump based on number of blades and blade angle for given values of fluid kinematic viscosity “ ν ”, fluid density “ ρ ”, volume flow rate “ Q ”, pump

output head “H”, Stodola coefficient with Wiesner correction $K_S = Z^{0.3} / (\pi \sqrt{\sin(\beta)})$, entrance-bend coefficient ($K_b = 1$) (Figure 4.5), and pump geometrical parameters “ b_1 , b_2 , d_1 , d_2 , t , δ , A_0 , A_e , D_0 , D_e , and t_0 ”, the following procedure was used:

- (1) Blade number, Z_k , was specified.
- (2) Blade angle, β_j , was specified.
- (3) Impeller Reynolds number, Re_i , was calculated, and the friction factor, λ , depends on $(Re_i \leq 2300)$ or $(Re_i > 2300)$.
- (4) Volute Reynolds number, Re_v , was calculated, and the friction factor, f , depends on $(Re_v \leq 2300)$ or $(Re_v > 2300)$.
- (5) Flow rate, q_o , was obtained by first calculating the fluid angle, α_o , and then, the angle, θ_o .
- (6) Pump output head, H_{kj}^{output} , and Pump input head, H_{kj}^{input} , were obtained by varying the impeller rotational speed, ω , so that $H_{kj} = H$, the pump output head required.
- (7) Efficiency η_{kj} was obtained for the speed, which gave $H_{kj} = H$.

The subscript, kj , is a notation representing the quantity for number of blades, Z_k , and the blade angle, β_j . The above procedure was repeated for various blade numbers and blade angles (see Appendix C and Appendix D).

4.7 Derivation of Euler’s Head Equation (H_e)

The theoretical head of a centrifugal pump is obtained by applying the principle of angular momentum to the mass of liquid flowing through the impeller passages. This principle defines that the time rate of change of angular momentum of a body with

respect to the axis of rotation is equal to the torque of the resultant force on the body with respect to the same axis.

Assume that a mass of liquid fills the space between two adjacent impeller blades (Figure 4.14). Its position at time “t” is “a-b-c-d”, and its position at time “t + dt” has changed to “e-f-g-h”. Then, assume that the mass of the liquid in “a-b-f-e”, just leaving the impeller channel, is “dm”. By applying assumption of incompressible fluid ($\rho = \text{constant}$), the mass of the liquid in “c-d-h-g”, just entering the channel of blade impeller in the same time interval “dt”, is equal to the mass of liquid in “a-b-f-e”, just leaving the channel of the blade impeller. The part of liquid, in “a-b-g-h”, contained between the two blades of impeller does not change its moment of momentum in time interval “dt”. Therefore, the change in moment of momentum of the whole content of the channel is given by the change of moment of momentum of the mass “dm” entering the impeller “c-d-h-g” and mass “dm” leaving the impeller “a-b-f-e”. This change of moment of momentum is equal to the moment of all external forces applied to the liquid contained between the two blades of impeller.

Let T indicate the moment of external forces. Applying the angular momentum principle gives:

$$T = F r = (ma) r = \left(V \frac{dm}{dt} \right) r \quad (4.134)$$

$$T = \frac{r_2 V_2 \cos \alpha_2 - r_1 V_1 \cos \alpha_1}{g_c} \frac{dm}{dt}$$

The external forces applied to the liquid contained between the blades are:

- (i) The difference in pressure, P_f , on the front-side and, P_b , on the back-side of each blade.

- (ii) Pressure, P_d , at the impeller discharge on the face “a-b” and P_s at the impeller inlet on the face “c-d”, which are radial forces and do not have moment about the axis of rotation.
- (iii) The hydraulic friction forces, F_b , and, F_f , on the back side “b-c” (pressure surface) and front side “a-d” (suction surface) of each blade, which oppose the relative flow and produce torque in addition to that exerted by the blades of impeller.

The mass flow rate, when exerted to all impeller channels, represents the constant time rate of mass flow rate through the impeller as:

$$(dm/dt) = Q\rho \quad (4.135)$$

Substituting “dm/dt” into torque equation “T”, and then multiplying both sides by angular velocity “ ω ” of the impeller, the following equation is obtained:

$$T \omega = Q \rho \omega \left(\frac{r_2 V_2 \cos \alpha_2 - r_1 V_1 \cos \alpha_1}{g_c} \right) \quad (4.136)$$

The term $(T \omega)$ is the power input (P_e) applied to the liquid by the impeller blades. Substituting the peripheral velocity ($U_2 = r_2 \omega$) at the impeller exit and ($U_1 = r_1 \omega$) at the impeller inlet into the above equation of “ $T\omega$ ”:

$$P_e = T \omega = Q \rho \left(\frac{U_2 V_2 \cos \alpha_2 - U_1 V_1 \cos \alpha_1}{g_c} \right) \quad (4.137)$$

Assuming that there is no loss of head between the impeller and the point where the total head (H_e) is measured. Bernoulli’s equation is expressed by:

$$Q \left(\frac{\rho V_2^2}{2} + P_2 + \rho g z_2 \right) = Q \left(\frac{\rho V_1^2}{2} + P_1 + \rho g z_1 \right) = \text{Constant Energy}$$

The ideal power of an ideal pump is:

$$P_e = Q \rho \left(\frac{g}{g_c} \right) H_e \quad (4.138)$$

Comparing the equation of power due to torque, T , and the equation of power due to total head, H_e , gives:

$$H_e = \frac{U_2 V_2 \cos \alpha_2 - U_1 V_1 \cos \alpha_1}{g} \quad (4.139)$$

The above equation is called as Euler's Head equation for a theoretical head. This equation can be expressed in another form. The following expressions are obtained from the velocity triangle diagrams as:

$$V_2 \cos \alpha_2 = U_2 - V_{r2} / \tan \beta \quad (4.140)$$

$$V_1 \cos \alpha_1 = U_1 - V_{r1} / \tan \beta \quad (4.141)$$

Substituting equations (4.140) and (4.141) into (4.139), the Euler's Head is given as:

$$H_e = \frac{U_2 (U_2 - V_{r2} / \tan \beta) - U_1 (U_1 - V_{r1} / \tan \beta)}{g} \quad (4.142)$$

The Euler's Head equation is derived for an infinite number of blades in the impeller. Moreover, this equation does not include a finite number of blades, the friction losses in the impeller, and the slip effect. In conclusion, there are some assumptions in the analysis of Euler's Head equation

1. Inviscid (frictionless) flow.
2. Fully constrained flow (an impeller with an infinite number of infinitely thin vanes).
3. Uniform steady flow, in which average velocity represents actual velocity.
4. One-dimensional analysis.

4.8 Determination of Logarithmic Blade Length (L)

Figure 4.15 shows a logarithmic profile with some setups as follows:

- (i) Point J on the curve is at a distance r from the origin O and subtends an angle “ θ ” with the X-axis.
- (ii) Line CD is tangent to the radius “ r ” of the circle at J.
- (iii) Line AB is tangent to the logarithmic profile at J.
- (iv) The length change “ dL ” is the elemental length of JJ’ of the curve.
- (v) The angle change “ $d\theta$ ” is the elemental angle JOJ’.
- (vi) The radius change “ $r + dr$ ” is the radius at point J’.
- (vii) The angle “ β ” is the angle between the line AB and CD.

The elemental length “ dL ” is given by:

$$dL = \left[(r d\theta)^2 + (dr)^2 \right]^{1/2} \quad (4.143)$$

$$\tan\beta = \frac{1}{r} \frac{dr}{d\theta} \Rightarrow \frac{d\theta}{dr} = \frac{1}{r \tan\beta} \quad (4.144)$$

Integrating equation of elemental radius “ dr ” gives a general equation of a logarithmic profile as:

$$\int_0^r \frac{dr}{r} = \int_0^\theta \tan(\beta) d\theta \quad (4.145)$$
$$\ln(r) = \theta \tan(\beta) + \ln(c)$$

Using a boundary condition $\theta = 0$ when $r = r_1$, the blade impeller radius “ r ” for the logarithmic profile of the blade is:

$$\begin{aligned}
\ln(r) &= \theta \tan(\beta) + \ln(c) \\
\theta = 0 \text{ as } r = r_1 &\Rightarrow c = r_1 \\
\ln(r) &= \theta \tan(\beta) + \ln(r_1) \\
\ln\left(\frac{r}{r_1}\right) &= \theta \tan(\beta)
\end{aligned} \tag{4.146}$$

$$\Rightarrow r = r_1 \exp(\theta \tan(\beta)) \tag{4.147}$$

Rewriting equation of the elemental length “dL” gives:

$$\frac{dL}{dr} = \left[\left(r \frac{d\theta}{dr} \right)^2 + 1 \right]^{1/2} \tag{4.148}$$

Substituting equation of “dθ/dr” into equation of “dL/dr” gives:

$$\frac{dL}{dr} = \left[\left(r \frac{1}{r \tan \beta} \right)^2 + 1 \right]^{1/2} \Rightarrow \frac{dL}{dr} = \frac{1}{\sin \beta} \tag{4.149}$$

Integrating equation of “dL/dr” gives:

$$\begin{aligned}
L = L_2 \quad r = r_2 \\
\int_{L=L_1}^{L=L_2} dL = \int_{r=r_1}^{r=r_2} \frac{1}{\sin \beta} dr \Rightarrow L_2 - L_1 = L = \frac{r_2 - r_1}{\sin \beta}
\end{aligned} \tag{4.150}$$

The above equation gives the length of the logarithmic blade “L” in terms of inlet radius “r₁”, and exit radius “r₂”, and the blade angle “β”.

FIGURES

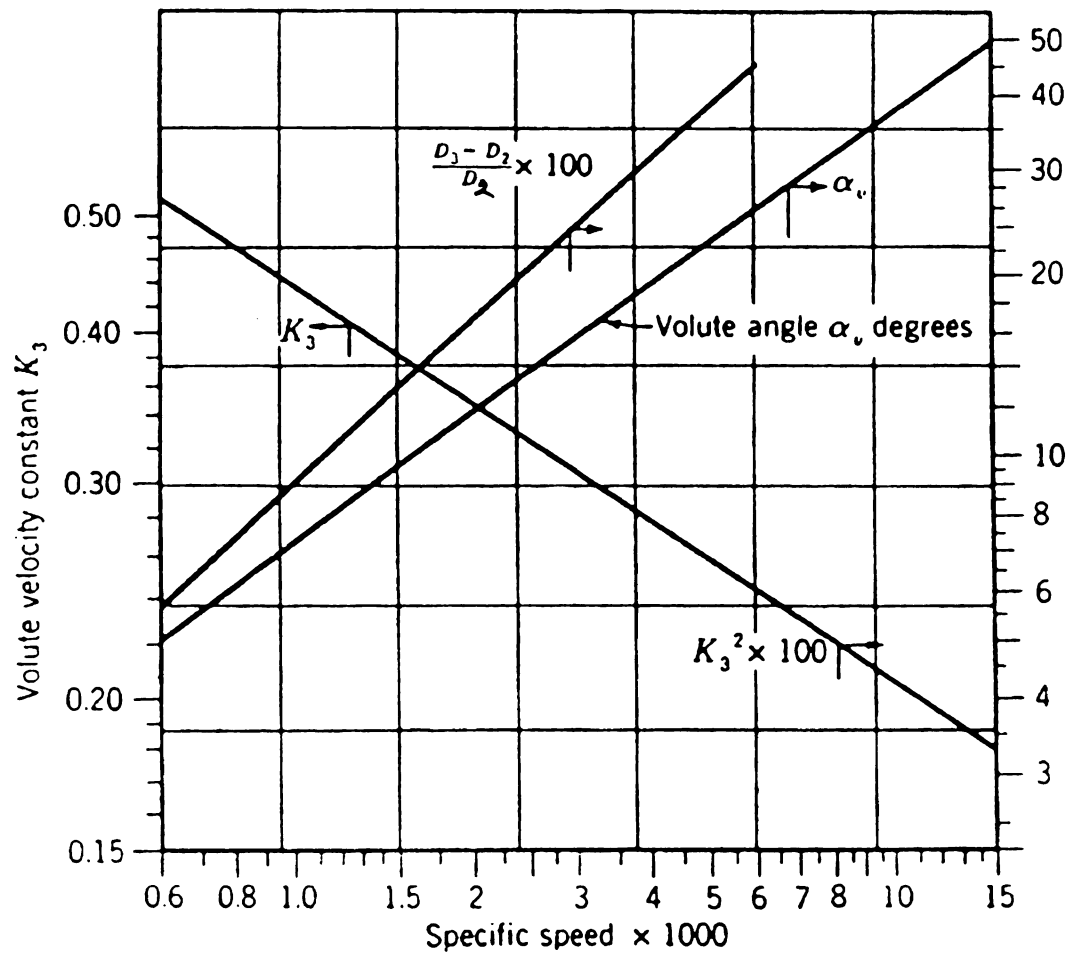


Figure 4.1 Volute Constants (after Stepanoff, A., 1993)

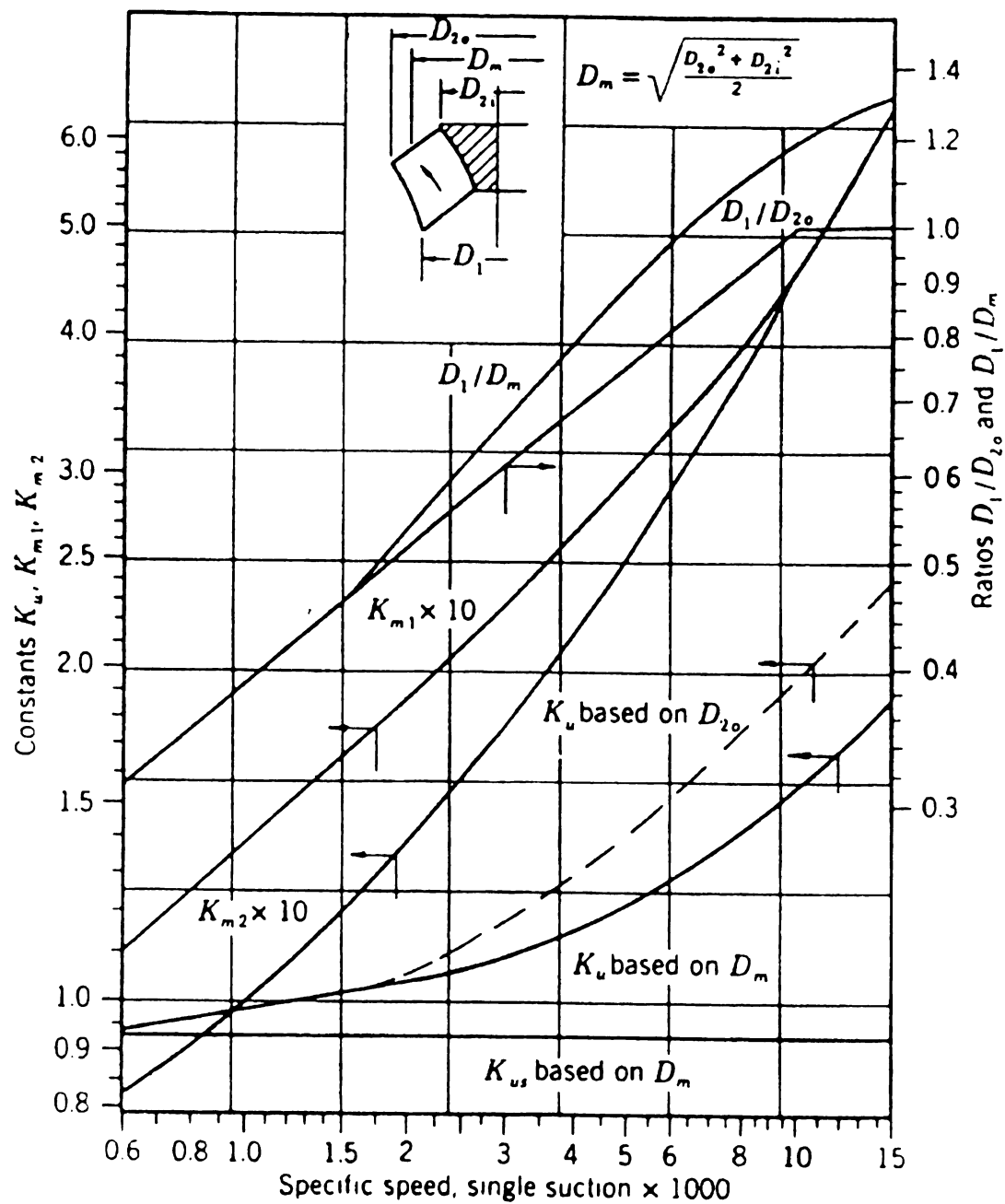
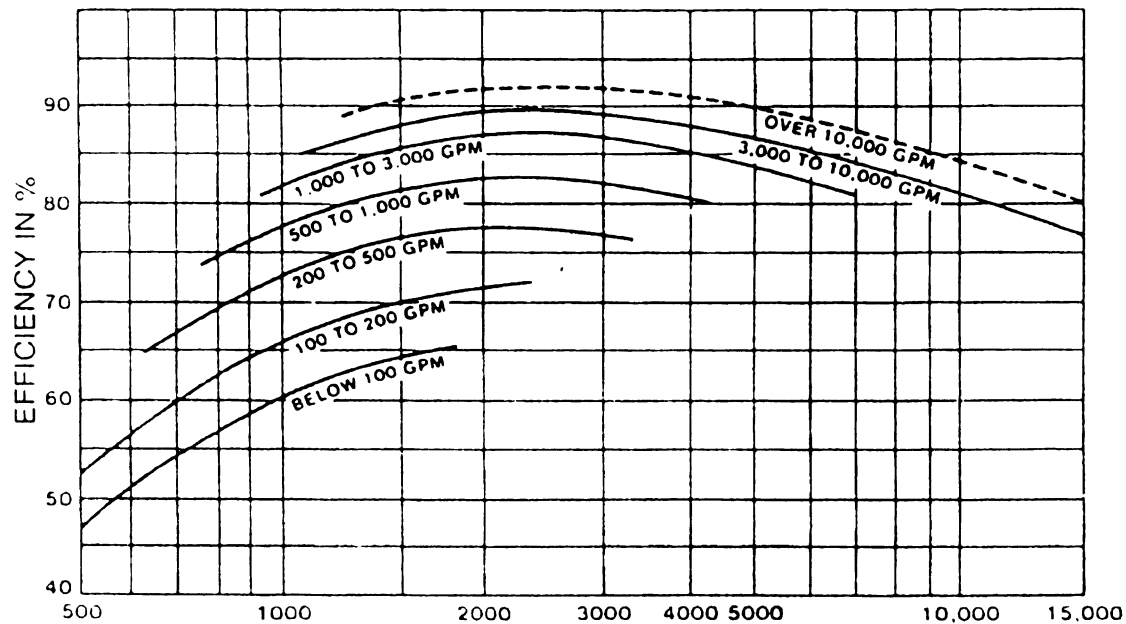


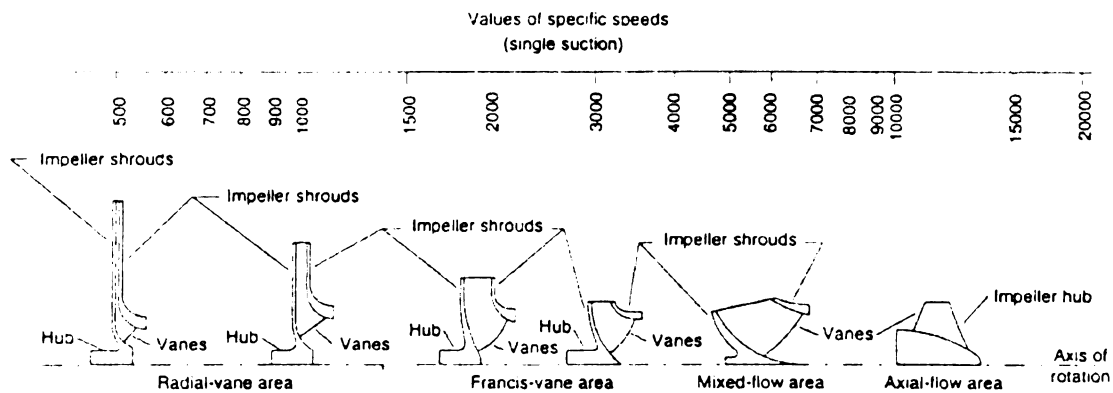
Figure 4.2 Impeller Constants (after Stepanoff, A., 1993)



$$\text{VALUES OF SPECIFIC SPEED } N_s = \frac{\text{rpm} \sqrt{\text{GPM}}}{H^{3/4}}$$

$$N_s = \frac{\phi^{1/2}}{\psi^{3/4}}; \phi = \frac{Q}{ND^3}; \psi = \frac{\Delta h}{(ND)^2}; N_s = \frac{N\sqrt{Q}}{H^{3/4}}$$

$$\text{VALUES OF SPECIFIC SPEED (SINGLE SUCTION); } N_s = \frac{N\sqrt{Q}}{H^{3/4}}$$



NOTE – Profiles of several pump impeller designs ranging from low specific speed radial flow on the left to a high specific speed axial flow on the right, placed according to where each design fits on the specific speed scale.

Figure 4.3 Pump Efficiency versus Specific Speed and Pump Size-Worthington (after Stepanoff, A., 1993)

Resistance of Bends

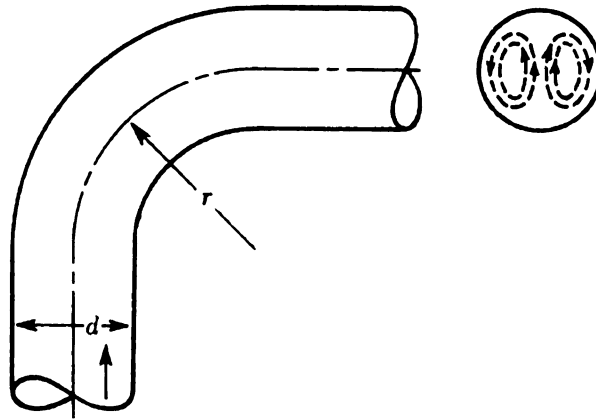
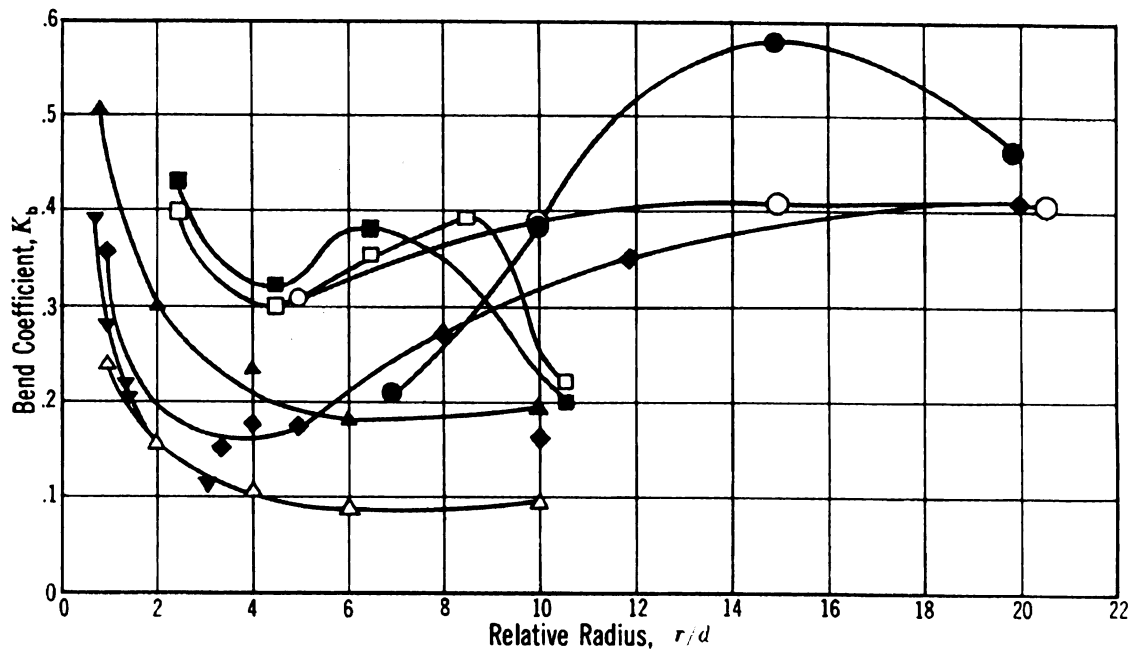


Figure 4.4 Secondary Flow in Bends (after Crane Company, 1969)



Investigator	Diameter	Symbol
Balch.....	3-inch.....	●
Davis.....	2-inch.....	○
Brightmore.....	3-inch.....	■
Brightmore.....	4-inch.....	□
Hofmann.....	1.7-inch (rough pipe).....	▲
Hofmann.....	1.7-inch (smooth pipe).....	△
Vogel.....	.6, 8, and 10-inch.....	▼
Beij.....	4-inch.....	◆

Figure 4.5 Bend Coefficients in Resistance of Bends Found by Various Investigators (after Crane Company, 1969)

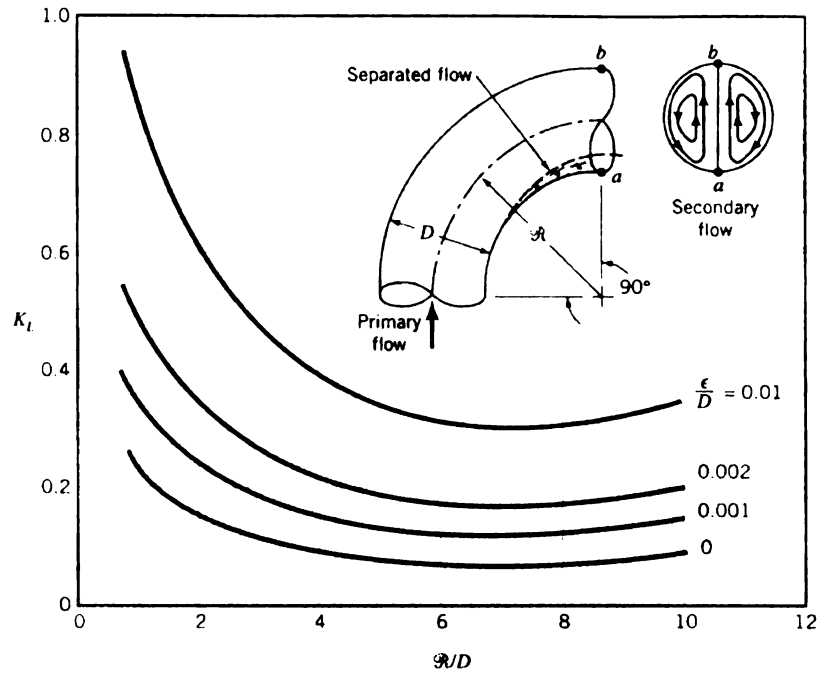


Figure 4.6 Character of the Flow in a 90° Bend and the Associated Loss Coefficient (after Munson, B., Young, D., Okiishi, T., 2002)

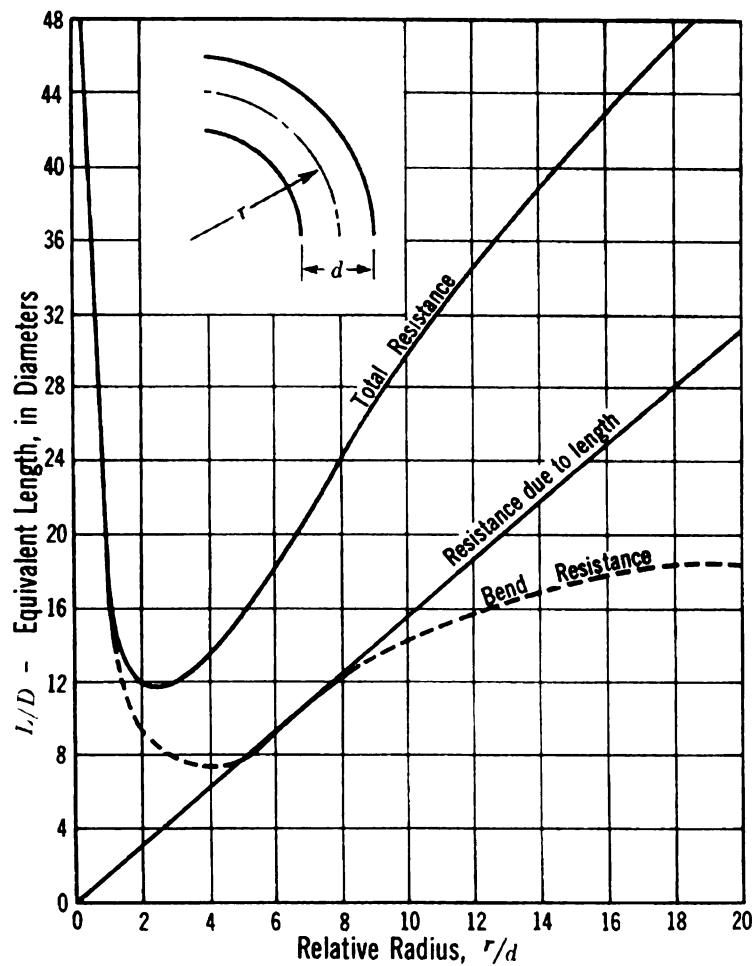
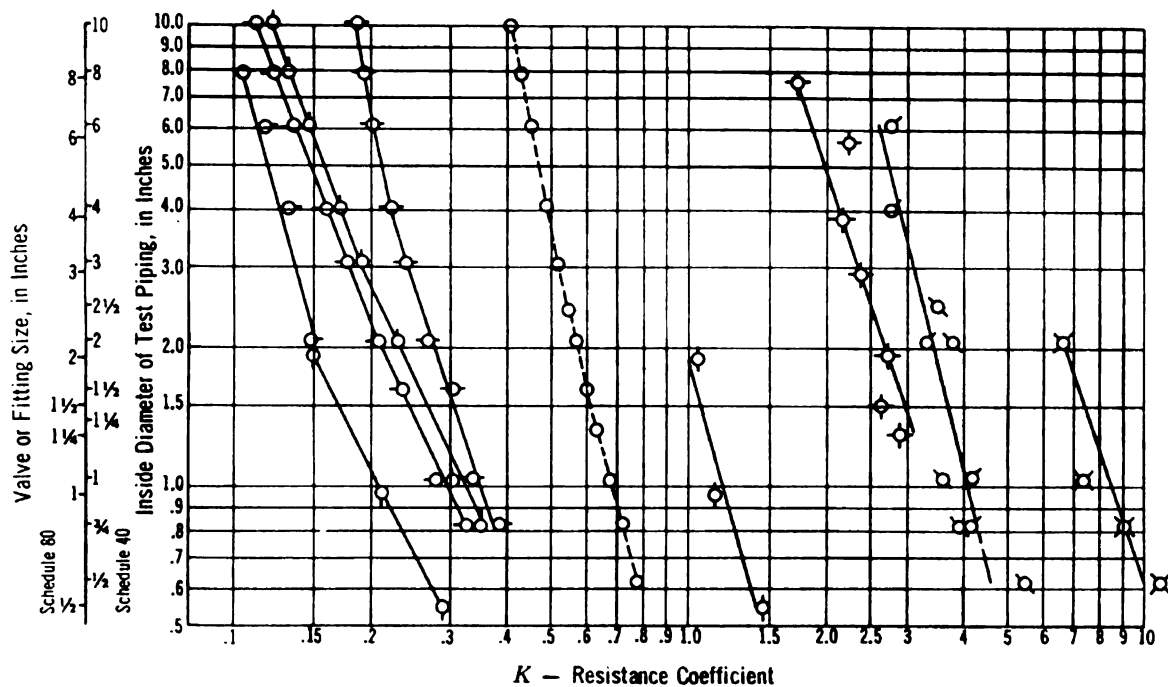


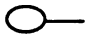



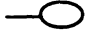



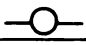


Figure 4.7 Resistance of 90° Bends (after Crane Company, 1969)



Symbol	Product tested	Symbol	Product tested
	Schedule 40 Pipe, 30 Diameters long ($K = 30 f$)		600-pound steel wedge gate valves, seat reduced
	125-pound Iron body wedge gate valves		600-pound steel venturi ball- cage gate valves
	600-pound steel wedge gate valves		125-pound iron body Y- pattern globe valves
	90 degree pipe bends, $R/D = 2$		125-pound brass angle valves, composition disc
	90 degree pipe bends, $R/D = 3$		125-pound brass globe valves, composition disc
	90 degree pipe bends, $R/D = 1$		

**Figure 4.8 Variation of Resistance Coefficient $K (= f L/D)$ with Size
(after Crane Company, 1969)**

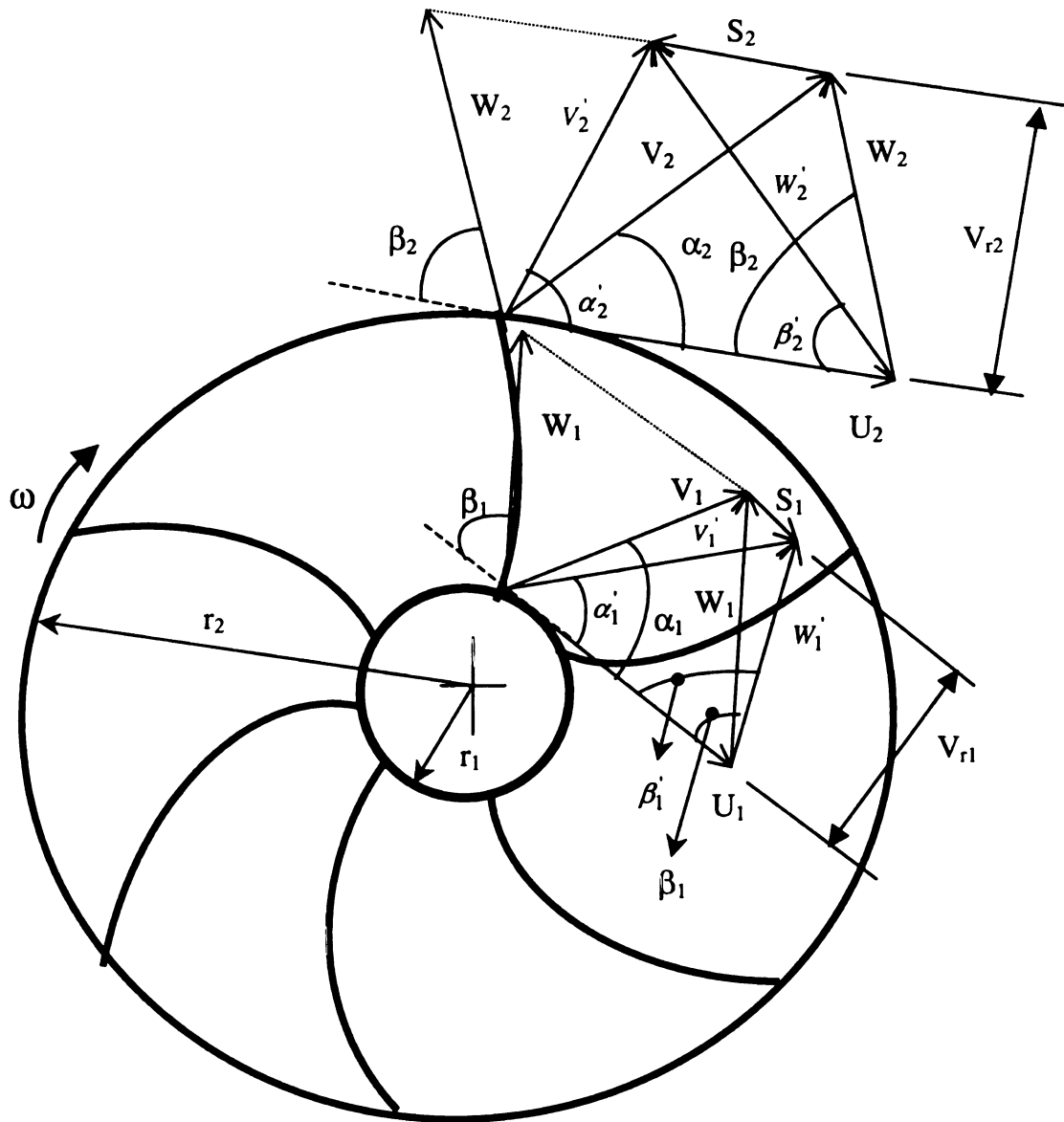


Figure 4.9 Ideal Impeller Velocities ($V_1, W_1; V_2, W_2$ Without Slip Effect) and Actual Impeller Velocities ($V'_1, W'_1; V'_2, W'_2$ With Slip Effect) at Inlet and Exit

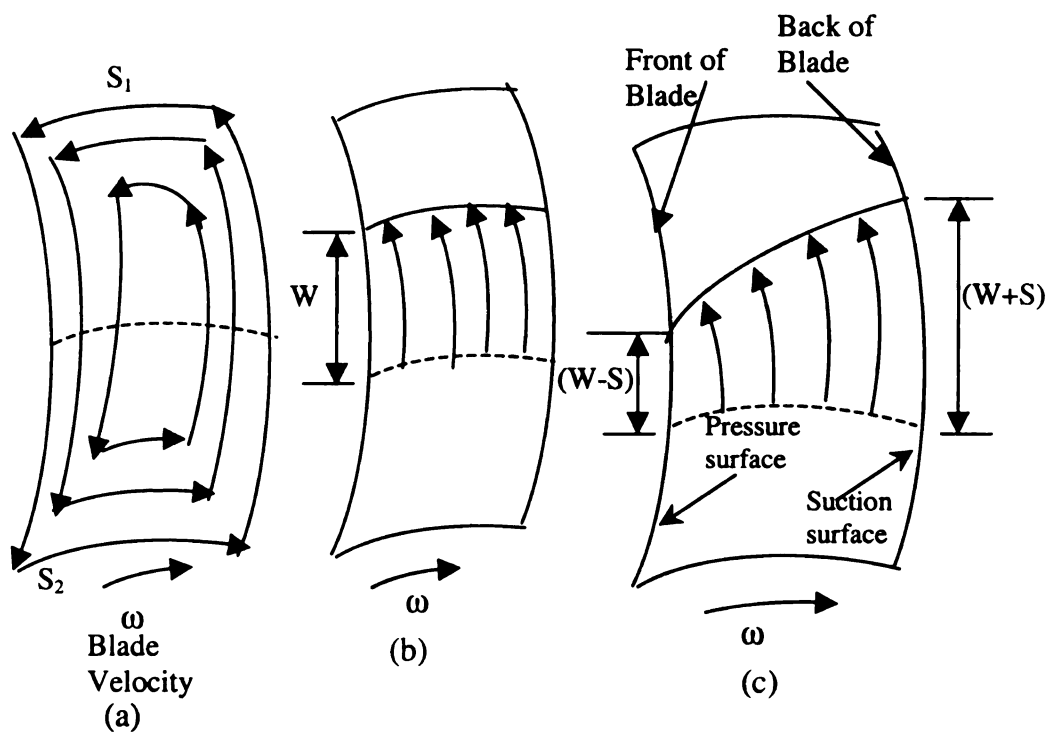


Figure 4.10 Flow Through A Blade Passage

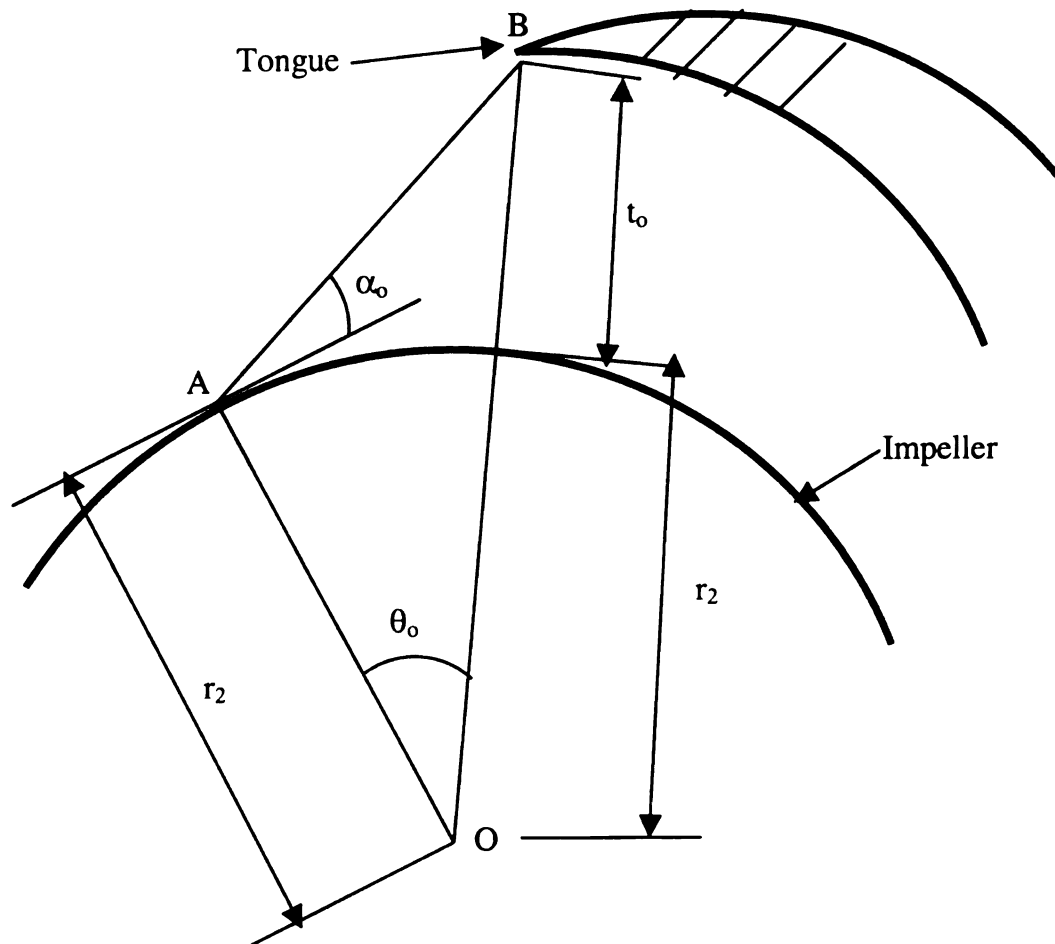
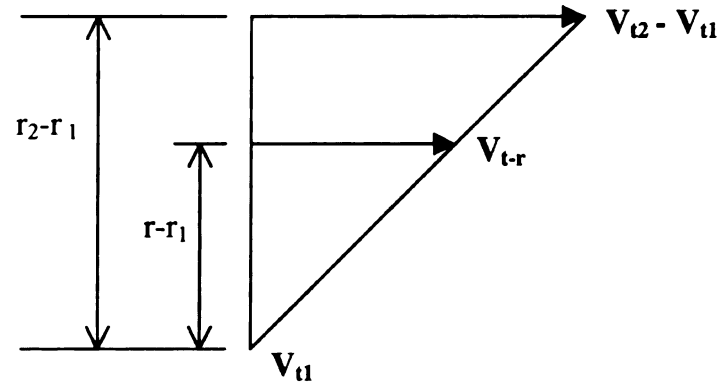


Figure 4.11 Determination of θ_0





$$\frac{V_{t2} - V_{t1}}{r_2 - r_1} = \frac{V_{t-r}}{r - r_1} \Rightarrow V_{t-r} = \frac{r - r_1}{r_2 - r_1} (V_{t2} - V_{t1})$$

$$V_{t(r)} = V_{t1} + V_{t-r} = V_{t1} + \frac{r - r_1}{r_2 - r_1} (V_{t2} - V_{t1})$$

Figure 4.13 Tangential Velocity of Fluid at any radius $V_{t(r)}$

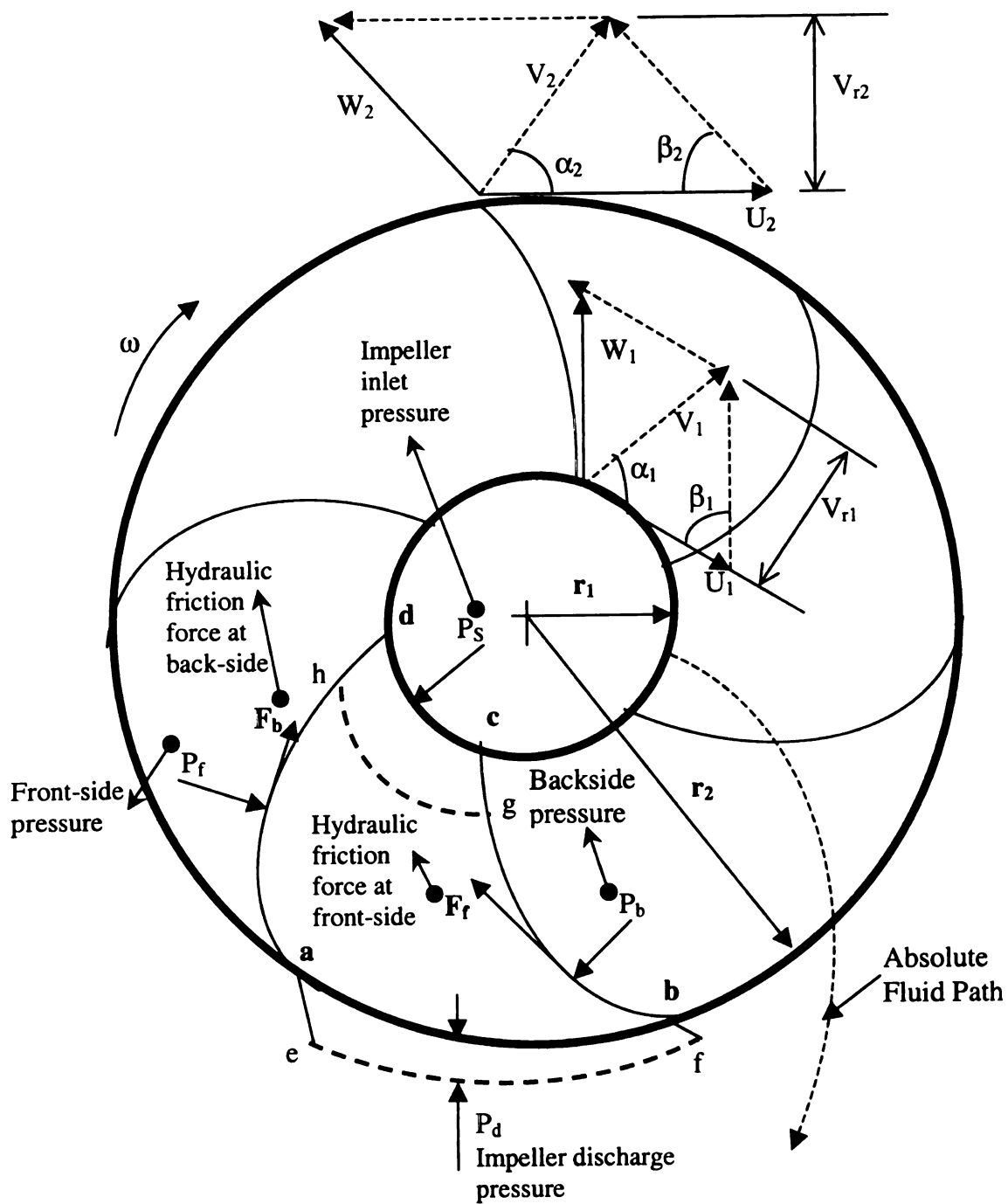


Figure 4.14 Forces and Velocities in an Impeller

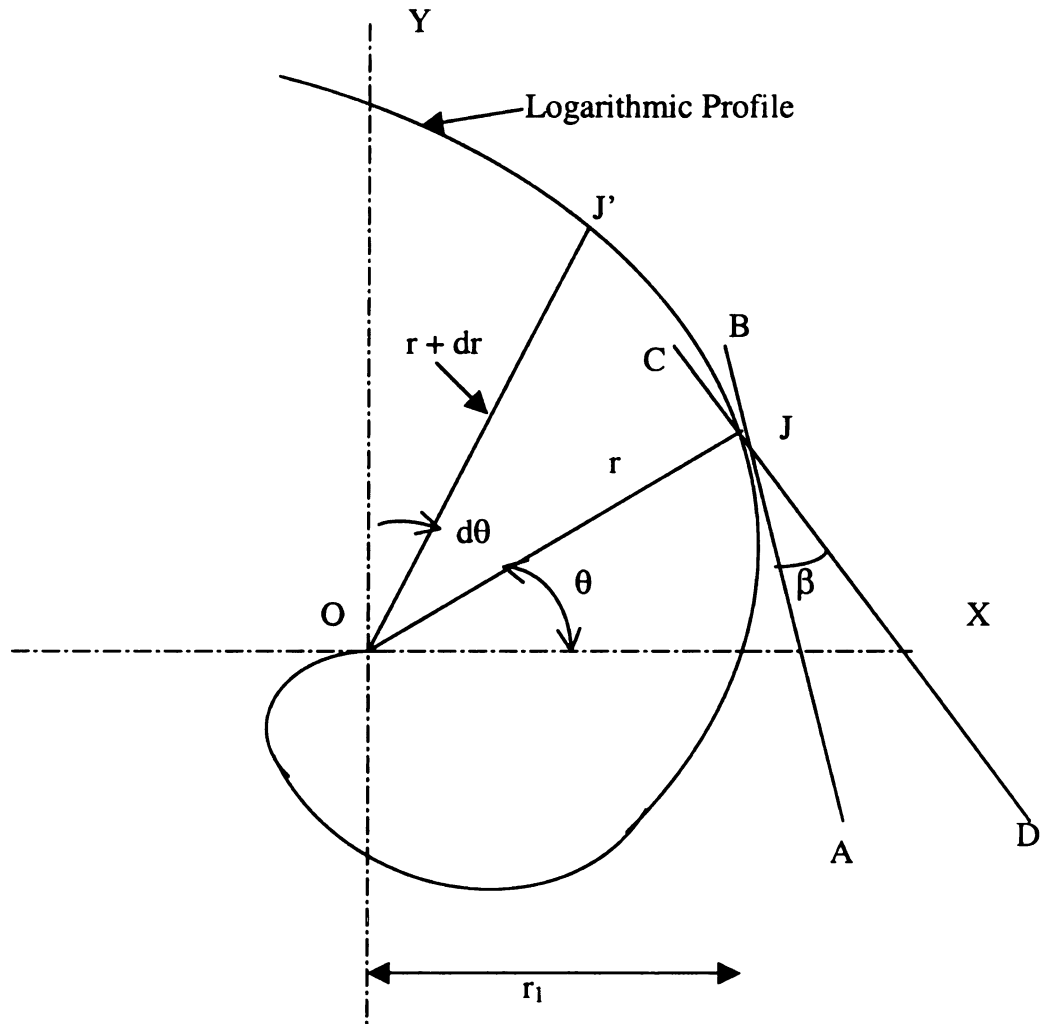


Figure 4.15 Logarithmic Profile

Line AB – Tangent to the Logarithmic Profile

Line CD – Perpendicular to Radius, r

Line JJ' – Elemental Length, dL

Chapter 5

DESIGN RECOMMENDATION

This chapter presented the optimized results of the pump efficiency from the un-conventional pump design. Besides this, some possible recommendations were also mentioned to improve the qualitative and quantitative evaluations of un-conventional pump performance more accurately and more reliably.

There were some assumptions used for the un-conventional pump design:

- Entrance-Bend-Resistance coefficient: K_b
- Blade thickness: t
- Front axial clearance between impeller and housing: δ

The following solution was recommended for increasing the pump efficiency:

- ✦ Optimize the results of the un-conventional pump design

In this solution, the geometrical parameters of pump would be the first optimization. Then, the pump efficiency was the second optimization. In order to implement the optimization process of the pump geometrical parameters, the fifteen possible cases of pump operation were set up for the optimizing process (Table 5.2). All the necessary impeller and volute constants were selected (Table 5.3). From the results of the pump geometrical parameters in fifteen cases, the final optimum data set of pump geometrical parameters was chosen after the optimization process of pump geometrical parameters had been executed. There were some small differences between the calculation and the selection of pump geometrical parameters. This was continuously carried out in the optimization process because of the following two reasons:

- The simplification and the feasibility of the manufacturing process for blade impeller.
- The experimental data of high pump efficiency of unconventional pump collected by Rathod.

From the optimized geometrical parameters of un-conventional centrifugal pump design, the pump efficiency was optimized from twelve design cases with different number of blades, different exit blade angles, and different rotational speed in terms of volume flow rate.

The twelve plots were made after collecting data from the two MATLAB programs of centrifugal pump geometrical parameters and centrifugal pump efficiency. These two MATLAB programs can be found in Appendix F.

At the design point, the volume flow rate is $Q = 39.0772 \text{ cm}^3/\text{sec}$, $N = 9000 \text{ rpm}$.

This volume flow rate can approximately equal $Q = 40 \text{ cm}^3/\text{sec}$.

Table 5.1 Un-conventional Pump Efficiencies of twelve design cases at Design Point

Design Point: $Q = 40 \text{ cm}^3/\text{s}$ and $N = 9000 \text{ rpm}$			
	Number of Blades	Exit Blade Angle	Pump Efficiency (%)
Case 1: P420	$Z = 4$	$\beta_2 = 20^\circ$	56.2303
Case 2: P430	$Z = 4$	$\beta_2 = 30^\circ$	60.2788
Case 3: P470	$Z = 4$	$\beta_2 = 70^\circ$	65.0489
Case 4: P490	$Z = 4$	$\beta_2 = 90^\circ$	65.5942
Case 5: P620	$Z = 6$	$\beta_2 = 20^\circ$	55.3285
Case 6: P630	$Z = 6$	$\beta_2 = 30^\circ$	54.0874
Case 7: P670	$Z = 6$	$\beta_2 = 70^\circ$	60.6298
Case 8: P690	$Z = 6$	$\beta_2 = 90^\circ$	61.0343
Case 9: P820	$Z = 8$	$\beta_2 = 20^\circ$	53.9138
Case 10: P830	$Z = 8$	$\beta_2 = 30^\circ$	55.2012
Case 11: P870	$Z = 8$	$\beta_2 = 70^\circ$	58.1729
Case 12: P890	$Z = 8$	$\beta_2 = 90^\circ$	58.4956

From Table 5.1, the centrifugal pump efficiency at design point is highest ($\eta = 65.5942\%$) when the number of blades is four and the exit blade angle is $\beta_2 = 90^\circ$. The

next optimal pump efficiency is $\eta = 65.0498\%$ when the number of blades is four and the exit blade angle is $\beta_2 = 70^\circ$.

From the twelve plots, the twelve feasible design cases of high pump efficiencies in twelve plots are recommended in terms of twelve different operating conditions as follows:

Figure 5.1: $Z = 4$, $\beta_2 = 20^\circ$; $\eta = 56.7066\%$ when $N = 10500$ rpm and $Q = 40 \text{ cm}^3/\text{s}$

Figure 5.2: $Z = 4$, $\beta_2 = 30^\circ$; $\eta = 68.0542\%$ when $N = 3000$ rpm and $Q = 140 \text{ cm}^3/\text{s}$

Figure 5.3: $Z = 4$, $\beta_2 = 70^\circ$; $\eta = 72.4829\%$ when $N = 3000$ rpm and $Q = 140 \text{ cm}^3/\text{s}$

Figure 5.4: $Z = 4$, $\beta_2 = 90^\circ$; $\eta = 72.8705\%$ when $N = 3000$ rpm and $Q = 140 \text{ cm}^3/\text{s}$

Figure 5.5: $Z = 6$, $\beta_2 = 20^\circ$; $\eta = 65.3501\%$ when $N = 3000$ rpm and $Q = 140 \text{ cm}^3/\text{s}$

Figure 5.6: $Z = 6$, $\beta_2 = 30^\circ$; $\eta = 54.9107\%$ when $N = 10500$ rpm and $Q = 40 \text{ cm}^3/\text{s}$

Figure 5.7: $Z = 6$, $\beta_2 = 70^\circ$; $\eta = 68.1302\%$ when $N = 3000$ rpm and $Q = 140 \text{ cm}^3/\text{s}$

Figure 5.8: $Z = 6$, $\beta_2 = 90^\circ$; $\eta = 68.377\%$ when $N = 3000$ rpm and $Q = 140 \text{ cm}^3/\text{s}$

Figure 5.9: $Z = 8$, $\beta_2 = 20^\circ$; $\eta = 63.1214\%$ when $N = 3000$ rpm and $Q = 140 \text{ cm}^3/\text{s}$

Figure 5.10: $Z = 8$, $\beta_2 = 30^\circ$; $\eta = 64.18\%$ when $N = 3000$ rpm and $Q = 140 \text{ cm}^3/\text{s}$

Figure 5.11: $Z = 8$, $\beta_2 = 70^\circ$; $\eta = 65.6456\%$ when $N = 3000$ rpm and $Q = 140 \text{ cm}^3/\text{s}$

Figure 5.12: $Z = 8$, $\beta_2 = 90^\circ$; $\eta = 65.8279\%$ when $N = 3000$ rpm and $Q = 140 \text{ cm}^3/\text{s}$

Table 5.2 Rotational speed, flow rate, head, specific speed in fifteen design cases of pump geometry determination

	N (rpm)	Q (cm ³ /s)	Q (ft ³ /s)	Q (gal/m)	H (ft)	N _s
Case 1	7500	10	3.53E-04	0.15831	165.23	64.752
Case 2	7500	30	1.06E-03	0.47493	165.23	112.153
Case 3	7500	39.0772	1.38E-03	0.61864	165.23	128.001
Case 4	7500	60	2.12E-03	0.94987	165.23	158.608
Case 5	7500	100	3.53E-03	1.58311	165.23	204.763
Case 6	9000	10	3.53E-04	0.15831	165.23	77.702
Case 7	9000	30	1.06E-03	0.47493	165.23	134.584
Case 8	9000	39.0772	1.38E-03	0.61864	165.23	153.601
Case 9	9000	60	2.12E-03	0.94987	165.23	190.330
Case 10	9000	100	3.53E-03	1.58311	165.23	245.715
Case 11	10500	10	3.53E-04	0.15831	165.23	90.652
Case 12	10500	30	1.06E-03	0.47493	165.23	157.014
Case 13	10500	39.0772	1.38E-03	0.61864	165.23	179.201
Case 14	10500	60	2.12E-03	0.94987	165.23	222.052
Case 15	10500	100	3.53E-03	1.58311	165.23	286.668

Table 5.3 Necessary Impeller and Volute constants in determining the optimized pump geometrical parameters from fifteen design cases

	Impeller Constants					Volute Constants		
	N _s	K _u	K _{m1}	K _{m2}	d ₁ /d ₂	K ₃	Phi (degree)	(D ₃ -D ₂)*100/D ₂ (2*to*100/d2)
Case 1	64.752	0.87	0.082	0.062	0.22	0.64	2.5	2.4
Case 2	112.153	0.88	0.085	0.063	0.23	0.62	2.7	2.6
Case 3	128.001	0.88	0.085	0.064	0.24	0.61	2.9	2.8
Case 4	158.608	0.89	0.086	0.065	0.27	0.6	3.5	3.4
Case 5	204.763	0.9	0.09	0.068	0.27	0.58	3.6	3.5
Case 6	77.702	0.87	0.087	0.062	0.22	0.64	2.6	2.5
Case 7	134.584	0.88	0.088	0.064	0.25	0.61	2.9	2.8
Case 8	153.601	0.89	0.086	0.065	0.26	0.6	3.5	3.4
Case 9	190.330	0.9	0.09	0.068	0.27	0.57	3.6	3.5
Case 10	245.715	0.93	0.096	0.072	0.28	0.55	3.7	3.6
Case 11	90.652	0.88	0.088	0.062	0.23	0.65	2.7	2.6
Case 12	157.014	0.89	0.086	0.065	0.26	0.6	3.5	3.4
Case 13	179.201	0.9	0.09	0.068	0.26	0.57	3.6	3.5
Case 14	222.052	0.92	0.092	0.07	0.27	0.58	3.6	3.5
Case 15	286.668	0.95	0.098	0.074	0.29	0.54	3.7	3.6

In order to have a more accurate prediction, a quantitative CFD analysis at off-design should be performed to validate the assumptions made in the un-conventional one-dimensional design.

From the conventional design and un-conventional design of centrifugal pump, the fluid dynamic design of a centrifugal pump is basically 1-D design. The 1-D design sets the principal pump dimensions in order to satisfy the expected performance data (rotational speed, specific speed, head, flow rate). Having applied 1-D design method, the centrifugal pump efficiency was calculated on the qualitative basis. Moreover, the calculations also rely on empirical correlations such as impeller constants and volute constants. Consequently, a high precision can be unattainable. In order to reach a more accurate improvement in the pump performance, 2-D design, 3-D design, and viscous design should be implemented.

The 2-D design refers to Blade-to-Blade and meridional surfaces. This allows a much deeper insight into the distribution of velocities and pressures in the flow field. The 2-D design can provide the qualitative evaluation of relevant phenomena such as flow separation due to excess of diffusion, cavitations because of local expansion conditions, re-circulation and so on. However, only a little quantitative data of flow conditions can be collected.

The 3-D design and viscous design can provide the detailed flow phenomena. This can be done by solving models for the two-dimensional boundary layers or for the propagation of secondary-flow vorticity.

With optimum geometry of centrifugal pump having low flow rate, low specific speed and high rotational speed, significant flow losses due to geometry size and

mechanical losses can be minimized. However, with low available NPSH, high-speed single stage pumps may still suffer the disagreeable compromises between the low NPSH and high rotational speed. Independent-stage speed capacity of multistage pump allows low suction pressure conditions to be met while maintaining maximum overall pump efficiency.

FIGURES

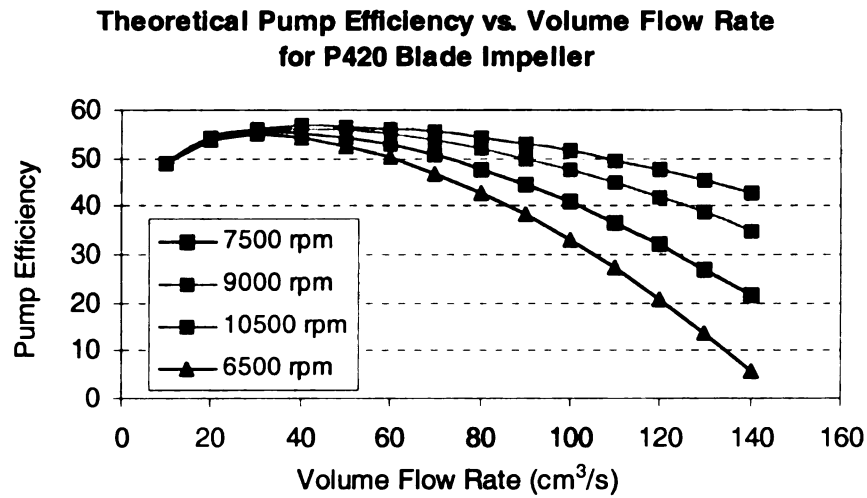


Figure 5.1 Pump Efficiency vs. Volume Flow Rate for P420 Blade Impeller

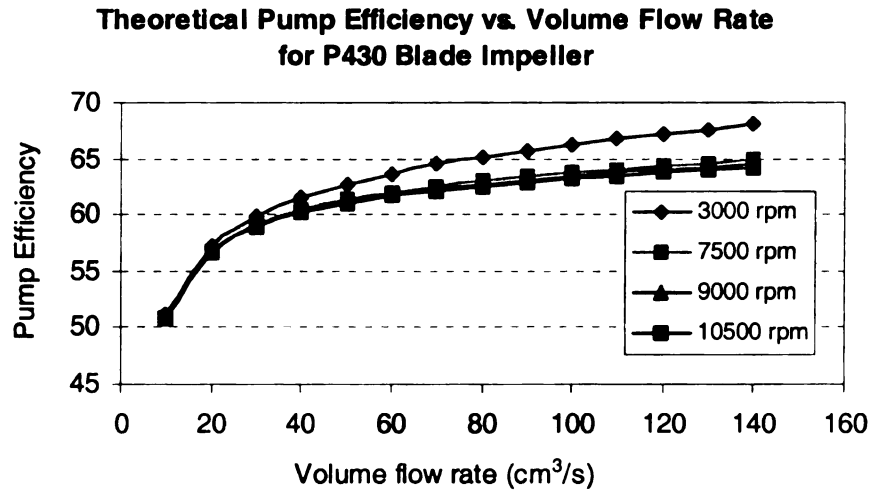


Figure 5.2 Pump Efficiency vs. Volume Flow Rate for P430 Blade Impeller

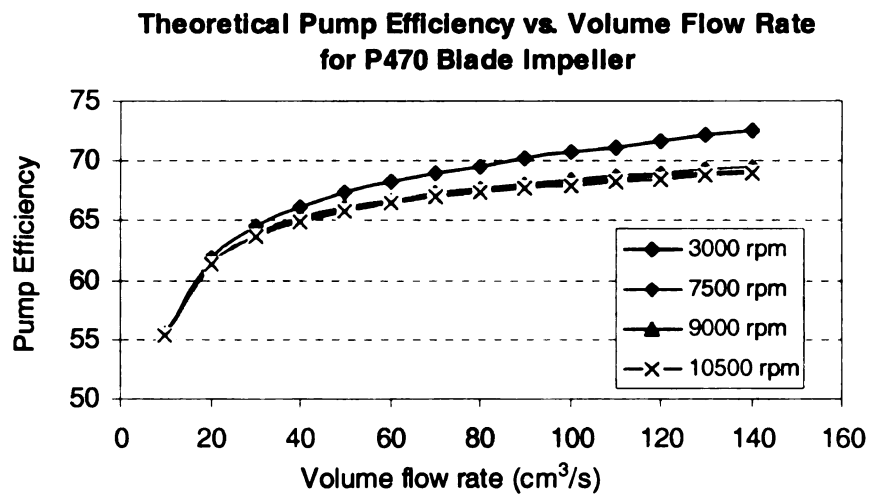


Figure 5.3 Pump Efficiency vs. Volume Flow Rate for P470 Blade Impeller

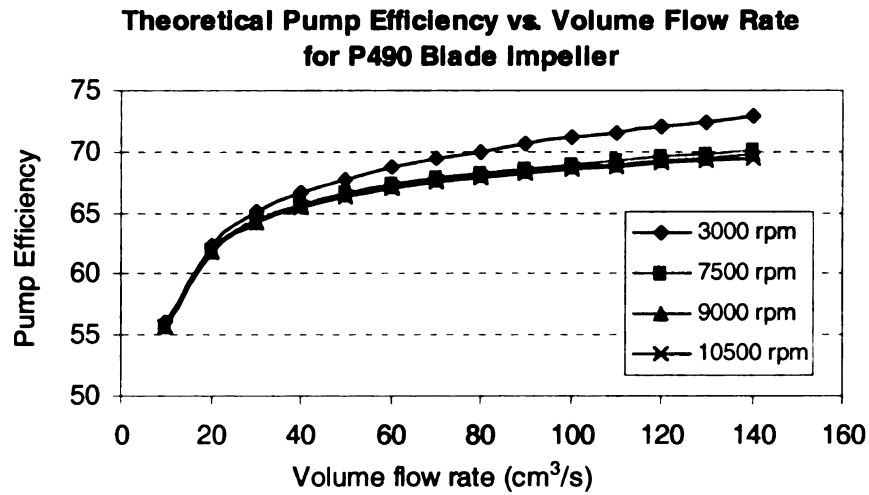


Figure 5.4 Pump Efficiency vs. Volume Flow Rate for P490 Blade Impeller

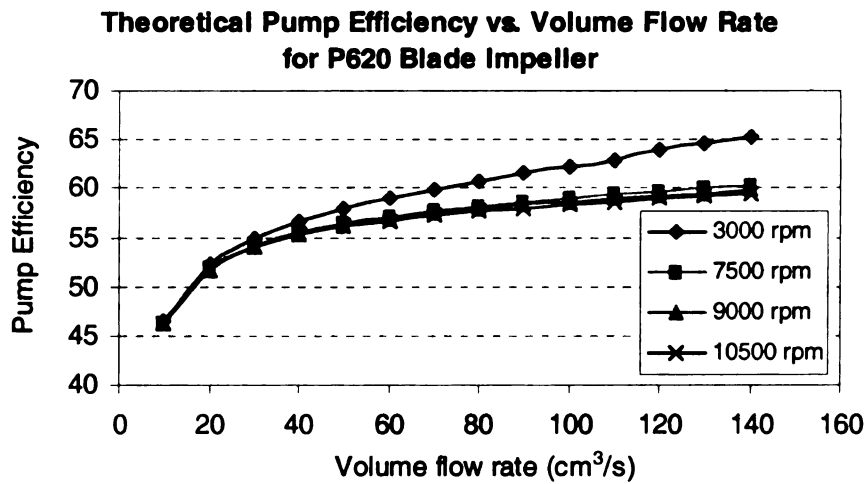


Figure 5.5 Pump Efficiency vs. Volume Flow Rate for P620 Blade Impeller

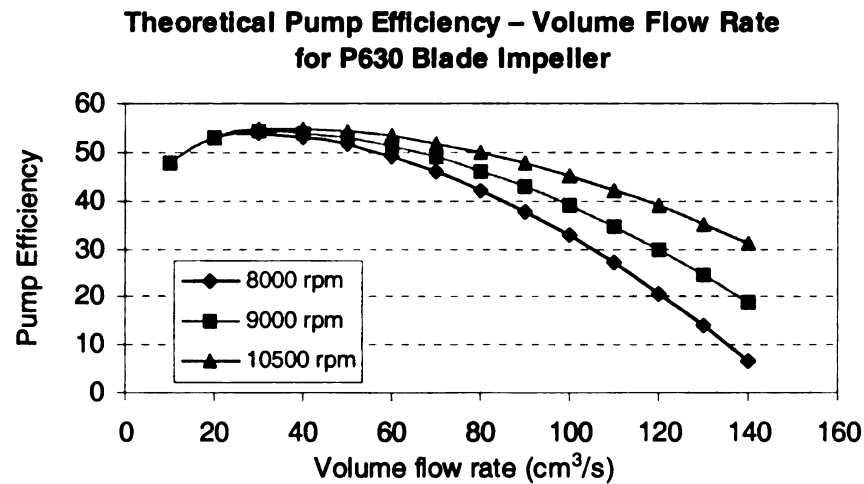


Figure 5.6 Pump Efficiency vs. Volume Flow Rate for P630 Blade Impeller

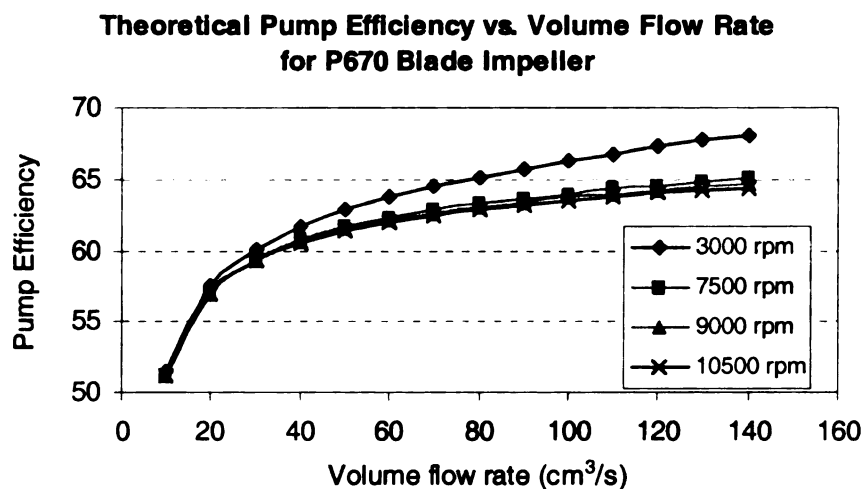


Figure 5.7 Pump Efficiency vs. Volume Flow Rate for P670 Blade Impeller

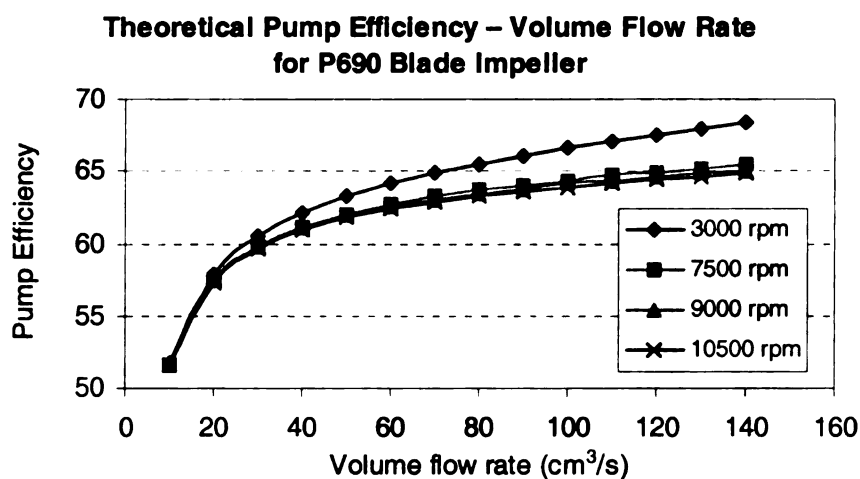


Figure 5.8 Pump Efficiency vs. Volume Flow Rate for P690 Blade Impeller

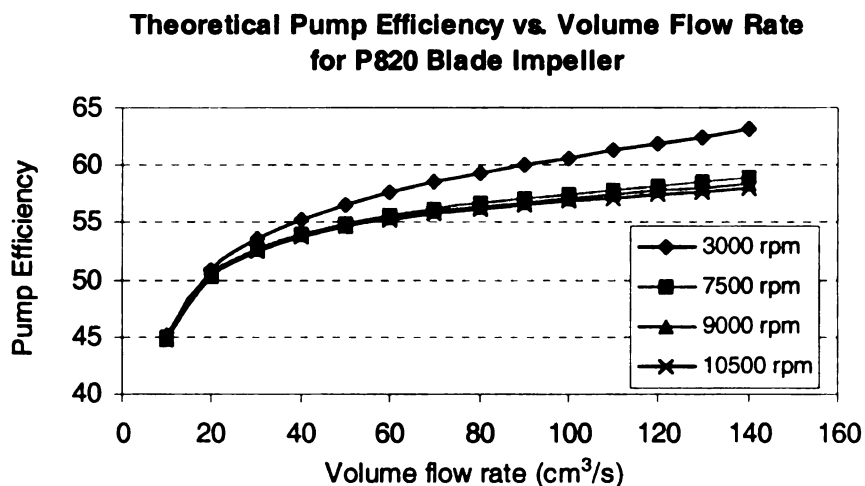


Figure 5.9 Pump Efficiency vs. Volume Flow Rate for P820 Blade Impeller

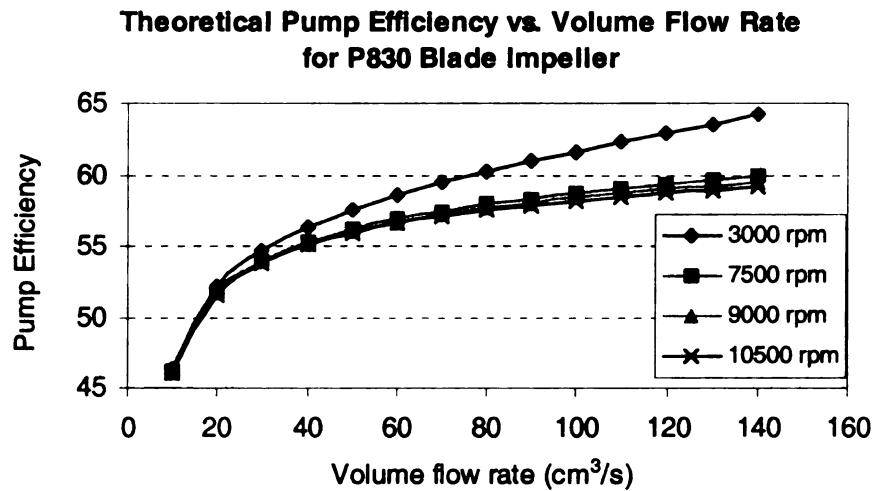


Figure 5.10 Pump Efficiency vs. Volume Flow Rate for P830 Blade Impeller

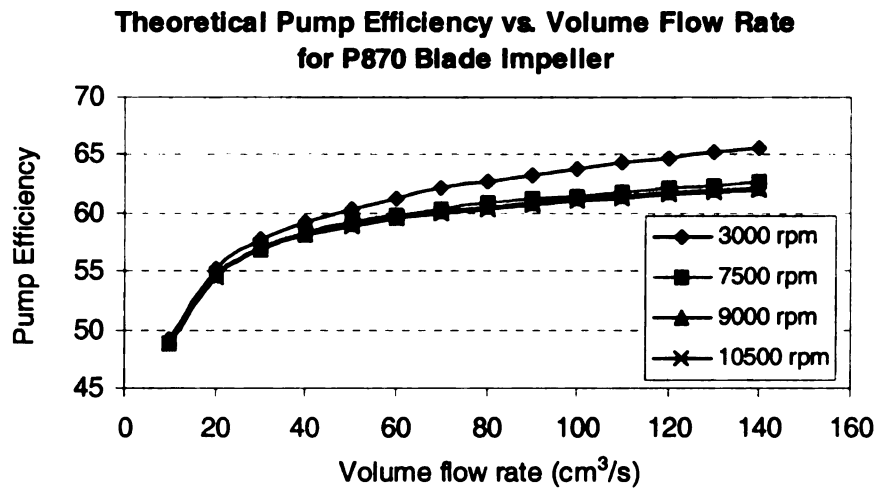


Figure 5.11 Pump Efficiency vs. Volume Flow Rate for P870 Blade Impeller

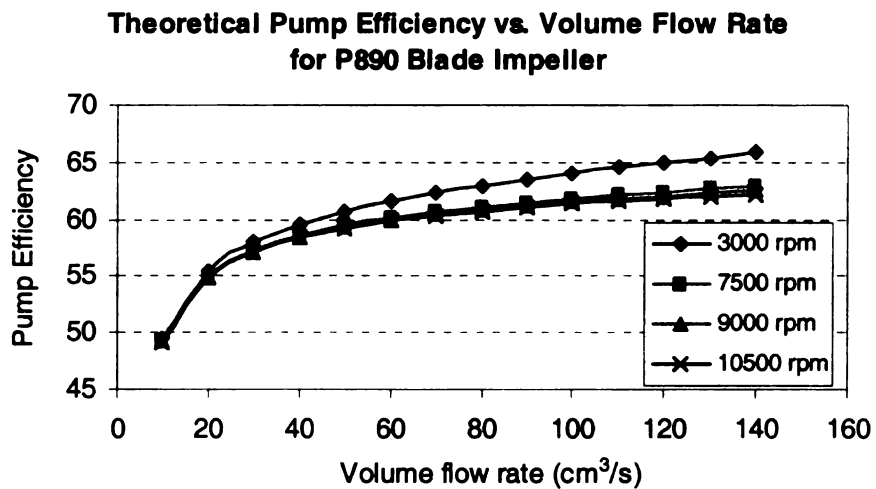


Figure 5.12 Pump Efficiency vs. Volume Flow Rate for P890 Blade Impeller

♣ Impeller geometry for Conventional and Un-Conventional Design

Table 5.4 Impeller Geometry of Conventional Centrifugal Pump Design

Conventional Centrifugal Pump Design ($Z = 7, \beta_2 = 30^\circ, \eta = 7\%$)		
1	Number of impeller blades	$Z = 7$
2	Flow angle ahead of the vane	$\beta_0 = 10^\circ$
3	Blade inlet angle	$\beta_1 = 29.84^\circ$
4	Blade exit angle	$\beta_2 = 30^\circ$
5	Exit impeller width	$b_2 = 0.016 \text{ mm}$
6	Inlet shroud impeller diameter	$d_{s1} = 31.029 \text{ mm}$
7	Inlet hub impeller diameter	$d_{h1} = 30.717 \text{ mm}$
8	Exit impeller diameter	$d_2 = 181.344 \text{ mm}$
9	Inlet blade thickness	$t_1 = s_1 = 4.8 \text{ mm}$
10	Outlet blade thickness	$t_2 = s_2 = 4.8 \text{ mm}$
11	Tongue clearance between impeller and tongue	$t = 6.347 \text{ mm}$
12	Throat radius (Volute hydraulic diameter at exit) (Figure 3.15 Volute casing)	$r_e = r_{thr} = 0.4921 \text{ mm}$
13	Throat area (Volute cross-sectional area at exit)	$A_{thr} = A_e = 0.7606 \text{ mm}^2$
14	Front axial clearance between impeller and housing	$\delta = 0.1 \text{ cm}$

In un-conventional design, the flow of fluid through a centrifugal pump is considered as a superposition of a free-vortex flow over a radial through-flow. The path of the incompressible fluid under this condition is a logarithmic or equiangular spiral with a constant angle between the tangents to the path of the fluid at any point and the radius at that point (Figure 3.21 Impeller with cylindrical vanes).

A logarithmic vane impeller would not force the fluid to follow any particular path. Hence, this impeller would let the fluid follow its own path and would not create adverse pressure gradients. The logarithmic vane impeller has an equiangular spiral with a constant angle. Therefore, the blade inlet and exit angles are equal, $\beta_1 = \beta_2 = \beta$ (Figure 3.22 Logarithmic spiral).

Table 5.5 Impeller Geometry of Un-Conventional Centrifugal Pump Design

Un-Conventional Centrifugal Pump Design ($Z = 4, \beta_2 = 70^\circ, \eta = 65.0498\%$)		
Design Pump Parameters		
1	Volume flow rate	$Q = 1.38 \times 10^{-3} \text{ ft}^3/\text{s} = 1.03 \times 10^{-2} \text{ gal/s}$ $= 3.9 \times 10^{-5} \text{ m}^3/\text{s} = 39.0772 \text{ cm}^3/\text{s}$
2	Rotational speed	$N = 9000 \text{ rpm}$
3	Head	$H = 380 \text{ kPa} = 50.36 \text{ m} = 165.23 \text{ ft}$
Fuel Property		
1	Dynamic viscosity	$\mu = 0.001 \text{ N-s/m}^2$
2	Kinematic viscosity	$\nu = 1.3 \times 10^{-6} \text{ m}^2/\text{s} = 1.3 \times 10^{-2} \text{ cm}^2/\text{s}$
3	Density	$\rho = 770 \text{ kg/m}^3 = 0.77 \text{ g/cm}^3$
Impeller Geometry Parameters		
1	Number of impeller blades	$Z = 4$
2	Flow angle ahead of the vane	$\beta_0 = 18^\circ$
3	Blade inlet angle	$\beta_1 = 70^\circ$
4	Blade exit angle	$\beta_2 = 70^\circ$
5	Inlet impeller width	$b_1 = 1.016 \text{ cm} = 0.4 \text{ in}$
6	Exit impeller width	$b_2 = 1.016 \text{ cm} = 0.4 \text{ in}$
7	Inlet impeller eye diameter (shroud diameter)	$d_1 = d_{s1} = 1.5850 \text{ cm} = 0.624 \text{ in}$
8	Inlet hub diameter	$d_{h1} = 0.262 \text{ in}$
9	Exit impeller diameter	$d_2 = 6.096 \text{ cm} = 2.4 \text{ in}$
10	Inlet blade thickness	$t_1 = 0.40 \text{ cm} = 0.1575 \text{ in}$
11	Inlet blade thickness	$t_2 = 0.40 \text{ cm} = 0.1575 \text{ in}$
12	Assumed front axial clearance between impeller and housing	$\delta = 0.127 \text{ cm} = 0.05 \text{ in}$
13	Volute cross - sectional area at tongue clearance	$A_0 = 0.2419 \text{ cm}^2$
14	Volute cross-sectional area at exit (throat area)	$A_e = 1.9355 \text{ cm}^2$
15	Volute hydraulic diameter at tongue clearance	$D_0 = 0.555 \text{ cm} = 0.2 \text{ in}$
16	Volute hydraulic diameter at exit (throat diameter)	$D_e = 1.5697 \text{ cm} = 0.6 \text{ in}$
17	Tongue clearance between impeller and tongue	$t_0 = 0.1905 \text{ cm} = 0.075 \text{ in}$
18	Volute radial clearance between impeller and housing at volute exit	$t_e = 1.524 \text{ cm} = 0.6 \text{ in}$
19	Housing inside axial width in the volute region	$b_0 = 1.27 \text{ cm} = 0.5 \text{ in}$
20	Housing axial width at exit	$b_e = 1.27 \text{ cm} = 0.5 \text{ in}$

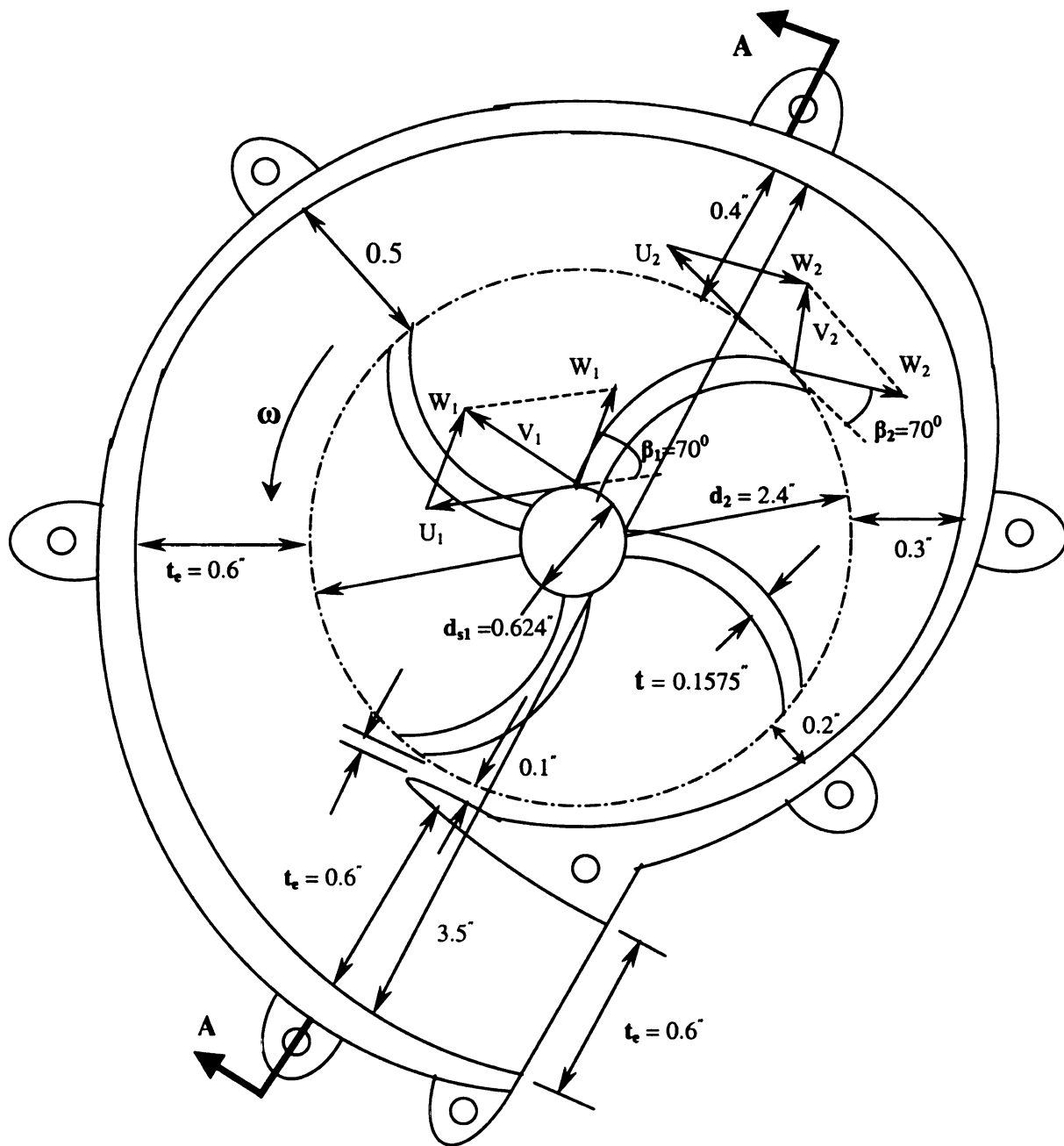


Figure 5.13 Un-conventional Centrifugal Pump Assembly
Volute cover is removed, ($Z = 4$, $\beta_2 = 70^\circ$, $\eta = 65.0498\%$)

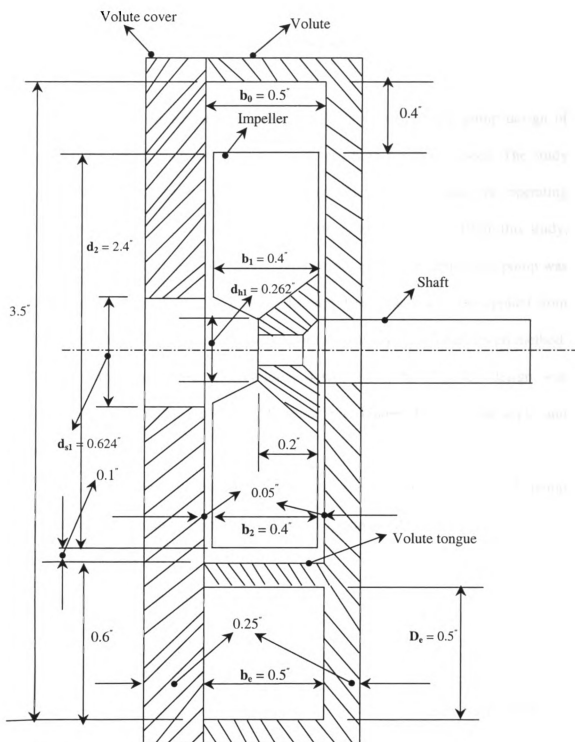


Figure 5.14 Un-conventional Centrifugal Pump Assembly
 Cutting Section A-A ($Z = 4$, $\beta_2 = 70^\circ$, $\eta = 65.0498\%$)

Chapter 6

CONCLUSIONS

This thesis has implemented a numerical study on centrifugal pump design of very low specific speed, very low flow rate and very high rotational speed. The study began with the introduction of centrifugal pump. On the other hand, the operating processes of the current automotive fuel pump systems were analyzed. From this study, the feasibility in the replacement of automotive fuel pumps by the centrifugal pump was considered and clarified. Then, the centrifugal pump design methods were applied from the conventional design method and approaching to the un-conventional design method. Finally, the optimization of un-conventional design from the required design was numerically obtained from the variables of the number of blades, the exit blade angle, and the flow rate.

In un-conventional pump design method, the following theoretical pump equations were substantiated with the assumption of Stodola's slip factor:

- (1) Circulation head.
- (2) Impeller friction head loss.
- (3) Volute head loss.
- (4) Disk friction loss, leakage loss, and entrance-bend loss.
- (5) Optimization with respect to number of blades and blade angle of a logarithmic vane impeller.
- (6) Derivation of Euler's Head.
- (7) Determination of Logarithmic blade length.

Four-blade impeller, six-blade impeller, and eight-blade impeller were used to analyze the variation of pump efficiency versus the pump capacity. The analyses of these impellers were based on four cases of exit blade angles ($\beta_2 = 20^\circ$, $\beta_2 = 30^\circ$, $\beta_2 = 70^\circ$, and $\beta_2 = 70^\circ$).

The change of the exit blade angles allowed the increase or the decrease of the centrifugal pump efficiency. The change of the rotational speed also made the pump efficiency increase or decrease.

The theoretical pump equations with Stodola's slip factor were numerically analyzed for the logarithmic vane impeller ($\beta_{2b} = 20^\circ$, $\beta_{2b} = 30^\circ$, $\beta_{2b} = 70^\circ$) and the radial vane impeller ($\beta_{2b} = 90^\circ$). The four-blade radial vaned impeller was theoretically more efficient than the four-blade 70° -logarithmic vaned impeller.

It was numerically observed that the optimal number of blades and the exit blade angle were the functions of the fluid properties and the geometrical parameters of the pump. These parameters are the inlet and exit impeller diameters, the inlet and exit blade widths, the inlet and exit blade thickness, the clearance between the impeller and the casing (housing), and the volute geometries.

The un-conventional one-dimensional design method provided a successful centrifugal pump design of very low specific speed, very low flow rate and very high rotational speed. The conventional centrifugal pump design was designed and analyzed from the foundation of the numerical method and experimental data from the current design trend of centrifugal pump design. Moreover, the twelve possible design cases of un-conventional one-dimensional design of centrifugal pump were also delved with more details in this preliminary design phase.

The quantitative performance prediction of pump efficiency with the calculated geometrical parameters cited in this thesis can only be quantified by implementing an research of an experimental testing program. Having based on comparing the experimental data collected by Rathod with design data in this thesis, the qualitatively predicted pump efficiencies appear to be reasonable.

This study would be able to show the qualitative and quantitative results. This will help improve the centrifugal pump design of very low specific speed and very high rotational speed with high efficiency and a large operating range.

The number of impeller blades was selected on a trial basis to increase the pump efficiency under the requirement of design point. The effect of more or fewer blades can be easily explored with the pump efficiency computer program of the un-conventional centrifugal pump design. More blades guide the flow better, increase the slip coefficient, and therefore increase the head. On the other hand, friction losses (leakage losses) are also increased, and the blockage produced by the blade thickness at the inlet could become excessive.

“Conventional centrifugal pump design” attempts to maximize efficiency by optimizing the specific speed (N_s). Since flow and head are usually dictated by the application, speed becomes the remaining variable to maximize the efficiency. However, the speeds necessary to optimize the specific speed within the considered head-flow condition can result in excessive NPSH requirements. This will put the rotating assembly under high stresses and so, cavitations erosion may become important. In reality, the optimum geometry of the centrifugal pump suffers substantial parasitic flow losses due to small impeller size, and mechanical losses may become significant.

For low specific speed ($N_s < 1000$), the hydraulic design will generally result in very small impeller flow passages. These small passages will promote high friction losses, and high degree sensitivity to clearance. In order to solve this problem, the “un-conventional centrifugal pump design” will allow the trade-offs of the following performance parameters prior to select the maximum overall pump efficiency from the design point (very low specific speed, very low flow rate and very high rotational speed).

1. Circulation head.
2. Impeller friction head loss (Impeller hydraulic losses).
3. Volute head loss (Volute hydraulic losses).
4. Disk friction loss, leakage loss, and entrance-bend loss (Mechanical losses).
5. Optimization with respect to number of blades and blade angle of a logarithmic vane impeller.

♣ Summary of Losses between Conventional and Un-Conventional Design

	Mechanical losses	Hydraulic losses	Volute losses
Total losses of Conventional Design	Disk friction loss on the impeller; Incidence loss	Leakage loss; Fluid friction loss; Through-flow loss (viscosity); Disk and ring friction loss (Reynolds number)	Volute loss
Total losses of Un-Conventional Design	Disk Friction loss; Entrance-bend Loss	Impeller friction head loss; Leakage Loss	Volute loss

A. Conventional Design

The Conventional centrifugal pump design calculates “all losses by the fluid parameters” (Specific speed and flow rate). Mechanical loss, hydraulic loss, and volute loss are quantified by mechanical efficiency, hydraulic efficiency, and volute efficiency, which are computed from the fluid parameters. As a result, “pump efficiency only

depends on fluid parameters”. Because of this, conventional design establishes “more constraint in selecting impeller geometry”. When the flow rate is high, the main sources of loss in pump design are generally resulted from the fluid parameters. Moreover, the loss from pump geometry is not significant.

B. Un-Conventional Design (H_f , H_v , H_d , H_L , H_{cb})

The Un-Conventional centrifugal pump design calculates “all losses (Mechanical loss, hydraulic loss, and volute loss) from impeller geometry and fluid parameters”. When the flow rate and specific speed are very low, and the rotational speed is very high; the loss from pump geometry is as significant as the loss from fluid parameters. This method accounts for Impeller friction head loss, Volute head loss, Power due to disk friction loss and leakage loss, Entrance-bend loss from pump geometry before estimating efficiency. “Pump efficiency is dependent on impeller geometry and fluid parameters”. There is “more flexible in selecting impeller geometry”.

B.1. Impeller Friction head losses (H_f) (Hydraulic losses)

The impeller friction head loss, H_f , takes into account of the following elements:

- ♣ Fluid friction and Friction factor.
- ♣ Impeller Reynolds number of Laminar flow or Turbulent flow.
- ♣ Total blockage area at inlet and outlet of vane impeller.
- ♣ The flow rate.
- ♣ Circulation because of slip velocities

Impeller Friction head loss is:

$$\begin{aligned}
H_f = & \frac{\lambda (d_2 - d_1) Q^2}{16 g \sin(\beta)} \left[\frac{\pi d_1 \sin(\beta) - Zt + Zb_1}{b_1^3 (\pi d_1 \sin(\beta) - Zt)^3} + \frac{\pi d_2 \sin(\beta) - Zt + Zb_2}{b_2^3 (\pi d_2 \sin(\beta) - Zt)^3} \right] + \\
& + \frac{\lambda (d_2 - d_1) K_s^2 \pi^2 \omega^2 \sin(\beta)}{64 g Z^2} \left[\frac{d_1^2 (\pi d_1 \sin(\beta) - Zt + Zb_1)}{b_1 (\pi d_1 \sin(\beta) - Zt)} + \right. \\
& \left. + \frac{d_2^2 (\pi d_2 \sin(\beta) - Zt + Zb_2)}{b_2 (\pi d_2 \sin(\beta) - Zt)} \right]
\end{aligned} \tag{6.1}$$

B.2. Volute head losses (H_v)

The Volute head loss, H_v , takes into account of the following elements:

- ♣ Friction surface area, Fluid Friction and mixing of flow in the volute.
- ♣ Wall shear stress, τ_w , with the presence of the friction factor, f .
- ♣ Total blockage area at inlet and outlet of blade impeller
- ♣ Clearance between the tongue and the impeller.

Volute head losses is:

$$\begin{aligned}
H_v = & \frac{1}{2g} \left[v_r^2 + \left(v_t - \frac{Q}{A_e} \right)^2 + \frac{2Q}{A_e} \left(v_t - \frac{Q}{A_e} \right) \left(\frac{A_0}{A_e} - \frac{q_0}{Q} \right) \ln \left(1 + \frac{A_e}{A_0} \right) + \right. \\
& \left. + \left(\frac{Q}{A_e} \right)^2 \left(\frac{A_0}{A_e} - \frac{q_0}{Q} \right)^2 \left(\frac{A_0}{A_e} \right)^{-1} \left(1 + \frac{A_0}{A_e} \right)^{-1} \right] + \\
& + \frac{\pi f r}{g D_e} \left(\frac{Q}{A_e} \right)^2 \left[1 + \left(\frac{A_0}{A_e} - \frac{q_0}{Q} \right)^3 \left(\frac{A_0}{A_e} \right)^{-1} \left(1 + \frac{A_0}{A_e} \right)^{-1} \left(\frac{A_0}{A_e} - \frac{D_0}{D_e} \right)^{-1} - \right. \\
& \left. - \left(\frac{D_0}{D_e} - \frac{q_0}{Q} \right)^3 \left(\frac{A_0}{A_e} - \frac{D_0}{D_e} \right)^{-2} \ln \left(1 + \frac{D_e}{D_0} \right) + \right. \\
& \left. + \left(\frac{A_0}{A_e} - \frac{q_0}{Q} \right)^2 \left(\frac{3D_0}{D_e} - \frac{2A_0}{A_e} - \frac{q_0}{Q} \right) \left(\frac{A_0}{A_e} - \frac{D_0}{D_e} \right)^{-2} \ln \left(1 + \frac{A_e}{A_0} \right) \right]
\end{aligned} \tag{6.2}$$

B.3. Disk friction losses (H_d) (Mechanical losses)

The Disk Friction Loss, H_d , takes into account of the following elements:

- ♣ Friction force of fluid due to the clearance between blade impeller and the housing.
- ♣ Friction between the impeller disk and the fluid.

♣ The surfaces, impeller speed, fluid properties, and the clearance.

The power due to Disk Friction Loss, P_d , is:

$$P_d = \frac{\pi \nu \rho}{2 g_c \delta} \left[\frac{(m_1)^2 ((d_2)^4 - (d_1)^4)}{8} + \frac{2m_1 m_2 ((d_2)^3 - (d_1)^3)}{3} + (m_2)^2 ((d_2)^2 - (d_1)^2) \right] \quad (6.3)$$

B.4. Leakage losses (H_L) (Hydraulic losses)

The Leakage Loss, H_L , takes into account of the following elements:

- ♣ Leakage in open impellers from the leading side to the trailing side of the vanes.
- ♣ Leakage across the vane edge at the clearance between the vane and the housing.

Power loss due to the leakage (P_L):

$$P_L = Z \rho \delta \omega^3 ((d_2)^4 - (d_1)^4) \frac{\sin^2(\beta)}{128 g_c} \quad (6.4)$$

B.5. Entrance-bend losses (H_{eb}) (Mechanical losses)

The Entrance-bend Loss, H_{eb} , takes into account of the following elements:

- ♣ A secondary flow in bend.

The head loss for the entrance-bend is:

$$H_{eb} = \frac{8 K_b Q^2}{\pi^2 g (d_i)^4} \quad (6.5)$$

BIBLIOGRAPHY

BIBLIOGRAPHY

- [1] Munson, B., Young, D., Okiishi, T., 1998. "Fundamentals of Fluid Mechanics", 3rd ed., John Willey & Sons, Inc, New York.
- [2] Munson, B., Young, D., Okiishi, T., 2002. "Fundamentals of Fluid Mechanics", 4th ed., John Willey & Sons, Inc, New York.
- [3] Tuzson, John, 2000. "Centrifugal Pump Design", John Willey & Sons, Inc, New York.
- [4] Turton, R. K., 1994. "Rotordynamic Pump Design", Cambridge University Press, New York.
- [5] Turton, R. K., 1984. "Principles of Turbomachinery", E. & F. N. Spon, New York.
- [6] Stepanoff, A., 1993. "Centrifugal and Axial Flow Pumps", Krieger Publishing Company, Malabar, Florida.
- [7] Stepanoff, A., 1957. "Centrifugal and Axial Flow Pumps", John Willey & Sons, Inc, New York.
- [8] Lobanoff, V., and Ross, R., 1985. "Centrifugal Pumps – Design & Application", Gulf Publishing Company, Houston, Texas.
- [9] Rathod, M. S., and Donovan, F. M., 1979. "Performance Evaluation of A Centrifugal Cardiac Pump", pp235-243, USA.
- [10] Rathod, M. S., 1975. "Theoretical Analysis and Design of a Centrifugal Blood Pump for Optimum Blade Number and Angle", Ph. D. Dissertation, Mississippi State University, Mississippi State, Mississippi.
- [11] Gopalakrishnan, S., 1979. "Performance prediction of centrifugal pumps and compressors", Fluids Engineering Division and the Gas Turbine Division, ASME, New York.
- [12] Logan, E. I., 1993. "Turbomachinery – Basic Theory and Applications", 2nd ed., Marcel Dekker, Inc, New York.
- [13] Logan, E. I., 1995. "Handbook of Turbomachinery", 2nd ed., Marcel Dekker, Inc, New York.
- [14] Finch, V., 1948. "Pump Handbook", National Press, USA.

- [15] Holland, F., and Chapman, F., 1966. "Pumping of Liquids", Reinhold Publishing Corporation, New York.
- [16] Karassik, I., Krutzsch, W., Fraser, W., Messina, J., C, 1986. "Pump Handbook", McGraw-Hill, Inc, New York.
- [17] Karassik, I. J., 1989. "Centrifugal Pump Clinic", 2nd ed., Marcel Dekker, Inc, New York.
- [18] Balje, O., 1981. "Turbomachines – A Guide to Design, Selection, and Theory", John Willey & Sons, Inc, New York.
- [19] Dixon, S., 1998. "Fluid Mechanics and Thermodynamics of Turbomachinery", 4th ed., Butterworth-Heinemann, Woburn, USA.
- [20] Sabersky, R., Acosta, A., Hauptmann, E., and Gates, E., 1999. "Fluid Flow – A First Course in Fluid Mechanics", 4th ed., Prentice-Hall, Inc, Upper Saddle River, New Jersey.
- [21] Newton, K., Steeds, W. and, Garrett, T. K., 1996. "The Motor Vehicle", 12th ed., Society of Automobile Engineers, Inc, Warrendale, PA.
- [22] Ellinger, H. E., 1976. "Automotive Systems – Fuel, Lubrication, and Cooling", Prentice-Hall, Inc, Englewood Cliffs, NJ.
- [23] Whitfield, A., and Baines, N. C., 1990. "Design of Radial Turbomachines", Longman Scientific and Technical, Essex, John Willey & Sons, Inc, New York.
- [24] Ferguson, T. B., 1963. "The Centrifugal Compressor Stage", Butterworths & Co. (Publishers) Ltd., London, Great Britain.
- [25] Stahler, Alfred F., 1965. "The Slip Factor of a Radial Bladed Centrifugal Compressor", Journal of Engineering for Power, Transactions of ASME, Pp.181-192.
- [26] Wiesner, F. J., 1967. "A Review of Slip Factors for Centrifugal Compressors", Journal of Engineering for Power, Transactions of ASME, Pp.558-572.
- [27] Whitfield, A, 1974. "Slip Factor of A Centrifugal Compressor and its Variation with Flow Rate", ImechE, Proc Instn Mech Engrs, Vol 188, Pp. 514-421.
- [28] Engeda, A., 2002. "Class Notes of Turbomachinery, Advanced Turbomachinery", Mechanical Engineering Department, Michigan State University.

- [29] Aungier, R. H., 2000. "Centrifugal Compressors: A Strategy for Aerodynamic Design and Analysis", The American Society of Mechanical Engineers, New York.
- [30] Wilson, D. G., and Korakianitis, T., 1998. "The Design of High-Efficiency Turbomachinery and Gas Turbine", 2nd ed., Prentice-Hall, Inc, Upper Saddle River, New Jersey.
- [31] Japikse, D., 1996. "Centrifugal Compressor Design and Performance", Concepts ETI, Inc, Vermont, USA.
- [32] Japikse, D., Marscher, W. D., and Furst, R. B., 1997. "Centrifugal Pump Design and Performance", Concepts ETI, Inc, Vermont, USA.
- [33] Robert, Neumaier, 1997. "Hermetic Pumps: The Latest Innovations and Industrial Applications of Sealless Pumps", Gulf Publishing Company, Houston, Texas.
- [34] Reddy, Y. R., Kar, S., 1971. "Optimum Vane Number and Angle for Centrifugal Pumps with Logarithmic Vanes", Journal of Basic Engineering, Transactions of ASME, Vol. 93, Pp. 411-425.
- [35] Iversen, H. W., Rolling, R. E., and Carlson, J. J., 1960. "Volute Pressure Distribution, Radial Force on Impellers, and Volute Mixing Losses of Radial Flow Centrifugal Pump", Journal of Engineering for Power, Transactions of ASME, Vol. 82, Pp. 136-144.
- [36] Daily, J. W., Nece, R. E., 1960. "Chamber Dimension Effects on Induced Flow and Frictional Resistance of Enclosed Rotating Disks", Journal of Basic Engineering, Transactions of ASME, Vol. 82, Pp. 217-232.
- [37] Cooper, P., 1964. "Application of Pressure and Velocity Criteria to the Design of Centrifugal Pump Impeller and Inlet", Journal of Engineering for Power, Transactions of ASME, Vol. 86, Pp. 181-190.
- [38] Jansen, W., 1964. "Steady Fluid Flow in a Radial Vaneless Diffuser", Journal of Basic Engineering, Transactions of ASME, Vol. 82, Pp. 607-619.
- [39] Agostinelli, A., Nobles D., and Mockridge, C. R., 1960. "An Experimental Investigation of Radial Thrust in Centrifugal Pumps", Journal of Engineering for Power, Transactions of ASME, Vol. 82, Pp. 120-126.
- [40] Kramer, J. J., Osborn, W. M., and Hamrick, J. T., 1960. "Design and Test of Mixed-Flow and Centrifugal Impellers", Journal of Engineering for Power, Transactions of ASME, Vol. 82, Pp. 127-135.

- [41] Yedidiah, Sh., 1964-65. "Centrifugal Pumps: Theories and Facts", Proc. Instn. Mech. Engrs, Vol. 179, Part 1, No. 20, Pp. 615-626.
- [42] Ippen, Arthur T., 1946. "The Influence of Viscosity on Centrifugal Pump Performance", Transactions of ASME, Pp. 823-848.
- [43] Peck, J. F., 1968-1969. "Design of Centrifugal Pumps with Computer Aid", Proc. Instn. Mech. Engrs., Vol. 183, Part 1, No. 17, Pp. 321-351.
- [44] Sixsmith, H., Giarratano, P., 1970. "A Miniature Centrifugal Pump", The Review Of Scientific Instruments, Vol. 41, No. 11, Pp. 1570-1573.
- [45] Sakurai, Teruo, 1972. "Study on Flow Inside Diffusers for Centrifugal Turbomachines", Bulletin of JSME, Vol. 15, No. 79, Pp. 81-92.
- [46] Brinkman, W., 1979. "Electro Magnetic Driven Fuel Injection Pump", Institution of Electrical Engineers, London, Vol. n 181, Pp. 145-149.
- [47] Itoh, S., Sasaki, S., and Arai, K., 1991. "Advanced In-Line Pump for Medium-Duty diesel Engines to Meet Future Emissions Regulations", Society of Automotive Engineers, Vol. 100, Sect 3, Pp. 221-231.
- [48] Kovats, A., Desmur, G., 1958. "Pumps, Fans, and Compressors", Blackie & Son Ltd, London, Great Britain.
- [49] Robert Scharff, 1989. "Complete Fuel Systems and Emission Control", Delmar Automotive, Delmar Publisher, Inc, New York.
- [50] Oberheide, G. C., and Tuckey, C. H., 1996. "Demand Delivery System-Returnless Fuel Delivery", Vol. Analyzing Fuel Systems Technology for Fuel Economy and Emissions, SP-1151, Society of Automotive Engineers, Inc., Warrendale, PA, Pp.35-46.
- [51] Garrett, T. K., 1991. "Automotive Fuels and Fuel Systems- Fuel, Tanks, Delivery, Metering, Mixing and Combustion and Environmental Considerations", Vol. 1 Gasoline, Pentech Press, London, and Society of Automotive Engineers, Inc., Warrendale, PA.
- [52] Garrett, T. K., 1991. "Automotive Fuels and Fuel Systems- Fuel, Tanks, Delivery, Metering, Mixing and Combustion and Environmental Considerations", Vol. 2 Diesel, Pentech Press, London, and Society of Automotive Engineers, Inc., Warrendale, PA.
- [53] Koichi, M., Shingo, N., Shigetaka, T., and Hitoshi, T., 1991. "Development of Brushless Fuel Pump", Transactions of Society of Automotive Engineers, Vol.100, Sect. 6, Pp. 522-527

- [54] Kemmner, U., Rollwage, M., and Rose, K., 1987. "New Generation of Bosh Electrical Fuel-pumps-Improvement in Hot-Fuel Handling and Noise", SAE Technical Paper Series, SAE International Congress and Exposition., Society of Automotive Engineers, Inc., Warrendale, PA.
- [55] Hattori, Y., Hisanori, K., and Kazuo, S., 1987. "Development of a Turbine In-Tank Fuel Pump", SAE Technical Paper Series, SAE International Congress and Exposition., Society of Automotive Engineers, Inc., Warrendale, PA.
- [56] Crane Company, 1969. "Flow of Fluids through Valves, Fittings, and Pipe", Technical paper No. 410, New York.
- [57] Jonhston, J. P., and Dean R. C. Jr., 1966. "Losses in Vaneless Diffusers of Centrifugal Compressors and Pumps", Journal of Engineering for Power, Transactions of ASME, Vol. 88, No. 1, Pp. 49-62.
- [58] Evghenide, C., 1969. "Effect of Viscosity on the Characteristics of Centrifugal Pumps", International Chemical Engineering, Vol. 9, No. 1, Pp. 69-74.
- [59] Ayyubi, S. K., Rao Y. V. N., 1971. "Theoretical Analysis of Flow Through Two-Dimensional Centrifugal Pump Impeller by Method of Singularities", Journal of Basic Engineering, Transactions of ASME, Vol. 93, Pp. 35-41.
- [60] Mine, K., Nakanishi, S., Takada, S., and Takeuchi, H., 1991. "Development of Brushless Fuel Pump", Transactions of SAE, Society of Automotive Engineers, Inc., Warrendale, PA, Pp. 522-527.
- [61] Karassik, I. J., Krutzsch, W., Fraser, W., Messina, J. P., Cooper, P., and Heald, C. C., 2001. "Pump Handbook", 3rd ed., McGraw-Hill, Inc, New York.
- [62] Manger, H., 1982. "Electronic Fuel Injection", Transactions of SAE, Society of Automotive Engineers, Inc., Warrendale, PA, Pp. 89-96.
- [63] Jansen, W., and Sunderland, P. B., 1990. "Off-Design Performance Prediction of Centrifugal Pumps", American Society of Mechanical Engineers, Fluids Engineering Division (Publication) FED, v 101, Pp 1-9.
- [64] Maceyka, T. D., 1987. "New Two-Stage Concept Optimizes High-Speed Pump Performance", I Mech E Conference Publications (Institution of Mechanical Engineers), Proceedings of the Institution of Mechanical Engineers Third European Congress, Pp. 185-191.

- [65] Grimaldi, Carlo N., and Manfreda, Giampaolo, 1992. "Interactive Design of Centrifugal Pumps: From 1-D to Blade-to Blade", American Society of Mechanical Engineers, Petroleum Division (Publication) PD, Proceedings of the 1992 Engineering Systems Design and Analysis Conference, Vol. 47-1, Pp. 23-30.
- [66] Salisbury, A. G., 1982. "Current Concept in Centrifugal Pump Hydraulic Design", I Mech E Conference Publications (Institution of Mechanical Engineers), Centrifugal Pumps - Hydraulic Design., London, England, Pp. 1-15.
- [67] Dahl, Trygve, and Nelik, Lev, 1985. "Computer Aided Design of Centrifugal Pump Impeller", American Society of Mechanical Engineers (Paper), 85-WA/FE-10, Pp. 1-7.
- [68] Grimaldi, Carlo N., Manfreda, Giampaolo, and Pacciani, Roberto, 1994. "Global Fluid Dynamics Design of Centrifugal Pumps", American Society of Mechanical Engineers, Petroleum Division (Publication) PD, Vol. 64, n 8-2; Proceedings of the 2nd Biennial European Joint Conference on Engineering Systems Design and Analysis: Part 8-B (of 8), London, England, Pp. 503-510.
- [69] Wilkie, Fergus, 1986. "Getting The Most out of Pumps", Process Engineering (London), Vol. 67, n 7, Pp. 61 and 63-64.
- [70] Franke, H.-J., 1986. "Design Methodology and Practice-A Critical Assessment", KSB Technische Berichte (Klein, Schanzlin & Becker Aktiengesellschaft), n 19e, Pp. 17-23
- [71] Cameron, Lee, and Maceyka, Thomas D., 1986. "Using Inducers to Improve High-Speed Pump Performance", Plant Engineering (Barrington, Illinois), Vol. 40, n 4, Pp. 41-43.
- [72] Liu, C.H., Vafidis, C., and Whitelaw, J. H., 1994. "Flow Characteristics of A Centrifugal Pump", Journal of Fluids Engineering, Transactions of the ASME, Vol. 116, n 2, Pp. 303-309.
- [73] AL-Zubaidy, Sarim, 1994. "Preliminary Design of Centrifugal Impellers Using Optimization Techniques", Journal of Fluids Engineering, Transactions of the ASME, Vol. 116, Pp. 310-315.
- [74] Cader, T., Masbernat, O., and Roco, M. C., 1994. "Two-Phase Velocity Distributions and Overall Performance of A Centrifugal Slurry Pump", Journal of Fluids Engineering, Transactions of the ASME, Vol. 116, Pp. 316-323.
- [75] Anderson, J. D., Jr., 1991. "Fundamentals of Aerodynamics", 2nd ed., McGraw-Hill, Inc, New York.

- [76] Vavra, M. H., 1960. "Aero-Thermodynamics and Flow in Turbomachines", John Willey & Sons, Inc, New York.
- [77] Somerton, W. S., and Potter, M. C., 1995. "Engineering Thermodynamics", 1st ed., McGraw-Hill, Inc, New York.
- [78] Moran, M. J., and Shapiro, H. N., 2000. "Fundamentals of Engineering Thermodynamics", 4th ed., John Willey & Sons, Inc, New York.
- [79] Ruskeepää, Heikki, 1999. "Mathematica Navigator, Graphics and Methods of Applied Mathematics", Academic Press, San Diego, CA, USA.
- [80] Friedman, F. L., and Koffman, E. B., 1993. "Fortran", 5th ed., Addison Wesley Longman, Inc, New York.
- [81] Chapman, S. J., 1998. "Fortran 90/95 for Scientists and Engineers", 1st ed., McGraw-Hill, Inc, New York.
- [82] Magrab, Edward B., 2000. "An Engineer's Guide to MATLAB", Prentice-Hall, Inc, Upper Saddle River, New Jersey.
- [83] Stewart, James, 1995. "Calculus, Early Transcendentals", 3rd ed., Brooks/Cole Publishing Company, A division of International Thomson Publishing Inc., CA, USA.
- [84] Wislicenus, G. F., 1965, "Fluid Mechanics of Turbomachinery", Vol. 1 and Vol. 2, Dover Publications, Inc., New York.
- [85] Wood, Benard D., 1982. "Applications of Thermodynamics", 2nd ed., Addison Wesley Publishing Company, Inc, USA.
- [86] Stepanoff, A., 1948. "Centrifugal and Axial Flow Pumps", John Willey & Sons, Inc, New York.
- [87] Bill Mc Nally, 2002, "Pump and Seal Reference Manual", The Mc Nally Institute, FL.

Appendix A

CALCULATION OF CONVENTIONAL CENTRIFUGAL PUMP DESIGN (Karassik, Krutzsch, Fraser, and Messina)

The centrifugal pump design requirements are:

- Head, $H = 380 \text{ Kpa}, 50.36\text{m}, 165.23 \text{ ft}$
- Flow, $Q = 3.9 \cdot 10^{-5} \text{ m}^3/\text{s}, 1.38 \cdot 10^{-3} \text{ ft}^3/\text{s}, 1.03 \cdot 10^{-2} \text{ gal}^3/\text{s}$
- Speed, $N = 9000\text{rpm}$
- Specific Speed, $N_s = 1.65 \text{ (m)}, 85.29 \text{ (US-gal)}, 4.03 \text{ (cf)}$

The fuel property requirements are:

- Density $\rho = 770 \text{ kg/m}^3$
- Viscosity $\mu = 0.001 \text{ N-sec/m}^2$

All the calculations are implemented in the S.I. unit system. There are some assumptions

- The number of vanes is $Z = 7$
- The coefficient a in the slip factor of Pfleiderer is affected by volute: $a = 0.65$
- The hub-tip ratio is assumed to be $k = 0.02$
- The flow angle β_0 is assumed to be $\beta_0 = 10^\circ$
- The inlet vane thickness is assumed to be $s_1 = 4.8 \text{ mm}$
- The outlet vane thickness is assumed to be $s_2 = 4.8 \text{ mm}$
- The initially assumed radius ratio $r_1/r_2 = 0.5$.
- The initially assumed area ratio should be smaller than $A_{II}/A_I = 1.3$.
- The tongue distance is assumed to be 7% of the impeller radius (r_2).

STEP 1. The specific speed

The specific rotation speed is defined by

$$N_s = \frac{N\sqrt{Q}}{H^{0.75}} = \frac{9000\sqrt{3.9*10^{-5}}}{50.36^{0.75}} = 2.9731$$

From Figure 3.1, the expected pump efficiency ($N_s = 2.9731$, $Q = 3.9*10^{-5} \text{ m}^3/\text{s} = 0.1404 \text{ m}^3/\text{h}$) is about $\eta = 5\%$.

STEP 2. Impeller discharge velocity triangle

With $N_s = 2.9731$, Figure 3.3 provides $C_{m3}/U_2 = 0.05$ and Figure 3.4 provides $\beta_2 = 30^\circ$. The slip factor by Pfleiderer is

$$\mu = \frac{1}{1 + \frac{a}{Z} \left(1 + \frac{\beta_2}{60}\right) \frac{2}{1 - (r_1^2 / r_2^2)}} = \frac{1}{1 + \frac{0.65}{7} \left(1 + \frac{30}{60}\right) \frac{2}{1 - (0.5)^2}} = 0.7292$$

The slip factor by Stodola is

$$\mu = 1 - \frac{\pi \sin \beta_2}{Z} = 1 - \frac{\pi \sin 30}{7} = 0.7756$$

The slip factor by Pfleiderer is smaller than the slip factor by Stodola. The slip factor by Pfleiderer is selected because this value takes into account of the important design parameters. $\mu = 0.7292$. The hydraulic efficiency is estimated from

$$\eta_H \approx 1 - \frac{0.071}{Q^{0.25}} \approx 1 - \frac{0.071}{(3.9*10^{-5})^{0.25}} \approx 0.1016$$

The head coefficient is computed by

$$\psi = 2\mu\eta_H \left(1 - \frac{C_{m3}}{U_2} \cot \beta_2\right) = 2 * 0.7292 * 0.1016 * (1 - 0.05 * \cot 30) = 0.1353$$

The necessary impeller peripheral (tangential) speed is

$$U_2 = \sqrt{\frac{2gH}{\psi}} = \sqrt{\frac{2 * 9.81 * 50.36}{0.1353}} = 85.4562 \text{ m/sec}$$

The meridional speed right after the impeller discharge is

$$C_{m3} = \left(\frac{C_{m3}}{U_2} \right) U_2 = 0.05 * 85.4562 = 4.2728 \text{ m/sec}$$

The peripheral speed of the absolute impeller-discharge velocity without slip is calculated with geometric relationships.

$$C_{u3} = U_2 - C_{m3} \cot \beta_2 = 85.4562 - 4.2728 * \cot 30 = 78.0555 \text{ m/sec}$$

With slip, the peripheral speed of the absolute impeller-discharge velocity is calculated with definition of slip factor.

$$C'_{u3} = \mu C_{u3} = 0.7292 * 78.0555 = 56.9181 \text{ m/sec}$$

STEP 3. Impeller discharge dimensions

$$\text{The impeller diameter is } D_2 = \frac{60 U_2 (1000)}{\pi N} = \frac{60 * 85.4562 * 1000}{\pi * 9000} = 181.344 \text{ mm}$$

$$\text{The impeller radius is } r_2 = \frac{D_2}{2} = \frac{181.344}{2} = 90.6718 \text{ mm}$$

The meridional velocity C_{m3} is calculated right after the impeller discharge width

$$C_{m3} = \frac{Q * 10^6}{2 \pi r_2 b_3} = \frac{Q * 10^6}{2 \pi r_2 b_2}$$

The impeller discharge width is calculated from

$$b_3 = b_2 = \frac{Q (10^6)}{2 \pi r_2 C_{m3}} = \frac{3.9 * 10^{-5} * 10^6}{2 * \pi * 90.6718 * 4.2728} = 0.016 \text{ mm}$$

STEP 4. Impeller inlet diameter

The hub-tip ratio is assumed to be $k = 0.02$

The flow angle β_0 is assumed to be $\beta_0 = 10^\circ$. The suction (shroud) diameter is

$$D_s = 2897 \left(\frac{Q}{k N \tan \beta_0} \right)^{1/3} = 2897 \left(\frac{3.9 * 10^{-5}}{0.02 * 9000 * \tan 10} \right)^{1/3} = 31.0294 \text{ mm}$$

The inlet radius is $r_1 = r_s = \frac{D_s}{2} = \frac{31.0294}{2} = 15.5147 \text{ mm}$

The hub radius is calculated from the hub-tip ratio

$$k = 1 - \left(\frac{D_H}{D_s} \right)^2 \Rightarrow D_H = D_s \sqrt{1 - k} = 31.0294 \sqrt{1 - 0.02} = 30.7175 \text{ mm}$$

$$r_H = \frac{D_H}{2} = \frac{30.7175}{2} = 15.3588 \text{ mm}$$

The mean inlet radius is

$$r_{1m} = \left(\frac{r_s^2 + r_H^2}{2} \right)^{1/2} = \left(\frac{15.5147^2 + 15.3588^2}{2} \right)^{1/2} = 15.4369 \text{ mm}$$

The radius ratio r_{1m}/r_2 is $\frac{r_{1m}}{r_2} = \frac{15.4369}{90.6718} = 0.1703$

The calculated radius ratio r_{1m}/r_2 is satisfied because this radius ratio is smaller than the initially assumed radius ratio $r_1/r_2 = 0.5$.

STEP 5. Inlet vane angles

The inlet vane angle at outer radius is calculated by

$$\tan(\beta_1) = \frac{\tan \beta_0}{1 - \frac{Z s_1}{2 \pi r_1 \sin(\beta_1)}} = \frac{\tan(10)}{1 - \frac{7 * 4.8}{2 * \pi * 15.5147 * \sin(\beta_1)}} \Rightarrow \beta_1 = 29.84^\circ$$

The Mean inlet vane angle at the Mean radius is calculated by

$$\tan(\beta_{1m}) = \frac{\tan \beta_0}{1 - \frac{Z s_1}{2 \pi r_{1m} \sin(\beta_{1m})}} = \frac{\tan(10)}{1 - \frac{7 * 4.8}{2 * \pi * 15.4369 * \sin(\beta_{1m})}} \Rightarrow \beta_{1m} = 29.94^\circ$$

STEP 6. Impeller inlet velocity triangle

The meridional velocity ahead of the vanes is

$$C_{m0} = \frac{Q(10^6)}{\pi r_1^2} = \frac{3.9 * 10^{-5} * 10^6}{\pi * 15.5147^2} = 0.0516 \text{ m/sec}$$

The peripheral vane velocity at the eye is

$$U_1 = \frac{\pi r_1 N}{30(1000)} = \frac{\pi * 15.5147 * 9000}{30 * 1000} = 14.6223 \text{ m/sec}$$

STEP 7. Flow areas between vanes

The inlet area between vanes is approximately

$$A_1 = Z a_1 \approx \pi r_1^2 \sin \beta_{1m} \approx \pi * 15.5147^2 \sin(29.9485) \approx 377.511 \text{ mm}^2$$

The discharge area between vanes is approximately

$$A_{II} = Z a_{II} \approx b_2 (2 \pi r_2 \sin \beta_2 - Z s_2)$$
$$A_{II} \approx 0.016 * (2 * \pi * 90.6718 * \sin(30) - 7 * 4.8) \approx 4.0201 \text{ mm}^2$$

The area ratio of A_{II}/A_1 is $\frac{A_{II}}{A_1} = \frac{4.0201}{377.511} = 0.0106$

The calculated area ratio A_{II}/A_1 is satisfied because this area ratio is smaller than the initially assumed area ratio $A_{II}/A_1 = 1.3$.

STEP 8. Volute casing

From Figure 3.13 and the calculated specific speed $N_s = 2.9731$, the velocity ratio of C_{thr}/U_2 is approximately estimated by $C_{thr}/U_2 = 0.6$. This estimation needs to be verified later by the experiment because the specific speed of the design is too low and is also outside the design range of Figure 3.13.

The throat velocity is calculated from $C_{thr} = \left(\frac{C_{thr}}{U_2} \right) U_2 = 0.6 * 85.4562 = 51.2737 \text{ m/sec}$

The throat area is $A_{thr} = \frac{Q (10^6)}{C_{thr}} = \frac{3.9 * 10^{-5} * 10^6}{51.2737} = 0.7606 \text{ mm}^2$

Assuming a circular throat section, the throat radius is

$$r_{thr} = \sqrt{\frac{A_{thr}}{\pi}} = \sqrt{\frac{0.7606}{\pi}} = 0.4921 \text{ mm}$$

The tongue distance is selected to be 7% of the impeller radius

$$t = 0.07 * r_2 = 0.07 * 90.6718 = 6.347 \text{ mm}$$

The distance of the throat center from the axis is

$$r_4 \approx r_2 + t + r_{thr} \approx 90.6718 * 6.347 * 0.4921 \approx 97.5109 \text{ mm}$$

The average throat velocity C (the flow factor) is calculated by

$$C = \frac{C_{thr} r_4}{C_{u3} r_2} = \frac{51.2737}{56.9181} * \frac{97.5109}{90.6718} = 0.9688$$

The flow factor $C = 0.9688$ is acceptable because this flow factor belongs to the design range $0.9 < C = 0.9688 < 1.0$.

The area ratio of A_{thr}/A_{II} is $\frac{A_{thr}}{A_{II}} = \frac{0.7606}{4.0201} = 0.1892$

This area ratio of $A_{thr}/A_{II} = 0.1892$ does not fall into the region of High Efficiency from the graph of Figure 3.14. This area ratio of $A_{thr}/A_{II} = 0.1892$ only falls into the region of Low Efficiency. The intermediate volute areas are approximated by Stepanoff's equation.

$$A_v = A_{thr} \frac{\phi_v}{360}$$

The volute radius is $r = \sqrt{\frac{A_v}{\pi}}$

The radius from the center of the pump to the center of the volute (the new center distances) is $r_v = r_2 + t + r$. The results of volute dimensions are tabulated in Table A.1.

All the results are tabulated for the central angle ϕ_v from 0° to 360° .

Table A.1 Volute Dimensions

ϕ_v (degree)	A_v (mm ²)	r (mm)	r_v (mm)
0	0.0000	0.00	97.02
45	0.0951	0.17	97.19
90	0.1902	0.25	97.26
135	0.2852	0.30	97.32
180	0.3803	0.35	97.37
225	0.4754	0.39	97.41
270	0.5705	0.43	97.44
315	0.6655	0.46	97.48
360	0.7606	0.49	97.51

The intermediate volute velocities are $C_v = \frac{r_2}{r_v} C(C'_{u3})$

The intermediate volute areas are $A_v = \frac{Q(10^6)}{C_v} \frac{\phi_v}{360}$

The newly calculated intermediate areas (A_v) result in new center distances r_v , which are then compared with the assumed values. These results (assumed r_v , C_v , A_v , r , calculated r_v) are tabulated in Table A.2.

Table A.2 Volute Dimensions

	Assumed Values				Calculated Values
ϕ_v (degree)	r_v (mm)	C_v (m/sec)	A_v (mm ²)	r (mm ²)	r_v (mm)
0	97.02	51.53	0.00	0.00	97.02
45	97.19	51.44	0.09	0.17	97.19
90	97.26	51.40	0.19	0.25	97.26
135	97.32	51.38	0.28	0.30	97.32
180	97.37	51.35	0.38	0.35	97.37
225	97.41	51.33	0.47	0.39	97.41
270	97.44	51.31	0.57	0.43	97.44
315	97.48	51.29	0.67	0.46	97.48
360	97.51	51.27	0.76	0.49	97.51

The calculated center distances r_v is very close to the initially assumed value.

The volute can be drawn using the section radii r and distance r_v of the volute centers from the axis.

STEP 9. Loss estimates, resultant efficiency, and shaft power

The hydraulic efficiency is

$$\eta_H \approx 1 - \frac{0.071}{Q^{0.25}} \approx 1 - \frac{0.071}{(3.9 \times 10^{-5})^{0.25}} \approx 0.1016$$

From the calculated specific speed $N_s = 2.9731$, the flow rate $Q = 3.9 \times 10^{-5} \text{ m}^3/\text{sec}$ = 0.1404 m³/hr and Figure 3.5, the volumetric efficiency η_v is computed by $(1 - \eta_v) = 0.05$. The volumetric efficiency η_v is $\eta_v = 0.95$. The ratio of impeller disk friction power to waterpower P_{DF}/P_w is determined by

$$\frac{P_{DF}}{P_w} = \frac{10.89}{N_s^{5/3}} = \frac{10.89}{2.9731^{5/3}} = 1.7715$$

From the calculated specific speed $N_s = 2.9731$, the flow rate $Q = 3.9 \times 10^{-5} \text{ m}^3/\text{sec}$
 $= 0.1404 \text{ m}^3/\text{hr}$ and Figure 3.19, the ratio of Mechanical Power loss to Water Power
 (P_M/P_W) is $P_M/P_W = 2$. The pump overall efficiency is calculated from

$$\eta = \frac{1}{\frac{1}{\eta_H \eta_v} + \frac{P_{DF}}{P_w} + \frac{P_M}{P_w}} = \frac{1}{\frac{1}{0.1016 * 0.95} + 1.7715 + 2.0} = 0.07$$

The pump efficiency calculated from estimated losses is close to the value of 0.05
 read from Figure 3.1. The pump overall efficiency is the ratio of water power P_w to shaft
 power P_s . With the pump overall efficiency $\eta = 0.05$, the power necessary to operate the
 pump is (specific gravity = 1).

$$P_s = \frac{(9.8) Q H (\text{specific gravity})}{\eta} = \frac{P_w}{\eta} = \frac{(9.8) * 3.9 * 10^{-5} * 50.36 * (1)}{0.07} = 0.275 \text{ W}$$

Appendix B

CALCULATION OF PUMP GEOMETRICAL PARAMETERS

UNCONVENTIONAL CENTRIFUGAL PUMP DESIGN

B.1 Specific Speed (N_s), Number of Blades (Z), Blade Exit Angle (β_2)

The specific speed depends on the rotational speed and is defined by

$$N_s = \frac{N Q^{0.5}}{H^{0.75}} = \frac{9000 * 0.618^{0.5}}{165.23^{0.75}} = 153.522$$

Select 6 blades $Z = 6$ and the blade exit angle is an important design element since it controls the slope of the head-capacity curve, and the normal head and capacity increase with angle β_2 . The range of this angle is $17.5^\circ < \beta_2 < 22.5^\circ$. In order to optimize the pump design, the 30° -logarithmic blade angle for the impeller is selected ($\beta_2 = 30^\circ$).

B.2 Speed Constants (K_u), Capacity Constant at Impeller Entrance (K_{m1}), Capacity Constant at Impeller Exit (K_{m2}), Diameter Ratio (d_1/d_2) from Calculated Specific Speed (N_s)

From Figure 4.2 and $N_s = 153.522$, the impeller constants K_u , K_{m1} , K_{m2} , d_1/d_2 are determined as follows:

$$K_u = 0.89$$

$$K_{m1} = 0.086$$

$$K_{m2} = 0.065$$

$$d_1/d_2 = 0.26$$

B.3 Inlet and Exit Diameter (d_1 , d_2), Inlet and Exit Width (b_1, b_2)

$$U_2 = K_u \sqrt{2 g H} = 0.89 \sqrt{2 * 32.2 * 165.23} = 91.8073 \text{ m/sec}$$

$$\omega = \frac{2\pi N}{60} = \frac{2 * \pi * 9000}{60} = 942.478 \text{ rad/sec}$$

$$d_2 = \frac{2 U_2}{\omega} = \frac{2 * 91.8073}{942.478} = 0.1948 \text{ ft} = 2.3376 \text{ in}$$

It was decided to select $d_2 = 2.4 \text{ in}$ and $d_1/d_2 = 0.26$

$$d_1 = 0.26 * d_2 = 0.26 * 2.4 = 0.624 \text{ in} = d_{s1}$$

The hub-shroud diameter ratio at inlet is in the range $0.3 < \frac{d_{h1}}{d_{s1}} < 0.5$. This range provides

a balance between blockage and high inlet velocities.

Assume that: $d_{h1} = 0.42 * d_{s1} = 0.42 * 0.624 = 0.262 \text{ in}$

$$V_{r1} = K_{m1} \sqrt{2 g H} = 0.086 * \sqrt{2 * 32.2 * 165.23} = 8.8713 \text{ ft/sec}$$

$$b_1 = \frac{Q}{\pi d_1 V_{r1}} = \frac{1.38 * 10^{-3}}{\pi * (0.624/12) * 8.8713} = 0.00095 \text{ ft} = 0.0114 \text{ in}$$

$$V_{r2} = K_{m2} \sqrt{2 g H} = 0.065 * \sqrt{2 * 32.2 * 165.23} = 6.7050 \text{ ft/sec}$$

$$b_2 = \frac{Q}{\pi d_2 V_{r2}} = \frac{1.38 * 10^{-3}}{\pi * (2.4/12) * 6.7050} = 0.00032757 \text{ ft} = 0.00393 \text{ in}$$

For simplicity in the manufacturing process, b_1 and b_2 are selected as follows:

$$b_1 = b_2 = 0.4 \text{ in}$$

The housing inside axial width: $b_0 = 0.5 \text{ in}$

B.4 Volute Velocity Constant K_3 , Volute Angle ϕ , and Ratio of $(2 * t_0/d_2) * 100$

From Figure 4.1 and $N_s = 153.522$, the volute constants are the volute velocity constant

K_3 , the estimated volute angle $\phi_{\text{estimated}}$, the ratio of $(2 * t_0/d_2) * 100$. These volute constants are determined as follows:

$$K_3 = 0.6$$

$$\alpha_v = \phi_{\text{estimated}} = 3.5^0$$

$$\frac{D_3 - D_2}{D_2} * 100 = \frac{2 * t_0}{d_2} * 100 = 3.4$$

The minimum gap between the casing diameter D_3 and the impeller outside diameter D_2 is called “ t_0 ”.

B.5 Volute Cross-Sectional Area at Exit (A_e), Volute Radial Clearance at Exit (t_e), Housing Axial Width in Volute Region at Exit (b_e), and Volute Hydraulic Diameter at Exit (D_e)

$$V_{mv} = K_3 \sqrt{2 g H} = 0.6 * \sqrt{2 * 32.2 * 165.23} = 61.8926 \text{ m/sec}$$

$$A_e = \frac{Q}{V_{mv}} = \frac{1.38 * 10^{-3}}{61.8926} = 0.00002223 \text{ ft}^2 = 0.003211 \text{ in}^2$$

For simplicity in the manufacturing process, it was decided to keep the housing axial width (b_e) constant in the volute region. It was decided to keep the housing axial width (b_e) constant in the volute region too $b_e = 0.5$ in. This gave the volute radial clearance (t_e) between the impeller and the housing at volute exit as:

$$t_e = \frac{A_e}{b_e} = \frac{0.003211}{0.5} = 0.006422 \text{ in}$$

For simplicity in the manufacturing process, the volute radial clearance was selected as $t_e = 0.6$ in. The Volute cross - sectional area at exit is calculated as:

$$A_e = t_e * b_e = 0.6 * 0.5 = 0.3 \text{ in}^2$$

The Volute hydraulic diameter at exit

$$D_e = \sqrt{\frac{4 A_e}{\pi}} = \sqrt{\frac{4 * 0.3}{\pi}} = 0.618 \text{ in}$$

C

T

i

A

D

B

(C

o

F

th

B

$$\frac{D_3 - D_2}{D_2} * 100 = \frac{2 * t_0}{d_2} * 100 = 3.4$$

$$t_0 = \frac{3.4 * d_2}{200} = \frac{3.4 * 2.4}{200} = 0.0408 \text{ in}$$

For simplicity in the manufacturing process, the clearance (t_0) between the impeller and the tongue was selected as: $t_0 = 0.075$ in

B.6 Volute Cross-Sectional Area at Tongue Clearance (A_0), Tongue Clearance between Impeller and Tongue (t_0), Housing Axial Width in Volute Region at Tongue Clearance (b_0), Volute Hydraulic Diameter at Tongue Clearance (D_0)

The value of t_0 is also called the minimum gap between the casing diameter D_3 and the impeller outside diameter D_2 .

$$A_0 = b_0 * t_0 = 0.5 * 0.075 = 0.0375 \text{ in}^2$$

$$D_0 = \sqrt{\frac{4 A_0}{\pi}} = \sqrt{\frac{4 * b_0 * t_0}{\pi}} = \sqrt{\frac{4 * 0.5 * 0.075}{\pi}} = 0.2185 \text{ in}$$

B.7 Verification of Calculated Volute Angle ($\phi_{\text{calculated}}$) and Estimated Volute Angle ($\phi_{\text{estimated}}$)

$$\phi_{\text{calculated}} = \tan^{-1} \left(\frac{t_e}{\pi d_2} \right) = \tan^{-1} \left(\frac{0.6}{\pi * 2.4} \right) = 4.55^\circ$$

From Figure 4.1, the estimated volute angle is $\phi_{\text{estimated}} = 3.5^\circ$. The difference between the $\phi_{\text{calculated}}$ and $\phi_{\text{estimated}}$ is acceptable.

B.8 Summary of All Geometrical Parameters of Un-Conventional Pump Design

	Given Design Pump Parameters	
1	Volume flow rate	$Q = 1.38 \times 10^{-3} \text{ ft}^3/\text{s} = 1.03 \times 10^{-2} \text{ gal/s}$ $= 3.9 \times 10^{-5} \text{ m}^3/\text{s} = 39.0772 \text{ cm}^3/\text{s}$
2	Rotational speed	$N = 9000 \text{ rpm}$
3	Head	$H = 380 \text{ kPa} = 50.36 \text{ m} = 165.23 \text{ ft}$
	Given Design Parameters of Fuel Property	
1	Dynamic viscosity	$\mu = 0.001 \text{ N-s/m}^2$
2	Kinematic viscosity	$\nu = 1.3 \times 10^{-6} \text{ m}^2/\text{s} = 1.3 \times 10^{-2} \text{ cm}^2/\text{s}$
3	Density	$\rho = 770 \text{ kg/m}^3 = 0.77 \text{ g/cm}^3$
	Geometrical Parameters	
1	Number of impeller blades	$Z = 6$
2	Blade inlet angle	$\beta_1 = 30^\circ$
3	Blade exit angle	$\beta_2 = 30^\circ$
4	Inlet impeller width	$b_1 = 1.016 \text{ cm} = 0.4 \text{ in}$
5	Exit impeller width	$b_2 = 1.016 \text{ cm} = 0.4 \text{ in}$
6	Inlet impeller eye diameter (shroud diameter)	$d_1 = d_{s1} = 1.5850 \text{ cm} = 0.624 \text{ in}$
7	Inlet hub diameter	$d_{h1} = 0.262 \text{ in}$
8	Exit impeller diameter	$d_2 = 6.096 \text{ cm} = 2.4 \text{ in}$
9	Assumed blade thickness	$t = 0.40 \text{ cm} = 0.1575 \text{ in}$
10	Assumed front axial clearance between impeller and housing	$\delta = 0.127 \text{ cm} = 0.05 \text{ in}$
11	Volute cross - sectional area at tongue clearance	$A_0 = 0.2419 \text{ cm}^2$
12	Volute cross - sectional area at exit	$A_e = 1.9355 \text{ cm}^2$
13	Volute hydraulic diameter at tongue clearance	$D_0 = 0.555 \text{ cm}$
14	Volute hydraulic diameter at exit	$D_e = 1.5697 \text{ cm} = 0.6 \text{ in}$
15	Tongue clearance between impeller and tongue	$t_0 = 0.1905 \text{ cm} = 0.075 \text{ in}$
16	Volute radial clearance between impeller and housing at volute exit	$t_e = 1.524 \text{ cm} = 0.6 \text{ in}$
17	Housing inside axial width in the volute region	$b_0 = 1.27 \text{ cm} = 0.5 \text{ in}$
18	Housing axial width at exit	$b_e = 1.27 \text{ cm} = 0.5 \text{ in}$
19	Calculated volute angle	$\phi_{\text{calculated}} = 4.55^\circ$

Appendix C

CALCULATION OF PUMP EFFICIENCY

UNCONVENTIONAL CENTRIFUGAL PUMP DESIGN

C.1 Description of Pump Geometrical Parameters

All the geometrical parameters of un-conventional pump design previously established will be used in this section.

C.2 Euler Head (H_e), Circulation Head (H_c), Head due to Finite Number of Blades (H_a), Head Loss due to Entrance-Bend-Resistance Loss (H_{eb})

$$\omega = \frac{2\pi N}{60} = \frac{2 * \pi * 9000}{60} = 942.478 \text{ rad/sec}$$

$$U_1 = \frac{\omega d_1}{2} = \frac{942.478 * 1.585}{2} = 746.914 \text{ cm/sec}$$

$$U_2 = \frac{\omega d_2}{2} = \frac{942.478 * 6.096}{2} = 2872.67 \text{ cm/sec}$$

$$K_s = \frac{Z^{0.3}}{\pi \sqrt{\sin(\beta)}} = \frac{6^{0.3}}{\pi \sqrt{\sin(30)}} = 0.7706$$

$$S_1 = U_1 K_s \left(\frac{\pi}{Z} \right) \sin(\beta) = 746.914 * 0.7706 * \left(\frac{\pi}{6} \right) * \sin(30) = 150.678 \text{ cm/sec}$$

$$S_2 = U_2 K_s \left(\frac{\pi}{Z} \right) \sin(\beta) = 2872.67 * 0.7706 * \left(\frac{\pi}{6} \right) * \sin(30) = 579.515 \text{ cm/sec}$$

$$V_{r1} = \frac{Q}{b_1 \left(\pi d_1 - \frac{Z t}{\sin(\beta)} \right)} = \frac{39.0772}{1.016 * \left(\pi * 1.585 - \frac{6 * 0.4}{\sin(30)} \right)} = 214.362 \text{ cm/sec}$$

$$V_{r2} = \frac{Q}{b_2 \left(\pi d_2 - \frac{Z t}{\sin(\beta)} \right)} = \frac{39.0772}{1.016 * \left(\pi * 6.096 - \frac{6 * 0.4}{\sin(30)} \right)} = 2.6801 \text{ cm/sec}$$

$$V_{t1} = U_1 + S_1 - \frac{V_{r1}}{\tan(\beta)} = 746.914 + 150.678 - \frac{214.362}{\tan(30)} = 526.306 \text{ cm/sec}$$

$$V_{t2} = U_2 - S_2 - \frac{V_{r2}}{\tan(\beta)} = 2872.67 - 579.515 - \frac{2.6801}{\tan(30)} = 2288.51 \text{ cm/sec}$$

$$V_{u2} = U_2 - \frac{V_{r2}}{\tan(\beta)} = 2872.67 - \frac{2.6801}{\tan(30)} = 2868.03 \text{ cm/sec}$$

$$H_e = \frac{U_2 V_{u2}}{g} = \frac{2872.67 * 2868.03}{981} = 8398.47 \text{ cm}$$

$$H_c = \frac{(U_2)^2 K_s \pi \sin(\beta)}{g Z} = \frac{(2872.67)^2 * 0.7706 * \pi * \sin(30)}{981 * 6} = 1697.07 \text{ cm}$$

$$H_a = H_e - H_c = 8398.47 - 1697.07 = 6701.4 \text{ cm}$$

$$H_{cb} = \frac{8 K_b Q^2}{\pi^2 g (d_1)^4} = \frac{8 * 0.2 * 39.0772^2}{\pi^2 * 981 * (1.585)^4} = 0.03998 \text{ cm}$$

The entrance-bend-resistance coefficient was selected with the assumption of having elbow of long radius, 90⁰, flanged. Therefore, the value of this entrance-bend-resistance coefficient is $K_b = 0.2$ (Loss coefficient).

C.3 Friction Head Loss (H_f)

$$W_1 = \frac{Q}{b_1 (\pi d_1 \sin(\beta) - Z t)} = \frac{39.0772}{1.016 * (\pi * 1.585 * \sin(30) - 6 * 0.4)} = 428.725 \text{ cm/sec}$$

$$W_2 = \frac{Q}{b_2 (\pi d_2 \sin(\beta) - Z t)} = \frac{39.0772}{1.016 * (\pi * 6.096 * \sin(30) - 6 * 0.4)} = 5.3601 \text{ cm/sec}$$

$$D_1 = \frac{2 b_1 (\pi d_1 \sin(\beta) - Z t)}{(\pi d_1 \sin(\beta) - Z t + Z b_1)} = \frac{2 * 1.016 * (\pi * 1.585 * \sin(30) - 6 * 0.4)}{(\pi * 1.585 * \sin(30) - 6 * 0.4 + 6 * 1.016)} = 0.0295 \text{ cm}$$

$$D_2 = \frac{2 b_2 (\pi d_2 \sin(\beta) - Z t)}{(\pi d_2 \sin(\beta) - Z t + Z b_2)} = \frac{2 * 1.016 * (\pi * 6.096 * \sin(30) - 6 * 0.4)}{(\pi * 6.096 * \sin(30) - 6 * 0.4 + 6 * 1.016)} = 1.0987 \text{ cm}$$

To calculate λ

$$d_m = \frac{d_1 + d_2}{2} = \frac{1.585 + 6.096}{2} = 3.8405 \text{ cm}$$

$$b_m = \frac{b_1 + b_2}{2} = \frac{1.016 + 1.016}{2} = 1.016 \text{ cm}$$

$$W_m = \frac{Q}{b_m (\pi d_m \sin(\beta) - Z t)} = \frac{39.0772}{1.016 * (\pi * 3.8405 * \sin(30) - 6 * 0.4)} = 10.5878 \text{ cm/sec}$$

$$S_m = \frac{S_1 + S_2}{2} = \frac{150.678 + 579.515}{2} = 365.097 \text{ cm/sec}$$

$$D_{mi} = \frac{2 b_m (\pi d_m \sin(\beta) - Z t)}{(\pi d_m \sin(\beta) - Z t + Z b_m)}$$

$$D_{mi} = \frac{2 * 1.016 * (\pi * 3.8405 * \sin(30) - 6 * 0.4)}{(\pi * 3.8405 * \sin(30) - 6 * 0.4 + 6 * 1.016)} = 0.7587 \text{ cm}$$

$$V_{mi} = \frac{1}{2} \left(\left| W_m + \frac{1}{2} S_m \right| + \left| W_m - \frac{1}{2} S_m \right| \right)$$

$$V_{mi} = \frac{1}{2} * \left(\left| 10.5878 + \frac{1}{2} * 365.097 \right| + \left| 10.5878 - \frac{1}{2} * 365.097 \right| \right) = 182.548 \text{ cm/sec}$$

$$Re_i = \frac{V_{mi} D_{mi}}{\nu} = \frac{182.548 * 0.7587}{1.3 * 10^{-2}} = 10654.4$$

Hence,

$$\lambda = \frac{64}{Re_i} \quad \text{if } Re_i \leq 2300$$

$$\lambda = \frac{0.3164}{(Re_i)^{1/4}} \quad \text{if } Re_i > 2300$$

The impeller Reynolds number is larger than 2300 and the following expression is used.

$$\lambda = \frac{0.3164}{(10654.4)^{1/4}} = 0.0311 \quad \text{if } R_i > 2300$$

$$H_f = \frac{\lambda (d_2 - d_1)}{4 g \sin(\beta)} \frac{1}{2} \left[\frac{(W_1)^2 + (1/4)(S_1)^2}{D_1} + \frac{(W_2)^2 + (1/4)(S_2)^2}{D_2} \right]$$

$$H_f = \frac{0.0311 * (6.096 - 1.585)}{4 * 981 * \sin(30)} * \frac{1}{2} * \left[\frac{(428.725)^2 + (1/4)(150.678)^2}{0.0295} + \frac{(5.3601)^2 + (1/4)(579.515)^2}{1.0987} \right]$$

$$H_f = 232.373 \text{ cm}$$

C.4 Volute Head Loss (H_v)

To calculate q_0

$$\alpha_0 = \tan^{-1} \left(\frac{V_r}{V_t} \right) = \tan^{-1} \left(\frac{V_{r2}}{V_{t2}} \right) = \tan^{-1} \left(\frac{2.6801}{2288.51} \right) = 0.001171 \text{ radian}$$

$$X_{13} = \frac{d_2}{d_2 + 2 t_0} = \frac{6.096}{6.096 + 2 * 0.1905} = 0.941176$$

$$X_{14} = \text{Cos} \alpha_0 \left\{ \left[1 - (X_{13} \text{Cos} \alpha_0)^2 \right]^{1/2} - X_{13} \text{Sin} \alpha_0 \right\}$$

$$X_{14} = \text{Cos}(0.001171) * \left\{ \left[1 - (0.941176 * \text{Cos}(0.001171))^2 \right]^{1/2} - 0.941176 * \text{Sin}(0.001171) \right\}$$

$$X_{14} = 0.336815$$

$$\theta_0 = \sin^{-1}(X_{14}) = \sin^{-1}(0.336815) = 0.343532 \text{ radian}$$

$$q_0 = \frac{Q \theta_0}{2\pi} = \frac{39.0772 * 0.343532}{2 * \pi} = 2.1365 \text{ cm}^3/\text{sec}$$

To calculate f

$$D_{mv} = \frac{1}{2} (D_0 + D_c) = \frac{1}{2} * (0.555 + 1.5697) = 1.0624 \text{ cm}$$

$$V_{mv} = \frac{1}{2} \left[\left(\frac{q_0}{A_0} \right) + \left(\frac{Q}{A_e} \right) \right] = \frac{1}{2} * \left[\left(\frac{2.1365}{0.2419} \right) + \left(\frac{39.0772}{1.9355} \right) \right] = 14.511 \text{ cm/sec}$$

$$Re_v = \frac{V_{mv} D_{mv}}{\nu} = \frac{14.511 * 1.0624}{1.3 * 10^{-2}} = 1185.83$$

The friction factor is determined from the volute Reynolds number

$$f = \frac{64}{Re_v} \quad \text{if } Re_v \leq 2300$$

$$f = \frac{0.3164}{(Re_v)^{1/4}} \quad \text{if } Re_v > 2300$$

The volute Reynolds number is smaller than 2300 and the following expression is used.

$$f = \frac{64}{1185.3} = 0.0539706 \quad \text{if } Re_v \leq 2300$$

There are some substitutions

$$V_r = V_{r2} = 2.6801 \text{ cm/s}$$

$$V_t = V_{t2} = 2288.51 \text{ cm/s}$$

$$V_e = Q/A_e = 39.0772/1.9355 = 20.1897 \text{ cm/s}$$

$$E_Q = q_0/Q = 2.1365/39.0772 = 0.0546738$$

$$E_A = A_0/A_e = 0.2419/1.9355 = 0.124981$$

$$E_D = D_0/D_e = 0.555/1.5697 = 0.353571$$

$$X_1 = E_A - E_Q = 0.124981 - 0.0546738 = 0.0703068$$

$$X_2 = \frac{\pi f d_2}{D_e} = \frac{\pi * 0.0539706 * 6.096}{1.5697} = 0.658469$$

$$X_3 = \frac{(E_A - E_Q)^2}{E_A (1 + E_A)} = \frac{(0.124981 - 0.0546738)^2}{0.124981 * (1 + 0.124981)} = 0.0351566$$

$$X_4 = \frac{(E_A - E_Q)^3}{E_A(1 + E_A)(E_A - E_D)} = \frac{(0.124981 - 0.0546738)^3}{0.124981 * (1 + 0.124981) * (0.124981 - 0.353571)}$$

$$X_4 = -0.010813$$

$$X_5 = \frac{(E_Q - E_D)^3}{(E_A - E_D)^2} = \frac{(0.0546738 - 0.353571)^3}{(0.124981 - 0.353571)^2} = -0.511034$$

$$X_6 = \frac{(E_D - E_Q)^2(3E_D - 2E_A - E_Q)}{(E_A - E_D)^2}$$

$$X_6 = \frac{(0.353571 - 0.0546738)^2 * (3 * 0.353571 - 2 * 0.124981 - 0.0546738)}{(0.124981 - 0.353571)^2}$$

$$X_6 = 1.29269$$

$$H_{v1} = \frac{[(V_r)^2 + (V_t - V_e)^2 + 2 V_e(V_t - V_e) X_1 \ln(1 + 1/E_A) + (V_e)^2 X_3]}{2g}$$

$$H_{v1} = \frac{[(2.6801)^2 + (2288.51 - 20.1897)^2]}{2 * 981} + \frac{2 * 20.1897 * (2288.51 - 20.1897) * 0.0703068 * \ln(1 + 1/0.124981)}{2 * 981} + \frac{(20.1897)^2 * 0.0351566}{2 * 981}$$

$$H_{v1} = 2629.69 \text{ cm}$$

$$H_{v2} = \frac{X_2(V_e)^2[1 + X_4 + X_5 \ln(1 + 1/E_D) + X_6 \ln(1 + 1/E_A)]}{2g}$$

$$H_{v2} = \frac{0.658469 * (20.1897)^2 *}{2 * 981} [1 + (-0.010813) + (-0.511034) * \ln(1 + 1/0.353571) + 1.29269 * \ln(1 + 1/0.124981)]$$

$$H_{v2} = 0.430065 \text{ cm}$$

$$H_v = H_{v1} + H_{v2} = 2629.69 + 0.430065 = 2630.12 \text{ cm}$$

C.5 Pump Output Head (H)

$$H = H_a - H_{cb} - H_f - H_v = 6701.4 - 0.0399 - 232.373 - 2630.12 = 3838.87 \text{ cm}$$

C.6 Pump Output Power (W_{out} , Experimental value)

To convert units of H_a and H from (cm) to (mmHg)

$$H_a = \left(\frac{10}{13.6} \right) * H_a (\text{cm}) = \left(\frac{10}{13.6} \right) * 6701.4 = 4927.5 \text{ mmHg}$$

$$H = \left(\frac{10}{13.6} \right) * H(\text{cm}) = \left(\frac{10}{13.6} \right) * 3838.87 = 2822.7 \text{ mmHg}$$

$$W_{out} = H(\text{mmHg}) \left(\frac{Q * 60}{1000} \right) * \frac{1}{450} = 2822.7 * \left(\frac{39.0772 * 60}{1000} \right) * \frac{1}{450} = 14.7071 \text{ Watt}$$

C.7 Power Loss due to Leakage (P_L), Power Loss due to Disk Friction (P_d), Pump

Input Power (W_{in} , Experimental value)

$$m_1 = \frac{2(V_{i2} - V_{i1})}{(d_2 - d_1)} = \frac{2 * (2288.51 - 526.306)}{(6.096 - 1.585)} = 781.292 \text{ rad/sec}$$

$$m_2 = V_{i1} - (V_{i2} - V_{i1}) \frac{d_1}{(d_2 - d_1)}$$

$$m_2 = 526.306 - (2288.51 - 526.306) * \frac{1.585}{(6.096 - 1.585)} = -92.8679 \text{ cm/sec}$$

$$y_{11} = \frac{(m_1)^2 [(d_2)^4 - (d_1)^4]}{8} = \frac{(781.292)^2 [(6.096)^4 - (1.585)^4]}{8} = 1.04888 * 10^8$$

$$y_{12} = 2 m_1 m_2 \frac{[(d_2)^3 - (d_1)^3]}{3} = 2 * 781.292 * (-92.8679) * \frac{[(6.096)^3 - (1.585)^3]}{3}$$

$$y_{12} = -1.07652 * 10^7$$

$$y_{13} = (m_2)^2 [(d_2)^2 - (d_1)^2] = (-92.8679)^2 * [(6.096)^2 - (1.585)^2] = 298828$$

$$P_d = \frac{\pi v \rho (y_{11} + y_{12} + y_{13})}{2 * \delta * 10^7}$$

$$P_d = \frac{\pi * 1.3 * 10^{-2} * 0.77 * [(1.04888 * 10^8) + (-1.07652 * 10^7) + (298828)]}{2 * 0.1 * 10^7}$$

$$P_d = 1.48466 \text{ Watt}$$

$$P_L = \frac{Z \rho \delta [(d_2)^4 - (d_1)^4] \sin^2(\beta)}{128 * g_c} \quad (\text{egr/sec})$$

Substitute $g_c = 1$ into the equation of calculating P_L and multiply by 10^{-7} to get power loss in Watt

$$P_L = \frac{Z \rho \delta [(d_2)^4 - (d_1)^4] \sin^2(\beta)}{128 * 10^7} = \frac{6 * 0.77 * 0.1 * [(6.096)^4 - (1.585)^4] * \sin^2(30)}{128 * 10^7}$$

$$P_L = 1.2404 * 10^{-7} \text{ Watt}$$

$$W_{in} = P_L + P_d + H_a (\text{mmHg}) \left(\frac{Q * 60}{1000} \right) * \frac{1}{450}$$

$$W_{in} = 1.2404 * 10^{-7} + 1.48466 + 4927.5 * \left(\frac{39.0772 * 60}{1000} \right) * \frac{1}{450} = 27.1584 \text{ Watt}$$

C.8 Pump Efficiency (Theoretical value)

$$\eta = 100 * \frac{W_{out}}{W_{in}} = 100 * \frac{14.707}{27.1584} = 54.15 \%$$

C.9 Summary of All Fluid Parameters of Un-Conventional Pump Design

	Calculated Fluid Parameters	
1	Angular velocity	$\omega = 942.478 \text{ rad/sec}$
2	Impeller Inlet peripheral velocity	$U_1 = 746.914 \text{ cm/sec}$
3	Impeller Exit peripheral velocity	$U_2 = 2872.67 \text{ cm/sec}$
4	Stodola coefficient	$K_S = 0.7706$
5	Impeller Inlet slip velocity	$S_1 = 150.678 \text{ cm/sec}$
6	Impeller Exit slip velocity	$S_2 = 579.515 \text{ cm/sec}$
7	Impeller Inlet radial velocity	$V_{r1} = 214.362 \text{ cm/sec}$
8	Impeller Exit radial velocity	$V_{r2} = 2.6801 \text{ cm/sec}$
9	Impeller Inlet tangential velocity	$V_{t1} = 526.306 \text{ cm/sec}$
10	Impeller Exit tangential velocity	$V_{t2} = 2288.51 \text{ cm/sec}$
11	Tangential velocity	$V_{u2} = 2868.03 \text{ cm/sec}$
12	Euler head	$H_e = 8398.47 \text{ cm}$
13	Circulation head	$H_c = 1697.07 \text{ cm}$
14	Head due to finite number of blades	$H_a = 6701.4 \text{ cm}$
15	Entrance-bend head	$H_{eb} = 0.03998 \text{ cm}$
16	Impeller Inlet relative velocity	$W_1 = 428.725 \text{ cm/sec}$
17	Impeller Exit relative velocity	$W_2 = 5.3601 \text{ cm/sec}$
18	Impeller Inlet hydraulic diameter	$D_1 = 0.0295 \text{ cm}$
19	Impeller Exit hydraulic diameter	$D_2 = 1.0987 \text{ cm}$
20	Impeller Reynolds number	$Re_i = 10654.4$
21	Impeller friction factor	$\lambda = 0.0311$
22	Friction head loss	$H_f = 232.373 \text{ cm}$
23	Flow angle at tongue clearance	$\alpha_o = 0.001171 \text{ radian}$
24	Imaginary angle subtended by fluid	$\theta_o = 0.343532 \text{ radian}$
25	Volume flow rate through A_o	$q_o = 2.1365 \text{ cm}^3/\text{s}$
26	Volute Reynolds number	$Re_v = 1185.83$
27	Volute friction factor	$f = 0.0539706$
28	Volute head loss	$H_v = 2630.12 \text{ cm}$
29	Pump output head	$H = 3838.87 \text{ cm}$
30	Pump output power	$W_{out} = 14.7071 \text{ Watt}$
31	Power loss due to disk friction	$P_d = 1.48466 \text{ Watt}$
32	Power loss due to leakage	$P_L = 1.2404 \times 10^{-7} \text{ Watt}$
33	Pump input power	$W_{in} = 27.1584 \text{ Watt}$
34	Pump efficiency	$\eta = 54.15 \%$

Appendix D

SUMMARY OF UNCONVENTIONAL CENTRIFUGAL PUMP DESIGN

D.1 Determination of Pump Geometrical Parameters

D.1.1 Specific Speed (N_s), Number of Blades (Z), Blade Exit Angle (β_2)

The specific speed depends on the rotational speed and is defined by

$$N_s = \frac{N Q^{0.5}}{H^{0.75}} \quad (D.1)$$

Select 6 blades $Z = 6$ and the blade exit angle is an important design element since it controls the slope of the head-capacity curve, and the normal head and capacity increase with angle β_2 . The range of this angle is $17.5^\circ < \beta_2 < 22.5^\circ$. The 30° -logarithmic blade angle for the impeller is selected ($\beta_2 = 30^\circ$).

D.1.2 Speed Constants (K_u), Capacity Constant at Impeller Entrance (K_{m1}), Capacity Constant at Impeller Exit (K_{m2}), Diameter Ratio (d_1/d_2) from Calculated Specific Speed (N_s)

From Figure 4.2, the constants K_u , K_{m1} , K_{m2} , d_1/d_2 are determined when N_s is calculated.

D.1.3 Inlet and Exit Diameter (d_1 , d_2), Inlet and Exit Width (b_1, b_2)

$$K_u = \frac{U_2}{\sqrt{2 g H}} \quad (D.2)$$

$$\omega = \frac{2 \pi N}{60} \quad (D.3)$$

$$U_2 = \omega \frac{d_2}{2} \quad (D.4)$$

$$K_{m1} = \frac{V_{r1}}{\sqrt{2 g H}} \quad (D.5)$$

$$V_{r1} = \frac{Q}{\pi d_1 b_1} \quad (D.6)$$

$$K_{m2} = \frac{V_{r2}}{\sqrt{2 g H}} \quad (D.7)$$

$$V_{r2} = \frac{Q}{\pi d_2 b_2} \quad (D.8)$$

D.1.4 Volute Velocity Constant K_3 , Volute Angle ϕ , Ratio of $(2*t_0/d_2)*100$

From Figure 4.1, the volute velocity constant K_3 , volute angle ϕ , ratio of $(2*t_0/d_2)*100$ are determined when N_S is calculated.

$$\frac{D_3 - D_2}{D_2} * 100 = \frac{2 * t_0}{d_2} * 100 \quad (D.9)$$

D.1.5 Volute Cross-Sectional Area at Exit (A_e), Volute Radial Clearance at Exit (t_e), Housing Axial Width in Volute Region at Exit (b_e), Volute Hydraulic Diameter at Exit (D_e)

$$V_{mv} = K_3 \sqrt{2 g H} \quad (D.10)$$

$$V_{mv} = \frac{Q}{A_e} \quad (D.11)$$

For simplicity in the manufacturing process, it was decided to keep the housing axial width (b_e) constant in the volute region.

$$t_e = \frac{A_e}{b_e} \quad (D.12)$$

$$D_e = \sqrt{\frac{4 A_e}{\pi}} \quad (D.13)$$

D.1.6 Volute Cross-Sectional Area at Tongue Clearance (A_0), Tongue Clearance between Impeller and Tongue (t_0), Housing Axial Width in Volute Region at Tongue Clearance (b_0), Volute Hydraulic Diameter at Tongue Clearance (D_0)

The value of t_0 is also called the minimum gap between the casing diameter D_3 and the impeller outside diameter D_2 .

$$A_0 = b_0 * t_0 \quad (D.14)$$

$$D_0 = \sqrt{\frac{4 A_0}{\pi}} \quad (D.15)$$

D.1.7 Verification of Calculated Volute Angle ($\phi_{\text{calculated}}$) and Estimated Volute Angle ($\phi_{\text{estimated}}$)

$$\phi_{\text{calculated}} = \tan^{-1} \left(\frac{t_e}{\pi d_2} \right) \quad (D.16)$$

D.1.8 Summary of All Geometrical Parameters of Un-Conventional Pump Design

	Given Design Pump Parameters	
1	Volume flow rate	Q
2	Rotational speed	N
3	Head	H
	Given Design Parameters of Fuel Property	
1	Dynamic viscosity	μ
2	Kinematic viscosity	ν
3	Density	ρ
	Calculated and Assumed Geometrical Parameters	
1	Number of impeller blades	Z
2	Blade exit angle	β_2
3	Inlet impeller width	b_1
4	Exit impeller width	b_2
5	Inlet impeller diameter	d_1
6	Exit impeller diameter	d_2
7	Assumed blade thickness	t
8	Assumed front axial clearance between impeller and housing	δ
9	Volute cross - sectional area at tongue clearance	A_0
10	Volute cross - sectional area at exit	A_e
11	Volute hydraulic diameter at tongue clearance	D_0
12	Volute hydraulic diameter at exit	D_e
13	Tongue clearance between the impeller and the tongue	t_0
14	Volute radial clearance at exit	t_e
15	Housing inside axial width in the volute region	b_0
16	Housing axial width at exit	b_e
17	Calculated volute angle	$\phi_{\text{calculated}}$

D.2 Determination of Pump Efficiency

D.2.1 Description of Pump Geometrical Parameters

All the geometrical parameters of un-conventional pump design previously established will be used in the section.

D.2.2 Euler Head (H_e), Circulation Head (H_c), Head due to Finite Number of Blades (H_a), Head Loss due to Entrance-Bend-Resistance Loss (H_{eb})

$$\omega = \frac{2\pi N}{60} \text{ (rad/sec)} \quad (D.17)$$

$$U_1 = \frac{\omega d_1}{2} \text{ (cm/sec)} \quad (D.18)$$

$$U_2 = \frac{\omega d_2}{2} \text{ (cm/sec)} \quad (D.19)$$

$$K_s = \frac{Z^{0.3}}{\pi \sqrt{\sin(\beta)}} \quad (D.20)$$

$$S_1 = U_1 K_s \left(\frac{\pi}{Z} \right) \sin(\beta) \text{ (cm/sec)} \quad (D.21)$$

$$S_2 = U_2 K_s \left(\frac{\pi}{Z} \right) \sin(\beta) \text{ (cm/sec)} \quad (D.22)$$

$$V_{r1} = \frac{Q}{b_1 \left(\pi d_1 - \frac{Z t}{\sin(\beta)} \right)} \text{ (cm/sec)} \quad (D.23)$$

$$V_{r2} = \frac{Q}{b_2 \left(\pi d_2 - \frac{Z t}{\sin(\beta)} \right)} \text{ (cm/sec)} \quad (D.24)$$

$$V_{t1} = U_1 + S_1 - \frac{V_{r1}}{\tan(\beta)} \text{ (cm/sec)} \quad (D.25)$$

D

V

W

D

D

To

d_m

b_m

$$V_{t2} = U_2 - S_2 - \frac{V_{r2}}{\tan(\beta)} \quad (\text{cm/sec}) \quad (\text{D.26})$$

$$V_{u2} = U_2 - \frac{V_{r2}}{\tan(\beta)} \quad (\text{cm/sec}) \quad (\text{D.27})$$

$$H_e = \frac{U_2 V_{u2}}{g} \quad (\text{cm}) \quad (\text{D.28})$$

$$H_c = \frac{(U_2)^2 K_s \pi \sin(\beta)}{g Z} \quad (\text{cm}) \quad (\text{D.29})$$

$$H_a = H_e - H_c \quad (\text{cm}) \quad (\text{D.30})$$

$$H_{eb} = \frac{8 K_b Q^2}{\pi^2 g (d_1)^4} \quad (\text{cm}) \quad (\text{D.31})$$

D.2.3 Friction Head Loss (H_f)

$$W_1 = \frac{Q}{b_1(\pi d_1 \sin(\beta) - Z t)} \quad (\text{cm/sec}) \quad (\text{D.32})$$

$$W_2 = \frac{Q}{b_2(\pi d_2 \sin(\beta) - Z t)} \quad (\text{cm/sec}) \quad (\text{D.33})$$

$$D_1 = \frac{2 b_1(\pi d_1 \sin(\beta) - Z t)}{(\pi d_1 \sin(\beta) - Z t + Z b_1)} \quad (\text{cm}) \quad (\text{D.34})$$

$$D_2 = \frac{2 b_2(\pi d_2 \sin(\beta) - Z t)}{(\pi d_2 \sin(\beta) - Z t + Z b_2)} \quad (\text{cm}) \quad (\text{D.35})$$

To calculate λ

$$d_m = \frac{d_1 + d_2}{2} \quad (\text{cm}) \quad (\text{D.36})$$

$$b_m = \frac{b_1 + b_2}{2} \quad (\text{cm}) \quad (\text{D.37})$$

$$W_m = \frac{Q}{b_m (\pi d_m \sin(\beta) - Z t)} \quad (\text{cm/sec}) \quad (4.38)$$

$$S_m = \frac{S_1 + S_2}{2} \quad (\text{cm/sec}) \quad (D.39)$$

$$D_{mi} = \frac{2 b_m (\pi d_m \sin(\beta) - Z t)}{(\pi d_m \sin(\beta) - Z t + Z b_m)} \quad (\text{cm}) \quad (D.40)$$

$$V_{mi} = \frac{1}{2} \left(\left| W_m + \frac{1}{2} S_m \right| + \left| W_m - \frac{1}{2} S_m \right| \right) \quad (\text{cm/sec}) \quad (D.41)$$

$$Re_i = \frac{V_{mi} D_{mi}}{\nu} \quad (D.42)$$

Hence,

$$\lambda = \frac{64}{Re_i} \quad \text{if } Re_i \leq 2300 \quad (D.43)$$

$$\lambda = \frac{0.3164}{(Re_i)^{1/4}} \quad \text{if } Re_i > 2300 \quad (D.44)$$

$$H_f = \frac{\lambda (d_2 - d_1)}{4 g \sin(\beta)} \frac{1}{2} \left[\frac{(W_1)^2 + (1/4)(S_1)^2}{D_1} + \frac{(W_2)^2 + (1/4)(S_2)^2}{D_2} \right] \quad (\text{cm}) \quad (D.45)$$

D.2.4 Volute Head Loss (H_v)

To calculate q_o

$$\alpha_0 = \tan^{-1} \left(\frac{V_r}{V_t} \right) \quad (D.46)$$

$$X_{13} = \frac{d_2}{d_2 + 2 t_0} \quad (D.47)$$

$$X_{14} = \text{Cosa}_0 \left\{ \left[1 - (X_{13} \text{Cosa}_0)^2 \right]^{1/2} - X_{13} \text{Sina}_0 \right\} \quad (D.48)$$

$$\theta_0 = \sin^{-1}(X_{14}) \quad (D.49)$$

$$q_0 = \frac{Q \theta_0}{2\pi} \quad (\text{cm}^3/\text{sec}) \quad (D.50)$$

To calculate f

$$D_{mv} = \frac{1}{2}(D_0 + D_e) \quad (\text{cm}) \quad (D.51)$$

$$V_{mv} = \frac{1}{2} \left[\left(\frac{q_0}{A_0} \right) + \left(\frac{Q}{A_e} \right) \right] \quad (\text{cm/sec}) \quad (D.52)$$

$$Re_v = \frac{V_{mv} D_{mv}}{\nu} \quad (D.53)$$

The friction factor is determined from the volute Reynolds number

$$f = \frac{64}{Re_v} \quad \text{if } Re_v \leq 2300 \quad (D.54)$$

$$f = \frac{0.3164}{(Re_v)^{1/4}} \quad \text{if } Re_v > 2300 \quad (D.55)$$

There are some substitutions

$$V_r = V_{r2} \quad (D.56)$$

$$V_t = V_{t2} \quad (D.57)$$

$$V_e = Q/A_e \quad (D.58)$$

$$E_Q = q_0/Q \quad (D.59)$$

$$E_A = A_0/A_e \quad (D.60)$$

$$E_D = D_0/D_e \quad (D.61)$$

$$X_1 = E_A - E_Q \quad (D.62)$$

$$X_2 = \frac{\pi f d_2}{D_e} \quad (D.63)$$

$$X_3 = \frac{(E_A - E_Q)^2}{E_A(1 + E_A)} \quad (4.64)$$

$$X_4 = \frac{(E_A - E_Q)^3}{E_A(1 + E_A)(E_A - E_D)} \quad (D.65)$$

$$X_5 = \frac{(E_Q - E_D)^3}{(E_A - E_D)^2} \quad (D.66)$$

$$X_6 = \frac{(E_D - E_Q)^2(3E_D - 2E_A - E_Q)}{(E_A - E_D)^2} \quad (D.67)$$

$$H_{v1} = \frac{[(V_r)^2 + (V_t - V_e)^2 + 2 V_e(V_t - V_e) X_1 \ln(1 + 1/E_A) + (V_e)^2 X_3]}{2g} \quad (D.68)$$

$$H_{v2} = \frac{X_2(V_e)^2[1 + X_4 + X_5 \ln(1 + 1/E_D) + X_6 \ln(1 + 1/E_A)]}{2g} \quad (D.69)$$

$$H_v = H_{v1} + H_{v2} \quad (\text{cm}) \quad (D.70)$$

D.2.5 Pump Output Head (H)

$$H = H_a - H_{cb} - H_f - H_v \quad (\text{cm}) \quad (D.71)$$

D.2.6 Pump Output Power (W_{out} , Experimental value)

To convert units of H_a and H from (cm) to (mmHg)

$$H_a = \left(\frac{10}{13.6} \right) * H_a (\text{cm}) \quad (\text{mmHg}) \quad (D.72)$$

$$H = \left(\frac{10}{13.6} \right) * H(\text{cm}) \quad (\text{mmHg}) \quad (D.73)$$

$$W_{\text{out}} = H \left(\frac{Q * 60}{1000} \right) * \frac{1}{450} \quad (\text{Watt}) \quad (D.74)$$

D.2.7 Power Loss due to Leakage (P_L), Power Loss due to Disk Friction (P_d), Pump

Input Power (W_{in} , Experimental value)

$$m_1 = \frac{2(V_{t2} - V_{t1})}{(d_2 - d_1)} \quad (\text{rad/sec}) \quad (\text{D.75})$$

$$m_2 = V_{t1} - (V_{t2} - V_{t1}) \frac{d_1}{(d_2 - d_1)} \quad (\text{cm/sec}) \quad (\text{D.76})$$

$$y_{11} = \frac{(m_1)^2 [(d_2)^4 - (d_1)^4]}{8} \quad (\text{D.77})$$

$$y_{12} = 2 m_1 m_2 \frac{[(d_2)^3 - (d_1)^3]}{3} \quad (\text{D.78})$$

$$y_{13} = (m_2)^2 [(d_2)^2 - (d_1)^2] \quad (\text{D.79})$$

$$P_d = \frac{\pi \nu \rho (y_{11} + y_{12} + y_{13})}{2 * \delta * 10^7} \quad (\text{Watt}) \quad (\text{D.80})$$

$$P_L = \frac{Z \rho \delta [(d_2)^4 - (d_1)^4] \sin^2(\beta)}{128 * g_c} \quad (\text{egr/sec}) \quad (\text{D.81})$$

Substitute $g_c = 1$ into the equation of calculating P_L and multiply by 10^{-7} to get power loss in Watt

$$P_L = \frac{Z \rho \delta [(d_2)^4 - (d_1)^4] \sin^2(\beta)}{128 * 10^7} \quad (\text{D.82})$$

$$W_{in} = P_L + P_d + H_a \left(\frac{Q * 60}{1000} \right) * \frac{1}{450} \quad (\text{Watt}) \quad (\text{D.83})$$

D.2.8 Pump Efficiency (Theoretical value)

$$\eta = 100 * \frac{W_{out}}{W_{in}} \quad (\text{D.84})$$

	Calculated Fluid Parameters	
1	Angular velocity	ω
2	Impeller Inlet peripheral velocity	U_1
3	Impeller Exit peripheral velocity	U_2
4	Stodola coefficient	K_S
5	Impeller Inlet slip velocity	S_1
6	Impeller Exit slip velocity	S_2
7	Impeller Inlet radial velocity	V_{r1}
8	Impeller Exit radial velocity	V_{r2}
9	Impeller Inlet tangential velocity	V_{t1}
10	Impeller Exit tangential velocity	V_{t2}
11	Tangential velocity	V_{u2}
12	Euler head	H_e
13	Circulation head	H_c
14	Head due to finite number of blades	H_a
15	Entrance-bend head	H_{eb}
16	Impeller Inlet relative velocity	W_1
17	Impeller Exit relative velocity	W_2
18	Impeller Inlet hydraulic diameter	D_1
19	Impeller Exit hydraulic diameter	D_2
20	Impeller Reynolds number	Re_i
21	Impeller friction factor	λ
22	Friction head loss	H_f
23	Flow angle at tongue clearance	α_o
24	Imaginary angle subtended by fluid	θ_o
25	Volume flow rate through A_o	q_o
26	Volute Reynolds number	Re_v
27	Volute friction factor	f
28	Volute head loss	H_v
29	Pump output head	H
30	Pump output power	W_{out}
31	Power loss due to disk friction	P_d
32	Power loss due to leakage	P_L
33	Pump input power	W_{in}
34	Pump efficiency	η

Appendix E

INTEGRATION OF VOLUTE ENERGY LOSS RATE EQUATION

The volute energy loss rate equation is:

$$E = \int_0^{2\pi} \frac{\rho C_2 (V_t^2 + V_r^2)}{2 g_c} d\theta - \int_0^{2\pi} \frac{\rho C_2 V_t (q_o + C_2 \theta)}{g_c (A_o + C_1 \theta)} d\theta + \int_0^{2\pi} \frac{\rho C_2 (q_o + C_2 \theta)^2}{2 g_c (A_o + C_1 \theta)^2} d\theta + \int_0^{2\pi} \frac{\rho f r (q_o + C_2 \theta)^3}{2 g_c (D_o + C_3 \theta) (A_o + C_1 \theta)^2} d\theta$$

This equation is expressed as:

$$E = E_1 - E_2 + E_3 + E_4$$

where:

$$E_1 = \int_0^{2\pi} \frac{\rho C_2 (V_t^2 + V_r^2)}{2 g_c} d\theta$$

$$E_2 = \int_0^{2\pi} \frac{\rho C_2 V_t (q_o + C_2 \theta)}{g_c (A_o + C_1 \theta)} d\theta$$

$$E_3 = \int_0^{2\pi} \frac{\rho C_2 (q_o + C_2 \theta)^2}{2 g_c (A_o + C_1 \theta)^2} d\theta$$

$$E_4 = \int_0^{2\pi} \frac{\rho f r (q_o + C_2 \theta)^3}{2 g_c (D_o + C_3 \theta) (A_o + C_1 \theta)^2} d\theta$$

◆ Evaluation E_1

$$E_1 = \int_0^{2\pi} \frac{\rho C_2 (V_t^2 + V_r^2)}{2 g_c} d\theta = \frac{\rho C_2 (V_t^2 + V_r^2)}{2 g_c} [\theta]_0^{2\pi} = \frac{\pi \rho C_2 (V_t^2 + V_r^2)}{g_c}$$

Substituting $C_2 = Q/(2\pi)$ into this equation and simplifying gives:

$$E_1 = \frac{\rho Q (V_t^2 + V_r^2)}{2 g_c}$$

◆ Evaluation E_2

$$E_2 = \int_0^{2\pi} \frac{\rho C_2 V_t (q_o + C_2 \theta)}{g_c (A_o + C_1 \theta)} d\theta = \frac{\rho C_2 V_t}{g_c} \left[\frac{C_2 \theta}{C_1} - \frac{q_o C_1 - A_o C_2}{C_1^2} \ln(A_o + C_1 \theta) \right]_0^{2\pi}$$

$$E_2 = \frac{\rho C_2 V_t}{g_c} \left[\frac{2\pi C_2}{C_1} - \left(\frac{q_o}{C_1} - \frac{A_o C_2}{C_1^2} \right) \ln \left(\frac{A_o + 2\pi C_1}{A_o} \right) \right]$$

The evaluation of E_2 is verified by using “Mathematica” software:

$$\text{Simplify} \left[\left(\frac{C_2}{C_1} * (2 * \pi) - \frac{q_o * C_1 - A_o * C_2}{(C_1)^2} * \text{Log}[A_o + C_1 * (2 * \pi)] \right) - \left(\frac{C_2}{C_1} * (0) - \frac{q_o * C_1 - A_o * C_2}{(C_1)^2} * \text{Log}[A_o + C_1 * (0)] \right) \right]$$

$$\frac{(-\text{Log}[A_o] + \text{Log}[A_o + 2\pi C_1]) A_o C_2 + C_1 (2\pi C_2 + (\text{Log}[A_o] - \text{Log}[A_o + 2\pi C_1]) q_o)}{C_1^2}$$

Substituting $C_1 = A_o/(2\pi)$ and $C_2 = Q/(2\pi)$ into this equation and simplifying gives:

$$E_2 = \frac{\rho Q}{2g_c} \left[2V_t \frac{Q}{A_e} - 2V_t \frac{Q}{A_e} \left(\frac{q_o}{Q} - \frac{A_o}{A_e} \right) \ln \left(1 + \frac{A_e}{A_o} \right) \right]$$

$$E_2 = \frac{\rho Q V_t}{g_c} \left[\frac{Q}{A_e} - \left(\frac{q_o}{A_e} - \frac{Q A_o}{A_e^2} \right) \ln \left(1 + \frac{A_e}{A_o} \right) \right]$$

The evaluation of E_2 is verified by using “Mathematica” software:

$$\text{Simplify} \left[\frac{\rho * (Q / (2 * \pi)) * V_t}{g_c} * \left(\left(\frac{Q / (2 * \pi)}{A_o / (2 * \pi)} * (2 * \pi) - \frac{q_o * A_o / (2 * \pi) - A_o * Q / (2 * \pi)}{(A_o / (2 * \pi))^2} * \text{Log}[A_o + A_o / (2 * \pi) * (2 * \pi)] \right) - \left(\frac{Q / (2 * \pi)}{A_o / (2 * \pi)} * (0) - \frac{q_o * A_o / (2 * \pi) - A_o * Q / (2 * \pi)}{(A_o / (2 * \pi))^2} * \text{Log}[A_o + A_o / (2 * \pi) * (0)] \right) \right) \right]$$

$$\frac{Q \rho (Q (-\text{Log}[A_o] + \text{Log}[A_e + A_o]) A_o + A_e (Q + (\text{Log}[A_o] - \text{Log}[A_e + A_o]) q_o)) V_t}{A_e^2 g_c}$$

♦ Evaluation E_3

$$E_3 = \int_0^{2\pi} \frac{\rho C_2 (q_o + C_2 \theta)^2}{2g_c (A_o + C_1 \theta)^2} d\theta = \frac{\rho C_2}{2g_c} \int_0^{2\pi} \frac{q_o^2 + 2q_o C_2 \theta + C_2^2 \theta^2}{(A_o + C_1 \theta)^2} d\theta$$

$$E_3 = \frac{\rho C_2}{2g_c} \left\{ -\frac{q_o^2}{C_1} \frac{1}{(A_o + C_1 \theta)} + \frac{2q_o C_2}{C_1^2} \left[\frac{A_o}{A_o + C_1 \theta} + \ln(A_o + C_1 \theta) \right] + \frac{C_2^2}{C_1^3} \left[(A_o + C_1 \theta) - 2A_o \ln(A_o + C_1 \theta) - \frac{A_o^2}{A_o + C_1 \theta} \right] \right\}_0^{2\pi}$$

$$E_3 = \frac{\rho C_2}{2 g_c} \left[\frac{2 \pi C_2^2}{A_o (A_o + 2 \pi C_1)} \left(\frac{q_o}{C_2} - \frac{A_o}{C_1} \right)^2 + \frac{2 \pi C_2^2}{C_1^2} + \frac{2 C_2^2}{C_1^2} \left(\frac{q_o}{C_2} - \frac{A_o}{C_1} \right) \ln \left(1 + \frac{2 \pi C_1}{A_o} \right) \right]$$

Substituting $C_1 = A_e/(2\pi)$ and $C_2 = Q/(2\pi)$ into this equation and simplifying gives:

$$E_3 = \frac{\rho Q}{2 g_c} \left[\left(\frac{Q}{A_e} \right)^2 \left(\frac{A_o}{A_e} \right)^{-1} \left(1 + \frac{A_o}{A_e} \right)^{-1} \left(\frac{q_o}{Q} - \frac{A_o}{A_e} \right)^2 + \left(\frac{Q}{A_e} \right)^2 + \left(\frac{Q}{A_e} \right)^2 \left(\frac{q_o}{Q} - \frac{A_o}{A_e} \right) 2 \ln \left(1 + \frac{A_e}{A_o} \right) \right]$$

♦ Evaluation E_4

$$E_4 = \int_0^{2\pi} \frac{\rho f r (q_o + C_2 \theta)^3}{2 g_c (D_o + C_3 \theta) (A_o + C_1 \theta)^2} d\theta$$

$$E_4 = \frac{\rho f r}{2 g_c} \int_0^{2\pi} \frac{q_o^3 + 3q_o^2 C_2 \theta + 3q_o C_2^2 \theta^2 + C_2^3 \theta^3}{(D_o + C_3 \theta) (A_o + C_1 \theta)^2} d\theta$$

$$E_4 = \frac{\rho f r}{2 g_c} (E_{41} + E_{42} + E_{43} + E_{44})$$

Where:

$$E_{41} = \int_0^{2\pi} \frac{q_o^3}{(D_o + C_3 \theta) (A_o + C_1 \theta)^2} d\theta$$

$$E_{42} = \int_0^{2\pi} \frac{3q_o^2 C_2 \theta}{(D_o + C_3 \theta) (A_o + C_1 \theta)^2} d\theta$$

$$E_{43} = \int_0^{2\pi} \frac{3q_o C_2^2 \theta^2}{(D_o + C_3 \theta) (A_o + C_1 \theta)^2} d\theta$$

$$E_{44} = \int_0^{2\pi} \frac{C_2^3 \theta^3}{(D_o + C_3 \theta) (A_o + C_1 \theta)^2} d\theta$$

Evaluation of sub-integral E_{41}

$$E_{41} = \int_0^{2\pi} \frac{q_o^3}{(D_o + C_3 \theta) (A_o + C_1 \theta)^2} d\theta$$

$$E_{41} = q_o^3 \left\{ \frac{1}{(A_o C_3 - D_o C_1)} \left[\frac{1}{(A_o + C_1 \theta)} + \frac{C_3}{(A_o C_3 - D_o C_1)} \ln \left(\frac{D_o + C_3 \theta}{A_o + C_1 \theta} \right) \right] \right\} \Bigg|_0^{2\pi}$$

E

E

E

E.

Sul
sim

E4

Eva

E43

E43

$$E_{41} = \frac{q_0^3}{A_o C_3 - D_o C_1} \left[\frac{1}{(A_o + 2\pi C_1)} - \frac{1}{A_o} + \frac{C_3}{(A_o C_3 - D_o C_1)} \ln \left(\frac{1 + 2\pi C_3/D_o}{A_o + 2\pi C_1/A_o} \right) \right]$$

Substituting $C_1 = A_e/(2\pi)$ and $C_3 = D_e/(2\pi)$ into this equation and simplifying gives:

$$E_{41} = \frac{2q_0^3}{(A_o D_e - D_o A_e)(A_o + A_e)} - \frac{2q_0^3}{A_o (A_o D_e - D_o A_e)} + \frac{2q_0^3 D_e}{(A_o D_e - D_o A_e)^2} \ln \left(\frac{1 + D_e/D_o}{A_o + A_e/A_o} \right)$$

Evaluation of sub-integral E_{42}

$$E_{42} = \int_0^{2\pi} \frac{3q_0^2 C_2 \theta}{(D_o + C_3 \theta)(A_o + C_1 \theta)^2} d\theta = 3q_0^2 C_2 \int_0^{2\pi} \frac{\theta}{(D_o + C_3 \theta)(A_o + C_1 \theta)^2} d\theta$$

$$E_{42} = 3q_0^2 C_2 \left[\frac{-A_o}{C_1 (A_o C_3 - D_o C_1)(A_o + C_1 \theta)} - \frac{D_o}{(A_o C_3 - D_o C_1)^2} \ln \left(\frac{D_o + C_3 \theta}{A_o + C_1 \theta} \right) \right]_0^{2\pi}$$

$$E_{42} = -\frac{3q_0^2 C_2 A_o}{C_1 (A_o C_3 - D_o C_1)(A_o + 2\pi C_1)} + \frac{3q_0^2 C_2}{C_1 (A_o C_3 - D_o C_1)} + \frac{3q_0^2 C_3 D_o}{(A_o C_3 - D_o C_1)^2} \ln \left(\frac{1 + 2\pi C_1/A_o}{1 + 2\pi C_3/D_o} \right)$$

Substituting $C_1 = A_e/(2\pi)$, $C_2 = Q/(2\pi)$, and $C_3 = D_e/(2\pi)$ into this equation and simplifying gives:

$$E_{42} = -\frac{6\pi q_0^2 A_o Q}{A_e (A_o + A_e)(A_o D_e - D_o A_e)} + \frac{6\pi q_0^2 Q}{A_e (A_o D_e - D_o A_e)} + \frac{6\pi q_0^2 Q D_o}{(A_o D_e - D_o A_e)^2} \ln \left(\frac{1 + A_e/A_o}{1 + D_e/D_o} \right)$$

Evaluation of sub-integral E_{43}

$$E_{43} = \int_0^{2\pi} \frac{3q_0 C_2^2 \theta^2}{(D_o + C_3 \theta)(A_o + C_1 \theta)^2} d\theta = 3q_0 C_2^2 \int_0^{2\pi} \frac{\theta^2}{(D_o + C_3 \theta)(A_o + C_1 \theta)^2} d\theta$$

$$E_{43} = 3q_0 C_2^2 \left[\frac{A_o^2}{C_1^2 (A_o C_3 - D_o C_1)(A_o + C_1 \theta)} + \frac{D_o^2}{C_3 (A_o C_3 - D_o C_1)^2} \ln(D_o + C_3 \theta) + \frac{A_o (A_o C_3 - 2D_o C_1)}{C_1^2 (A_o C_3 - D_o C_1)^2} \ln(A_o + C_1 \theta) \right]_0^{2\pi}$$

E₂

Su
sim

E₂

Ev

E₂

E₂

E₂

$$E_{43} = \frac{3q_o C_2^2 A_o^2}{C_1^2 (A_o C_3 - D_o C_1) (A_o + 2\pi C_1)} - \frac{3q_o C_2^2 A_o}{C_1^2 (A_o C_3 - D_o C_1)} +$$

$$+ \frac{3q_o C_2^2 D_o^2}{C_3 (A_o C_3 - D_o C_1)^2} \ln(D_o + 2\pi C_3/D_o) +$$

$$+ \frac{3q_o C_2^2 A_o (A_o C_3 - 2D_o C_1)}{C_1^2 (A_o C_3 - D_o C_1)^2} \ln(1 + 2\pi C_1/A_o)$$

Substituting $C_1 = A_o/(2\pi)$, $C_2 = Q/(2\pi)$, and $C_3 = D_o/(2\pi)$ into this equation and simplifying gives:

$$E_{43} = \frac{6\pi q_o Q^2 A_o^2}{A_e^2 (A_o D_e - D_o A_e) (A_o + A_e)} - \frac{6\pi q_o Q^2 A_o}{A_o^2 (A_o D_e - D_o A_e)} +$$

$$+ \frac{6\pi q_o Q^2 D_o^2}{D_e (A_o D_e - D_o A_e)} \ln(1 + D_e/D_o) +$$

$$+ \frac{6\pi q_o Q^2 A_o (A_o D_e - 2D_o A_e)}{A_e^2 (A_o D_e - D_o A_e)^2} \ln(1 + A_e/A_o)$$

Evaluation of sub-integral E_{44}

$$E_{44} = \int_0^{2\pi} \frac{C_2^3 \theta^3}{(D_o + C_3 \theta) (A_o + C_1 \theta)^2} d\theta = C_2^3 \int_0^{2\pi} \frac{\theta^3}{(D_o + C_3 \theta) (A_o + C_1 \theta)^2} d\theta$$

$$E_{44} = \frac{C_2^3}{C_1^2 C_3} \int_0^{2\pi} \left[1 - \frac{D_o^3 C_1^2}{(D_o C_1 - A_o C_3)^2 (D_o + C_3 \theta)} + \frac{A_o^2 C_3 (3D_o C_1 - 2A_o C_3)}{(D_o C_1 - A_o C_3)^2 (A_o + C_1 \theta)} + \right.$$

$$\left. + \frac{A_o^3 C_3}{(A_o C_3 - D_o C_1) (A_o + C_1 \theta)^2} \right] d\theta$$

$$E_{44} = \frac{C_2^3}{C_1^2 C_3} \left[\theta - \frac{D_o^3 C_1^2}{(D_o C_1 - A_o C_3)^2 C_3} \ln(D_o + C_3 \theta) + \right.$$

$$\left. + \frac{A_o^2 C_3 (3D_o C_1 - 2A_o C_3)}{(D_o C_1 - A_o C_3)^2 C_1} \ln(A_o + C_1 \theta) - \frac{A_o^3 C_3}{(A_o C_3 - D_o C_1) C_1 (A_o + C_1 \theta)} \right]_0^{2\pi}$$

$$E_{44} = \frac{C_2^3}{C_1^2 C_3} \left[2\pi - \frac{D_o^3 C_1^2}{C_3 (D_o C_1 - A_o C_3)^2} \ln(1 + 2\pi C_3/D_o) + \right. \\ \left. + \frac{A_o^2 C_3 (3D_o C_1 - 2A_o C_3)}{C_1 (D_o C_1 - A_o C_3)^2} \ln(1 + 2\pi C_1/A_o) - \right. \\ \left. - \frac{A_o^3 C_3}{C_1 (A_o C_3 - D_o C_1)} \left(\frac{1}{A_o + 2\pi C_1} - \frac{1}{A_o} \right) \right]$$

Substituting $C_1 = A_e/(2\pi)$, $C_2 = Q/(2\pi)$, and $C_3 = D_e/(2\pi)$ into this equation and simplifying gives:

$$E_{44} = \frac{2\pi Q^3}{A_e^2 D_e} - \frac{2\pi Q^3 D_o^3}{D_e^2 (A_o D_e - D_o A_e)^2} \ln(1 + D_e/D_o) - \\ - \frac{2\pi Q^3 A_o^2 (2A_o D_e - 3D_o A_e)}{A_e^3 (A_o D_e - D_o A_e)^2} \ln(1 + A_e/A_o) - \\ - \frac{2\pi Q^3 A_o^3}{A_e^3 (A_o D_e - D_o A_e)(A_o + A_e)} + \frac{2\pi Q^3 A_o^3}{A_e^3 (A_o D_e - D_o A_e)}$$

Substituting E_{41} , E_{42} , E_{43} , and E_{44} , into E_4 gives:

$$E_4 = \frac{\pi \rho Q f r}{g_c D_e} \left[\left(\frac{Q}{A_e} \right)^2 + \left(\frac{Q}{A_e} \right)^2 \left(\frac{A_o}{A_e} - \frac{q_o}{Q} \right) \left(\frac{A_o}{A_e} \right)^{-1} \left(1 + \frac{A_o}{A_e} \right)^{-1} \left(\frac{A_o}{A_e} - \frac{D_o}{D_e} \right)^{-1} - \right. \\ \left. - \left(\frac{Q}{A_e} \right)^2 \left(\frac{D_o}{D_e} - \frac{q_o}{Q} \right) \left(\frac{A_o}{A_e} - \frac{D_o}{D_e} \right)^{-2} \ln \left(1 + \frac{D_e}{D_o} \right) + \right. \\ \left. + \left(\frac{Q}{A_e} \right)^2 \left(\frac{A_o}{A_e} - \frac{q_o}{Q} \right)^2 \left(\frac{3D_o}{D_e} - \frac{2A_o}{A_e} - \frac{q_o}{Q} \right) \left(\frac{A_o}{A_e} - \frac{D_o}{D_e} \right)^{-2} \ln \left(1 + \frac{A_e}{A_o} \right) \right]$$

Substituting E_1 , E_2 , E_3 , and E_4 , into E gives:

$$E = E_1 - E_2 + E_3 + E_4$$

$$\begin{aligned}
E = & \frac{\rho Q (V_t^2 + V_r^2)}{2 g_c} - \frac{\rho Q}{2 g_c} \left[2V_t \frac{Q}{A_e} + 2V_t \frac{Q}{A_e} \left(\frac{q_o}{Q} - \frac{A_o}{A_e} \right) \ln \left(1 + \frac{A_e}{A_o} \right) \right] + \\
& + \frac{\rho Q}{2 g_c} \left[\left(\frac{Q}{A_e} \right)^2 \left(\frac{A_o}{A_e} \right)^{-1} \left(1 + \frac{A_o}{A_e} \right)^{-1} \left(\frac{q_o}{Q} - \frac{A_o}{A_e} \right)^2 + \right. \\
& \left. + \left(\frac{Q}{A_e} \right)^2 + \left(\frac{Q}{A_e} \right)^2 \left(\frac{q_o}{Q} - \frac{A_o}{A_e} \right) 2 \ln \left(1 + \frac{A_e}{A_o} \right) \right] + \\
& + \frac{\pi \rho Q f r}{g_c D_e} \left[\left(\frac{Q}{A_e} \right)^2 + \left(\frac{Q}{A_e} \right)^2 \left(\frac{A_o}{A_e} - \frac{q_o}{Q} \right)^3 \left(\frac{A_o}{A_e} \right)^{-1} \left(1 + \frac{A_o}{A_e} \right)^{-1} \left(\frac{A_o}{A_e} - \frac{D_o}{D_e} \right)^{-1} - \right. \\
& \left. - \left(\frac{Q}{A_e} \right)^2 \left(\frac{D_o}{D_e} - \frac{q_o}{Q} \right)^3 \left(\frac{A_o}{A_e} - \frac{D_o}{D_e} \right)^{-2} \ln \left(1 + \frac{D_e}{D_o} \right) + \right. \\
& \left. + \left(\frac{Q}{A_e} \right)^2 \left(\frac{A_o}{A_e} - \frac{q_o}{Q} \right)^2 \left(\frac{3D_o}{D_e} - \frac{2A_o}{A_e} - \frac{q_o}{Q} \right) \left(\frac{A_o}{A_e} - \frac{D_o}{D_e} \right)^{-2} \ln \left(1 + \frac{A_e}{A_o} \right) \right]
\end{aligned}$$

$$\begin{aligned}
E = & \frac{\rho Q}{2 g_c} \left[V_r^2 + V_t^2 - 2V_t \frac{Q}{A_e} + \left(\frac{Q}{A_e} \right)^2 + \left(2V_t \frac{Q}{A_e} + \left(\frac{Q}{A_e} \right)^2 \right) \left(\frac{q_o}{Q} - \frac{A_o}{A_e} \right) \ln \left(1 + \frac{A_e}{A_o} \right) + \right. \\
& \left. + \left(\frac{Q}{A_e} \right)^2 \left(\frac{A_o}{A_e} \right)^{-1} \left(1 + \frac{A_o}{A_e} \right)^{-1} \left(\frac{q_o}{Q} - \frac{A_o}{A_e} \right)^2 \right] \\
& + \frac{\pi \rho Q f r}{g_c D_e} \left[\left(\frac{Q}{A_e} \right)^2 + \left(\frac{Q}{A_e} \right)^2 \left(\frac{A_o}{A_e} - \frac{q_o}{Q} \right)^3 \left(\frac{A_o}{A_e} \right)^{-1} \left(1 + \frac{A_o}{A_e} \right)^{-1} \left(\frac{A_o}{A_e} - \frac{D_o}{D_e} \right)^{-1} - \right. \\
& \left. - \left(\frac{Q}{A_e} \right)^2 \left(\frac{D_o}{D_e} - \frac{q_o}{Q} \right)^3 \left(\frac{A_o}{A_e} - \frac{D_o}{D_e} \right)^{-2} \ln \left(1 + \frac{D_e}{D_o} \right) + \right. \\
& \left. + \left(\frac{Q}{A_e} \right)^2 \left(\frac{A_o}{A_e} - \frac{q_o}{Q} \right)^2 \left(\frac{3D_o}{D_e} - \frac{2A_o}{A_e} - \frac{q_o}{Q} \right) \left(\frac{A_o}{A_e} - \frac{D_o}{D_e} \right)^{-2} \ln \left(1 + \frac{A_e}{A_o} \right) \right]
\end{aligned}$$

Simplifying the above equation gives:

$$\begin{aligned}
E = & \frac{\rho Q}{2g_c} \left[v_r^2 + \left(v_t - \frac{Q}{A_e} \right)^2 + \frac{2Q}{A_e} \left(v_t - \frac{Q}{A_e} \right) \left(\frac{A_o}{A_e} - \frac{q_o}{Q} \right) \ln \left(1 + \frac{A_e}{A_o} \right) + \right. \\
& \left. + \left(\frac{Q}{A_e} \right)^2 \left(\frac{A_o}{A_e} - \frac{q_o}{Q} \right)^2 \left(\frac{A_o}{A_e} \right)^{-1} \left(1 + \frac{A_o}{A_e} \right)^{-1} \right] + \\
& + \frac{2\pi\rho Q f r}{2g_c D_e} \left(\frac{Q}{A_e} \right)^2 \left[1 + \left(\frac{A_o}{A_e} - \frac{q_o}{Q} \right)^3 \left(\frac{A_o}{A_e} \right)^{-1} \left(1 + \frac{A_o}{A_e} \right)^{-1} \left(\frac{A_o}{A_e} - \frac{D_o}{D_e} \right)^{-1} - \right. \\
& \quad \left. - \left(\frac{D_o}{D_e} - \frac{q_o}{Q} \right)^3 \left(\frac{A_o}{A_e} - \frac{D_o}{D_e} \right)^{-2} \ln \left(1 + \frac{D_e}{D_o} \right) + \right. \\
& \quad \left. + \left(\frac{A_o}{A_e} - \frac{q_o}{Q} \right)^2 \left(\frac{3D_o}{D_e} - \frac{2A_o}{A_e} - \frac{q_o}{Q} \right) \left(\frac{A_o}{A_e} - \frac{D_o}{D_e} \right)^{-2} \ln \left(1 + \frac{A_e}{A_o} \right) \right]
\end{aligned}$$

1
+
+
U
(
θ
St

Supplement of Integral Evaluation for E_2, E_3, E_4

◆ Evaluating E_2 without limit $(0, 2\pi)$

$$E_2 = \int \frac{\rho C_2 V_t (q_o + C_2 \theta)}{g_c (A_o + C_1 \theta)} d\theta = \frac{\rho C_2 V_t}{g_c} \int \left[\frac{q_o}{(A_o + C_1 \theta)} + \frac{C_2 \theta}{(A_o + C_1 \theta)} \right] d\theta$$

Using Integration by Partial Fractions gives:

$$\frac{C_2 \theta}{(A_o + C_1 \theta)} = \frac{C_1 C_2 \theta}{C_1 (A_o + C_1 \theta)} = \frac{A}{C_1} + \frac{B}{(A_o + C_1 \theta)}$$

$$C_1 C_2 \theta = A(A_o + C_1 \theta) + B C_1$$

$$\text{Substitute } \theta = -\frac{A_o}{C_1} \Rightarrow B = -\frac{C_2}{C_1} A_o$$

$$\text{Substitute } \theta = 0 \Rightarrow A = C_2$$

$$E_2 = \frac{\rho C_2 V_t}{g_c} \int \left[\frac{q_o}{(A_o + C_1 \theta)} + C_2 \frac{1}{C_1} - \frac{C_2}{C_1} A_o \frac{1}{(A_o + C_1 \theta)} \right] d\theta$$

$$E_2 = \frac{\rho C_2 V_t}{g_c} \left[\frac{q_o}{C_1} \ln(A_o + C_1 \theta) + \frac{C_2 \theta}{C_1} - \frac{C_2 A_o}{C_1} \frac{\ln(A_o + C_1 \theta)}{C_1} \right] + \text{constant}$$

$$E_2 = \frac{\rho C_2 V_t}{g_c} \left[\frac{C_2 \theta}{C_1} + \frac{q_o C_1 - A_o C_2}{C_1^2} \ln(A_o + C_1 \theta) \right] + \text{constant}$$

◆ Evaluating E_3 without limit $(0, 2\pi)$

$$E_3 = \int \frac{\rho C_2 (q_o + C_2 \theta)^2}{2 g_c (A_o + C_1 \theta)^2} d\theta = \frac{\rho C_2}{2 g_c} \int \frac{q_o^2 + 2 q_o C_2 \theta + C_2^2 \theta^2}{(A_o + C_1 \theta)^2} d\theta$$

$$E_3 = \frac{\rho C_2}{2 g_c} \int \left[\frac{q_o^2}{(A_o + C_1 \theta)^2} + \frac{2 q_o C_2 \theta}{(A_o + C_1 \theta)^2} + \frac{C_2^2 \theta^2}{(A_o + C_1 \theta)^2} \right] d\theta = \frac{\rho C_2}{2 g_c} [E_{31} + E_{32} + E_{33}]$$

$$\clubsuit E_{31} = \int \left[\frac{q_o^2}{(A_o + C_1 \theta)^2} \right] d\theta = \frac{-q_o^2}{C_1 (A_o + C_1 \theta)} + \text{constant}$$

$$\clubsuit E_{32} = \int \left[\frac{2 q_o C_2 \theta}{(A_o + C_1 \theta)^2} \right] d\theta = 2 q_o C_2 \int \left[\frac{\theta}{(A_o + C_1 \theta)^2} \right] d\theta$$

Using Integration by Partial Fractions gives:

$$\frac{\theta}{(A_o + C_1 \theta)^2} = \frac{A}{(A_o + C_1 \theta)} + \frac{B}{(A_o + C_1 \theta)^2}$$

$$\theta = A(A_o + C_1 \theta) + B$$

$$\text{Substitute } \theta = -\frac{A_o}{C_1} \Rightarrow B = -\frac{A_o}{C_1}$$

Substitute $\theta = 0 \Rightarrow A = \frac{1}{C_1}$

$$E_{32} = 2q_o C_2 \int \left[\frac{1}{C_1} \frac{1}{(A_o + C_1\theta)} - \frac{A_o}{C_1} \frac{1}{(A_o + C_1\theta)^2} \right] d\theta$$

$$E_{32} = 2q_o C_2 \left[\frac{1}{C_1} \frac{\ln(A_o + C_1\theta)}{C_1} + \frac{A_o}{C_1} \frac{1}{C_1(A_o + C_1\theta)} \right] + \text{constant}$$

$$\clubsuit E_{33} = \int \left[\frac{C_2^2 \theta^2}{(A_o + C_1\theta)^2} \right] d\theta = C_2^2 \int \left[\frac{\theta^2}{(A_o + C_1\theta)^2} \right] d\theta = C_2^2 \int \left[\frac{\theta^2}{(C_1^2\theta^2 + 2A_o C_1\theta + A_o^2)} \right] d\theta$$

Using the method of Long Division gives:

$$\frac{\theta^2}{(C_1^2\theta^2 + 2A_o C_1\theta + A_o^2)} = \frac{1}{C_1^2} + \frac{\frac{-2A_o}{C_1}\theta - \frac{A_o^2}{C_1^2}}{(C_1^2\theta^2 + 2A_o C_1\theta + A_o^2)} = \frac{1}{C_1^2} + \frac{\frac{-2A_o}{C_1}\theta - \frac{A_o^2}{C_1^2}}{(A_o + C_1\theta)^2}$$

$$E_{33} = \int \left[\frac{C_2^2 \theta^2}{(A_o + C_1\theta)^2} \right] d\theta = C_2^2 \int \left[\frac{1}{C_1^2} + \frac{\frac{-2A_o}{C_1}\theta - \frac{A_o^2}{C_1^2}}{(A_o + C_1\theta)^2} \right] d\theta$$

$$E_{33} = C_2^2 \left\{ \int \left[\frac{1}{C_1^2} \right] d\theta + \int \left[\frac{\frac{-2A_o}{C_1}\theta - \frac{A_o^2}{C_1^2}}{(A_o + C_1\theta)^2} \right] d\theta \right\} = C_2^2 \left\{ \frac{\theta}{C_1^2} + \int \left[\frac{\frac{-2A_o}{C_1}\theta - \frac{A_o^2}{C_1^2}}{(A_o + C_1\theta)^2} \right] d\theta \right\}$$

Using Integration by Partial Fractions gives:

$$\frac{\frac{-2A_o}{C_1}\theta - \frac{A_o^2}{C_1^2}}{(A_o + C_1\theta)^2} = \frac{A}{(A_o + C_1\theta)} + \frac{B}{(A_o + C_1\theta)^2}$$

$$\frac{-2A_o}{C_1}\theta - \frac{A_o^2}{C_1^2} = A(A_o + C_1\theta) + B$$

Substitute $\theta = -\frac{A_o}{C_1} \Rightarrow B = \left(\frac{A_o}{C_1} \right)^2$

Substitute $\theta = 0 \Rightarrow A = -\frac{2}{A_o} \left(\frac{A_o}{C_1} \right)^2 = -\frac{2A_o}{C_1^2}$

The partial fraction decomposition is verified by using "Mathematica" software:

$$\frac{-2A_o}{C_1}\theta - \frac{A_o^2}{C_1^2} = -\frac{2A_o}{C_1^2}(A_o + C_1\theta) + \left(\frac{A_o}{C_1}\right)^2$$

$$\text{Simplify}\left[\frac{-2*(A_o)}{(C_1)^2}*(A_o + C_1*\theta) + \frac{(A_o)^2}{(C_1)^2}\right]$$

$$\frac{A_o (A_o + 2 \theta C_1)}{C_1^2}$$

$$\frac{-2A_o}{C_1}\theta - \frac{A_o^2}{C_1^2} = -\frac{2A_o}{C_1^2} \frac{1}{(A_o + C_1\theta)} + \frac{A_o^2}{C_1^2} \frac{1}{(A_o + C_1\theta)^2}$$

$$E_{33} = C_2^2 \left\{ \frac{\theta}{C_1^2} + \int \left[-\frac{2A_o}{C_1^2} \frac{1}{(A_o + C_1\theta)} + \frac{A_o^2}{C_1^2} \frac{1}{(A_o + C_1\theta)^2} \right] d\theta \right\}$$

$$E_{33} = C_2^2 \left[\frac{\theta}{C_1^2} - \frac{2A_o}{C_1^2} \frac{\ln(A_o + C_1\theta)}{C_1} - \frac{A_o^2}{C_1^2} \frac{1}{C_1(A_o + C_1\theta)} \right] + \text{constant}$$

$$E_3 = \frac{\rho C_2}{2g_c} [E_{31} + E_{32} + E_{33}]$$

$$E_3 = \frac{\rho C_2}{2g_c} \left\{ \left(\frac{-q_o^2}{C_1(A_o + C_1\theta)} \right) + 2q_o C_2 \left[\frac{1}{C_1} \frac{\ln(A_o + C_1\theta)}{C_1} + \frac{A_o}{C_1} \frac{1}{C_1(A_o + C_1\theta)} \right] + \right.$$

$$\left. + C_2^2 \left[\frac{\theta}{C_1^2} - \frac{2A_o}{C_1^2} \frac{\ln(A_o + C_1\theta)}{C_1} - \frac{A_o^2}{C_1^2} \frac{1}{C_1(A_o + C_1\theta)} \right] \right\}$$

$$E_3 = \frac{\rho C_2}{2g_c} \left\{ -\frac{q_o^2}{C_1} \frac{1}{(A_o + C_1\theta)} + \frac{2q_o C_2}{C_1^2} \left[\frac{A_o}{A_o + C_1\theta} + \ln(A_o + C_1\theta) \right] + \right.$$

$$\left. + \frac{C_2^2}{C_1^3} \left[(C_1\theta) - 2A_o \ln(A_o + C_1\theta) - \frac{A_o^2}{A_o + C_1\theta} \right] \right\} + \text{constant}$$

◆ Evaluating E_{41} without limit $(0, 2\pi)$

$$E_{41} = \int \frac{q_o^3}{(D_o + C_3\theta)(A_o + C_1\theta)^2} d\theta = q_o^3 \int \frac{1}{(D_o + C_3\theta)(A_o + C_1\theta)^2} d\theta$$

Applying the theory of the "integration of rational functions" by partial fraction decomposition gives:

$$\frac{1}{(D_o + C_3\theta)(A_o + C_1\theta)^2} = \frac{A}{(D_o + C_3\theta)} + \frac{B}{(A_o + C_1\theta)} + \frac{C}{(A_o + C_1\theta)^2}$$

$$1 = A(A_o + C_1\theta)^2 + B(D_o + C_3\theta)(A_o + C_1\theta) + C(D_o + C_3\theta)$$

$$\text{Substitute } \theta = -\frac{D_o}{C_3} \Rightarrow A = \frac{C_3^2}{(A_o C_3 - D_o C_1)^2}$$

$$\text{Substitute } \theta = -\frac{A_o}{C_1} \Rightarrow C = \frac{C_1}{(D_o C_1 - A_o C_3)}$$

$$\text{Substitute } \theta = 0 \Rightarrow B = \frac{(-C_1 C_3)}{(A_o C_3 - D_o C_1)^2}$$

The partial fraction decomposition is verified by using "Mathematica" software:

$$1 = \frac{C_3^2}{(A_o C_3 - D_o C_1)^2} (A_o + C_1\theta)^2 + \frac{-C_1 C_3}{(A_o C_3 - D_o C_1)^2} (D_o + C_3\theta)(A_o + C_1\theta) + \frac{C_1}{(D_o C_1 - A_o C_3)} (D_o + C_3\theta)$$

$$\text{Simplify} \left[\left(\frac{(C_3)^2}{(A_o * C_3 - D_o * C_1)^2} \right) * (A_o + C_1 * \theta)^2 + \left(\frac{(-C_1 * C_3)}{(A_o * C_3 - D_o * C_1)^2} \right) * (D_o + C_3 * \theta) * (A_o + C_1 * \theta) + \left(\frac{(-C_1)}{(A_o * C_3 - D_o * C_1)} \right) * (D_o + C_3 * \theta) \right]$$

1

$$E_{41} = q_o^3 \int \frac{1}{(D_o + C_3\theta)(A_o + C_1\theta)^2} d\theta$$

$$E_{41} = q_o^3 \int \left[\frac{C_3^2}{(A_o C_3 - D_o C_1)^2} \frac{1}{(D_o + C_3\theta)} + \frac{(-C_1 C_3)}{(A_o C_3 - D_o C_1)^2} \frac{1}{(A_o + C_1\theta)} + \frac{C_1}{(D_o C_1 - A_o C_3)} \frac{1}{(A_o + C_1\theta)^2} \right] d\theta$$

$$E_{41} = q_o^3 \left\{ \frac{C_3^2}{(A_o C_3 - D_o C_1)^2} \frac{\ln(D_o + C_3\theta)}{C_3} - \frac{C_1 C_3}{(A_o C_3 - D_o C_1)^2} \frac{\ln(A_o + C_1\theta)}{C_1} + \frac{C_1}{(D_o C_1 - A_o C_3)} \frac{1}{C_1 (A_o + C_1\theta)} \right\}$$

$$E_{41} = q_o^3 \left\{ \left(\frac{C_3}{(A_o C_3 - D_o C_1)^2} \right) \ln \left(\frac{D_o + C_3\theta}{A_o + C_1\theta} \right) + \frac{C_1}{(D_o C_1 - A_o C_3)} \frac{1}{C_1 (A_o + C_1\theta)} \right\} + \text{constant}$$

$$E_{41} = q_o^3 \left\{ \frac{1}{(A_o C_3 - D_o C_1)} \left[\frac{1}{(A_o + C_1 \theta)} + \frac{C_3}{(A_o C_3 - D_o C_1)} \ln \left(\frac{D_o + C_3 \theta}{A_o + C_1 \theta} \right) \right] \right\} + \text{constant}$$

◆ Evaluating E_{42} without limit $(0, 2\pi)$

$$E_{42} = \int \frac{3q_o^2 C_2 \theta}{(D_o + C_3 \theta)(A_o + C_1 \theta)^2} d\theta = 3q_o^2 C_2 \int \frac{\theta}{(D_o + C_3 \theta)(A_o + C_1 \theta)^2} d\theta$$

Applying the theory of the “integration of rational functions” by partial fraction decomposition gives:

$$\frac{\theta}{(D_o + C_3 \theta)(A_o + C_1 \theta)^2} = \frac{A}{(D_o + C_3 \theta)} + \frac{B}{(A_o + C_1 \theta)} + \frac{C}{(A_o + C_1 \theta)^2}$$

$$\theta = A(D_o + C_3 \theta) + B(D_o + C_3 \theta)(A_o + C_1 \theta) + C(D_o + C_3 \theta)$$

$$\text{Substitute } \theta = -\frac{D_o}{C_3} \Rightarrow A = \left(\frac{-D_o}{C_3} \right) \frac{C_3^2}{(A_o C_3 - D_o C_1)^2}$$

$$\text{Substitute } \theta = -\frac{A_o}{C_1} \Rightarrow C = \left(\frac{-A_o}{C_1} \right) \frac{C_1}{(D_o C_1 - A_o C_3)}$$

$$\text{Substitute } \theta = 0 \Rightarrow B = \frac{(-D_o C_1)}{(A_o C_3 - D_o C_1)^2}$$

The partial fraction decomposition is verified by using “Mathematica” software:

$$\theta = \left(\frac{-D_o}{C_3} \right) \frac{C_3^2}{(A_o C_3 - D_o C_1)^2} (A_o + C_1 \theta)^2 + \frac{-D_o C_1}{(A_o C_3 - D_o C_1)^2} (D_o + C_3 \theta)(A_o + C_1 \theta) + \left(\frac{-A_o}{C_1} \right) \frac{C_1}{(D_o C_1 - A_o C_3)} (D_o + C_3 \theta)$$

$$\text{Simplify} \left[\left(\frac{(-D_o * C_3)}{(A_o * C_3 - D_o * C_1)^2} \right) * (A_o + C_1 * \theta)^2 + \left(\frac{(D_o * C_1)}{(A_o * C_3 - D_o * C_1)^2} \right) * (D_o + C_3 * \theta) * (A_o + C_1 * \theta) + \left(\frac{(A_o)}{(A_o * C_3 - D_o * C_1)} \right) * (D_o + C_3 * \theta) \right]$$

$$E_{42} = 3q_o^2 C_2 \int \frac{\theta}{(D_o + C_3 \theta)(A_o + C_1 \theta)^2} d\theta$$

$$E_{42} = 3q_o^2 C_2 \int \left[\left(\frac{-D_o}{C_3} \right) \frac{C_3^2}{(A_o C_3 - D_o C_1)^2} \frac{1}{(D_o + C_3 \theta)} + \frac{(-D_o C_1)}{(A_o C_3 - D_o C_1)^2} \frac{1}{(A_o + C_1 \theta)} + \left(\frac{-A_o}{C_1} \right) \frac{C_1}{(D_o C_1 - A_o C_3)} \frac{1}{(A_o + C_1 \theta)^2} \right] d\theta$$

$$E_{42} = 3q_o^2 C_2 \left[\frac{-D_o C_3}{(A_o C_3 - D_o C_1)^2} \frac{\ln(D_o + C_3 \theta)}{C_3} - \frac{D_o C_1}{(A_o C_3 - D_o C_1)^2} \frac{\ln(A_o + C_1 \theta)}{C_1} + \frac{A_o}{(D_o C_1 - A_o C_3)} \frac{1}{C_1 (A_o + C_1 \theta)} \right] + \text{constant}$$

$$E_{42} = 3q_o^2 C_2 \left[\frac{-A_o}{C_1 (A_o C_3 - D_o C_1) (A_o + C_1 \theta)} - \frac{D_o}{(A_o C_3 - D_o C_1)^2} \ln \left(\frac{D_o + C_3 \theta}{A_o + C_1 \theta} \right) \right] + \text{constant}$$

◆ **Evaluating E_{43} without limit $(0, 2\pi)$**

$$E_{43} = \int \frac{3q_o C_2^2 \theta^2}{(D_o + C_3 \theta)(A_o + C_1 \theta)^2} d\theta = 3q_o C_2^2 \int \frac{\theta^2}{(D_o + C_3 \theta)(A_o + C_1 \theta)^2} d\theta$$

Using Integration by Partial Fractions gives:

$$\frac{\theta^2}{(D_o + C_3 \theta)(A_o + C_1 \theta)^2} = \frac{A}{(D_o + C_3 \theta)} + \frac{B}{(A_o + C_1 \theta)} + \frac{C}{(A_o + C_1 \theta)^2}$$

$$\theta^2 = A(A_o + C_1 \theta)^2 + B(D_o + C_3 \theta)(A_o + C_1 \theta) + C(D_o + C_3 \theta)$$

$$\text{Substitute } \theta = -\frac{D_o}{C_3} \Rightarrow A = \frac{D_o^2}{(A_o C_3 - D_o C_1)^2}$$

$$\text{Substitute } \theta = -\frac{A_o}{C_1} \Rightarrow C = \frac{-A_o^2}{C_1 (D_o C_1 - A_o C_3)}$$

$$\text{Substitute } \theta = 0 \Rightarrow B = \frac{A_o^2 C_3 - 2C_1 A_o D_o}{C_1 (A_o C_3 - D_o C_1)^2}$$

The partial fraction decomposition is verified by using “Mathematica” software:

$$\theta^2 = \frac{D_o^2}{(A_o C_3 - D_o C_1)^2} (A_o + C_1 \theta)^2 + \frac{A_o^2 C_3 - 2C_1 A_o D_o}{C_1 (A_o C_3 - D_o C_1)^2} (D_o + C_3 \theta)(A_o + C_1 \theta) + \frac{-A_o^2}{C_1 (D_o C_1 - A_o C_3)} (D_o + C_3 \theta)$$

$$\text{Simplify} \left[\left(\frac{(D_o)^2}{(A_o * C_3 - D_o * C_1)^2} \right) * (A_o + C_1 * \theta)^2 + \left(\frac{(A_o)^2 * C_3 - 2 * C_1 * A_o * D_o}{C_1 * (A_o * C_3 - D_o * C_1)^2} \right) * (D_o + C_3 * \theta) * (A_o + C_1 * \theta) + \left(\frac{- (A_o)^2}{C_1 * (A_o * C_3 - D_o * C_1)} \right) * (D_o + C_3 * \theta) \right]$$

$$\theta^2$$

$$\begin{aligned}
E_{43} &= 3q_o C_2^2 \int \frac{\theta^2}{(D_o + C_3\theta)(A_o + C_1\theta)^2} d\theta \\
E_{43} &= 3q_o C_2^2 \int \left[\frac{D_o^2}{(A_o C_3 - D_o C_1)^2} \frac{1}{(D_o + C_3\theta)} + \frac{A_o^2 C_3 - 2C_1 A_o D_o}{C_1 (A_o C_3 - D_o C_1)^2} \frac{1}{(A_o + C_1\theta)} + \right. \\
&\quad \left. + \frac{-A_o^2}{C_1 (D_o C_1 - A_o C_3)} \frac{1}{(A_o + C_1\theta)^2} \right] d\theta \\
E_{43} &= 3q_o C_2^2 \left[\frac{D_o^2}{(A_o C_3 - D_o C_1)^2} \frac{\ln(D_o + C_3\theta)}{C_3} + \frac{A_o^2 C_3 - 2C_1 A_o D_o}{C_1 (A_o C_3 - D_o C_1)^2} \frac{\ln(A_o + C_1\theta)}{C_1} \right. \\
&\quad \left. + \frac{A_o^2}{C_1 (D_o C_1 - A_o C_3)} \frac{1}{C_1 (A_o + C_1\theta)} \right] \\
E_{43} &= 3q_o C_2^2 \left[\frac{A_o^2}{C_1^2 (A_o C_3 - D_o C_1) (A_o + C_1\theta)} + \frac{D_o^2}{C_3 (A_o C_3 - D_o C_1)^2} \ln(D_o + C_3\theta) + \right. \\
&\quad \left. + \frac{A_o (A_o C_3 - 2D_o C_1)}{C_1^2 (A_o C_3 - D_o C_1)^2} \ln(A_o + C_1\theta) \right] + \text{constant}
\end{aligned}$$

◆ **Evaluating E_{44} without limit $(0, 2\pi)$**

$$E_{44} = \int \frac{C_2^3 \theta^3}{(D_o + C_3\theta)(A_o + C_1\theta)^2} d\theta = C_2^3 \int \frac{\theta^3}{(D_o + C_3\theta)(A_o + C_1\theta)^2} d\theta$$

$$\text{Evaluate } \int \frac{\theta^3}{(D_o + C_3\theta)(A_o + C_1\theta)^2} d\theta$$

To make the calculations simpler, let $D_o = d$; $C_3 = c$; $A_o = a$; $C_1 = e$; $x = \theta$

$$\int \frac{x^3}{(d + cx)(a + ex)^2} dx = \frac{1}{da^2} \int \frac{x^3}{\left(1 + \frac{c}{d}x\right)\left(1 + \frac{e}{a}x\right)^2} dx$$

To further simplify the calculations, substitute $p = \frac{c}{d}$; $q = \frac{e}{a}$:

$$\frac{1}{da^2} \int \frac{x^3}{(1 + px)(1 + qx)^2} dx = \frac{1}{da^2} \int \frac{x^3}{(1 + px)(1 + 2qx + q^2x^2)} dx$$

$$\frac{1}{da^2} \int \frac{x^3}{pq^2x^3 + (2pq + q^2)x^2 + (2q + p)x + 1} dx$$

$$\frac{x^3}{pq^2x^3 + (2pq + q^2)x^2 + (2q + p)x + 1} =$$

The method of Long Division can be implemented as follows:

$$\begin{array}{r|l}
 x^3 & pq^2x^3 + (2pq + q^2)x^2 + (2q + p)x + 1 \\
 - & \\
 x^3 + \frac{(2pq + q^2)x^2}{pq^2} + \frac{(2q + p)x}{pq^2} + \frac{1}{pq^2} & \frac{1}{pq^2} \\
 \hline
 -\frac{(2pq + q^2)x^2}{pq^2} - \frac{(2q + p)x}{pq^2} - \frac{1}{pq^2} &
 \end{array}$$

Using the method of Long Division gives:

$$\frac{x^3}{pq^2x^3 + (2pq + q^2)x^2 + (2q + p)x + 1} = \frac{1}{pq^2} + \frac{-\frac{(2pq + q^2)}{pq^2}x^2 - \frac{(2q + p)}{pq^2}x - \frac{1}{pq^2}}{pq^2x^3 + (2pq + q^2)x^2 + (2q + p)x + 1}$$

$$\frac{1}{pq^2} - \frac{\left(\frac{2}{q} + \frac{1}{p}\right)x^2 + \left(\frac{2}{pq} + \frac{1}{q^2}\right)x + \frac{1}{pq^2}}{(1 + px)(1 + qx)^2}$$

Applying the theory of the “integration of rational functions” by partial fraction decomposition gives:

$$\frac{\left(\frac{2}{q} + \frac{1}{p}\right)x^2 + \left(\frac{2}{pq} + \frac{1}{q^2}\right)x + \frac{1}{pq^2}}{(1 + px)(1 + qx)^2} = \frac{A}{(1 + px)} + \frac{B}{(1 + qx)} + \frac{C}{(1 + qx)^2}$$

$$\left(\frac{2}{q} + \frac{1}{p}\right)x^2 + \left(\frac{2}{pq} + \frac{1}{q^2}\right)x + \frac{1}{pq^2} = A(1 + qx)^2 + B(1 + px)(1 + qx) + C(1 + px)$$

$$\text{Substitute } x = -\frac{1}{q} \Rightarrow C = \frac{1}{q^3 - pq^2}$$

$$\text{Simplify} \left[\left(\left(\frac{2}{q} + \frac{1}{p} \right) * \left(\frac{-1}{q} \right)^2 + \left(\frac{2}{p \cdot q} + \frac{1}{q^2} \right) * \left(\frac{-1}{q} \right) + \frac{1}{p \cdot q^2} \right) / \left(1 - \frac{p}{q} \right) \right]$$

$$\text{Substitute } x = -\frac{1}{p} \Rightarrow A = \frac{1}{p(p - q)^2}$$

$$\text{Simplify} \left[\left(\left(\frac{2}{q} + \frac{1}{p} \right) * \left(\frac{-1}{p} \right)^2 + \left(\frac{2}{p \cdot q} + \frac{1}{q^2} \right) * \left(\frac{-1}{p} \right) + \frac{1}{p \cdot q^2} \right) / \left(1 - \frac{p}{q} \right)^2 \right]$$

$$\frac{1}{p(p-q)^2}$$

$$\text{Substitute } x = 0 \Rightarrow B = \frac{(2p-3q)}{q^2(p-q)^2}$$

$$\text{Simplify}\left[\frac{1}{p \cdot q^2} - \left(\frac{1}{p(p-q)^2} + \frac{1}{q^2(-p+q)}\right)\right]$$

$$\frac{2p-3q}{(p-q)^2 q^2}$$

$$x = -\frac{1}{p} \Rightarrow A = \frac{1}{p(p-q)^2}$$

$$x = 0 \Rightarrow B = \frac{(2p-3q)}{q^2(p-q)^2}$$

$$x = -\frac{1}{q} \Rightarrow C = \frac{1}{q^3 - pq^2}$$

The partial fraction decomposition is verified by using “Mathematica” software:

$$\left(\frac{2}{q} + \frac{1}{p}\right)x^2 + \left(\frac{2}{pq} + \frac{1}{q^2}\right)x + \frac{1}{pq^2} = A(1+qx)^2 + B(1+px)(1+qx) + C(1+px)$$

$$\text{Simplify}\left[\frac{1}{p(p-q)^2} \cdot (1+q \cdot x)^2 + \frac{2p-3q}{(p-q)^2 q^2} \cdot (1+p \cdot x) \cdot (1+q \cdot x) + \frac{1}{q^2(-p+q)} \cdot (1+p \cdot x)\right]$$

$$\frac{(1+qx)^2 + px(1+2qx)}{pq^2}$$

$$\text{Simplify}\left[\left(\frac{2}{q} + \frac{1}{p}\right) \cdot (x)^2 + \left(\frac{2}{pq} + \frac{1}{q^2}\right) \cdot (x) + \frac{1}{pq^2}\right]$$

$$\frac{(1+qx)^2 + px(1+2qx)}{pq^2}$$

$$\frac{1}{da^2} \int \frac{x^3}{(1+px)(1+qx)^2} dx = \frac{1}{da^2} \int \frac{x^3}{(1+px)(1+2qx+q^2x^2)} dx$$

$$\frac{1}{da^2} \int \left[\frac{1}{pq^2} - \frac{\left(\frac{2}{q} + \frac{1}{p}\right)x^2 + \left(\frac{2}{pq} + \frac{1}{q^2}\right)x + \frac{1}{pq^2}}{(1+px)(1+qx)^2} \right] dx$$

$$\begin{aligned} & \frac{1}{da^2} \int \left[\frac{1}{pq^2} - \left(\frac{A}{(1+px)} + \frac{B}{(1+qx)} + \frac{C}{(1+qx)^2} \right) \right] dx \\ & \frac{1}{da^2} \int \left[\frac{1}{pq^2} - \left(\frac{1}{p(p-q)^2} \frac{1}{(1+px)} + \frac{(2p-3q)}{q^2(p-q)^2} \frac{1}{(1+qx)} + \frac{1}{q^3-pq^2} \frac{1}{(1+qx)^2} \right) \right] dx \\ & \frac{1}{da^2} \left[\frac{x}{pq^2} - \frac{1}{p(p-q)^2} \frac{\ln(1+px)}{p} - \frac{(2p-3q)}{q^2(p-q)^2} \frac{\ln(1+qx)}{q} + \frac{1}{q^3-pq^2} \frac{1}{q(1+qx)} \right] + \text{constant} \end{aligned}$$

Integrate[

$$\begin{aligned} & \frac{1}{p \cdot q^2} - \left(\frac{1}{p(p-q)^2} * \frac{1}{(1+p \cdot x)} + \frac{2p-3q}{(p-q)^2 q^2} * \frac{1}{(1+q \cdot x)} + \right. \\ & \left. \frac{1}{q^2(-p+q)} * \frac{1}{(1+q \cdot x)^2} \right), x] \end{aligned}$$

$$\frac{x}{pq^2} - \frac{1}{(p-q)q^3(1+qx)} - \frac{\text{Log}[1+px]}{p^2(p-q)^2} + \frac{(-2p+3q)\text{Log}[1+qx]}{(p-q)^2q^3}$$

Substituting $p = \frac{c}{d}$; $q = \frac{e}{a}$ into the integral equation gives:

$$\begin{aligned} & \frac{1}{da^2} \left[\frac{x}{pq^2} - \frac{1}{p(p-q)^2} \frac{\ln(1+px)}{p} - \frac{(2p-3q)}{q^2(p-q)^2} \frac{\ln(1+qx)}{q} + \frac{1}{q^3-pq^2} \frac{1}{q(1+qx)} \right] \\ & \frac{1}{da^2} \left[\frac{x}{(c/d)(e/a)^2} - \frac{\ln(1+(c/d)x)}{(c/d)^2((c/d)-(e/a))^2} - \frac{(2(c/d)-3(e/a))\ln(1+(e/a)x)}{(e/a)^3((c/d)-(e/a))^2} + \right. \\ & \left. + \frac{1}{(e/a)^3-(c/d)(e/a)^2} \frac{1}{(e/a)(1+(e/a)x)} \right] \end{aligned}$$

Substituting $D_o = d$; $C_3 = c$; $A_o = a$; $C_1 = e$ into the above equation gives:

$$\begin{aligned} & \frac{1}{D_o(A_o)^2} \left[\frac{x}{(C_3/D_o)(C_1/A_o)^2} - \frac{\ln(1+(C_3/D_o)x)}{(C_3/D_o)^2((C_3/D_o)-(C_1/A_o))^2} - \right. \\ & \left. - \frac{(2(C_3/D_o)-3(C_1/A_o))\ln(1+(C_1/A_o)x)}{(C_1/A_o)^3((C_3/D_o)-(C_1/A_o))^2} + \right. \\ & \left. + \frac{1}{(C_1/A_o)^3-(C_3/D_o)(C_1/A_o)^2} \frac{1}{(C_1/A_o)(1+(C_1/A_o)x)} \right] \end{aligned}$$

Substitute $x = \theta$ and evaluating E_{44} without limit $(0, 2\pi)$ gives:

$$E_{44} = C_2^3 \int \frac{\theta^3}{(D_o + C_3\theta)(A_o + C_1\theta)^2} d\theta$$

$$E_{44} = C_2^3 \frac{1}{D_o A_o^2} \left[\frac{D_o A_o^2 \theta}{C_3 C_1^2} - \frac{D_o^4 A_o^2}{C_3^2 (D_o C_1 - C_3 A_o)^2} \frac{\ln(D_o + C_3 \theta)}{\ln(D_o)} - \frac{A_o^3 (2C_3 A_o) - 3C_1 D_o}{D_o A_o C_1^3} \frac{D_o^2 A_o^2}{(D_o C_1 - C_3 A_o)^2} \frac{\ln(A_o + C_1 \theta)}{\ln(A_o)} + \frac{A_o^3 D_o}{(C_1^3 D_o - C_3 C_1^2 A_o)} \frac{A_o^2}{C_1 (A_o + C_1 \theta)} \right] + \text{constant}$$

Assuming: $\ln(D_o) = 1$; $\ln(A_o) = 1$ and simplifying gives:

$$E_{44} = \frac{C_2^3}{C_3 C_1^2} \left[\theta - \frac{D_o^3 C_1^2}{C_3 (D_o C_1 - C_3 A_o)^2} \ln(D_o + C_3 \theta) + \frac{A_o^2 C_3 (3C_1 D_o - 2C_3 A_o)}{C_1 (D_o C_1 - C_3 A_o)^2} \ln(A_o + C_1 \theta) - \frac{A_o^3 C_3}{(C_1^3 D_o - C_3 C_1^2 A_o) C_1 (A_o + C_1 \theta)} \right] + \text{constant}$$

Appendix F

COMPUTER PROGRAMS OF PUMP GEOMETRY DETERMINATION & PUMP EFFICIENCY DETERMINATION

F.1 Pump Geometry Determination

```
str1=sprintf('    * WELCOME TO THE GEOMETRY CALCULATION PROGRAM *');
disp(str1);
%
clear all
%-----
-----
str2=sprintf('Enter Flowrate, Head, Rotational speed, Gravitational
acceleration');
disp(str2);

Q = input(' Enter Flowrate in ft^3/sec:      ');
H = input(' Enter Head in ft, 165.32:      ');
N = input(' Enter Rotational speed in rpm:   ');
g = input(' Enter Gravitational acceleration in ft/sec^2, 32.2:
');
t = input(' Enter assumed blade thickness in cm, 0.4:      ');
delta = input(' Enter assumed front axial clearance between impeller
and housing in cm, 0.1:      ');

%-----
-----
str3=sprintf('Enter all constants');
disp(str3);

Ku = input(' Constant Ku:      ');
Km1 = input(' Constant Km1:    ');
Km2 = input(' Constant Km2:    ');
d1_d2 = input(' Constant d1/d2:      ');
K3 = input(' Constant K3:      ');
phi = input(' Constant phi:      ');
to2_100_d2 = input(' Constant 2to_100_d2:      ');

U2 = Ku*sqrt(2*g*H) ; % ft/sec

omega = 2*pi*N/60 ; % rad/sec

d2 = (2*U2/omega) ;
d2_cm = (2*U2/omega)*12*2.54 ;

d1 = d1_d2*d2 ;
d1_cm = d1_d2*d2_cm ;

Vr1 = Km1*sqrt(2*g*H) ; % ft/sec

b1_cm = (Q/(pi*d1*Vr1))*12*2.54 ;

Vr2 = Km2*sqrt(2*g*H) ; % ft/sec
```

```

b2_cm = (Q/(pi*d2*Vr2))*12*2.54 ;

b1_assumed_cm = 0.4*2.54 ;
b2_assumed_cm = 0.4*2.54 ;

Vmv = K3*sqrt(2*g*H) ; % ft/sec

Ae_cm2 = (Q/Vmv)*144*2.54^2 ;
be_assumed_cm = 0.5*2.54 ;

te_cm = Ae_cm2/be_assumed_cm ;
te_assumed_cm = 0.6*2.54 ;

Ae_assumed_cm2 = te_assumed_cm*be_assumed_cm ;

De_cm = sqrt(4*Ae_assumed_cm2/pi) ;

to_cm = to2_100_d2*d2_cm/200 ;
to_assumed_cm = 0.075*2.54 ;
bo_assumed_cm = 0.5*2.54 ;

Ao_assumed_cm2 = (to_assumed_cm*bo_assumed_cm)*12^2*2.54^2 ;

Do_cm = sqrt(4*Ao_assumed_cm2/pi) ;

phi_new = atan(te_assumed_cm/(pi*d2_cm))*180/pi ;

str20=sprintf(' Calculated impeller width at inlet: %7.4f cm',b1_cm );
str21=sprintf(' Calculated impeller width at exit: %7.4f cm',b2_cm );
str22=sprintf(' Assumed impeller width at inlet: %7.4f
cm',b1_assumed_cm);
str23=sprintf(' Assumed impeller width at exit: %7.4f
cm',b2_assumed_cm);

str24=sprintf(' Inlet impeller diameter: %7.4f cm',d1_cm );
str25=sprintf(' Exit impeller diameter: %7.4f cm',d2_cm );

str26=sprintf(' Blade thickness: %7.4f cm',t );
str27=sprintf(' Front axial clearance between impeller and housing:
%7.4f cm',delta );
str28=sprintf(' Volute cross - sectional area at tongue clearance:
%7.4f cm^2',Ao_assumed_cm2 );
str29=sprintf(' Calculated Volute cross - sectional area at exit: %7.4f
cm^2',Ae_cm2 );
str30=sprintf(' Assumed Volute cross - sectional area at exit: %7.4f
cm^2',Ae_assumed_cm2 );

str31=sprintf(' Volute hydraulic diameter at tongue clearance: %7.4f
cm',Do_cm );
str32=sprintf(' Volute hydraulic diameter at exit: %7.4f cm',De_cm );
str33=sprintf(' Calculated Tongue clearance between the impeller and
the tongue: %7.4f cm',to_cm );
str34=sprintf(' Assumed Tongue clearance between the impeller and the
tongue: %7.4f cm',to_assumed_cm );
str35=sprintf(' Calculated Volute radial clearance at exit: %7.4f
cm',te_cm );

```

```

str36=sprintf(' Assumed Volute radial clearance at exit: %7.4f
cm',te_assumed_cm );

str37=sprintf(' Assumed Housing inside axial width in the volute
region: %7.4f cm',bo_assumed_cm );
str38=sprintf(' Assumed Housing axial width at exit: %7.4f
cm',be_assumed_cm );
str39=sprintf(' Calculated volute angle : %7.4f degree',phi_new );
str40=sprintf(' Old volute angle : %7.4f degree',phi );

disp(str20);
disp(str21);
disp(str22);
disp(str23);
disp(str24);
disp(str25);
disp(str26);
disp(str27);
disp(str28);
disp(str29);
disp(str30);
disp(str31);
disp(str32);
disp(str33);
disp(str34);
disp(str35);
disp(str36);
disp(str37);
disp(str38);
disp(str39);
disp(str40);

```

F.2 Pump Efficiency Determination

```

clear all ;
% Step 1: Pump Geometrical Input Parameters
% Variable Parameters for variable efficiencies

Q = 0;
for i=1:14
    Q(i)=(i)*10;
    Q = Q(i)

% Varied Parameters
N = 10500 ; % rpm
% Q = 80 ; % cm^3/sec
Z = 8 ;
beta = 90 ; % beta = beta2

% Fixed Parameters
nu = 1.3*10^-2 ; % cm^2/sec Kinematic Viscosity
rho = 0.77 ; % g/cm^3 Density
g = 981 ; % cm/sec^2
b1 = 1.016 ; % cm
b2 = 1.016 ; % cm
d1 = 1.585 ; % cm

```

```

d2 = 6.096          ; % cm
t = 0.4             ; % cm, Assumed
delta = 0.1         ; % cm, Assumed
Kb = 0.2            ; % Assumed entrance-bend-resistance coefficient
Ao = 0.2419         ; % cm^2
Ae = 1.9355         ; % cm^2
Do = 0.555          ; % cm
De = 1.5697         ; % cm
to = 0.1905         ; % cm

% Step 2:
% Euler Head He, Head due to finite number of blades Ha
% Head Loss due to Entrance-Bend-Resistance Loss Heb

omega = 2*pi*N/60   ;
U1 = omega*d1/2      ;
U2 = omega*d2/2      ;

Ks = (Z^0.3)/(pi*sqrt(sin(beta*pi/180))) ;

S1 = U1*Ks*(pi/Z)*sin(beta*pi/180) ;
S2 = U2*Ks*(pi/Z)*sin(beta*pi/180) ;

Vr1 = Q/(b1*(pi*d1 - Z*t/sin(beta*pi/180))) ;
Vr2 = Q/(b2*(pi*d2 - Z*t/sin(beta*pi/180))) ;

Vt1 = U1 + S1 - Vr1/tan(beta*pi/180) ;
Vt2 = U2 - S2 - Vr2/tan(beta*pi/180) ;

Vu2 = U2 - Vr2/tan(beta*pi/180) ;

He = U2*Vu2/g ;
Hc = (U2^2)*Ks*pi*sin(beta*pi/180)/(g*Z) ;
Ha = He - Hc ;
Heb = 8*Kb*Q^2/(pi^2*g*d1^4) ;

% Step 3: Friction Head Loss Hf
W1 = Q/(b1*(pi*d1*sin(beta*pi/180) - Z*t)) ;
W2 = Q/(b2*(pi*d2*sin(beta*pi/180) - Z*t)) ;

D1 = 2*b1*(pi*d1*sin(beta*pi/180) - Z*t)/(pi*d1*sin(beta*pi/180) - Z*t + Z*b1) ;
D2 = 2*b2*(pi*d2*sin(beta*pi/180) - Z*t)/(pi*d2*sin(beta*pi/180) - Z*t + Z*b2) ;

d_m = 0.5*(d1 + d2) ;
b_m = 0.5*(b1 + b2) ;

W_m = Q/(b_m*(pi*d_m*sin(beta*pi/180) - Z*t)) ;

S_m = 0.5*(S1 + S2) ;

D_mi = 2*b_m*(pi*d_m*sin(beta*pi/180) - Z*t)/(pi*d_m*sin(beta*pi/180) - Z*t + Z*b_m) ;

V_mi = 0.5*(abs(W_m + 0.5*S_m) + abs(W_m - 0.5*S_m)) ;

```

```

Re_i = V_mi*D_mi/nu ;
if Re_i > 2300
    lamda = 0.3164/Re_i^0.25 ;
else
    lamda = 64/Re_i ;
end

Hf = (lamda*(d2-d1)*0.5/(4*g*sin(beta*pi/180)))*((W1^2 + 0.25*S1^2)/D1
+ (W2^2 + 0.25*S2^2)/D2) ;

% Step 4: Volute Head Loss
alpha_o = atan(Vr2/Vt2) ;

X13 = d2/(d2 + 2*to) ;
X14 = cos(alpha_o)*((1 - (X13*cos(alpha_o))^2)^0.5 - X13*sin(alpha_o))
;
teta_o = asin(X14) ;

q_o = Q*teta_o/(2*pi) ;
D_mv = 0.5*(Do + De) ;
V_mv = 0.5*((q_o/Ao) + (Q/Ae)) ;
Re_v = V_mv*D_mv/nu ;
if Re_v > 2300
    f = 0.3164/Re_v^0.25 ;
else
    f = 64/Re_v ;
end

Vr = Vr2 ;
Vt = Vt2 ;
Ve = Q/Ae ;
E_Q = q_o/Q ;
E_A = Ao/Ae ;
E_D = Do/De ;
X1 = E_A - E_Q ;
X2 = pi*f*d2/De ;
X3 = (E_A - E_Q)^2/(E_A*(1 + E_A)) ;
X4 = (E_A - E_Q)^3/(E_A*(1 + E_A)*(E_A - E_D)) ;
X5 = (E_Q - E_D)^3/(E_A - E_D)^2 ;
X6 = (E_D - E_Q)^2*(3*E_D - 2*E_A - E_Q)/(E_A - E_D)^2 ;
Hv1 = (1/(2*g))*(Vr^2 + (Vt - Ve)^2 + 2*Ve*(Vt - Ve)*X1*log(1 + 1/E_A)
+ Ve^2*X3) ;

Hv2 = (1/(2*g))*X2*Ve^2*(1 + X4 + X5*log(1 + 1/E_D) + X6*log(1 +
1/E_A)) ;
Hv = Hv1 + Hv2 ;

% Step 5: Pump Output Head H
H = Ha -Heb -Hf - Hv ;

% Step 6: Pump Output Power W_out
Ha_mm = (10/13.6)*Ha ;
H_mm = (10/13.6)*H ;

W_out = H_mm*(Q*60/1000)*(1/450) ;

% Step 7:

```

```

% Power Loss due to Leakage PL
% Power Loss due to Disk Friction Pd
% Pump Input Power W_in

m1 = 2*(Vt2 - Vt1)/(d2 - d1) ;
m2 = Vt1 - (Vt2 - Vt1)*d1/(d2 - d1) ;
y11 = m1^2*(d2^4 - d1^4)/8 ;
y12 = 2*m1*m2*(d2^3 - d1^3)/3 ;
y13 = m2^2*(d2^2 - d1^2) ;

Pd = pi*nu*rho*(y11 + y12 + y13)/(2*delta*10^7) ;
PL = Z*rho*delta*(d2^4 - d1^4)*(sin(beta*pi/180))^2/(128*10^7) ;
W_in = PL + Pd + Ha_mm*(Q*60/1000)*(1/450) ;

% Step 8: Pump Efficiency
efficiency = 100*W_out/W_in
end

```